2018

Toxicity Evaluations of Nanoclays and an Associated Nanocomposite throughout their Life Cycle

Alixandra Wagner

Toxicity Evaluations of Nanoclays and an Associated Nanocomposite throughout their Life Cycle

Alixandra Wagner

Dissertation submitted to the Benjamin M. Statler College of Engineering and Mineral Resources at West Virginia University
In partial fulfillment of the requirements for the degree of
Doctor of Philosophy in Chemical Engineering

Cerasela Zoica Dinu, Ph.D. Committee Chairperson

Rakesh K. Gupta, Ph.D.

Konstantinos A. Sierros, Ph.D.

Charter Stinespring, Ph.D.

Todd A. Stueckle, Ph.D.

Department of Chemical and Biomedical Engineering

Morgantown, West Virginia

2018

Keywords: Nanoclay, Nanocomposite, Life cycle, Toxicity, Lung cell

Abstract

Toxicity Evaluations of Nanoclays and an Associated Nanocomposite throughout their Life Cycle

Alixandra Wagner

Nanoclays are layered mineral silicates that originate from the clay fraction of soil and carry a platelet thickness of about 1 nm and lengths and widths of up to several microns. Due to their nanoscale dimensions, they have been used for numerous applications ranging from media for oil well drilling to sorbents in treatment of waste-water. Additionally, upon functionalization with organic modifiers, nanoclays have been incorporated into polymers to form nanocomposites with increased mechanical strength, barrier properties, UV dispersion, and fire resistance to be implemented in food packaging or medical devices related applications. Such increased implementation into industrial and commercial products has brought scrutiny onto nanoclays and associated nanocomposites toxicity. Previous studies have shown for instance that nanoclays induce cytotoxic and genotoxic effects upon cellular or model animal exposure, however little investigations were performed to identify how nanoclay functionalization may influence such toxicological profiles. Moreover, most of the studies related to nanoclays and nanocomposites toxicity only refer to their consumption/usage exposure and fail to assess manufacturing or disposal exposures.

Herein, we aimed to understand how the physical and chemical properties of nanoclay systems (i.e. pristine and organically modified, along with a nanoclay-enforced nanocomposite) in both their as-received (mimicking manufacturing) and thermally degraded (mimicking end of life cycle incineration) forms influence lung cells, used to model inhalation toxicity. Physical and chemical properties of the materials were investigated via microscopical and spectroscopical approaches, while toxicity profiles were assessed both in real-time or at disparate time points via *in vitro* cellular and molecular assays, cell imaging, and electric cell-substrate impedance sensing. Our analyses showed that nanoclays and nanocomposites properties (both physical and chemical) influence the materials' degradation profile and ultimately their induced toxicity in model cellular systems. The toxic effects were displayed either by reductions in cell proliferation and viability, changes in cell morphology, and/or alterations in the cell cytoskeleton. Overall, our results provide unique insights into how materials properties, both physical and chemical dictate materials' toxicological profiles throughout their life cycle (from manufacturing to disposal) with such information to be possibly aiding in safe-by-design strategies as well as safety protocols implementation in areas of exposure.

Dedication

To my family

Acknowledgements

First and foremost, I would like to express my sincere gratitude to my advisor Dr. Cerasela Zoica Dinu for all her guidance, advice, and support throughout my graduate studies. Without her encouragement, I would not have entered the Ph.D. program and been given the opportunities I have now. Further, her continuous assistance on all aspects of these studies have made such research a possibility and helped me learn and grow as a researcher.

In addition, I would like to thank Dr. Todd A. Stueckle for all his advice and assistance on the projects performed throughout my studies. I would also like to thank my committee members Dr. Rakesh K. Gupta, Dr. Konstantinos A. Sierros, and Dr. Charter Stinespring for all their assistance on these projects, as well as for serving on my committee. In addition, I would like to thank Dr. Yon Rojanasakul and Dr. Sushant A. Agarwal for their advice and assistance in laboratory space and materials that helped support this research.

I would like to thank the staff of the WVU Shared Research Facilities for all their help on equipment used for the material characterization studies in this research, with special thanks to Dr. Marcela Redigolo, Dr. Weiqiang Ding, and Dr. Qiang Wang. I would also like to thank Gabriela Perhinschi for her help with the TGA and the members of Dr. Sierros's lab for help with the DLS.

I would also like to express my gratitude for the current and former members of Dr. Dinu's and Dr. Rojanasakul's lab with whom I have worked with over the years and have helped greatly with numerous aspects of my graduate studies. I would also like to give a special thanks to the former and current faculty, staff, and students of the Chemical and Biomedical Engineering Department for all their help and support over the years.

Finally, I would like to thank my family and friends for all their continuous support over the years and for always being there for me.

TABLE OF CONTENTS

LIST OF FIGURES

Chapter 1: Nanoclays: A Review of their Toxicological Reports and Risk Assessment Implementation Strategies

Chapter 2: Toxicity Evaluations of Nanoclays and Thermally Degraded Byproducts through Spectroscopical and Microscopical Approaches

Chapter 3: Early Assessment and Correlations of Nanoclay's Toxicity to their Physical and Chemical Properties

Chapter 4: Toxicity Assessment of Byproducts Resulted from Nanoclay Composite Disposal by Incineration

LIST OF TABLES

Chapter 1: Nanoclays: A Review of their Toxicological Reports and Risk Assessment Implementation Strategies

Chapter 2: Toxicity Evaluations of Nanoclays and Thermally Degraded Byproducts through Spectroscopical and Microscopical Approaches

Chapter 3: Early Assessment and Correlations of Nanoclay's Toxicity to their Physical and Chemical Properties

LIST OF SYMBOLS / NOMENCLATURE

- ANOVA: analysis of variance
- BEAS-2B: immortalized human lung epithelial cells
- CC: as-received Cloisite 30B
- CC900: thermally degraded Cloisite 30B
- DLS: dynamic light scattering
- DMEM: Dulbecco's Modified Eagle's Medium (cellular media for BEAS-2B cells)
- ECIS: electric cell-substrate impedance sensing
- EDX: Energy dispersive X-ray spectroscopy
- FACS: fluorescence activated cell sorting
- FBS: fetal bovine serum
- FTIR: Fourier Transform Infrared Spectroscopy
- I.31PS: as-received Nanomer I.31PS
- I.31PS900: thermally degraded Nanomer I.31PS
- I.34TCN: as-received Nanomer I.34TCN
- I.34TCN900: thermally degraded Nanomer I.34TCN
- I.44P: as-received Nanomer I.44P
- I.44P900: thermally degraded Nanomer I.44P
- MMT: montmorillonite
- PBS: phosphate buffered saline
- PGV: as-received Nanomer PGV
- PGV900: thermally degraded Nanomer PGV
- PLA: polylactic acid
- PLACC: polylactic acid-Cloisite 30B nanocomposite
- PLACC900: thermally degraded polylactic acid-Cloisite 30B nanocomposite
- ROS: reactive oxygen species
- SAECs: small airway epithelial cells
- SAGM: small Airway Growth Medium (cellular media for SAECs)
- SEM: scanning electron microscopy

- TGA: thermogravimetric analysis
- UC: as-received Cloisite Na^+
- UC900: thermally degraded Cloisite Na^+
- WST: tetrazolium salt (cellular viability assay)
- XRD: X-ray diffraction

INTRODUCTION

Montmorillonite (MMT) is the most common type of phyllosilicate nanoclay, which consist of 2 silicate-oxygen tetrahedral sheets and an aluminum octahedral sheet. However, MMT has a negative charge due to the substitution of aluminum for silicon in its tetrahedral sheets and magnesium for aluminum in its octahedral sheets, respectively. Positively charged ions, such as sodium and calcium, are attracted to the inner galleries of such a negative nanoclay, allowing for its functionalization with organic modifiers through ion exchange reactions. The organic modifier increases nanoclay's basal spacing and leads to a more hydrophobic material with substantially improved ease of implementation into polymer mixtures for nanocomposites formation.

Nanoclays high aspect ratio along with their abundance in soil and low cost have made nanoclays applicable to numerous areas from sorbents for the treatment of waste water or hazardous spills, to rheological modifiers for oil well drilling fluids, paints, and cosmetics. Additionally, their functionalization with organic modifiers and incorporation into polymers to form a nanocomposite with increased mechanical strength, barrier properties, UV dispersion, and fire resistance, extended their usages to areas such as food packaging, medical devices, or automotive industry. However, with larger consumer implementation, nanoclays and nanocomposites have the extended potential for human exposure throughout their life cycle, i.e., from manufacturing, consumption/usage, to disposal. Impactful assessment strategies are needed to evaluate their possible toxicity profiles in order to establish consumer and worker exposure limits or design strategies that minimize their possible deleterious effects.

This thesis looks at identifying the toxicological profiles of nanoclays or nanoclay-enforced composites (nanocomposites) during their life-cycle, i.e. from manufacturing to disposal. Specifically:

Chapter one introduces structural and functional characteristics of nanoclays that have led to their increased ability for processing and applicability in numerous areas from sorbents in pollution prevention, to environmental remediation, paints, and cosmetics. Additionally, the chapter highlights the properties and applications of nanocomposites in the food packaging industry. Further, a comprehensive summary of the current studies differentiating toxicity and toxicity-related mechanisms resulted from cellular exposures to commercially available nanoclays (e.g., with different physico-chemical characteristics as provided by the organic modifier or the size of the nanoclay itself etc.) currently in use is presented. Lastly, this chapter highlights the gaps

in knowledge related to the toxicological profiles of the nanoclays and proposes that the logistical burden associated with their toxicological risk assessment could be circumvented through implementation of tailored strategies that ensure a greener route for nanoclay functionalization and implementation. (**Book Chapter:** Wagner, A., Gupta, R., Dinu, C.Z. Nanoclays: A Review of their Toxicological Profiles and Risk Assessment Implementation Strategies, in Nanotechnology Commercialization: Manufacturing Processes and Products. 2017. John Wiley & Sons, Inc., Hoboken, NJ, USA.)

Chapter two details the specific investigation as related to the potential inhalation toxicity of a pristine nanoclay, Cloisite Na^+, and an organically modified nanoclay, Cloisite 30B, as well as their thermally degraded byproducts, thus uniquely accounting for exposure in both manufacturing and disposal environments. With studies showing that nanoclays have the potential to come into contact with humans during manufacturing and handling, and considering that their disposal potentially leads to increased reactivity at interfaces with biological systems, this chapter highlights why it is important to understand nanoclays' life cycle and induced interactions with cellular systems. Through material characterization and toxicity analyses, the chapter demonstrates that the greatest degree of toxicity occurs for the organically modified nanoclay. Further, different toxicological profiles were obtained for the thermally degraded nanoclays relative to their as-received counterparts. The results show that both manufacturing and disposal exposures need to be considered when evaluating materials' toxicity profiles; further, the chapter emphasizes that viable safety protocols need to be implemented when nanoclays are being considered for consumer products. (**Publication:** Wagner, A., Eldawud, R., White, A., Agarwal, S., Stueckle, T.A., Sierros, K.A., Rojanasakul, Y., Gupta, R.K., Dinu, C.Z. Toxicity Evaluations of Nanoclays and Thermally Degraded Byproducts through Spectroscopical and Microscopical Approaches. Biochimica et Biophysica Acta. 2017, 1861 (1 Pt A), 3406-3415.)

Chapter three extends the existing literature and provides a comprehensive analysis of the physical and chemical characteristics of four types of nanoclays used in food packaging applications as well as differentiates their toxicity-related mechanisms based on their different physico-chemical characteristics. A variety of microscopical and spectroscopical materials characterization techniques, as well as two *in vitro* model lung cell lines, an immortalized and a primary line (to provide a more realistic view of nanoclay-related toxicity and a verification of results in pertinent human-related exposure models), were used. Additionally, the toxicity of the

nanoclays was investigated at levels of exposure that mimic a manufacturing and a disposal environment to thus establish valid toxicity pathways during the life cycle of the nanoclays. (**Publication:** Wagner, A., White, A.P., Stueckle, T.A., Banerjee. D., Sierros, K.A., Rojanasakul, Y., Agarwal, S., Gupta, R.K., Dinu, C.Z. Early Assessment and Correlations of Nanoclay's Toxicity to their Physical and Chemical Properties. ACS Applied Materials & Interfaces. 2017, 9 (37), 32323-32335.)

Chapter four establishes that toxicity studies do not only need to account for nanoclays themselves or for their exposure at both manufacturing and disposal areas, but further, have to account for nanoclays implementation. As such, this chapter establishes correlations between the consumption/usage and disposal stages of a nanocomposite while also allowing the individual toxicological impacts of the components themselves, i.e. polymer (model polymer considered is polylactic acid) and nanoclay, as well as their associated byproducts (i.e. products resulted from incineration), to be explored. The results of this chapter show that the byproduct of such a nanocomposite does induce changes to human lung cellular systems with effects being associated with the multiple stages of the nanocomposite life cycle. (**Publication:** Wagner, A., White, A.P., Tang, M.C., Agarwal, S., Stueckle, T.A., Rojanasakul, Y., Gupta, R.K., Dinu, C.Z. Incineration of Nanoclay Composites Leads to Byproducts with Reduced Cellular Reactivity. Scientific Reports. 2018, 8, 10709.)

CHAPTER 1

Nanoclays: A Review of their Toxicological Reports and Risk Assessment Implementation Strategies

Abstract

Nanoscale properties and increased ability for processing, along with abundance in soil and low cost, make nanoclays applicable to numerous areas from sorbents in pollution prevention to environmental remediation, paints, and cosmetics. Further, reinforcement of polymer films with nanoclays has led to implementation of nanoclays in the next generation of nanocomposites with increased mechanical strength, barrier properties, UV dispersions, and fire resistance capabilities, to be applied in the food packaging industry.

The first part of this review describes the characteristics of nanoclays and how they can be exploited for synthetic applications, especially food packaging applications, while the second part of the review focuses on the challenges associated with nanoclay integration in consumer products and their potential to induce deleterious effects that could affect humans at the exposure levels of manufacturing, consumption, and disposal. Lastly, the review highlights the potential mechanisms of toxicity resulted upon cellular exposure to nanoclays and proposes that logistical burden associated with risk assessment resulted from such exposures could be circumvented through implementation of tailored strategies to ensure a greener route for nanoclay functionalization and implementation.

Nanoclay structure and resulting applications

Nanoclays are layered, mineral silicates that originate from the clay fraction of the soil.[1,2] Carrying platelet thickness of around 1 nm and lengths and widths of up to several microns,[3,4] the smectite group of nanoclays are largely made up of 2:1 phyllosilicates, a silicate-oxygen tetrahedral and an aluminum octahedral sheet.[1,5] Such features differentiate them from chlorite and kaolinite nanoclays which consist of two tetrahedral and two octahedral sheets and one tetrahedral and one octahedral sheet, respectively.[1,6] Montmorillonite, the most common type of phyllosilicate clay,[1] has a negative charge due to the substitution of aluminum for silicon in its tetrahedral sheets and magnesium for aluminum in its octahedral sheets.[7] Bentonite, a source of montmorillonite, also contains crystalline quartz, cristobalite, and feldspar,[8] and due to the presence of inorganic cations in its galleries is hydrophilic in nature.[7,5]

Positively charged ions, such as, sodium, potassium, and calcium, are attracted to the inner galleries of negative nanoclays,[7] allowing for cations exchange and organic modification via an ion exchange reaction[9]. The addition of the organic modifier increases basal spacing to allow for a relatively larger distance between nanoclay platelets further allowing for the naturally hydrophilic clay to become more hydrophobic.[7,8,10] Smectite clays for instance have a cation exchange capacity (CEC) of 70-130 meq/100g,[6] where CEC is a measure of the number of positively charged ions that are able to be held by the negatively charged surface of the clay platelets.[8]

Due to their nanoscale thickness and longer relative lengths and widths, nanoclays have a high aspect- and surface area-to-volume ratios that lead to an increase of their reactivity.[1,9] This, along with their abundance in soil[1] and low cost,[1] have made nanoclays applicable to numerous areas from sorbents in pollution prevention,[7] to environmental remediation,[7] waste water treatment,[11,12] as well as rheological modifiers for oil well drilling fluids,[11,13] paints,[11] and cosmetics,[11] food packaging,[14,15] automotive,[16,17] medical devices,[18,19] and coatings-related industry.[20,21] A comprehensive list of the numerous organically modified nanoclays currently in use in consumer applications is shown in Table 1.

Table 1: Examples of nanoclays researched along with their organic modifiers, applications, and associated references.

Nanoclay	**Organic Modifier**	**Applications**	**References**
Montmorillonite (MMT)	None	Adsorbents in water and wastewater treatment, drilling fluid, paints, cosmetics, coatings, drug delivery	Pluta et al.[33] Mondal et al.[24] Meera et al.[20] Introzzi et al.[21] Baek et al.[63] Rawat et al.[64] Li et al.[65] Liu et al.[66] Murphy et al.[70]
	Octadecyl amine	Food packaging	Barua et al.[19] Manikantan et al.[40]
	Trimethyl stearyl ammonium	Coatings	Meera et al.[20]
Halloysite	None	Coatings, drug delivery, implants, food packaging, composites	Alipoormazandarant et al.[26] Sadegh-Hassani and Nafchi[38] Verma et al.[58] Vergaro et al.[67]
Bentonite	None	Drilling mud, absorbent, groundwater barrier, cosmetics, pharmaceutical	Barua et al.[19] Meibian et al.[44] Murphy et al.[70] Meibian et al.[75] Yuwen et al.[83]
	3-5 wt.% Na_2CO_3		Geh et al.[48]
	HCl		Geh et al.[48]
	Distearyl-dimethylamonium-chloride		Geh et al.[48]
	H_2SO_4		Meibian et al.[44] Meibian et al.[75]
Quartz	None	Drilling, glass making, foundry sand, electronics, abrasives	Gao et al.[59]
Kaolin	None	Coatings, cosmetics, paints, adsorbents in water and wastewater treatment, medical	Gao et al.[59]
	None	Cosmetics, food technology, medical	Yoshida et al.[46]

Amorphous nanosilica particles	Amine groups		Yoshida et al.[46]
	Carboxyl groups		Yoshida et al.[46]
Montmorillonite dellite	None	Adsorbents in water and wastewater treatment, drilling fluid, paints, cosmetics, coatings, drug delivery	Janer et al. [45]
Cloisite Na^+ (MMT)	None	Adsorbents in water and wastewater treatment, drilling fluid, paints, cosmetics, coatings, drug delivery	Shojaee-Aliabadi et al.[35] Rhim et al.[25] Houtman et al.[49] Maisanaba et al.[50] Maisanaba et al.[52] Lordan et al.[53] Verma et al.[58] Maisanaba et al.[62] Sharma et al.[47]
Cloisite 10A	Dimethyl, benzyl, hydrogenated tallow, quaternary ammonium	Composites, food packaging, paints, coatings	Molinero et al.[31]
Cloisite 11B	Benzyl(hydrogenated tallow alkyl)dimethyl	Composites, food packaging, automotive	Dalir et al.[17]
Cloisite 15A (MMT)	Dimethyl, dihydrogenated tallow, quaternary ammonium	Composites, drilling fluid, food packaging, medical, automotive	Agarwal et al.[13] Krikorian et al.[28] Pereira de Abreu et al.[14] Plackett et al.[22] Dalir et al.[17]
Cloisite 20A (MMT)	Dimethyl dihydrogenated tallow quaternary ammonium chloride	Composites, drilling fluid, food packaging, paints, coatings	Agarwal et al.[13] Molinero et al.[31] Rhim et al.[25] Lertwimolnun and Vergnes[36] Lertwimolnun and Vergnes[37] Choi et al.[15] Houtman et al.[49]
Cloisite 25A (MMT)	Dimethyl, hydrogenated tallow, 2-ethylhexyl quaternary ammonium methyl sulfate	Composites, drilling fluid, medical, food packaging	Agarwal et al.[13] Krikorian et al.[28] Plackett et al.[22]
Cloisite 30B (MMT)	Methyl, tallow, bis-2-hydroxyethyl, quaternary ammonium	Composites, drilling fluid, food packaging, medical, automotive, paints, coatings	Agarwal et al.[13] Krikorian et al.[28] Molinero et al.[31] Plackett et al.[22] Rhim et al.[25] Beltrán et al.[39] Dalir et al.[17]

			Abreu et al.[41] Maisanaba et al.[50] Maisanaba et al.[52] Sharma et al.[47] Sharma et al.[80]
Cloisite 93A (MMT)	Methyl dehydrogenated tallow ammonium	Composites, paints, coatings, food packaging	Molinero et al.[31] Lordan et al.[53]
Montmorillonite dellite (MMTdell 72T, MMTdell 72Ts, MMTdell 67G, MMTdell 67Gs)	Dimethyl dihydrogenated tallow ammonium	Composites, drilling fluids, medical, food packaging	Janer et al.[45]
Montmorillonite dellite (MMTdell 43B, MMTdell 43Bs)	Dimethyl benzyl hydrogenated tallow ammonium	Composites, drilling fluids, medical, food packaging	Janer et al.[45]
PSAN-MMT	Oligo(styrene-*co*-acrylonitrile)	Drug delivery	Liu et al.[66]
Halloysite MP1	None	Coatings, drug delivery, implants, food packaging, composites	Verma et al.[58]
Delilite LVF (Bentonite)	None	Composites	Verma et al.[58]
Nanomer PGV (Bentonite)	None	Composites, rheological modifier	Verma et al.[58]
Clay 1	Quaternary ammonium salt hexadecyltrimethyl-ammonium bromide (HDTA)	Composites, food packaging	Houtman et al.[49] Maisanaba et al.[51] Jorda-Beneyto et al.[54] Maisanaba et al.[81] Maisanaba et al.[82]
Clay 2	HDTA and acetylcholine chloride (ACO)	Composites, food packaging	Houtman et al.[49] Maisanaba et al.[51] Jorda-Beneyto et al.[54]

Anionic Nanoclay	Carbonate	Composites, catalyst, pharmaceuticals, filters	Chung et al.[60]
	Chloride	Composites, catalyst, pharmaceuticals, filters	Chung et al.[60]
Bentone MA (hectorite clay)	None	Cosmetics, adhesives, paints, cleaners, coatings	Verma et al.[58]
ME-100 (Somasif—a synthetic fluoromica clay)	None	Composites	Verma et al.[58]

Nanoclays in food packaging applications

Polymers such as polylactic acid (PLA),[22,23] polycaprolactone (PCL),[23] methylcellulose, starch, lignin, and poly(vinyl alcohol) have been of interest to replace the petroleum-based, non-biodegradable packaging materials.[22,24,23] However, such polymers do not always have the thermal stability,[25] strength,[24] or barrier properties[25] of conventional, synthetic polymers thus making their implementation as effective food packaging materials challenging. Further, gases, such as oxygen, carbon dioxide, water vapor, or ethylene, can penetrate the polymer matrix and diffuse throughout it[14] in the process decreasing matrix quality.[14,26]

The addition of nanoclays into a polymer matrix at a low silicate content[3,27] allows for better reinforcement within the polymer plane,[28,29] as well as an increase in its mechanical strength,[30,28] barrier properties,[3,31,14] UV dispersions,[31] and fire resistance, [32,33] and makes it applicable to food packaging industry.[14,15] As such, nanoclay-enforced polymers were shown to maintain their transparency,[14,26] with further research showing that nanoclay addition into a polymer matrix creates a tortuous path in which the nanoclays are acting as physical barriers to slow down the movement of gases[14] and create a greener route for production and disposal of packaging.[14,26,25,34] For instance, Plackett et al. found that nanoclays only caused a slight reduction in light transparency when incorporated into PLA-PCL films,[22] with Shojaee-Aliabadi et al. showing that the addition of up to 10% weight of nanoclays into polymers can still lead to translucent films when kappa-carrageenan/Cloisite Na^+ (a pristine montmorillonite with Na^+ between the platelets) were used for instance.[35] However, Rhim et al. found that nanoclays

significantly reduced the light transmittance when introduced in PLA alone, with a better exfoliation within PLA being observed for Cloisite 20A (a hydrophobic dimethyl dihydrogenated tallow quaternary ammonium chloride nanoclay).[25]

The degree of exfoliation[14] was shown to depend on the organic modifiers being used, as well as the temperature,[36] processing time,[22] and processing conditions.[37] For example, Pereira de Abreu et al. showed that longer processing mixing times generally have a positive influence on the dispersion of nanoclays.[14] Studies also found that between 180° and 200°C, better exfoliation of Cloisite 20A in polypropylene (PP) was obtained at 180°C presumably as a result of the polymer stress in this domain of temperature.[36] Further, Lertwimolnun and Vergnes showed that exfoliation of Cloisite 20A in PP films increased with decreasing feeding rate from 29 to 4.5 kg/h and increasing the screw speed from 100 to 300 rpm.[37]

Other studies showed that the addition of a low percent weight of nanoclays can increase mechanical properties of polymers.[14, 24] The displayed increases in mechanical strength was shown to help nanocomposite packaging materials withstand the stresses encountered during handling and transportation of food products.[38] Pereira de Abreu et al. for instance showed that the addition of Cloisite 15A (nanoclay organically modified with dimethyl, dihydrogenated tallow, quaternary ammonium) into PP increased the Young's modulus of the material by 692 MPa relative to the control PP[14] while the addition of halloysite (a 1:1 aluminosilicate) nanoclay to soluble soybean polysaccharide (SSPS) films increased their tensile strength by 4.1 MPa relative to SSPS with no halloysite.[26] Shojaee-Aliabadi et al. showed increases in tensile strength of 8.38 MPa when montmorillonite (MMT) was exfoliated in kappa-carrageenan (KC) films relative to KC films without MMT.[35] Sadegh-Hassani and Nafchi showed that tensile strength increased 2.49 MPa for potato starch films containing halloysite nanoclay[38] while Beltrán et al. showed that the addition of Cloisite 30B (nanoclay organically modified with methyl, tallow, bis-2-hydroxyethyl, quaternary ammonium) increased elongation at break for PCL.[39]

Studies also revealed that addition of nanoclays to polymers such as PLA reduced water vapor permeability (WVP) by 6-33% when compared to control PLA alone.[25] Sadegh-Hassani and Nafchi also showed a decrease in oxygen permeability upon addition of halloysite nanoclay,[38] while Alipoormazandarani et al. showed that halloysite nanoclay reduced water vapor and oxygen permeability by 56% and 58%, respectively, when incorporated into soluble soybean polysaccharide (SSPS).[26] Complementarily, Manikantan et al. found that nanoclays added into

polypropylene (PP) also decreased the WVP with banana chips packaged in 2% nanoclay/ PP films showing 22% lower moisture content and banana chips packaged in 4% nanoclay/PP films having 24% lower moisture content respectively all relative to the control,[40] while Shojaee-Aliabadi et al. showed a decrease in WVP by around 78% upon addition of MMT into kappa-carrageenan (KC) films.[35] Numerous other studies have shown similar results with different nanoclays and polymer matrices, [26,35,24,38,39,40] with further analysis of PLA reinforced with Cloisite 30B also displaying antimicrobial activity against *L. monocytogenes*[25] while starch films containing Cloisite 30B decreased microbial growth for *S. aureus* and *E. Coli.*[41]

Possible toxicity upon implementation of nanoclay in consumer applications

The large consumer implementation of nanoclays, especially in food packaging applications as indicated above, has the potential to affect humans at the exposure levels of manufacturing, consumption/usage, and disposal.[42,43] As such, studies aimed to differentiate toxicity and toxicity-induced mechanisms based on the organic modifier or the size of the nanoclays. For the organic modifier for instance, Meibian et al. found that activated bentonite particles had a greater cytotoxic response relative to untreated counterparts, indicating that surface characteristics may be playing a large role in mechanisms of toxicity, such as the adsorption capacity, cation exchange, charge interactions, and surface area.[44] Janer et al. also observed differences in toxicity based on the organic modifier being used, with the modifier dimethyl benzyl hydrogenated tallow ammonium displaying greater toxic effects relative to the modifier dimethyl dehydrogenated tallow ammonium for instance.[45] However, Yoshinda et al. found that the organically modified silica particles coated with amine or carboxyl groups were less toxic than the unmodified silica particle, as the modified particles reduced the amount of reactive oxygen generated in a human keratinocyte cell line (HaCat) and a murine hepatocyte cell line (TLR-1) and the amount of DNA damage in HaCaT cells.[46]

For the size, Sharma et al. showed that samples of Cloisite 30B that had been filtered through a 0.2 μm filter, thus eliminating particles in the micro range, were less cytotoxic than their unfiltered counterparts.[47] However, Janer et al. did not observe any differences in cytotoxicity between the small (100-822 nm) and large (100-3230 nm) sized pristine MMT particles.[45] Size played a role in the uptake of bentonite particles, with a maximum uptake for particles in the size range of 0.4-1.6 μm for the activated bentonite particles, and a less selective size range for the unactivated particles.[48] Other *in vitro* studies evaluated the toxicity of nanoclays (both pristine and

organically modified nanoclays) and differentiated the observed nanoclay-induced effects based on the exposure levels or the cell type being used, with the majority of studies focusing on understanding toxicity at the consumption level of exposure (i.e. around 48%, 24%, and 28% for consumption exposure, inhalation exposure, and other, respectively) and assuming that nanoclays will eventually migrate out of the polymer matrix into food stocks when used for food packaging applications.[49,50,51,52,53,54] Detailed below are several investigations that mean to identify the deleterious effects that nanoclays can have and possibly propose means to reduce the logistical burden associated with developing meaningful risk assessment strategies for evaluating their potential and feasibility for implementation in food packaging industry.

***In vitro* studies reveal the potential of nanoclay to induce changes in cellular viability**

Studies proposed that the small size and platelet morphology of nanoclays have the potential to allow for their inhalation and deposition in the bronchial or alveolar regions of the lung.[42,55,56,57] In support of this hypothesis, Verma et al. investigated the inhalation toxicity of both platelet and tubular shaped nanoclays using *in vitro* models, i.e., human alveolar epithelial cells (A549), and a dosage ranging from 1 to 250 µg/ml.[58] Analyses showed that tubular nanoclays did not induce toxicity until doses of 250 µg/ml, which was in contrast with the platelet nanoclays that induced toxicity at only 25 µg/ml and 24 h exposure.[58] Further studies by the same authors showed that the pristine nanoclay, i.e., Cloisite Na^+ was internalized by the exposed cells and accumulated in their perinuclear region (Figure 1b,c; nanoclays were labeled in red using rhodamine dyes and their localization is indicated with white arrowheads).[58] Figure 1a displays the control cells; all cells were also counterstained with Alexa Fluor 488 phalloidin (green) for cellular cytoskeleton and Hoechst (blue) for nucleus identification. Analysis showed that the uptake was time dependent with increases in the amount of Cloisite Na^+ occurring accumulatively over the 24 h exposure time. Geh et al. also observed uptake of bentonite particles into human lung fibroblasts (IMR90 cells) over 24 h exposure at a dose of 10 µg/cm^2, with uptake increasing when the bentonite particles were activated with quartz (5-6%).[48] Such nanoclays were also more cytotoxic when compared to non-activated or lower quartz content particles with the observed cytotoxicity being attributed to the lysis of the cell membrane upon translocation of the activated nanoclays.[48]

Complementarily, Janer et al. found that organically modified nanoclays induced a greater toxicity than the pristine nanoclays.[45] For instance, when A549 cells were treated with pristine clay or nanoclays modified with dimethyl dihyrdrogenated tallow ammonium or dimethyl benzyl

hydrogenated tallow ammonium respectively (doses <500 μg/ml), a greater loss in cellular viability was experienced even though both the nanoclays were taken up by the cell during the 72 h window of incubation, with the internalization being more prevalent for the pristine clay.[45] Other studies showed that quartz and kaolin dust decreased pulmonary alveolar macrophage viability within 1 day of exposure at doses of 40 μg/cm^2 and 20 μg/cm^2 respectively,[59] however quartz and kaolin treated with the surfactant dipalmitoyl phosphatidylcholine (DPPC) did not induce significant decreases in viability even after 3 or 5 days of treatment.[59] Lastly, Chung et al. examined both the short- and long-term toxicity of anionic nanoclays (carbonate and chloride forms) on A549 cells and found no toxic effects at high exposure doses of 1000 μg/ml,[60] however the anionic nanoclay seemed to have inhibited colony formation after 10 days of exposure to doses ranging from 250 to 500 μg/ml.[60]

However, due to the nanoclay incorporation into nanocomposites for food packaging applications,[14,15,61] it is likely that nanoclays will not only come into contact with humans through the route of inhalation but also through the route of ingestion. Studies aimed to examine the toxicity of nanoclays upon exposure to cell lines isolated or belonging to the ingestion track have shown toxic effects induced by Cloisite 30B on human hepatocellular carcinoma epithelial cell line (HepG2) for instance, with significant decreases in both cellular growing rate and viability (Figure 1d,e).[50] In particular, analyses showed that significant decreases in uptake occurred starting at the dose of 62.5 μg/ml to 500 μg/ml upon both 24 and 48 h cellular exposure to Cloisite 30B (Figure 1e). However, analyses on pristine nanoclay Cloisite Na^+ did not reveal any cytotoxic effects on the HepG2 cells up to a dose of 62.5 μg/ml upon the same time of exposure (Figure 1d).[50] Further, Cloisite Na^+ again did not show any cytotoxicity after 24 h of exposure to cells in doses up to 62.5 μg/ml.[62] Similarly, Sharma et al. found that Cloisite 30B showed increased toxicity relative to Cloisite Na^+ (40% toxicity in human colon carcinoma cells-Caco-2) after 24 h exposure to a dose of 226 μg/ml,[47] with Cloisite 30B inducing greater toxicity than Cloisite Na^+ and also causing both time and dose-dependent decreases in protein content (PC), 3-(4,5-dimethylthiazol-2-yl)-5-(3-carboxymethoxyphenyl)-2-(4-sulfophenyl)-2H-tetrazolium (MTS) reduction,[52] all standards for the *in vitro* evaluation of cytotoxicity. A significant toxic effect for Cloisite Na^+ was only obtained using the MTS assay after 48 h of exposure to doses of 31.25 μg/ml, all relative to control cells.[52]

Janer et al. complemented the above studies showing that the organically modified nanoclays were more toxic than the pristine ones when a colorectal carcinoma cell line (HCT116)

and HepG2 cells were assessed, with all organoclays displaying IC_{50}'s at doses below 25 µg/ml whereas the IC_{50} of pristine clays were above 100 µg/ml.[45] Houtman et al. treated HepG2 and Caco-2 cells with 3 other types of clays used in packaging namely Cloisite 20A, Clay 1 (modified with quaternary ammonium salt hexadecyltrimethyl-ammonium bromide (HDTA)), and Clay 2 (modified with HDTA and acetylcholine chloride (ACO)) respectively.[49] Analyses showed that Clay 2 caused significant decreases in viability in both HepG2 cells and Caco-2 cells, with more prevalent effects being observed in Caco-2 cells.[49] In another study, Clay 1 was shown to cause significant reductions for HepG2 cells at the same dosage.[54] Both Cloisite Na^+ and Cloisite 93A (modified with methyl dehydrogenated tallow ammonium) caused significant dose-dependent decreases in HepG2 cell viability after 24 h starting from a dose of 1 µg/ml.[53] Similarly, MMT caused significant decreases in the viability of human normal intestinal cells (INT-407) in a dose and time-dependent manner at doses of 100 µg/ml or above, all over 24-72 h.[63] For instance, Rawat et al. found that MMT induced 50% cytotoxicity in the human embryonic kidney cell line at a dose as low as 0.005 µg/ml.[64] When examining the effects on HepG2 or Caco-2 cells after 24 and 48 h of exposure to extracts of PLA-Clay 1 and PLA-Clay 2 nanocomposites for instance, Maisanaba et al. did not observe any cytotoxic effects up to 2.5-100% extracts.[51] Li et al. showed that nanosilicate platelets (NSP) originated from MMT produced significant decreases in viability of Chinese Hamster Ovary (CHO) cells after 24 h of treatment with doses from 62.5 to 1000 µg/ml,[65] while Meibian et al. treated a human B lymphocyte cell line (HMy2.CIR) with active and native bentonite particles and showed that both the active (treated with 10-15% H_2SO_4) and native bentonite particles resulted in dramatic decreases in cellular viability within only 4 h of exposure, with 1000 µg/ml exposure dose causing almost complete loss of cellular viability.[44] Mouse embryonic fibroblast (NIH 3T3) and Human Embryonic Kidney 293 (HEK) cells however did not show a loss in cellular viability when treated with MMT or MMT modified with oligo(styrene-*co*-acrylonitrile) (PSAN-MMT) until exposure doses of 1 g/L, with MMT showing a greater loss in viability relative to PSAN-MMT.[66] Complementarily, human breast cancer cell line (MCF-7) and human cervical cancer cell line (HeLa) displayed decreases in viability after concentrations of 75 µg/ml of the tubular nanoclay, halloysite,[67] and halloysite coated with amino-propyl-triethoxysilane (APTES) produced similar trends in toxicity relative to its uncoated counterpart.[67]

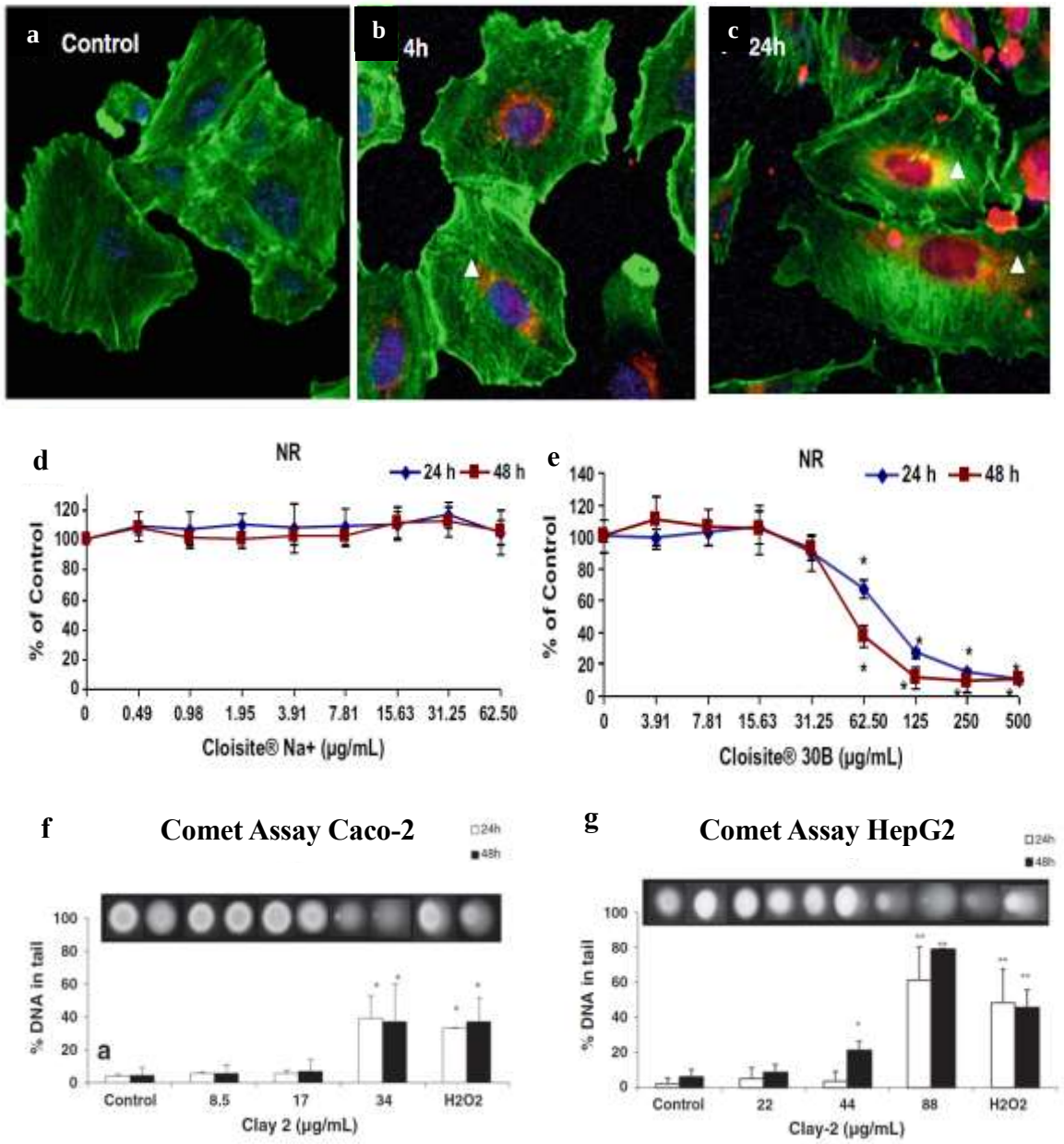

Figure 1: Cellular uptake of nanoclays by A549 cells. A549 cells grown onto 8-well chamber slides were (a) fixed (control) or (b) incubated with rhodamine (red) labeled Cloisite Na^+ (25 µg/mL) for 4 h, (c) or 24 h. Cells were also counterstained with Alexa Fluor 488 phalloidin (green) for their cytoskeletal organization identification and Hoechst (blue) for their nuclear localization. Intracellular accumulation of the nanoclays was detected by confocal microscopy; the representative images show the nanoclays localization mostly concurrent with the nuclear regions. (Copyright after Verma et al. 2012). HepG2 cells uptake (d) 0-62.5 µg/ml Cloisite Na^+ labeled

with Neutral red uptake (NR) or (e) 0-500 µg/ml Cloisite 30B labeled with NR. All values are expressed as mean ± SD. *Significantly different from control ($p \leq 0.05$). (Copyright after Maisanaba et al. 2013). Comet assay results of: (f) Caco-2 cells after 24 and 48 h of exposure to 8.5, 17, or 34 µg/ml Clay 2; (g) HepG2 cells after 24 and 48 h of exposure to 22, 44, and 88 µg/ml Clay 2. Results from 3 independent experiments with 2 replicates/experiment. All values are expressed as mean ± s.d. *Significantly different from control ($p < 0.05$). **Significantly different from control ($p \leq 0.01$). (Copyright after Houtman et al. 2014).

Proposed mechanisms of toxicity for the *in vitro* cellular studies

Due to the observed changes in cellular viability upon exposure to different types of nanoclays, studies aimed to determine the nanoclay-induced mechanisms of toxicity. For this, the strategies have considered the effects of nanoclays exposure to cell morphology, structure, cell signaling, cell-cell and cell-substrate interactions, as well as cell progression through cell cycle and appropriate cellular proliferation since all these aspects are known to be influencing cell viability and ultimately determine cellular fate.[68,69] Further, the evaluations of such changes were meant to provide the means for assessing and differentiating the nanoclay-induced cyto and/or genotoxic mechanisms in a clay type-dependent manner.

Analyses showed that HepG2 cells had dilated endo-membranes after treatment with Cloisite 30B,[50] while Caco-2 cells treated with 20 and 40 µg/ml of the same nanoclay displayed changes in cell morphology, intense vacuolization and euchromatic irregular nuclei.[52]

Nanoclays exposure led to membrane damage and changes in cellular structure, likely due to their induced charge interactions with the membrane and resulting membrane lysing ability.[70] For instance, Murphy et al. determined that primary murine spinal cord neurons were lysed after 60 min of incubation with 0.1 mg/ml bentonite or MMT, whereas differentiated N1E-115 cells did not appear to be lysed or undergo any morphological damage.[70] Studies by Meibian et al. found that both active and native bentonite particles induced significant lactate dehydrogenase (LDH) leakage in human B lymphocyte cells after 4 h of exposure to doses of 60 and 120 µg/ml, respectively.[44] Li et al. also observed significant membrane damage in CHO cells after cell treatment with NSP particles in 62.5-1000 µg/ml doses.[65] Both Cloisite Na^+ and Cloisite 93A caused significant increases in LDH release in HepG2 cells, with the organically modified clay inducing the greater response.[53] However, Baek et al. only observed significant LDH release in

INT-407 cells at the top dose of 1000 µg/ml MMT after 48 and 72 h.[63] The organically modified MMT, i.e., PSAN-MMT, showed lower LDH release relative to MMT.[66]

Combined with effects on cellular morphology and structure, changes in mitochondrial function were proposed as another viable mean to explain nanoclay-induced toxicity since it is known that the mitochondria regulates redox signaling to cellular cytosol and nucleus.[71,72] Studies by Maisanaba et al. have showed that mitochondria of cells treated with nanoclays exhibited both matrix and inner membrane degradation.[52] However, when reactive oxygen species (ROS) were assessed in the HepG2 cell line treated with Cloisite Na^+ or Cloisite 30B up to a dose of 88 µg/ml for instance, no significant increases were recorded.[50] Further both the HepG2 and Caco-2 cells showed no ROS generation when treated with Clay 2 up to a dose of 88 µg/ml for 48 h.[49] However, Lordan et al. found that both Cloisite Na^+ and Cloisite 93A produced ROS in HepG2 cells, with Cloisite Na^+ inducing more ROS than the organically modified counterpart and with the significant increases being recorded for smaller doses of 50 µg/ml over 24 h of exposure.[53] This is in contrast with studies performed with both active and native bentonite which showed significant ROS levels upon only 30 min of exposure to human B lymphocyte cells.[44] ROS was also generated in Caco-2 cells upon treatment with 40 µg/ml of Cloisite 30B,[52] while MMT generated ROS in INT-407 cells at concentrations above 50 µg/ml after 48-72 h.[63] One possible explanation for the observed dose and nanoclay-dependent ROS generation was that the toxic effects of nanoclays could be potentially circumvented by changes in the endogenous antioxidant glutathione (GSH), a known regulator of the intracellular redox balance.[73] Maisanaba et al. for instance found that Cloisite 30B caused significant decreases in GSH cellular concentration for both HepG2 cells and Caco-2 cells,[50,52] with the GSH concentration being dependent on both the type of clay used (e.g., Clay 2 did not affect the GSH content of Caco-2 cells) and the dose of nanoclay.[49]

With changes in cellular structure and energetic activity being known to influence cell cycle and overall fate,[69,74] the role of nanoclays to induce genotoxicity was also investigated. Studies of NIH 3T3 cells exposed to 1 g/L MMT for 24 h identified nuclei fragmentation and condensed chromatin, however the changes were minimal for cells exposed to organically modified PSAN-MMT.[66] Maisanaba et al. also showed that Cloisite 30B caused significant time dependent DNA breaks in HepG2 cell,[50] while Houtman et al. showed that Clay 2 induced DNA changes in both HepG2 and Caco-2 cells respectively, with Clay 2 having a slightly greater effect on Caco-2 cells (Figure 11.1f,g).[49] However, exposures to Cloisite 20A and Clay 1 did not induce

DNA strand breaks in either Caco-2 or HepG2 cells after 48 h and concentrations up to 62.5 and 8 µg/ml, respectively.[49] Additionally, neither of the extracts of the PLA-Clay 1 or PLA-Clay 2 nanocomposites induced any genotoxicity after 24 or 48 h of exposure.[51] Studies by Sharma et al. also complemented previous findings and showed DNA damage in a nanoclay dose-dependent manner when Caco-2 cells were treated with Cloisite 30B, with the 2 highest doses of 113 and 170 µg/ml respectively being significantly different from the control (not exposed cells) after 24 h of exposure.[47] However, no change was recorded for the Caco-2 cells treated with Cloisite Na^+,[47] or Cloisite 30B.[52] However, Cloisite Na^+ caused an increase in micronuclei frequency in HepG2 cells after 24 h at exposure levels of 62.5 µg/ml.[62] Similarly, when CHO cells were treated with nanosilicate platelets from MMT, DNA dose-dependent damage was observed within the exposure dose range of 62.5 to 1000 µg/ml.[65] An increase in DNA damage was observed when human B lymphoblast cells were treated with active or native bentonite particles from doses of 120 µg/ml for 24 h, 60 µg/ml for 48 h, or 30 µg/ml over 72 h, with active bentonites showing a greater effect, and with both particles causing significant increases in micronucleus frequency.[75] Untreated quartz particles induced significant DNA damage in rat pulmonary alveolar macrophages within 1 day of exposure at a dose of 20 µg/cm^2, whereas quartz/DPPC induced damage after 3 days at double that dose.[59] Additionally, untreated kaolin induced DNA damage after 1 day at an exposure dose of 40 µg/cm^2 and kaolin/DPPC inducing DNA damage after 5 days at a dose of 40 µg/cm^2.[59] Lastly, Janer et al. observed a slight increase in caspase 3/7 for HepG2 cells exposed to 100 µg/ml nanoclay.[45] Caspases 3 and 7 are cysteine asparate proteases with similar structures[76,77] that control apoptotic pathways. Briefly, intrinsic apoptosis is mediated by mitochondrial outer membrane permeabilization with cytosol release of pro-apoptotic proteins such as cytochrome c activating caspase-9.[78,79] The resulting activated caspase-9 then cleaves and actives caspase-3 and 7 respectively to initiate the degradation of cellular structures and cell detachment, eventually leading to cell death.[78]

Maisanaba et al. proposed to further investigate genotoxicity of nanoclays by investigating the effect of Cloisite Na^+ on the regulation of genes in HepG2 cells.[62] Cloisite Na^+ was found to deregulate genes associated with cellular metabolism, immediate-early response/signaling, DNA damage response, oxidative stress, and apoptosis/survival.[62] Specifically, 4 out of the 5 genes studied for metabolism and 2 DNA damage responsive genes were found to be upregulated at the tested concentrations of 6.25 µg/ml or 62.5 µg/ml of Cloisite Na^+ after 24 h of exposure. Catalase,

an oxidative stress responsive gene, was down regulated however at both concentrations used. Complementarily, both apoptosis responsive genes and early response/signaling genes were also affected after 24 h, with early response/signaling also having a gene (JUNB) affected at 4 h at the dose of 62.5 µg/ml.[62]

***In vivo* evaluation of nanoclay toxicity**

While the mechanism of toxicity is still not completely understood, the deleterious effects observed upon exposure to both pristine and organically modified nanoclays from the *in vitro* studies have prompted increased interest for their *in vivo* evaluations at a consumer level of exposure. Herein the consumer level of exposure is defined as exposures to nanoclays when in use by the public who buys the product embedding nanoclay. Analyses by Sharma et al. found that Wistar rats orally exposed for two times to Cloisite 30B ranging from 250-1000 mg/kg of their body weight, with 24 h apart the exposures, did not induce changes in their organs nor DNA strand breaks in the cells isolated from the colon, liver, or kidney (Figure 2a).[80] Specifically, analyses showed that the Wistar rats treated with Cloisite 30B suspended in water or cell culture media had no significant differences in % tail DNA relative to the controls, even up to a dose of 1000 mg/kg body weight for the liver, kidney, or colon. However, the tracer element aluminum was found in the rat's feces thus indicating there was no absorption of the clay from the gastrointestinal tract. Complementarily, results by Maisanaba et al. administering Clay 1 over 90 days at 40 mg/kg/d showed that rats underwent an adaptive response in result of an increased oxidative stress.[81] Specifically, significant increases in catalase (CAT; responsible in maintaining ROS levels) activity in the kidney (Figure 2b) as well as changes in proteins expressions level of CAT in the kidney of the rat were observed, which was in contrary to no significant effects on the antioxidant enzymes, superoxide dismutase (SOD), glutathione peroxidase (GPx), and gluthatione S-transferase (GST) responsible for maintaining ROS levels respectively (Figure 2c).[81]

Maisanaba et al. also tested the migrant extract of a PLA-Clay 1 (4%) nanocomposite on the same animal models over an exposure of 90 days and showed no significant effects on their biomarkers, which included the oxidative stress biomarkers of enzymes gluthatione S-transferase (GSH)/ glutathione disulfide (GSSG) ratios, lipid peroxidation via thiobarbituric acid (TBA), and antioxidant enzyme activities (CAT, SOD, GPx, and GST).[82] Further, unlike the previous study dealing with Clay 1, the migrant extract did not cause any changes in CAT activity or in genetic and protein expressions of CAT.[81,82]

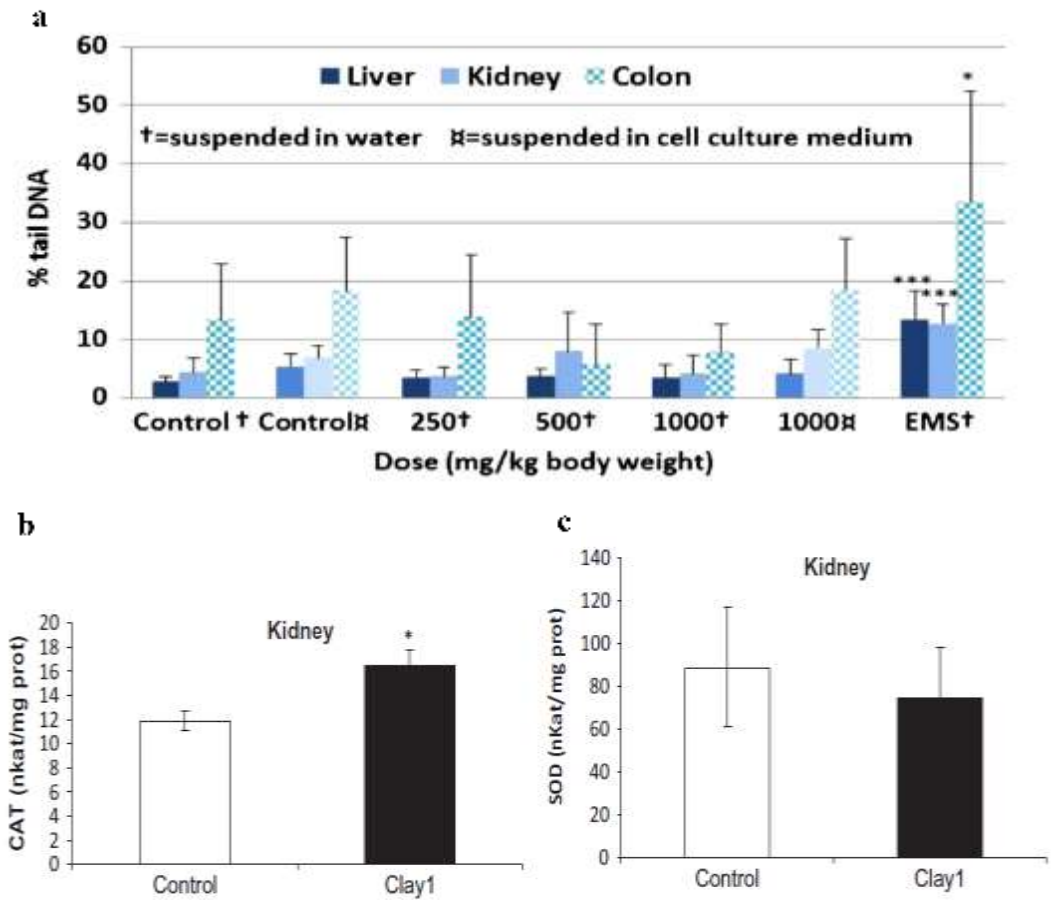

Figure 2: (a) Comet assay performed on Wistar rats (n = 6) exposed to Cloisite 30B suspended in water (being administered at 250, 500 and 1000 mg/kg body weight of rat) or cell-culture medium (being administered at 1000 mg/kg body weight of rat). Ethylmethane sulfonate (EMS) suspended in water was the positive control. For the experiments, six rats were exposed to 250 mg/kg body weight. Data from liver, kidney and colon cells of the EMS-exposed group were statistically significantly different ($p < 0.001$, $p < 0.001$: *** and $p < 0.05$: *), respectively, from the values in the corresponding control group (two-tailed, unpaired t-test). Internal standards: positive controls (Caco-2 cells exposed to 0.05% ethylmethane sulfonate):16 slides, % tail DNA, mean ± S.D., 21.6 ± 6.6; negative controls (untreated Caco-2 cells): 16 slides, % tail DNA, mean ± S.D., 1.8 ± 0.6. (Copyright after Sharma et al. 2014). (b) Catalase (CAT) and (c) superoxide dismutase (SOD) activities (nKat/mg protein) in kidney of rat exposed to Clay 1. The values are expressed as mean ± SD (n=10). The levels observed are significant at *$p<0.05$ in comparison to control group values. (Copyright after Maisanaba et al. 2014).

There were also no major differences being observed in the histopathology of the control versus the exposed groups to the migrant extract of PLA-Clay 1 (Figure 3). Specifically, Figure 3a and 3b display the unexposed rat liver and kidney tissues, respectively, stained with hematoxylin and eosin (HE).[82] Figure 3c and 3d displays the exposed rat liver and kidney tissues, with analyses showing that the liver tissue displayed hepatocytes similar to that of the control and with the kidney tissue displaying a normal parenchyma and normal proximal convoluted tubules (Pct) and distal convoluted tubules (Dct) relative to the control group.[82] Li et al. also evaluated the LD_{50} of NSP particles being fed to Sprague-Dawley rats at doses of 1500, 3000, and 5700 mg/kg over 14 days and showed no acute oral toxicity of these nanoclays,[65] while results by Baek et al. obtained in ICR mice exposed to MMT particles orally in single administered doses in between 5-1000 mg/kg showed that after 14 days there was no significant accumulation of nanoclay in any specific organs and the LD_{50} was estimated to be over 1000 mg/kg.[63]

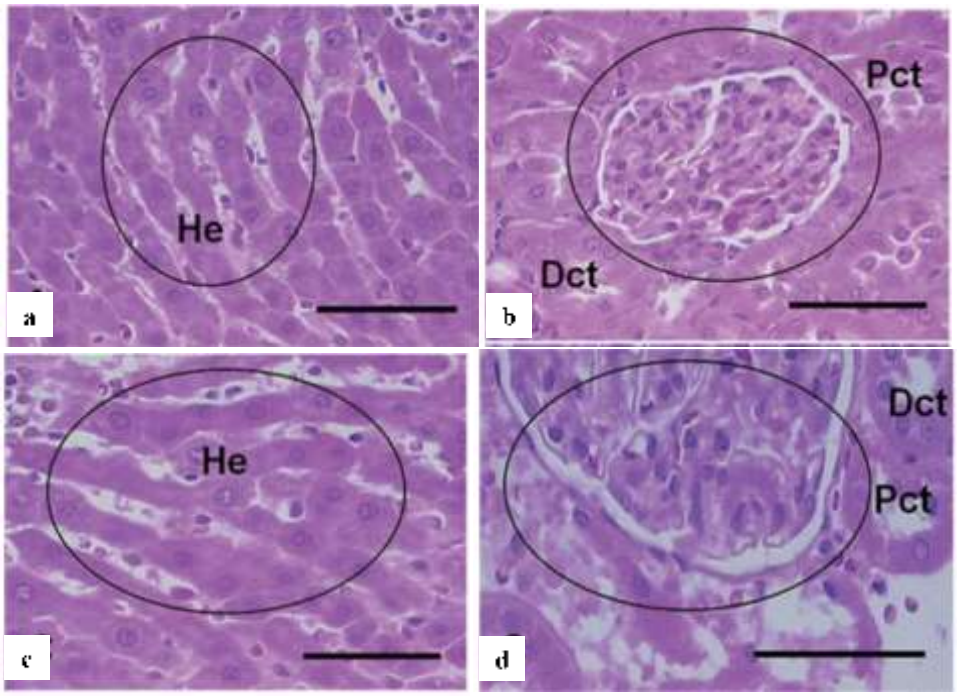

Figure 3: Histopathological evaluations of liver of Wistar rats exposed to a PLA-Clay1 extract as beverage for 90 days. (a) He-stained liver section and (b) He-stained kidney sections. Bars, 100 μm. (a,b) Control rats. (a) Liver parenchyma with hepatocytes with normal morphology, central nuclei and light cytoplasm (He), organized in hepatic cords (circle). (b) Normal structure of kidney parenchyma with glomerulus (circle), proximal convoluted tubules (Pct), and distal convoluted

tubules (Dct). (c,d) Exposed rats (c) Liver parenchyma with hepatocytes with normal morphology, central nuclei, and light cytoplasm (He), organized in hepatic cords (circle). (d) Normal structure of kidney parenchyma with glomerulus (circle), proximal convoluted tubules (Pct), and distal convoluted tubules (Dct). (Copyright after Maisanaba et al. 2014).

Conclusions and Outlook

In the past decades, research has been trying to answer critical questions related to the properties and characteristics of nanoclays that could allow for enhancing their consumer-related utility at minimum toxicological risks. However, even though extensive body of evidence from *in vitro* studies supports that nanoclay could be toxic at the exposure level of consumption and inhalation, it is still unclear as to what extent they could potentially affect humans. The isolated study performed by Yuwen et al. for instance showed that organic bentonite particles could affect workers in two different factories producing such nanoclays. Specifically, group I was exposed to high concentration (around 13 mg/m^3), while group II was exposed to moderate concentration (around 8 mg/m^3) of bentonites.[83] Preliminary analyses performed in the study identified that group I had a higher frequency of micronuclei, nucleus buds, micronucleated cells, nucleoplasmic bridges, apoptotic cell rate, and necrotic cell rate relative to group II and the control (unexposed individuals) in all the isolated human lymphocytes. Further, group II had higher frequencies of all the above parameters relative to the control group, indicating that genetic damage can occur. Further, both groups showed an increase in lipid peroxidation, responsible for cell damage due to oxidation of lipids in cell membranes, all relative to the control groups, with the age factor further accentuating such correlations.

We propose that circumventing strategies to limit toxicological risks of nanoclays should consider that their toxicity is a combination of both cyto and genotoxic effects (Scheme 1), where effect differentiation is based on the cell and nanoclay type being studied, as well as on the nanoclay physical and chemical characteristics (size, organic modifier etc.). For risk prevention for instance, one could envision controlling the synergistically induced toxicological effects by reducing the nanoclay-induced generation of ROS through direct activation of nanoclay degradation upon their cellular uptake. As such, if the potential of nanoclays implementation in user-directed applications is to be fully reached at the minimum human and environmental logistical burden, both the development of functionalization strategies that allow for such

activation strategy to occur, as well as the confirmative body of evidence to demonstrate the feasibility of the activation need to be established. A technical approach in which the addition of user-tailored copolymers to the surface of the nanoclay would facilitate both their cellular uptake as well as their cellular-based autophagy, i.e., the lysosome-based degradation, could be implemented prior to consumer integration. With degradative pathways being activated at minimum changes of the lysosome-encapsulated enzymes, the continuous cellular degradation of any uptaken nanoclays will then take place to maintain cellular homeostasis and reduce any cellular toxicity. The underlying functionalization techniques that would ensure such a greener route to nanoclay degradation as well as the lysosome-based degradative pathways will still need to be elucidated. However, until such means are achieved, the "no harm" policy for the worker implementing nanoclays in food packaging or derived products can only account for a proper system of safety measures to be implemented. They could impose limiting the amount of any airborne particles in workplaces or developing personal protective equipment such as respirators capable of removing nanoclays in a reliable and timely fashion, and with a high efficiency. Lastly, high-throughput screening tests to quickly gain an idea of the toxicity of the numerous types of nanoclays in a time efficient manner could be developed and implemented to allow for realistic human and environmentally relevant concentrations rather than excessively high concentrations to be determined and assessed for toxicity of nanoclay risk mitigation.

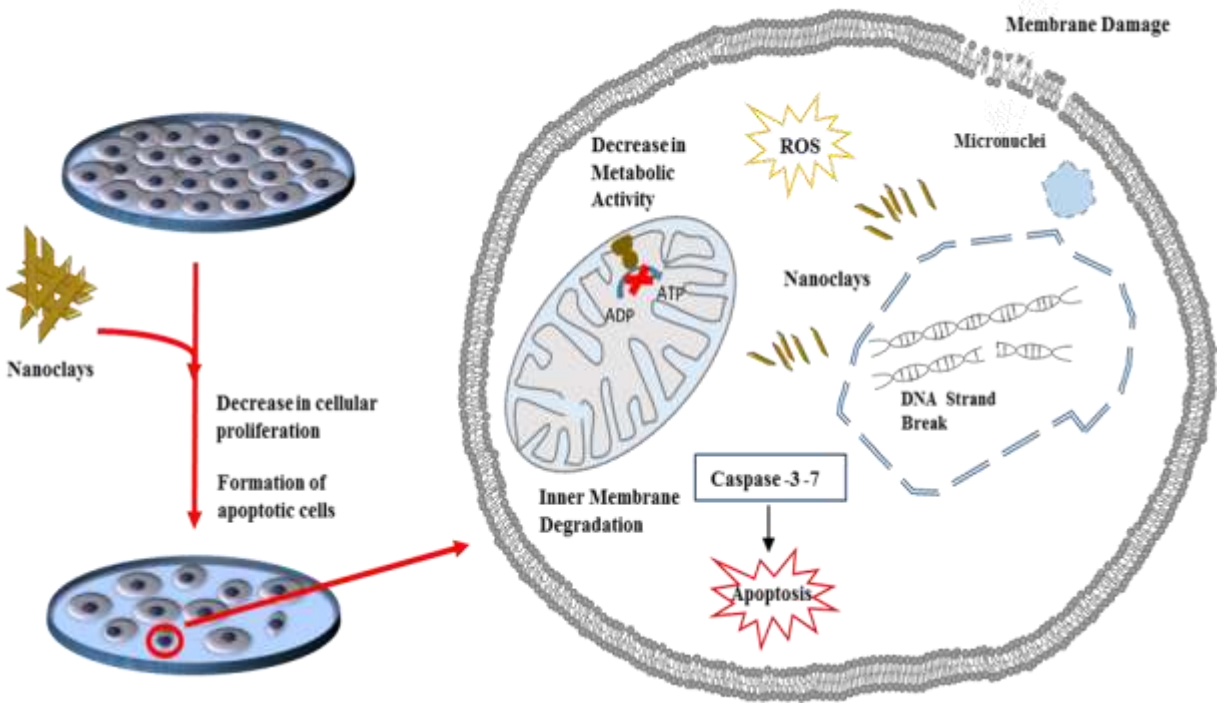

Scheme 1: Schematic representation of the proposed mechanisms of toxicity induced by cellular exposure to nanoclays. *In vitro* exposure of cells to nanoclays with different physico-chemical properties undergo changes in their structure and functions, with such changes being directly correlated with cellular morphology or proliferation rates controlled at the genetic level.

Acknowledgements

This work was supported by National Science Foundation (NSF) grant EPS-1003907, NSF 1434503, and the National Institute of Health (NIH; R01-ES022968).

References

1. Floody, M. C.; Theng, B. K. G.; Reyes, P.; Mora, M. L., Natural nanoclays: applications and future trends-a Chilean perspective. *Clay Minerals* **2009,** *44*, 161-176.

2. Calabi, M.; Jara, A.; Bendall, J.; Welland, M.; Mora, M., Structural characterization of natural nanomaterials: potential use to increase the phosphorus mineralization. In *19th World Congress of Soil Science, Soil Solutions for a Changing World*, Brisbane, Australia, 2010; Vol. 1-6, pp 29-32.

3. Patel, H. A.; Somani, R. S.; Bajaj, H. C.; Jasra, R. V., Nanoclays for polymer nanocomposites, paints, inks, greases and cosmetics formulations, drug delivery vehicle and waste water treatment. *Bulletin of Material Science* **2006,** *29* (2), 133-145.

4. Ray, S. S.; Okamoto, M., Polymer/layered silicate nanocomposites: a review from preparation to processing. *Progress in Polymer Science* **2003,** *28*, 1539-1641.

5. Liu, G.; Wu, S.; van de Ven, M.; Molenaar, A.; Besamusca, J., Characterization of Organic Surfacant on Montmorillonite Nanoclay to be used in Bitumen. *Journal of Materials in Civil Engineering* **2010**, 794-799.

6. Odom, I. E., Smectite clay Minerals: Properties and Uses. *Philosophical Transactions of the Royal Society of London. Series A. Mathematical and Physical Sciences* **1984,** *311*, 391-409.

7. Xi, Y.; Ding, Z.; He., H.; Frost, R. L., Structure of organoclays-an X-ray diffraction and thermogravimetric analysis study. *Journal of Colloid and Interface Science* **2004,** *277*, 116-120.

8. Udon, F., Clays, Nanoclays, and Montmorillonite Minerals. *Metallurgical and Materials Transactions A* **2008,** *39A*, 2804-2814.

9. Lewis, D. R., Ion exchange reactions of clays. *Proc. First National Conference on Clays and Clay Technology* **1955,** *169*, 54-69.

10. Singla, P.; Mehta, R.; Upadhyay, S. N., Clay modification by the use of organic cations. *Green and Sustainable Chemistry* **2012,** *2*, 21-25.

11. Beall, G. W.; Goss, M., Self-assembly of organic molecules on montmorillonite. *Applied Clay Science* **2004,** *27*, 179-186.

12. Beall, G. W., The use of organo-clays in water treatment. *Applied Clay Science* **2003,** *24*, 11-20.

13. Agarwal, S.; Tran, P.; Soong, Y.; Martello, D.; Gupta, R. K., Flow behavior of nanoparticles stabilized drilling fluids and effect of high temperature aging. *Journal of Petroleum Science and Engineering* **2014,** *117*, 15-27.

14. Pereira de Abreu, D. A.; Paseiro Losada, P.; Angulo, I.; Cruz, J. M., Development of new polyolefin films with nanoclays for application in food packaging. *European Polymer Journal* **2007,** *43*, 2229-2243.

15. Choi, R.; Cheigh, C.; Lee, S.; Chung, M., Preparation and Properties of Polypropylene/Clay Nanocomposites for Food Packaging. *Journal of Food Science* **2011,** *76*, 62-67.

16. Okada, A.; Usuki, A., The chemistry of polymer-clay hybrids. *Material Science and Engineering: C* **1995,** *3*, 109-115.

17. Dalir, H.; Farahani, R. D.; Nhim, V.; Samson, B.; Lévesque, M.; Therriault, D., Preparation of Highly Exfoliated Polyester-Clay Nanocomposites: Process-Property Correlations. *Langmuir* **2012,** *28*, 791-803.

18. Sahoo, R.; Sahoo, S.; Nayak, P. L., Synthesis and Characterization of Gelatin-Chitosan Nanocomposite to Explore the Possible Use as Drug Delivery Vehicle. *European Scientific Journal* **2013,** *9*, 135-141.

19. Barua, S.; Dutta, N.; Karmakar, S.; Chattopadhyay, P.; Aidew, L.; Buragohain, A. K.; Karak, N., Biocompatible high performance hyperbranched epoxy/clay nanocomposite as an implantable material. *Biomedical Materials* **2014,** *9*.

20. Meera, K. M. S.; Sankar, R. M.; Murali, A.; Jaisankar, S. N.; Mandal, A. B., Sol–gel network silica/modified montmorillonite clay hybrid nanocomposites for hydrophobic surface coatings. *Colloids and Surfaces B: Biointerfaces* **2012,** *90*, 204-210.

21. Introzzi, L.; Blomfeldt, T. O. J.; Trabattoni, S.; Tavazzi, S.; Santo, N.; Schiraldi, A.; Piergiovanni, L.; Farris, S., Ultrasound-Assisted Pullulan/Montmorillonite Bionanocomposite Coating with High Oxygen Barrier Properties. *Langmuir* **2012,** *28*, 11206-11214.

22. Plackett, D. V.; Holm, V. K.; Johansen, P.; Ndoni, S.; Nielsen, P. V.; Sipilainen-Malm, T.; Södergård, A.; Verstichel, S., Characterization of L-Polylactide and L-Polyactide-Polycaprolactone Co-Polymer Films for Use in Cheese-Packaging Applications. *Packaging Technology and Science* **2006,** *19*, 1-24.

23. Rhim, J.; Park, H.; Ha, C., Bio-nanocomposites for food packaging and applications. *Progress in Polymer Science* **2013,** *38* (10-11), 1629-1652.

24. Mondal, D.; Bhowmick, B.; Mollick, M. M. R.; Maity, D.; Mukhopadhyay, A.; Rana, D.; Chattopadhyay, D., Effect of clay concentration on morphology and properties of hydroxypropylmethylcellulose films. *Carbohydrate Polymers* **2013,** *96*, 57-63.

25. Rhim, J.; Hong, S.; Ha, C., Tensile, water vapor barrier and antimicrobial properties of PLA/nanoclay composite films. *LWT-Food Science and Technology* **2009,** *42*, 612-617.

26. Alipoormazandarani, N.; Ghazihoseini, S.; Nafchi, A. M., Preparation and characterization of novel bionanocomposite based on soluble soybean polysaccharide and halloysite nanoclay. *Carbohydrate Polymers* **2015,** *134*, 745-751.

27. Lebaron, P. C.; Wang, Z.; Pinnavaia, T. J., Polymer-layered silicate nanocomposites: an overview. *Applied Clay Science* **1999,** *15*, 11-29.

28. Krikorian, V.; Pochan, D. J., Poly (L-Lactic Acid)/Layered silicate nanocomposite: fabrication, characterization, and properties. *Chemistry of Materials* **2003,** *15*, 4317-4324.

29. Wang, Z.; Pinnavaia, T. J., Nanolayer reinforcement of elastomeric polyurethane. *Chemistry of Materials* **1998a,** *10*, 3769-3771.

30. Paul, D. R.; Robeson, L. M., Polymer nanotechnology: Nanocomposites. *Polymer* **2008,** *49*, 3187-3204.

31. Molinaro, S.; Romero, M. C.; Boaro, M.; Sensidoni, A.; Lagazio, C.; Morris, M.; Kerry, J., Effect of nanoclay-type and PLA optical purity on the characteristics of PLA-based nanocomposite films. *Journal of Food Engineering* **2013,** *117*, 113-123.

32. Zheng, X.; Wilkie, C. A., Flame retardancy of polystyrene nanocomposites based on an oligomeric organically-modified clay containing phosphate. . *Polymer Degradation and Stability* **2003,** *81*, 539-550.

33. Pluta, M.; Galeski, A.; Alexandra, M.; Paul, M. A.; Dubois, P., Polylactide/Montmorillonite Nanocomposites and Microcomposites Prepared by Melt Blending: Structure and Some Physical Properties. *Journal of Applied Polymer Science* **2002,** *86*, 1497-1506.

34. Majeed, K.; Jawaid, M.; Hassan, A.; Abu Baker, A.; Abdul Khalil, H. P. S.; Salema, A. A.; Inuwa, I., Potential materials for food packaging from nanoclay/natural fibres filled hybrid composites. *Material and Design* **2013,** *46*, 391-410.

35. Shojaee-Aliabadi, S.; Mohammadifar, M. A.; Hosseini, H.; Mohammadi, A.; Ghasemlou, M.; Hosseini, S. M.; Haghshenas, M.; Khaksar, R., Characterization of nanobiocomposite kappa-carrageenan film with *Zataria multiflora* essential oil and nanoclay. *International Journal of Biological Macromolecules* **2014,** *69*, 282-289.

36. Lertwimolnun, W.; Vergnes, B., Influence of compatibilizer and processing conditions on the dispersion of nanoclay in a polypropylene matrix. *Polymer* **2005,** *46*, 3462-3471.

37. Lertwimolnun, W.; Vergnes, B., Effect of Processing Conditions on the Formation of Polypropylene/Organoclay Nanocomposites in a Twin Screw Extruder. *Polymer Engineering and Science* **2006**, 314-323.

38. Sadegh-Hassani, F.; Nafchi, A. M., Preparation and characterization of bionanocomposite films based on potato starch/halloysite nanoclay. *International Journal of Biological Macromolecules* **2014,** *67*, 458-462.

39. Beltrán, A.; Valente, A. J. M.; Jiménez, A.; Garrigós, M. C., Characterization of Poly(Ɛ-caprolactone)-Based Nanocomposites Containing Hydroxytyrosol for Active Food Packaging. *Journal of Agricultural and Food Chemistry* **2014,** *62*, 2244-2252.

40. Manikantan, M. R.; Sharma, R.; Kasturi, R.; Varadharaju, N., Storage stability of banana chips in polypropylene based nanocomposite packaging films. *Journal of Food Science and Technology* **2014,** *51* (11), 2990-3001.

41. Abreu, A. S.; Oliveira, M.; de Sá, A.; Rodrigues, R. M.; Cerqueira, M. A.; Vicente, A. A.; Machado, A. V., Antimicrobial nanostructured starch based films for packaging. *Carbohydrate Polymers* **2015,** *129*, 127-134.

42. Stern, S. T.; McNeil, S. E., Nanotechnology Safety Concerns Revisited. *Toxicological Sciences* **2008,** *101* (1), 4-21.

43. Souza, P. M. S.; Morales, A. R.; Marin-Morales, M. A.; Mei, L. H. I., PLA and Montmorillonite Nanocoposites: Properties, Biodegradation, and Potential Toxicity. *Journal of Polymers and the Environment* **2013,** *21*, 738-759.

44. Meibian, Z.; Yezhen, L.; Xiaoxue, L.; Qing, C.; Longxi, L.; Mingluan, X.; Hua, Z.; Jiliang, H., Studying the cytotoxicity and oxidative stress induced by two kinds of bentonite particles on human B lymphoblast cells in vitro. *Chemico-Biological Interactions* **2010,** *183*, 390-396.

45. Janer, G.; Fernández-Rosas, E.; Mas del Molino, E.; González-Gáalvez, D.; Vilar, G.; López-Iglesias, C.; Ermini, V.; Vázquez-Campos, S., In vitro toxicity of functionalised nanoclays is mainly driven by the presence of organic modifier. *Nanotoxicology* **2014,** *8*, 279-294.

46. Yoshida, T.; Yoshioka, Y.; Matsuyama, K.; Nakazato, Y.; Tochigi, S.; Hirai, T.; Kondoh, S.; Nagano, K.; Abe, Y.; Kamada, H.; Tsunoda, S.; Nabeshi, H.; Yoshikawa, T.; Tsutsumi, Y., Surface modification of amorphous nanosilica particles suppresses nanosilica-induced cytotoxicity, ROS generation, and DNA damage in various mammalian cells. *Biochemical and Biophysical Research Communications* **2012,** *427*, 748-752.

47. Sharma, A. K.; Schmidt, B.; Frandsen, H.; Jacobsen, N. R.; Larsen, E. H.; Binderup, M., Genotoxicity of unmodified and organo-modified montmorillonite. *Mutation Research/Genetic Toxicology and Environmental Mutagenesis* **2010,** *700*, 18-25.

48. Geh, S.; Yücel, R.; Duffin, R.; Albrecht, C.; Borm, P. J. A.; Armbruster, L.; Raulf-Heimsoth, M.; Brüning, T.; Hoffman, E.; Rettenmeier, A. W.; Dopp, E., Cellular uptake and cytotoxic potential of respirable bentonite particles with different quartz contents and chemical modifications in human lung fibroblasts. *Archives of Toxicology* **2006,** *80*, 98-106.

49. Houtman, J.; Maisanaba, S.; Puerto, M.; Gutièrrez-Praena, D.; Jordá, M.; Aucejo, S.; Jos, A., Toxicity assessment or organomodified clays used in food contact materials on human target cell lines. *Applied Clay Science* **2014,** *90*, 150-158.

50. Maisanaba, S.; Puerto, M.; Pichardo, S.; Jorda, M.; Moreno, F. J.; Aucejo, S.; Jos, A., In vitro toxicological assessment of clays for their use in food packaging application. *Food and Chemical Toxicology* **2013,** *57*, 266-275.

51. Maisanaba, S.; Pichardo, S.; Jordá-Beneyto, M.; Aucejo, S.; Cameán, A. M.; Jos, A., Cytotoxicity and mutagenicity studies on migration extracts from nanocomposites with potential use in food packaging. *Food and Chemical Toxicology* **2014,** *66*, 366-372.

52. Maisanaba, S.; Gutièrrez-Praena, D.; Pichardo, S.; Moreno, F. J.; Jordá, M.; A.M., C.; Aucejo, S.; Jos, A., Toxic effects of a modified montmorillonite clay on the human intestinal cell line Caco-2. *Journal of Applied Toxicology* **2013,** *34*, 714-725.

53. Lordan, S.; Kennedy, J. E.; Higginbotham, C. L., Cytotoxic effects induced by unmodified and organically modified nanoclays in human hepatic HepG2 cell line. *Journal of Applied Toxicology* **2011,** *31*, 27-35.

54. Jorda-Beneyto, M.; Ortuño, N.; Devis, A.; Aucejo, S.; Puerto, M.; Gutiérrez-Praena, D.; Houtman, J.; Pichardo, S.; Maisanaba, S.; Jos, A., Use of nanoclay platelets in food packaging materials: technical and cytotoxicity approach. *Food Additives & Contaminants: Part A* **2014,** *31* (3), 354-363.

55. Hoet, P. H.; Brüske-Hohlfeld, I.; Salata, O. V., Nanoparticles-known and unknown health risks. *Journal of Nanobiotechnology* **2004,** *2* (12).

56. Bakand, S.; Hayes, A.; Dechsakulthorn, F., Nanoparticles: a review of particle toxicology following inhalation exposure. *Inhalation Toxicology* **2012,** *24* (2), 125-135.

57. Schinwald, A.; Murphy, F. A.; Jones, A.; MacNee, W.; Donaldson, K., Graphene-Based Nanoplatelets: A New Risk to the Respiratory System as a Consequence of Their Unusual Aerodynamic Properties. *ACS Nano* **2012,** *6*, 736-746.

58. Verma, N. K.; Moore, E.; Blau, W.; Volkov, Y.; Babu, P. R., Cytotoxicity evaluation of nanoclays in human epithelial cell line A549 using high content screening and real-time impedance analysis. *Journal of Nanoparticle Research* **2012,** *14*.

59. Gao, N.; Keane, M. J.; Ong, T.; Wallace, W. E., Effects of simulated pulmonary surfactant on the cytotoxicity and DNA-damaging activity of respirable quartz and kaolin. *Journal of Toxicology and Environmental Health, Part A: Current Issues* **2000,** *60*, 153-167.

60. Chung, H.; Kim, I.; Baek, M.; Yu, J.; Choi, S., Long-term Cytotoxicity Potential of Anionic Nanoclays in Human Cells. *Toxicology and Environmental Health Sciences* **2011,** *3*, 129-133.

61. Laufer, G.; Kirkland, C.; Cain, A. A.; Grunlan, J. C., Oxygen barrier of multilayer thin films comprised of polysaccharides and clay. *Carbohydrate Polymers* **2013,** *95*, 299-302.

62. Maisanaba, S.; Hercog, K.; Filipic, M.; Jos, A.; Zegura, B., Genotoxic potential of montmorillonite clay mineral and alteration in the expression of genes involved in toxicity mechanisms in the human hepatoma cell line HepG2. *Journal of Hazardous Materials* **2016,** *304*, 425-433.

63. Baek, M.; Lee, J.; Choi, S., Toxicological effects of cationic clay, montmorillonite in vitro and in vivo. *Molecular and Cellular Toxicology* **2012,** *8*, 95-101.

64. Rawat, K.; Agarwal, S.; Tyagi, A.; Verma, A. K.; Bohidar, H. B., Aspect ratio dependent cytotoxicity and antimcrobial properties of nanoclay. *Applied Biochemistry and Biotechnology* **2014,** *174*, 936-944.

65. Li, P.; Wei, J.; Chiu, Y.; Su, H.; Peng, F.; Lin, J., Evaluation on cytotoxicity and genotoxicity of the exfoliated silicate nanoclay. *Applied Materials & Interfaces* **2010,** *2*, 1608-1613.

66. Liu, Q.; Liu, Y.; Xiang, S.; Mo, X.; Su, S.; Zhang, J., Apoptosis and cytotoxicity of oligo(styrene-*co*-acrylonitrile)-modified montmorillonite. *Applied Clay Science* **2011,** *51*, 214-219.

67. Vergaro, V.; Abdullayev, E.; Lvov, Y. M.; Zeitoun, A.; Cingolani, R.; Rinaldi, R.; Leporatti, S., Cytocompatibility and Uptake of Halloysite Clay Nanotubes. *Biomacromolecules* **2010,** *11*, 820-826.

68. Frisch, S. M.; Francis, H., Disruption of Epithelial Cell-Matrix Interactions Induces Apoptosis. *The Journal of Cell Biology 124* (4), 619-626.

69. Huang, S.; Ingber, D. E., The structural and mechanical complexity of cell-growth control. *Nature Cell Biology* **1999,** *1*, E131-E138.

70. Murphy, E. J.; Roberts, E.; Anderson, D. K.; Horrocks, L. A., Cytotoxicity of aluminum silicates in primary neuronal cultures. *Neuroscience* **1993,** *57*, 483-490.

71. Murphy, M. P., How mitochondria produce reactive oxygen species. *Biochemical Journal* **2009,** *417*, 1-13.

72. Handy, D. E.; Loscalzo, J., Redox Regulation of Mitochondrial Function. *Antioxidants & Redox Signaling* **2012,** *16*, 1323-1367.

73. Trachootham, D.; Lu, W.; Ogasawara, M. A.; Valle, N. R.; Huang, P., Redox Regulation of Cell Survival. *Antioxidants & Redox Signaling* **2008,** *10* (8), 1343-1374.

74. da Veiga Moreira, J.; Peres, S.; Steyaert, J.; Bigan, E.; Paulevé, L.; Nogueira, M. L.; Schwartz, L., Cell Cycle progression is regulated by intertwined redox oscillators. *Theoretical Biology and Medical Modelling* **2015,** *12*.

75. Meibian, Z.; Xiaoxue, L.; Yezhen, L.; Xinglin, F.; Qing, C.; Mingluan, X.; Jiliang, H., Studying the genotoxic effects induced by two kinds of bentonite particles on human B lymphoblast cells in vitro. *Mutation Research/Genetic Toxicology and Environmental Mutagenesis* **2011,** *720*, 62-66.

76. Lakhani, S. A.; Masud, A.; Kuida, K.; Porter Jr., G. A.; Booth, C. J.; Mehal, W. Z.; Inayat, I.; Flavell, R. A., Caspases 3 and 7: Key Mediators of Mitochondrial Events of Apoptosis. *Science* **2006,** *311*, 847-851.

77. Wei, Y.; Fox, T.; Chambers, S. P.; Sintchak, J.; Coll, J. T.; Golec, J. M. C.; Swenson, L.; Wilson, K. P.; Charifson, P. S., The structures of caspases-1, -3, -7 and -8 reveal the basis for substrate and inhibitor selectivity. *Chemistry & Biology* **2000,** *7*, 423-432.

78. Brentnall, M.; Rodriguez-Menocal, L.; Ladron De Guevara, R.; Cepero, E.; Boise, L. H., Caspase-9, caspase-3 and caspase-7 have distinct roles during intrinsic apoptosis. *BMC Cell Biology* **2013,** *13*, 1-9.

79. Mcllwain, D. R.; Berger, T.; MAk, T. W., Caspase Functions in Cell Death and Disease. *Cold Spring Harbor Perspectives in Biology* **2013,** *3*.

80. Sharma, A. K.; Mortensen, A.; Schmidt, B.; Frandsen, H.; Hadrup, N.; Larsen, E. H.; Binderup, M.-L., In-vivo study of genotoxic and inflammatory effects of the organo-modified Montmorillonite Cloisite 30B. *Mutation Research/Genetic Toxicology and Environmental Mutagenesis* **2014,** *770*, 66-71.

81. Maisanaba, S.; Puerto, M.; Gutièrrez-Praena, D.; Llan-Ruíz-Cabello, M.; Pichardo, S.; Mate, A.; Jordá-Beneyto, M.; Cameán, A. M.; Aucejo, S.; Jos, A., In vivo evaluation of activities and expression of antioxidant enzymes in Wistar rats exposed for 90 days to a modified clay. *Journal of Toxicology and Environmental Health, Part A: Current Issues* **2014,** *77*, 456-466.

82. Maisanaba, S.; Gutiérrez-Praena, D.; Puerto, M.; Llan-Ruíz-Cabello, M.; Pichardo, S.; Moyano, R.; Blanco, A.; Jordá-Beneyto, M.; Jos, A., In vivo Toxicity Evaluation of the Migration Extract of an Organomodified Clay-Poly(lactic) Acid Nanocomposite. *Journal of Toxicology and Environmental Health, Part A: Current Issues* **2014,** *77*, 731-746.

83. Yuwen, H.; Meibian, Z.; Hua, Z.; Xiaxue, L.; Mingluan, X.; Xinglin, F.; Jiliang, H., Genetic damage and lipid peroxidation in workers occupationally exposed to organic bentonite particles. *Mutation Research/Genetic Toxicology and Environmental Mutagenesis* **2013,** *751*, 40-44.

CHAPTER 2

Toxicity Evaluations of Nanoclays and Thermally Degraded Byproducts through Spectroscopical and Microscopical Approaches

Abstract

Montmorillonite is a type of nanoclay that originates from the clay fraction of the soil and is incorporated into polymers to form nanocomposites with enhanced mechanical strength, barrier and flammability properties used for food packaging, automotive, and medical devices. However, with implementation in such consumer applications, the interaction of montmorillonite-based composites or derived byproducts with biological systems needs to be investigated. Herein we examined the potential of Cloisite Na^+ (pristine) and Cloisite 30B (organically modified montmorillonite nanoclay) and their thermally degraded byproducts' to induce toxicity in model human lung epithelial cells. The experimental set-up mimicked biological exposure in manufacturing and disposal areas and employed cellular treatments with occupationally relevant doses of nanoclays previously characterized using spectroscopical and microscopical approaches. For nanoclay-cellular interactions and for cellular analyses respectively, biosensorial-based analytical platforms were used, with induced cellular changes being confirmed via live cell counts, viability assays, and cell imaging. Our analysis of nanoclays' or byproducts' chemical and physical properties revealed both structural and functional changes. Real-time high throughput analyses of exposed cellular systems confirmed that nanoclay induced significant toxic effects, with Cloisite 30B showing time-dependent decreases in live cell count and cellular viability relative to control and pristine nanoclay respectively. Thermally degraded byproducts produced less toxic effects; all treatments caused alterations in the cell morphology upon exposure. Our morphological, behavioral, and viability cellular changes show that nanoclays have the potential to produce toxic effects when used both in manufacturing or disposal environments. The reported toxicological mechanisms prove the extensibility of a biosensorial-based platform for cellular behavior analysis upon treatment with a variety of nanomaterials.

Introduction

Nanotechnology is quickly establishing itself as the next revolution in commercial and industrial products, with about one third of all produced engineered nanomaterials to occur within the U.S..[1,2] Naturally occurring montmorillonite nanoclays[3,4] are readily available, negatively charged,[5] low cost,[6] and consist of aluminum or magnesium octahedral sheets sandwiched between two silica-oxygen tetrahedral sheets. Isolated from the clay fraction of the soil,[7] nanoclays are currently used as sorbents in the treatment of waste water or hazardous spills[8] or as media for oil well drilling,[9] paints,[10] and cosmetics.[11] Functionalization with organic modifiers via an ion exchange reaction confers montmorillonite increased basal spacing and separation between its platelets[4,12] as well as better mixing ability, and facilitates its interactions with hydrophobic polymers.[3,4,13] Complementary, its high aspect ratio[5] ensures better reinforcement within the polymeric plane itself[14] by enhancing polymer's properties at a fairly low silicate content[13] and leading to the formation of nanoclay-polymer-based composites with increased mechanical strength,[3,14] barrier properties,[3,15] UV dispersion,[15] and fire resistance capabilities,[3,16] to be used for food packaging,[17,18] automotive,[19,20] medical devices,[21,22] and for coatings-related applications.[23,24]

With nanoclay or nanoclay-plastic composites wide implementation,[25] analyses of potential risks of these nanomaterials to exposed workers' lung health have started to emerge. As such, recent studies aiming to unravel the nanoclay toxicological profiles showed that its high aspect ratio resulted from its platelet thickness of about 1 nm and length and width of up to several microns,[5] has led to increased cellular uptake and interactions.[26] While such *in vitro* analyses allowed for elimination of animal subjects, lower processing time, and cost effectiveness,[27,28] they rely on usage of synthetic compounds such as tetrazolium salts (MTT) to measure mitochondrial reduction/cellular viability for instance.[28] Specific results based on such analyses revealed that cellular exposure to nanoclays lead to mitochondrial damage,[29,30] decreased cellular proliferation,[31] reactive oxygen species (ROS) generation,[29,30] as well as membrane[29,32] and DNA damage,[33,34,35] with the type and range of toxicity being dependent on the cell model being used, the dosage, and the organic modifier functionalizing the nanoclay, respectively.[5] However, based on our knowledge no analyses are currently available to report the toxicological profiles of nanoclays upon the end of composite life cycle.[26,36] High temperatures, oxidation, reduction, and potential chemical reactions occurring during the incineration process normally used for

composites disposal[37] could induce physical and chemical changes[38] and lead to increased reactivities of the resulting nanoclay-resulting byproducts. Further, previous analyses on other types of nanomaterials have showed that single-walled carbon nanotubes (SWCNTs), carbon black nanoparticles, fullerenes, and silica for instance, all interact with indicator dyes such as the MTT by binding to the formazan crystals and making them insoluble and thus creating false positives.[27,39,40] Additionally, the high adsorptive capacities of nanomaterials due to their large surface per unit mass have shown interferences with annexin V/PI binding, ELISA and ROS assays.[27,28] Finally, Casey et al. found considerable variation in the toxicity of carbon nanomaterials on human alveolar carcinoma cells (A549) from MTT, Commassie Blue, Neutral Red, and WST-1 assays, all of which help indicate cellular viability. [41]

Given the complex effects of nanoclays on increased cellular instability, previous research showing possible interference between nanomaterials in general and the assays being used, and lastly, given that smaller particles resulting from incineration are more likely to escape filters[37] and travel greater distances through the air by Brownian diffusion[26] thus leading to deeper inhalation, larger sedimentation and diffusion rates into the lungs[26,42] it is important that we perform a systemic analyses to assess how parallel exposures to nanoclay or byproducts resulted during their manipulation, handling, and disposal affects cellular systems' fate. Such tests should be cheap, not time intensive[43] or invasive,[43] and provide results in real-time in contrast with discrete time points currently achieved through the standard assays named above.[44,45] Further, such assays should be high throughput and should have the ability to provide accurate results that avoid the artifacts known to result from the interaction of nanomaterials with dyes or chemical compounds normally found in such standard assays.[39,41]

Herein we propose to assess toxicological profiles of nanoclays, both during the duration as well as at the end of their life cycle. Further, to eliminate the concern associated with using standardized single point assays and chemical compounds interference with nanoclays or their byproducts, we propose to use an electrical cell-substrate impedance sensing (ECIS) previously applied to monitor changes in cell adherence, proliferation, motility, and morphology. Our analysis will allow quantitative measurements, at a nanoscale resolution, and in a noninvasive, real-time manner[44,46] to establish whether nanoclays and their thermally degraded byproducts are leading to cellular changes when exposed to model target inhalation systems at an occupationally relevant dose for particles otherwise not regulated.[47,48] Exploitation of our findings can further advance

implementation of nanoclays or nanoclay-polymer-based composites in "safe-by-design" consumer-based applications, as well as confirm that ECIS has the potential to be a powerful tool for quickly, efficiently and non-invasively determining toxicity of a large variety of nanomaterials.

Materials and Methods

Nanoclay Preparation

Raw (as-received) Cloisite Na^+ (UC) and Cloisite 30B (CC) were obtained from Southern Clay Products (Gonzales, TX, USA). Cloisite Na^+ is an unmodified montmorillonite while Cloisite 30B is organically modified via an ion-exchange reaction (per the manufacturer specifications) with methyl, tallow, bis-2-hydroxyethyl, quaternary ammonium at a concentration of 90 meq/100 g clay.[4,5]

Thermal Degradation

UC and CC samples were thermally degraded using a TGA701 Thermogravimetric Analyzer from LECO to mimic the end of life cycle of the nanoclay. In order to determine the moisture content of the samples, around 0.5 g of each of the samples was heated in nitrogen at a rate of 6 °C/min and in a range of temperatures from 25 °C to 105 °C. To determine the volatile content, the samples were heated from 105 °C to 950 °C in nitrogen at a rate of 43 °C/min. Finally, to determine the ash content, the samples were heated from 550 °C to 900 °C in oxygen at a rate of 15 °C/min. The resulted ash was collected to serve as a model of the byproducts resulted from incineration i.e., thermally degraded Cloisite Na^+ (UC900) and thermally degraded Cloisite 30B (CC900) respectively.

Materials Characterization

Chemical composition of the samples (i.e., unsterile and sterilized clays, and their thermally degraded byproducts) was determined using Fourier Transform Infrared Spectroscopy (FTIR, Digilab FTS 7000) equipped with diamond Attenuated Total Reflection (ATR). Unsterile and samples sterilized under UV for 30 min were investigated to compare whether the sterilization, otherwise necessary for further biological-based studies, changes the physical and chemical properties of the nanoclays. Scans were collected in the range of 4000-400 cm^{-1} at a resolution of 4 cm^{-1}; a total of 100 scans were co-added to form the final spectrum for each of the samples.

Surface morphology and elemental composition of the samples were investigated using a Hitachi S-4700 Field Emission Scanning Electron Microscope (SEM, Hitachi High-Technologies

Corporation) equipped with an energy dispersive X-ray spectroscopy (EDX). Surface morphology was examined at 5.0 kV while elemental composition was determined at 20.0 kV. For the analyses, dry powder samples were mounted onto a carbon tape and then sputter coated for 10 s in vacuum injected with argon using a gold/palladium target. The argon atoms were ionized and collided with the gold/palladium target, causing the metal ions to deposit on the sample in a thin conductive layer of about 3 nm as calculated using the equation d=KIVt, where d is thickness, k is a constant value of 0.17, I is plasma current, V is voltage, and t is the time.

The size distribution of the samples was determined by dynamic light scattering (DLS) via the Mastersizer 2000 with a Hydro 2000S accessory (Malvern Instruments). For this, solutions of UC, CC, UC900, or CC900 dispersed and bath sonicated in cell culture media (Dulbecco's Modified Eagle Medium: DMEM) containing 5% fetal bovine serum (FBS) or in phosphate buffered saline (PBS) were dropped into the Hydro 2000S until laser obscuration was within 10-20%. The size analysis was performed 3 consecutive times with a stirrer speed of 1750 rpm and under continuous sonication.

Samples' sedimentation studies were performed by tracking changes in absorbance upon different incubation time when using an Evolution 300 UV-VIS spectrophotometer (Thermo Scientific). Briefly, concentrations of 100 µg/ml of UC, CC, UC900, and CC900 were prepared in media as described above. The maximum absorbance of each sample was obtained by scanning the absorbance in the 400-1100 nm range. Sedimentation was determined by measuring the changes in absorbance of each solution at the obtained maximum absorbance of 560 nm after 0, 0.5, 1, 2, 3, 4, 5, and 6 h incubation in media respectively, with media serving as the blank at each time point.

Cell Culture

Immortalized human bronchial epithelial cells (BEAS-2B) were cultured in media containing 1 % L-glutamine, and 1 % penicillin-streptomycin (all reagents were purchased from Life Technologies, USA). The cells were passaged regularly using 0.25 % trypsin (Invitrogen, USA) and incubated at 37 ^{0}C, 5 % CO_2 and 80 % relative humidity. Before each experiment cells were grown to a confluent monolayer.

Electrical Cell-substrate Impedance Testing

Real-time measurements of cellular resistance and attachment were performed using an electrical cell-substrate impedance sensing instrument (ECIS-ZΘ, Applied Biophysics, NY). For

the cellular studies, a 96 well plate (96W10idf) that contained inter-digitated finger connection electrodes covering an area of 3.985 mm^2 of the each well were used. Before addition of the cells, the electrodes were stabilized for 2 h with 200 µl media to minimize electrode drift during the experiment. After stabilization the cells were added at a density of 1.50E+05 cells/ml in a volume of 150 µl/well. The cells were allowed to grow for 24 h until they reached a confluent monolayer, as indicated by a constant level resistance.[49] After 24 h, 100 µg/ml of UC, CC, UC900, or CC900 (unsterilized) dispersed in media was added to their respective wells; cells in media served as the control. Subsequently, 24 h after treatment, the media was removed and the cells were washed 2 times with PBS. Fresh media was added to all of the wells, and the recovery of the cells was monitored for 48 h.

Live Cell Count

BEAS-2B cells were seeded in a 12 well plate (Thermo Scientific, USA) at a density of 2.0E+05 cells/ml. After 24 h, the cells were treated with UC, CC, or thermally degraded byproducts at a dose of 100 µg/ml. Before addition to the respective wells, each of the samples was sonicated for 8-10 min in media in a bath sonicator (2510 Branson); cells in only media served as controls. Twenty-four, 48, and 72 h post exposure to UC, CC, or thermally degraded byproducts, the cells were trypsinized and stained with 0.4% trypan blue solution (Invitrogen, USA). Subsequently, 10 µl of the sample containing the stained cells was added to a hemocytometer, and the number of cells in the 4 outer grids was counted through the use of the Leica DM IL optical microscope (Leica Microsystems) using a 10X objective. Analyses of cellular proliferation after exposure to UC, CC, UC900, and CC900, along with their sterilized counterparts, respectively were performed through direct live cell counts to eliminate concerns associated with false positive as resulted from the similar sizes of the cells and clay suspensions.

Cellular Viability

BEAS-2B cells were seeded in a 96 well plate (Thermo Scientific, USA); 2.0E+05 cells/ml were used. After 24 h, 100 µg/ml of UC, CC, UC900, or CC900 (unsterilized and sterilized) dispersed in media was added to their respective wells while cells in media served as control samples. The 4-[3-(4-Idophenyl)-2-(4-nitrophenyl)-2H-5-tetrazolio]-1,3-benzene disulfonate known as WST-1 assay (Roche, USA) was used to determine cellular viability as a change in color produced when cellular dehydrogenases reduced WST-1 to formazan.[50] The color change is known to be directly correlated with the number of metabolically active cells.[50] Briefly, after 24, 48, and

72 h of exposure, 10 µl of WST was added to the wells. Cells (exposed and control) were incubated for 2.5 h and changes in their absorbances were evaluated using a FLUOstar OPTIMA plate reader (BMG LABTECH) and 485 nm absorbance. Media, UC+media, CC+media, UC900+media, and CC900+media (unsterilized and sterilized) served as blanks and resulted absorbance values were subtracted from the cellular measurements counterparts.

Cell Imaging

BEAS-2B cells were seeded on glass coverslips in a 12 well plate at a density of 1.5E+05 cells/ml overnight. The cells were subsequently exposed to 100 µg/ml of UC, CC, UC900, or CC900 (unsterilized) dispersed in media. After 24 h, the media was removed and the cells were washed two times with Hank's Balanced Salt Solution (HBSS) (Corning, USA), fixed with 4% formaldehyde (Sigma-Aldrich, USA) for 15 min at 37 ^{0}C, and subsequently washed 3x with HBSS to remove any remaining formaldehyde. The cells plasma membrane and nuclei were then stained with 3 µg/ml Alexa Fluor 594 wheat germ agglutinin (WGA) and 2 µM Hoechst 33342 (Image-iT LIVE Plasma Membrane and Nuclear Labeling Kit, Life Technologies) in HBSS for 10 min at 4 ^{0}C. After incubation, cells were washed 2x with HBSS, mounted on glass coverslips, and imaged under a Nikon Inverted Microscope Eclipse Ti Series using a 40x objective. The NIS-Elements BR 3.1 software was used to define and analyze the size and morphology of cells. Around 75 cells per treatment were considered to allow for 375 cell measurements per replicate; a total of 3 replicates were used.

Statistical Analyses

All cellular experiments were repeated at least 6 times for all samples, with the exception of cell imaging which was repeated 3 times for unsterilized clay samples and ECIS which was repeated 4 times for unsterilized clay samples. All tables are presented as the average value with (+/-) SD values. All graphs are presented as the mean value of the number of indicated replicates with (+/-) SE bars. Significance was determined by one- or two-way analysis of variance ANOVA with $p<0.05$* indicating significance; a post-hoc test was also run to identify which groups were different from each other if statistical differences were recorded.

Results and Discussion

We aimed to investigate the toxicological profiles of as-received pristine and organically modified nanoclays and their thermally degraded, end of life cycle byproducts using non-

destructive and high throughput real-time electroanalytical approaches.[44,51,46] Cloisite Na^+ (UC), a pristine montmorillonite, and Cloisite 30B (CC), an organically modified montmorillonite frequently used in food packaging[17,18] and medical industry,[21] were used as testing materials to mimic potential human inhalation exposure during nanocomposites manufacturing and usage, while thermally degraded forms of these nanoclays, i.e., Cloisite Na^+ (UC900) and Cloisite 30B (CC900), were used to mimic the municipal solid waste incineration disposal environment generated at the product-based nanoclay end of life cycle.

Nanoclays and Their Thermally Degraded Byproducts Characterization

First, to mimic the incineration conditions of pristine (UC) or organically modified nanoclay (CC) and thus generate end of life cycle nanoclay byproducts, thermogravimetric analysis (TGA) was used. Briefly, samples degraded under temperatures ranging from 25 to 950 ^{0}C allowed moisture, volatile, fixed carbon content, and ash content identifications (Table 1). If initially UC had a greater weight loss, with about 20 % weight loss by 105 °C and 5 % more in the 105 to 800 °C temperature range, CC experienced the vast majority of its weight loss (about 30 %) in the 105 to 800 °C temperature range (Figure 1a).[33] Further, a significant higher volatile and ash content were observed for CC relative to the pristine sample, presumably resulted from the functionalization of CC with methyl, tallow, bis-2-hydroxyethyl, quaternary ammonium (per the manufacturer specifications).

Table 1: Amount of moisture, volatile, ash, and fixed carbon present in UC and CC as determined by TGA. The symbol * indicates a significant difference between UC and CC.

	Moisture (%)	**Volatile (%)**	**Ash (%)**	**Fixed Carbon (%)**
UC	17.76 +/- 0.12	6.31 +/- 0.04	75.72 +/- 0.13	0.22 +/- 0.03
CC	2.81 +/- 0.01*	28.87 +/-0.01*	67.28 +/-0.01*	1.05 +/-0.00*

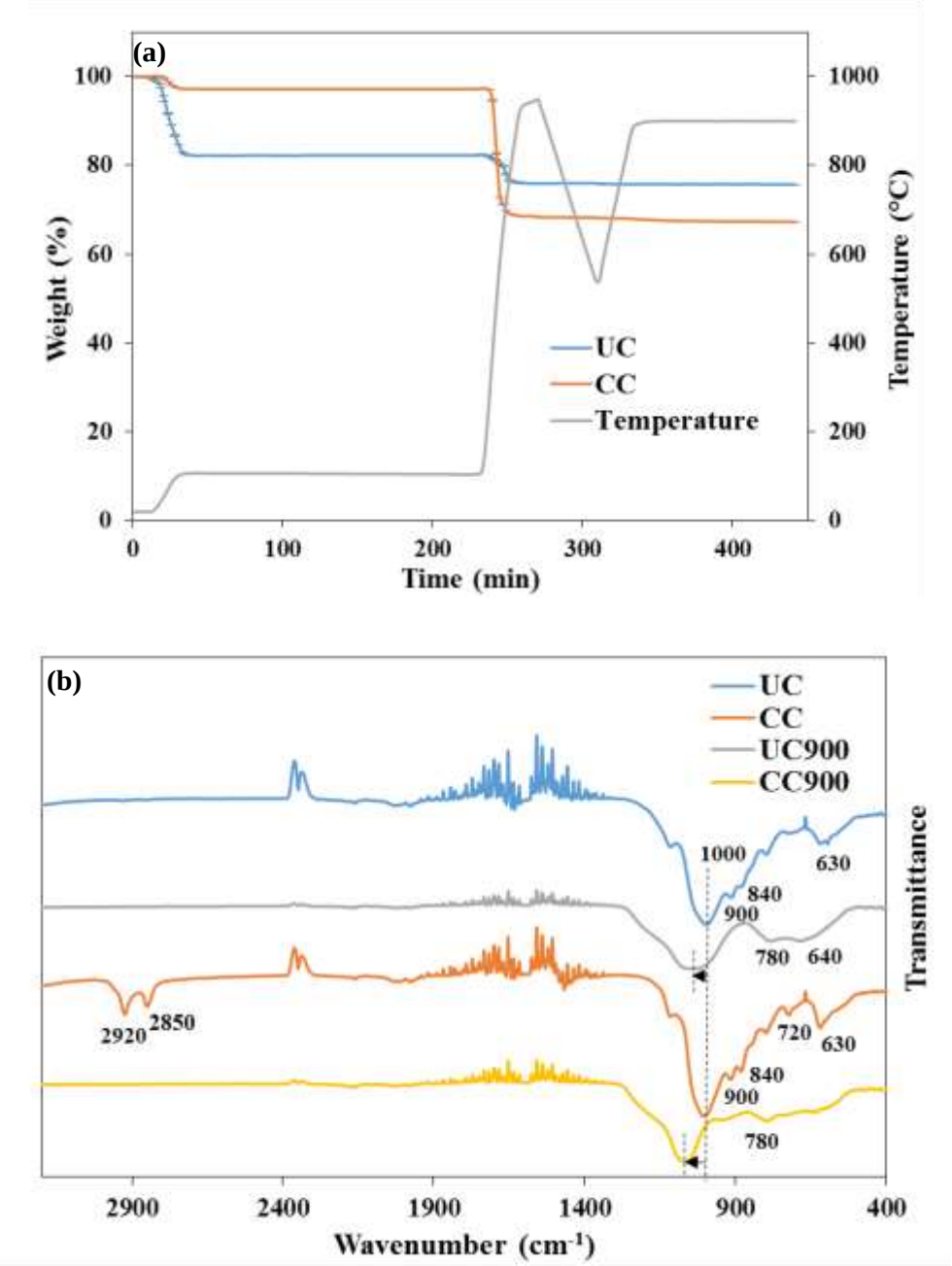

Figure 1: (a) Thermal degradation profile of UC and CC (n=2). (b) FTIR spectrum for UC and CC along with their thermally degraded byproducts (n=2).

Differences in chemical composition between UC, CC, and their thermally degraded byproducts were confirmed using Fourier transform infrared spectroscopy (FTIR) and are shown in Figure 1b. Both clays revealed the characteristic peaks indicative of the Si-O-Si stretching vibration of silicate[29,52] at 1000 cm^{-1} and of the Al-OH-Al deformation of aluminates[29,53] at 900 cm^{-1} respectively, while peak shifting was observed after their thermal degradation. The peak around 840 cm^{-1} was a result of the deformation of the OH linked to Al^{3-} and Mg^{2-} [53] while the peak around 630 cm^{-1} was associated with the out of plane vibration of the Al-O group.[54,55] Complementarily, UC900 had an additional peak around 640 cm^{-1} presumably due to Si-O-Si bending[53] while CC900 no longer retained the peaks normally present in its CC form at 2920, 2850, and 720 cm^{-1} respectively, thus confirming the degradation of the organic modifier.[56] Such peaks were likely resulted from the asymmetric or symmetric stretching of the C-H groups included in methylene groups or alkane rock of CH_2 for alkanes with 7 or more carbons, respectively[29,53] as resulted from the incorporation of the methyl, tallow, bis-2-hydroxyethyl, quaternary ammonium organic modifier during the nanoclay processing.[29,53] Molecular composition of UC, CC, and their thermally degraded counterparts was not changed after UV sterilization (Figure S1).

Scanning Electron Microscopy (SEM) allowed surface morphologies analyses of the as-received and end of life cycle samples (Figure 2). Generally, UC appeared to have less layering and smoother edges relative to CC (Figure 2a,b); similarly, UC900 and CC900 existed in agglomerated forms however, they displayed a fairly uniform surface with smooth edges for UC900 (Figure 2c) and a more fragmented surface with platelets jutting out for CC900 (Figure 2d). The observed changes in morphology from pristine nanoclay to thermally degraded nanoclay could be due to both the dehydroxylation of the crystal lattice structure of montmorillonite that occurs around 700 °C [56] as well as from the presence of the organic modifier which causes an increase in the nanoclay's basal spacing[57] and thus possible differences in the platelet structure breakdown during thermal degradation. UV sterilization did not produce significant changes in the surface morphology of UC, CC, or their thermally degraded byproducts (Figure S2a-d).

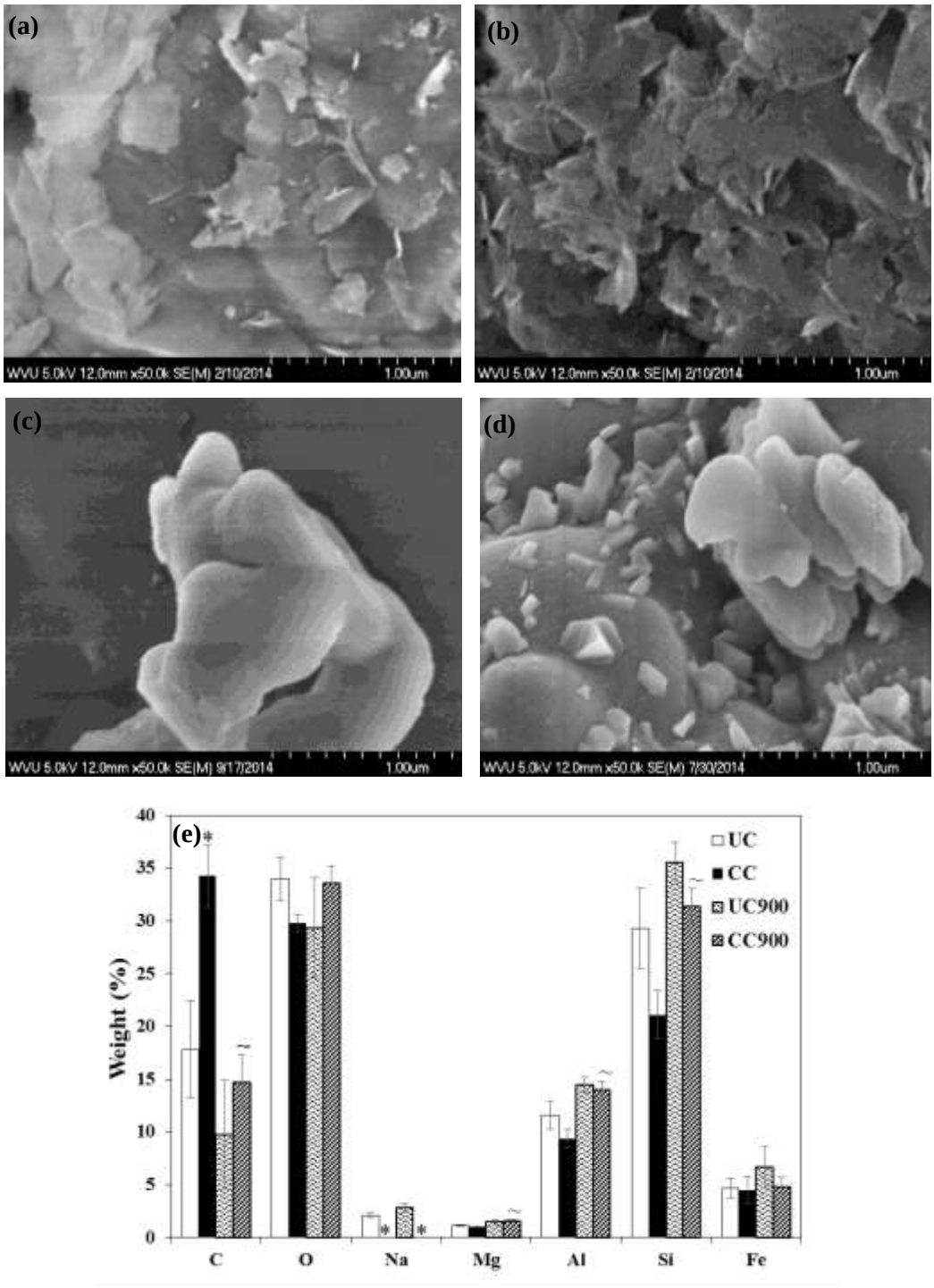

Figure 2: Surface morphology of (a) UC, (b) CC, and thermally degraded (c) UC900, and (d) CC900 as determined by SEM. (e) Elemental composition of as-received nanoclay and their thermally degraded byproducts as determined by EDX at 1 µm (n=5). The symbols * and ~ indicate significant differences between UC and CC and between as received nanoclay and its thermally degraded byproduct, respectively.

UC and CC differed significantly in their elemental composition as determined by energy dispersive X-ray (EDX) spectroscopy (Figure 2e). Specifically, CC showed a higher weight percent of carbon and a lower weight percent of sodium, both relative to UC, thus confirming the modification with the organic modifier.[58] After thermal degradation however, the weight percent of carbon decreased significantly for CC900, while the weight percent of magnesium, aluminum, and silicon increased; further, no sodium was observed. Complementarily, no significant differences were observed between the elemental composition of UC and its thermally degraded byproduct, UC900. The lower amount of carbon present in CC900 versus CC, as well as the fact that there was no longer a carbon difference between the two forms of thermally degraded clay is consistent with the previous studies and confirms the loss of the organic modifier after thermal degradation[56] Analyses also showed that the elemental composition of UC, CC, and their thermally degraded counterparts was not affected by UV sterilization (Figure S2e).

All of the samples displayed size distributions in the micrometer range upon sonication in either cellular media (Table 2) or phosphate buffer saline (PBS; Table 3), indicating that samples formed agglomerates. Agglomerate's size distribution was a function of the sample's chemical signature (Figure 3), with cell culture media with 5% serum containing appropriate cell growth proteins favoring larger agglomerates formation than PBS alone, likely due to the interactions of the clays with the proteins in the media forming coronas.[59,60] Interestingly, analyses showed that CC displayed smaller diameter sizes in both media and PBS relative to the other three samples, likely due to the presence of the organic modifier (Figure 3a,c). Contrary, thermally degraded samples of CC900 formed larger conglomerates relative to their non-degraded counterparts presumably due to their reduction of OH contents, with a 35 % and 36 % increase in size for CC900 in media and PBS, respectively, relative CC (Figure 3b,d). Table S1 and S2 and Figure S3a-d (both in Supplementary Information) display particle diameter sizes based upon % volume, with results confirming that while there were a greater number of small sized particles, the larger sized particles were taking up more volume. Sedimentation analysis showed that all of the samples had around 85% or more particles settled by 6 h ((Supplementary Information Figure S4), with the samples experiencing the greatest sedimentation within the first 3 h.

Table 2: Average particle diameter distribution sizes (μm) in solutions of media relative to the number of particles.

	UC	CC	UC900	CC900
<10%	4.66 +/- 0.25	2.63 +/- 0.06	3.58 +/- 0.08	3.75 +/- 0.13
<50%	7.70 +/- 0.40	3.85 +/- 0.17	5.50 +/- 0.18	5.89 +/- 0.23
<90%	13.91 +/- 0.48	7.23 +/- 0.36	10.86 +/- 0.24	11.22 +/- 0.29

Table 3: Average particle diameter distribution sizes (μm) in solutions of PBS relative to the number of particles.

	UC	CC	UC900	CC900
<10%	3.88 +/- 0.16	2.66 +/- 0.06	3.32 +/- 0.01	3.75 +/- 0.01
<50%	6.16 +/- 0.26	3.99 +/- 0.12	5.41 +/- 0.02	6.23 +/- 0.00
<90%	11.02 +/- 0.30	7.86 +/- 0.23	11.28 +/- 0.04	11.88 +/- 0.02

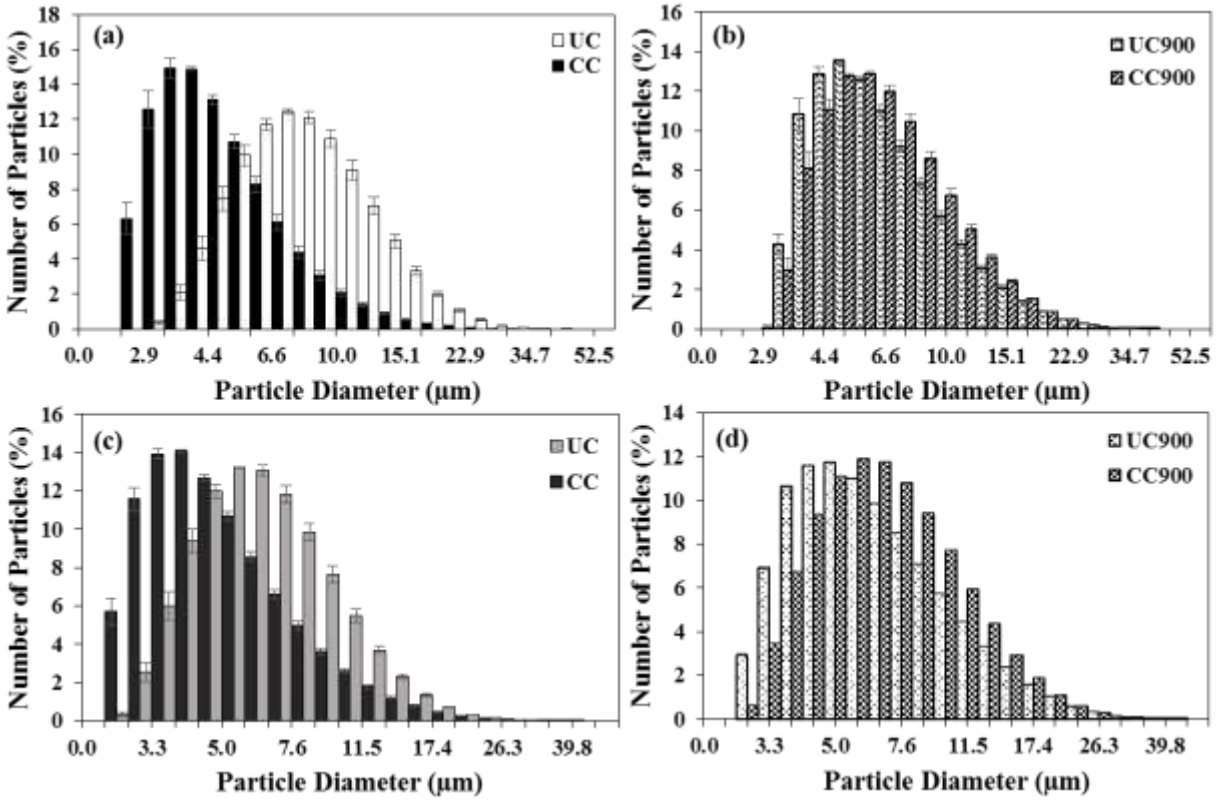

Figure 3: Average particle diameter size distribution of UC, CC, UC900, and CC900 in solutions of (a and b) media or (c and d) PBS.

The measured clay or thermally degraded byproducts sizes were similar to those found in manufacturing and disposal environments.[61] Specifically, manufacturing workplaces showed particle sizes from around 2.3 nm to 50 µm.[62,63] Further, the fly ash from incinerators was shown to display particles of size distributions ranging from 1 nm to 1000 µm, with a large fraction of such particles being under 100 µm.[37,64,65] This is in contrast with bottom ash[64,65] which was generally shown to contain larger particles normally ranging from around 250 µm to more than 8 mm, though the majority of the bottom ash was around 2-8 mm.[65]

Evaluate Cellular Behavior upon Exposure to Nanoclays or Thermally Degraded Byproducts

Changes in cell-induced impedance signals' were used to evaluate the characteristics of epithelial lung cells before and after exposure to as-received pristine, organically modified and end of life cycle nanoclay byproducts, as well as cellular ability to recover from any potential deleterious effects. Specifically, electric cell-substrate impedance sensing (ECIS) quantified changes in cell-substrate interactions and cell morphology, in real-time and non-invasively, all after exposure of human bronchial epithelial cells (BEAS-2B) to 100 µg/ml doses of the above-characterized samples. ECIS was previously used to monitor the morphology, attachment, and movement of cells,[51,46] while BEAS-2B's were previously used as model systems[66] to mimic inhalation toxicity. Previous studies have showed that the size of particles greatly influences their translocation in biological systems, with particles below 2.5 µm reaching the alveoli[42] and larger ones likely affecting cells in the upper airways.[42] Another study showed that the platelet-shaped particle with a projected area diameter up to 25 µm and thickness up to 0.1 µm is able to be respired and deposited in the lungs.[67] BEAS-2B epithelial cells were shown to serve as the first line of defense when a material is introduced into the human lung by respiration. The dose was chosen to represent a 6-year working lifetime, based on 8 h/day and 50 weeks/year as derived from particle deposition studies in rat lungs or computer modeling involving variables related to particle characteristics and lung characteristics of humans respectively.[48,68]

For analysis, the BEAS-2B cells were seeded onto the ECIS electrodes and exposed to clays or end of life cycle clay-based byproducts for 24 h (Figure 4, Region A and Region B respectively). To assess cellular recovery after clay or byproduct-based treatment, the clays and byproducts were removed and cellular behavior was recorded in real-time for another 48 h, using 4000 Hz, (Figure 4, Region C). The chosen frequency allows for resistance evaluation without effects on cell's plasma membrane.[69] Further, at this frequency, previous analyses have showed

that the impedance is dependent on the cell bodies, whereas at the lower or higher frequencies, parameters such as impedance of the electrode/electrolyte interface or the medium, and the constriction resistance of the working electrode dominate the impedance measurements.[70]

Our results showed that the resistance of cells treated with the clay or byproduct dropped when compared to the control (Figure 4a); in particular, CC showed the greatest drop in resistance, with an almost complete loss after 6 h of treatment (Region B). Upon 24 h of treatment and removal of the clays or end of life cycle byproducts, cells treated with UC, UC900, and CC900 were able to regain/maintain their resistance values (Region C). Further, the trends in resistance were similar for both UC and UC900, and slightly lower for CC900; no regain in resistance was however recorded for cells exposed to CC.

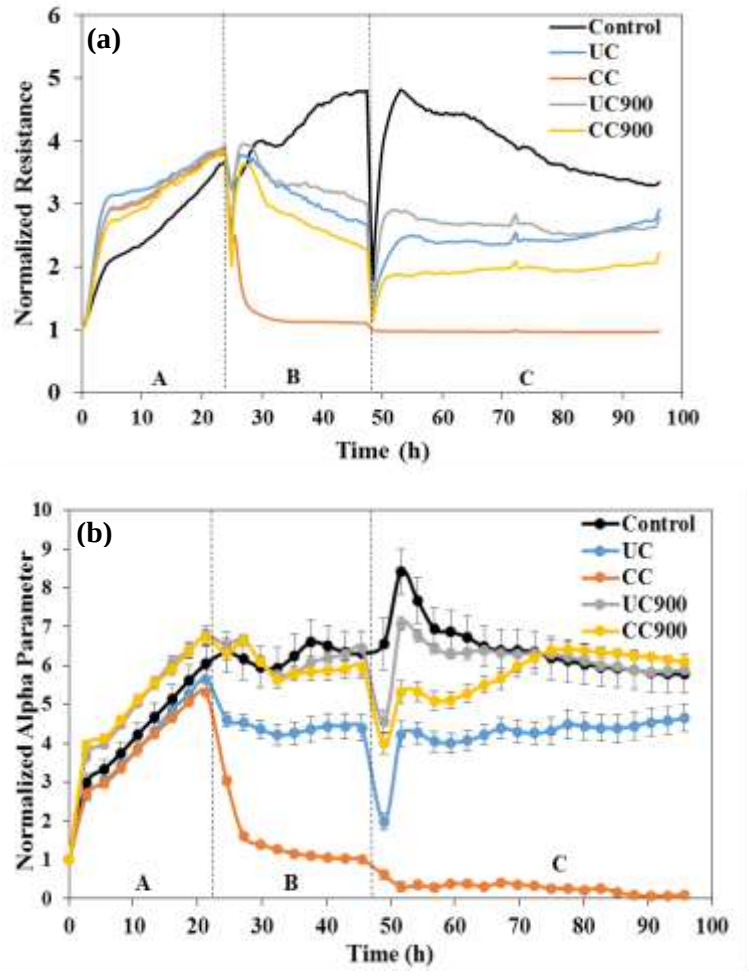

Figure 4: (a) Representative real-time measurements of normalized resistance for BEAS-2B cells before (Region A), during (Region B), and after treatment (Region C) with as-received and

thermally degraded nanoclays. (b) Real-time measurements of normalized alpha (α) parameter for BEAS-2B cells before (Region A), during (Region B), and after treatment (Region C) with as-received and thermally degraded nanoclays.

Mechanisms Responsible for Nanoclays or Thermally Degraded Byproducts Cellular Changes

Previous analysis have showed that a drop in resistance could be associated with changes in cell-substrate interactions,[71] in cell viability and proliferation,[72] or in cell shape as resulted from cell death, since flatter, more spread cells are responsible for higher resistance than rounder or apoptotic cells.[51,46] Complementary, complete loss in resistance was shown to be due to cell death and detachment from the electrode.[71]

To evaluate the first, namely whether cells exposed to nanoclays show changes in cell-substrate interactions, we used the α parameter which details the current through the ventral surfaces of the cells and electrodes[73] (Figure 4b). Indeed, while CC showed a complete loss in cell-substrate interaction within the course of the study time, cells treated with UC showed a decrease in α relative to the control cells within Region B, however, after clay removal, they maintained their cell-substrate interaction (Region C). Complementary, UC900 and CC900 had similar α values relative to the control, thus indicating that interactions between the cells and the substrate were maintained; however, resistance was lower for both relative to the control, possibly indicating that changes to the cell morphology had occurred. CC900 also showed an increase in the α parameter within the 48 h post treatment removal (Region C) confirming cell recovery.

To evaluate the second, namely whether changes in resistance are due to decreases in cellular viability and proliferation, we used cellular assays. Indeed, analyses showed that UC and CC displayed significant decreases, with CC causing a time-dependent decrease in cellular proliferation and viability over 72 h of exposure, relative to the control, UC, and the thermally degraded byproducts. Similar results were obtained by Maisanaba et al. who showed decreases in cellular viability in a time dependent manner at doses above 3.91 µg/ml upon treatment with CC of the human colon cell line, Caco-2.[30] UC900 and CC900 showed a more varied response in both live cell counts and cellular viability relative to their non-degraded counterparts. In particular, UC900 had a significant decrease in live cell count (Figure 5a), while no significant decreases in cellular viability were obtained for the thermally degraded clays, both relative to the control (Figure 5b). CC900 displayed an increase in cellular proliferation at 72 h relative to 48 h and

further confirmed the observed Region C changes in the α parameter. The ability of CC900 to display increased proliferation, may hint at its potential to produce effects similar to carcinogen carbon black; complementary study noted for instance that carbon black caused an increase in epithelial cell proliferation, as well as increases in mutation frequency in these cells, therefore hinting at an increased prevalence of cancer incidence upon such exposures.[74] No significant differences were obtained between UC and UC900 and overall there were no major differences between sterilized and unsterilized nanoclays (Figure S5a,b). Verma et al. complement our results on as-received nanoclays by showing differences in toxicity in A549 cells based on the clay morphology, with platelet type nanoclays showing lower cell numbers relative to the tubular type, as well as varying toxicity between the platelet types.[31]

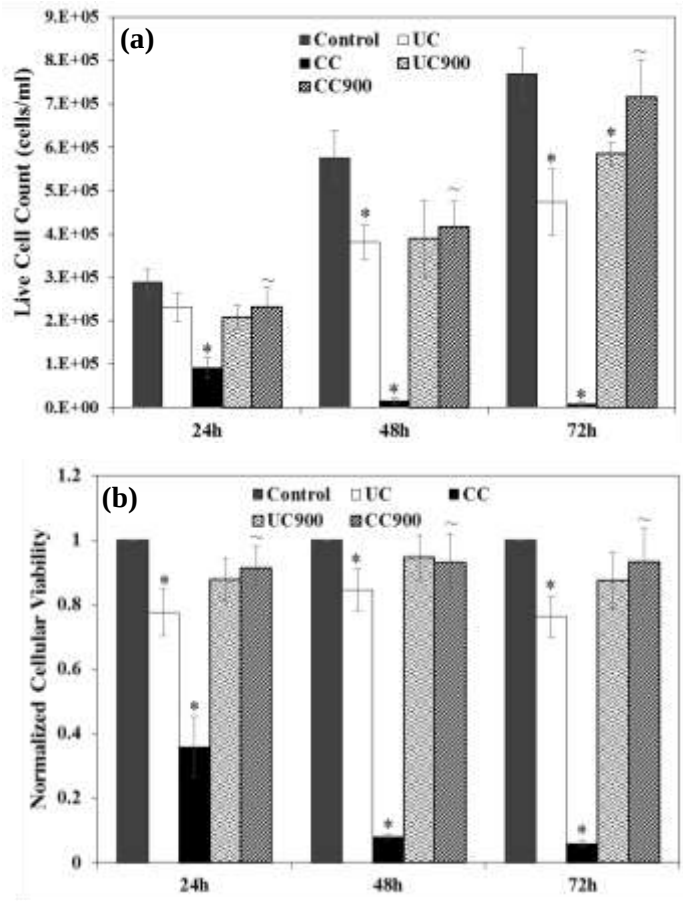

Figure 5: Toxicity of as-received and thermally degraded nanoclays determined by (a) live cell count and (b) cellular viability via WST assay, for unsterilized nanoclay (n=6). The symbols * and ~ indicate significant differences between the control and nanoclay treatments and between as-received nanoclay and thermally degraded byproducts, respectively.

To evaluate the last, namely whether changes in cell shape were correlated with the ECIS results, cellular imaging was used. Indeed, analysis showed that all of the clays and thermally degraded byproducts altered cellular shape and size, as well as cells confluence (Figure 6a-e). For instance, the treated cells displayed abnormal cell shapes with a more stretched and altered profile away from the more oval shape of the control cells. Further, the membranes of the cells exposed to UC900 and CC900 did not appear as distinct as those of the control cells and further, the integrity of the exposed cell monolayer seemed compromised. Moreover, treatment with UC and CC caused significant decreases in the area of the cells relative to the control therefore further confirming the ECIS results (Figure 6f); i.e., smaller cells would be taking up less room on the electrode, causing for more current to pass through and thus a lower resistance as shown by ECIS. Further, the dramatic loss of resistance and α shown for cells treated with CC along with the circular shape observed in cell imaging, show that alterations are likely occurring in these cells morphology as a first step towards cell transformation.

The larger effect observed for CC is presumably due to the presence of its organic modifier known to induce toxicity[33,30,35] through decrease in cellular proliferation,[31] as well as membrane changes[29,32] and DNA damage.[33,34,35] It is our hypothesis that the route of the displayed toxicity of cells treated with CC could be through alteration of the cytoskeleton, causing for the observed decreases in resistance and α. Specifically, previous analysis for instance have shown that circular cells have lost their ability to attach to the substrate (electrode), as well as to other cells eventually leading to and/or serving as a signal of cell death.[75,76] Such changes in morphology are known to be occurring due to cytoskeleton reorganization[76] with alteration in cytoskeleton[44] leading to changes in cell mechanics,[77] migration,[78] differentiation,[79] and organization.[80] Further, it is likely that cells exposed to UC are also experiencing alterations of their cytoskeleton. While UC900 and CC900 did not experience as much a loss in the α parameter relative to the as-received clays, they still showed decreases in resistance, possibly associated with reduced membrane integrity as observed in cellular imaging. Such changes in cell morphology, structure, and cell-substrate interactions may eventually lead to loss of cell-cell signaling.[76,81]

Similar to our results, the presence of the organic modifier in clays was associated to greater toxicity.[29,30,35,82] Janer et al. for instance tested dose-response (<500 µg/ml) of 5 cell lines and 1 primary cell line and found that clays organically modified with dimethyl dihydrogenated tallow ammonium and dimethyl benzyl hydrogenated tallow ammonium respectively had higher

cytotoxicity relative to pristine clays.[82] When testing the modifier, quaternary ammonium compound (QAC), Sharma et al. found that the QAC had the same effect as the coated clay on the genotoxicity of Caco-2 cells, suggesting that the toxic effects were due to QAC.[35] Further, one study by Yoshida et al. found that organically modified silica particles coated with amine or carboxyl groups reduced the amount of reactive oxygen generation in HaCaT and TLR-1 cells. They also observed reduced DNA damage in HaCaT cells all relative to the unmodified silica particle, showing that the type of organic modifier and not just its presence plays a key role in toxicity.[83]

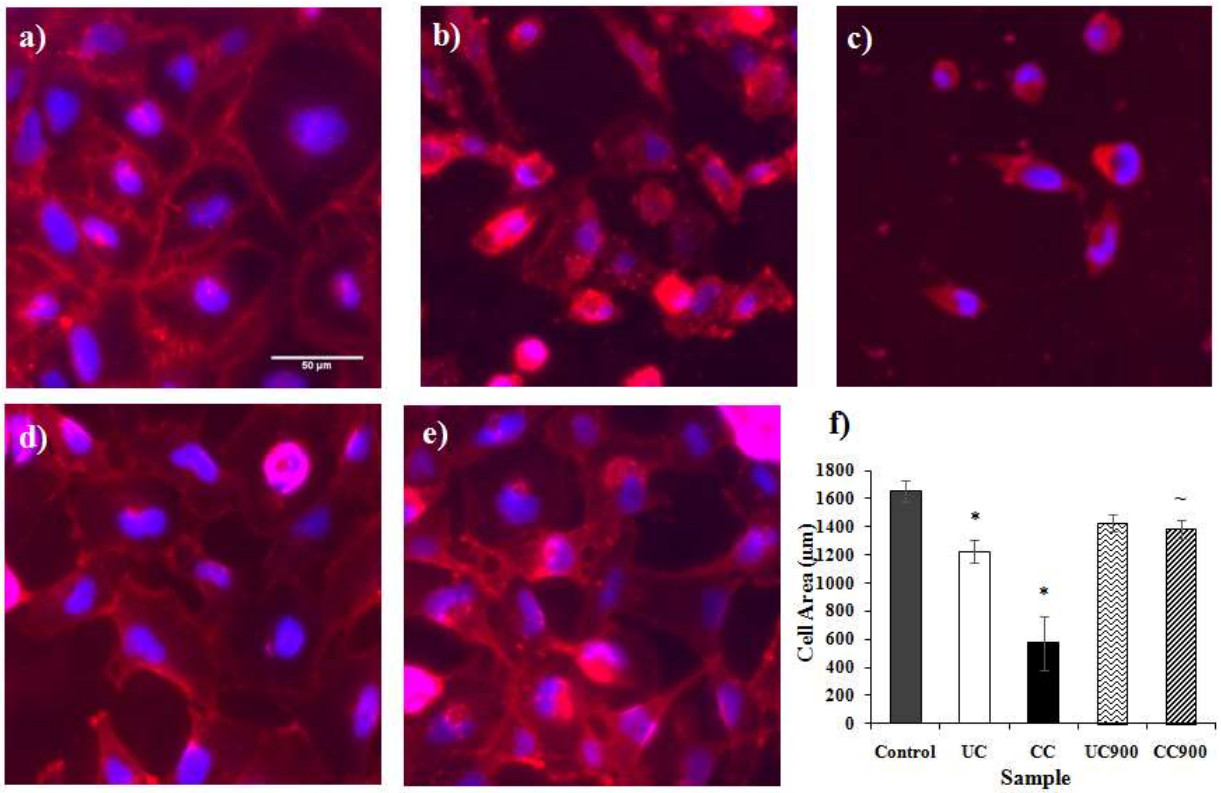

Figure 6: Fluorescent images of the cell membrane (red) and nucleus (blue) for (a) control cells and cells treated with (b) UC, (c) CC, (d) UC900, and (e) CC900 after 24 h. (f) Cell area (µm) after 24 h of treatment with nanoclays (n=3).

While the full picture of the mechanistic toxicity of the nanoclays or end of life byproducts is still undergoing, to our knowledge, these are the first studies to identify toxicological profiles associated with cellular exposure to thermally degraded byproducts using a non-invasive and real-

time cellular based platform. Further, while in our study we evaluated 4 different samples, one could envision creating a combinatorial assay to allow for profiles identification based on both sample as well as cellular characteristics thus extending the flexibility of this experimental set-up for toxicity evaluation of a large variety of nanomaterials, all in real-time and in a high-throughput manner.

Conclusions

The ECIS provided new means to identify the toxicity profiles of the clays or byproducts, in a non-invasive, high-throughput, and real-time manner. Specifically, the morphological, behavioral, and viability changes observed in BEAS-2B cells after treatment with as-received clay or thermally degraded byproducts show that such samples have the potential to produce toxic effects when used both in manufacturing or disposal environments. Organically modified nanoclay, CC, had the greatest toxic effects, with large losses in cell-substrate and cell-cell interactions and near maximal cell population loss by 72 h. Contrary, its thermally degraded byproduct, CC900, induced cell proliferation possibly hinting to similar toxic profiles to known carcinogen carbon black. UC, and its thermally degraded counterpart, UC900, displayed less significant toxic effects.

Acknowledgements

This work was supported by National Science Foundation (NSF) grant EPS-1003907, NSF 1434503, the National Institute of Health (NIH; R01-ES022968). The authors acknowledge use of WVU Shared Research Facilities.

Supporting Information

Chapter 2: Toxicity Evaluations of Nanoclays and Thermally Degraded Byproducts through Spectroscopical and Microscopical Approaches

Materials and Methods

Material Characterization

In order to determine if UV sterilization caused changes in molecular composition, samples of UC, CC, UC900, and CC900 were sterilized for 30 min under UV light and examined via Fourier Transform Infrared Spectroscopy (FTIR, Digilab FTS 7000) equipped with diamond Attenuated Total Reflection (ATR). Scans were collected in the range of 4000-400 cm^{-1} at a resolution of 4 cm^{-1}; a total of 100 scans were co-added to form the final spectrum of each one of the samples being analyzed. Samples were used as dry powders.

In order to determine if UV sterilization caused changes in surface morphology and chemical composition, samples of UC, CC, UC900, and CC900 were sterilized for 30 min under UV light and examined using a Hitachi S-4700 Field Emission Scanning Electron Microscope (SEM, Hitachi High-Technologies Corporation) equipped with an energy dispersive X-ray spectrographic detector (EDX). Surface morphology was examined at 5.0 kV while elemental composition was determined at 20.0 kV. For the analyses, the samples (dry powder forms) were mounted onto a carbon tape and then sputter coated for 10 s in vacuum injected with argon using a gold/palladium target.

Sedimentation over 6 h of the clays was performed by measuring absorbance via the spectrophotometer. Briefly, a concentration of 100 µg/ml of the two clays and their thermally degraded byproducts was prepared in media. The maximum absorbance of each clay was obtained by scanning the absorbance of each solution from 400-1100 nm. Sedimentation was determined by measuring the absorbance of each solution at the obtained maximum absorbance of 560 nm for 0, 0.5, 1, 2, 3, 4, 5, and 6 h with media serving as the blank at each time point.

Toxicity Analyses

UC, CC, and their thermally degraded byproducts were sterilized under UV light for 30 min in order to verify that the toxic effects obtained from the clay were due to the clay and not due to contaminants on the clay before sterilization. Therefore, live cell counts and cellular viability via

the WST assay were also performed with UV sterilized clay samples. Live cell counts were performed by seeding BEAS-2B cells in a 12 well plate (Thermo Scientific, USA) at a density of 2.0E+05 cells/ml. After 24 h, the cells were treated with UC(UV), CC(UV), or UV sterilized thermally degraded byproducts at a dose of 100 µg/ml. Before addition to the respective wells, the samples were sonicated for 8-10 min in media. Cells in only media served as controls. After 24, 48, and 72 h post exposure to UC(UV), CC(UV), UC900(UV) or CC900(UV), the cells were trypsinized and stained with 0.4% trypan blue solution (Invitrogen, USA). Subsequently, 10 µl of the sample containing the stained cells was added to a hemocytometer, and the number of cells in the four outer grids was counted through the use of the Leica DM IL optical microscope (Leica Microsystems) at 100X magnification. Cellular viability of cells treated with UV sterilized clays was performed by seeding BEAS-2B cells in a 96 well plate (Thermo Scientific, USA) at a density of 2.0E+05 cells/ml. After 24 h, 100 µg/ml of UC(UV), CC(UV), UC900(UV), or CC900(UV) dispersed in media was added to their respective wells; cells in media served as control samples. After 24, 48, and 72 h of exposure, 10 µl of WST was added to the wells. The cells were incubated for 2.5 h and then read by a FLUOstar OPTIMA plate reader (BMG LABTECH) at 485 nm absorbance. Media, UC(UV)+media, CC(UV)+media, UC900(UV)+media, and CC900(UV)+media served as blanks and their obtained absorbance values were subtracted from their cellular counterparts.

Results

Table S1: Average particle diameter distribution sizes (µm) in solutions of media relative to % volume.

	UC	**CC**	**UC900**	**CC900**
<10%	7.93 +/- 0.27	4.25 +/- 0.16	6.25 +/- 0.01	6.36 +/- 0.20
<50%	14.41 +/- 0.46	9.76 +/- 0.08	13.53 +/- 0.21	12.71 +/- 0.30
<90%	24.21 +/-1.08	21.73 +/- 1.32	25.81 +/-0.76	23.05 +/- 1.11

Table S2: Average particle diameter distribution sizes (µm) in solutions of PBS relative to % volume.

	UC	**CC**	**UC900**	**CC900**
<10%	6.29 +/- 0.16	4.68 +/- 0.12	6.69 +/- 0.03	6.79 +/- 0.01
<50%	11.68 +/- 0.12	11.12 +/- 0.12	14.64 +/- 0.05	13.16 +/- 0.03
<90%	21.27 +/- 0.60	23.00 +/- 0.15	28.14 +/- 0.09	23.53 +/- 0.07

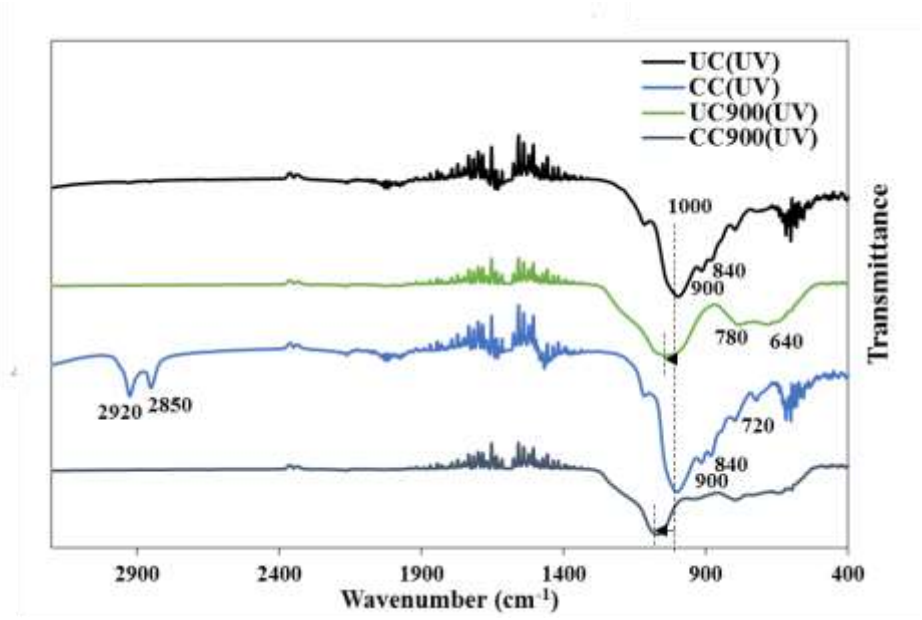

Figure S1: FTIR spectrum of as-received and thermally degraded nanoclay sterilized by UV light for 30 min (n=2).

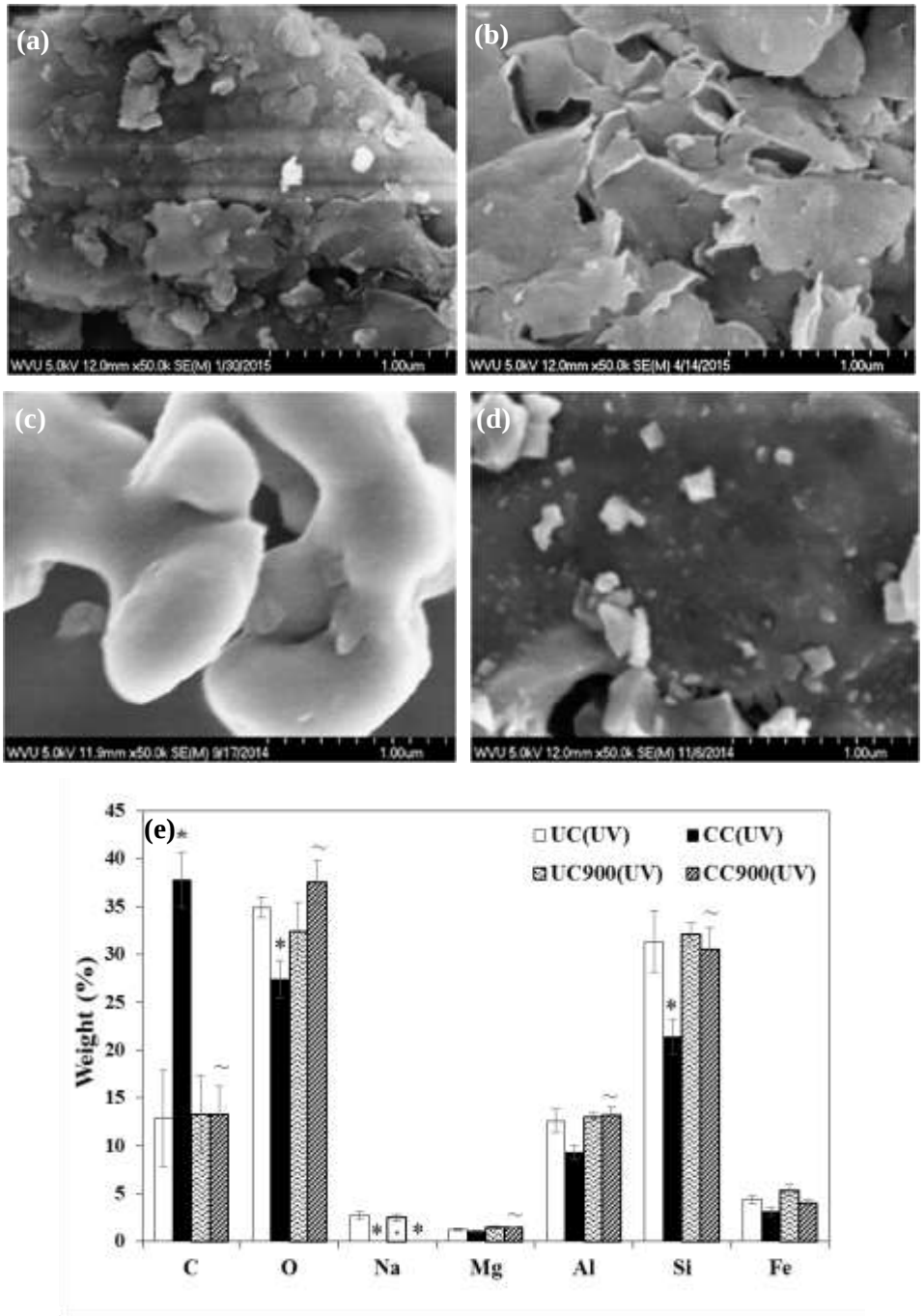

Figure S2: Surface morphology of sterilized (a) UC(UV), (b) CC(UV), and thermally degraded (c) UC900(UV), and (d) CC900(UV) as determined by SEM. (e) Elemental composition of as-received and thermally degraded nanoclay sterilized by UV light for 30 min determined by EDX at 1µm (n=5). The symbols * and ~ indicate significant differences between UC and CC and between as-received nanoclay and thermally degraded byproducts, respectively.

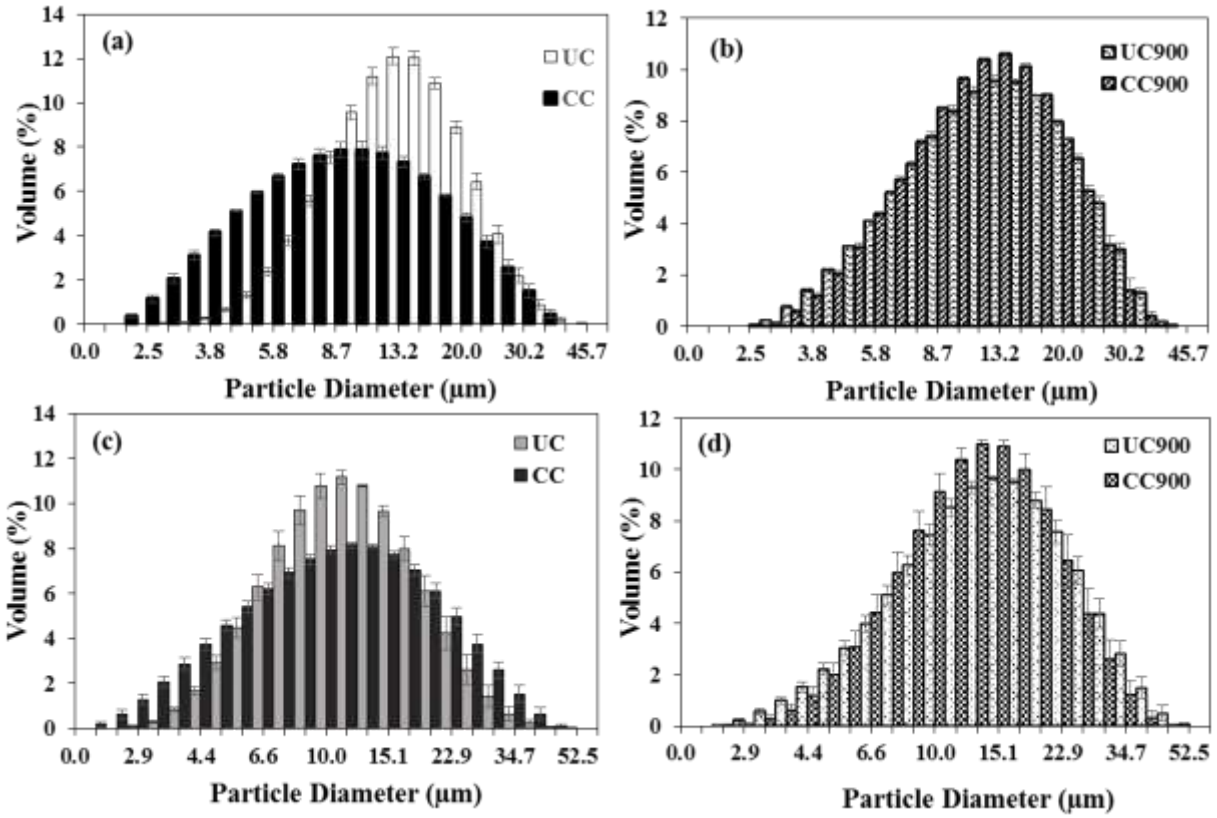

Figure S3: Average particle diameter size distribution of UC, CC, UC900, and CC900 in solutions of (a-b) media or (c-d) PBS based on % volume (n=3).

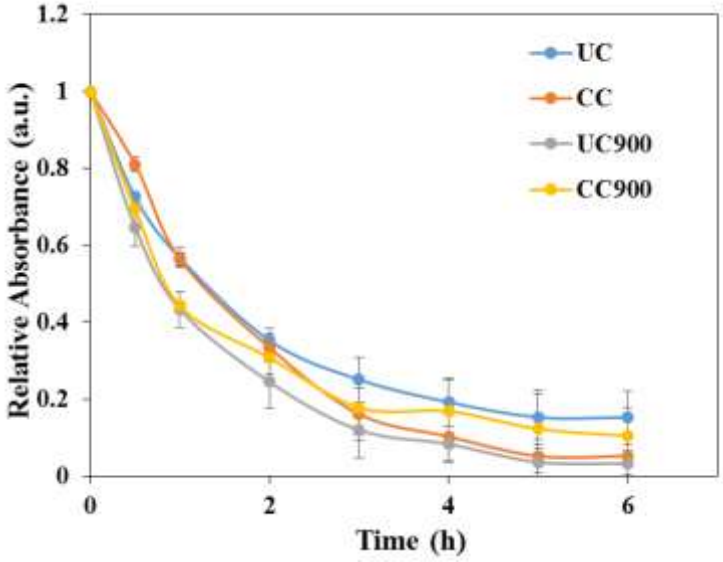

Figure S4: Sedimentation of as-received and thermally degraded nanoclays over 6 h as determined via spectrophotometer (n=4).

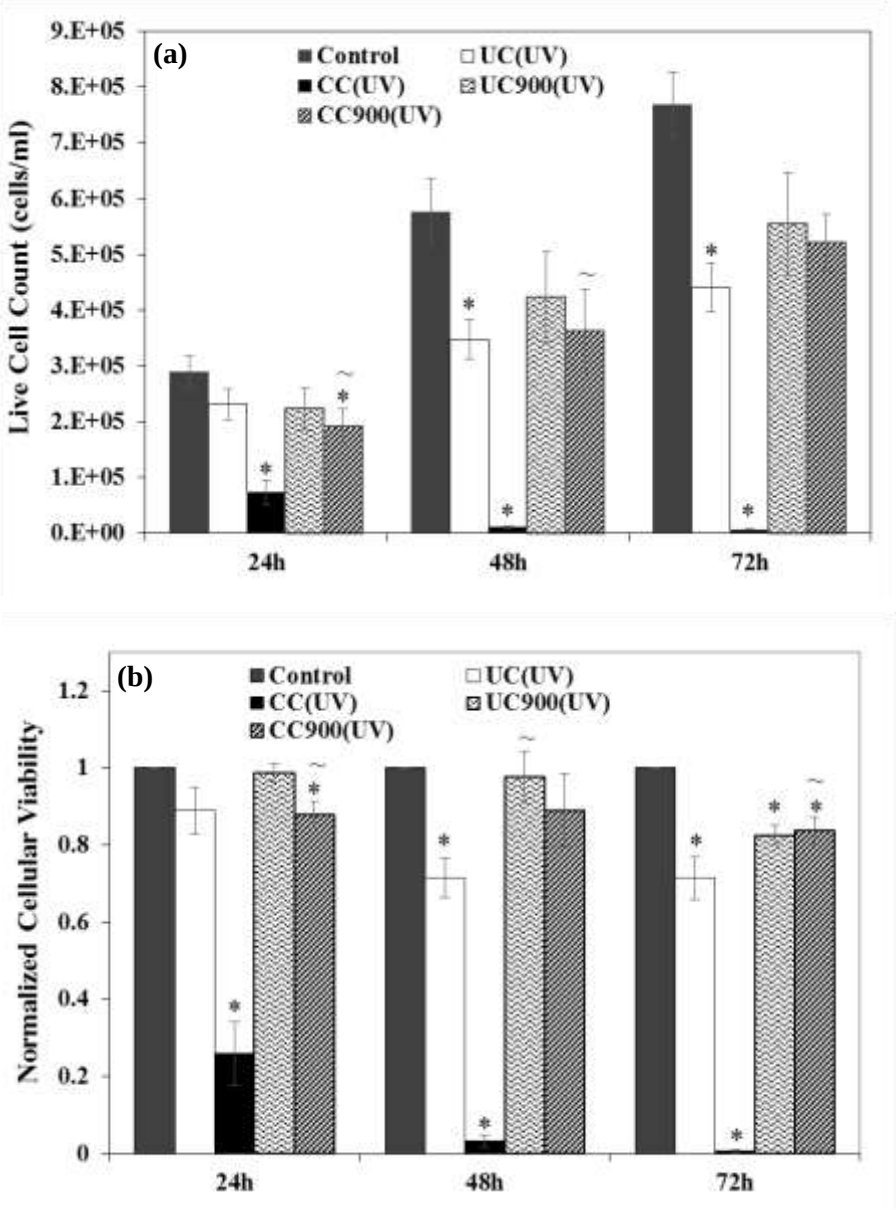

Figure S5: Toxicity of as-received and thermally degraded nanoclays sterilized by UV light for 30 min determined by (a) live cell count and (b) cellular viability via WST assay. The symbols * and ~ indicate significant differences between the control and nanoclay treatments and between as-received nanoclay and thermally degraded byproducts, respectively. The symbol ¤ indicates significant differences between unsterilized nanoclay and its sterilized counterpart.

References

1. Roco, M. C., The long view of nanotechnology development: The National Nanotechnology Initiative at 10 years. *Journal of Nanoparticle Research* **2011,** *13*, 427-445.

2. Sargent Jr., J. F., The National Nanotechnology Initiative: Overview, Reauthorization, and Appropriations Issues. *Congressional Research Service* **2014**.

3. Paul, D. R.; Robeson, L. M., Polymer nanotechnology: Nanocomposites. *Polymer* **2008,** *49*, 3187-3204.

4. Singla, P.; Mehta, R.; Upadhyay, S. N., Clay modification by the use of organic cations. *Green and Sustainable Chemistry* **2012,** *2*, 21-25.

5. Ray, S. S.; Okamoto, M., Polymer/layered silicate nanocomposites: a review from preparation to processing. *Progress in Polymer Science* **2003,** *28*, 1539-1641.

6. Ultracki, L. A.; Sepehr, M.; Boccaleri, E., Synthetic, layered nanoparticles for polymeric nanocomposites (PNCs). *Polymers for Advanced Technologies* **2007,** *18* (1), 1-37.

7. Floody, M. C.; Theng, B. K. G.; Reyes, P.; Mora, M. L., Natural nanoclays: applications and future trends-a Chilean perspective. *Clay Minerals* **2009,** *44*, 161-176.

8. Beall, G. W., The use of organo-clays in water treatment. *Applied Clay Science* **2003,** *24*, 11-20.

9. Agarwal, S.; Tran, P.; Soong, Y.; Martello, D.; Gupta, R. K., Flow behavior of nanoparticles stabilized drilling fluids and effect of high temperature aging. *Journal of Petroleum Science and Engineering* **2014,** *117*, 15-27.

10. Jones, T. R., The Properties and Uses of Clays Which Swell in Organic Solvents. *Clay Minerals* **1983,** *18*, 399-410.

11. Elmore, A. R. *Final Report on the Safety Assessment of Aluminum Silicate, Calcium Silicate, Magnesium Aluminum Silicate, Magnesium Silicate, Magnesium Trisilicate, Sodium Magnesium Silicate, Zirconium Silicate, Attapulgite, Bentonite, Fuller's Earth, Hectorite, Kaolin, Lithium Magnesium Silicate, Lithium Magnesium Sodium Silicate, Montmorillonite, Pyrophyllite, and Zeolite*; International Journal of Toxicology, 2003; pp 37-102.

12. Tiwari, R. R.; Khilar, K. C.; Natarajan, U., Synthesis and characterization of novel organo-montmorillonites. *Applied Clay Science* **2008,** *38*, 203-208.

13. Lebaron, P. C.; Wang, Z.; Pinnavaia, T. J., Polymer-layered silicate nanocomposites: an overview. *Applied Clay Science* **1999,** *15*, 11-29.

14. Krikorian, V.; Pochan, D. J., Poly (L-Lactic Acid)/Layered silicate nanocomposite: fabrication, characterization, and properties. *Chemistry of Materials* **2003,** *15*, 4317-4324.

15. Molinaro, S.; Romero, M. C.; Boaro, M.; Sensidoni, A.; Lagazio, C.; Morris, M.; Kerry, J., Effect of nanoclay-type and PLA optical purity on the characteristics of PLA-based nanocomposite films. *Journal of Food Engineering* **2013,** *117*, 113-123.

16. Zheng, X.; Wilkie, C. A., Flame retardancy of polystyrene nanocomposites based on an oligomeric organically-modified clay containing phosphate. . *Polymer Degradation and Stability* **2003,** *81*, 539-550.

17. Choi, R.; Cheigh, C.; Lee, S.; Chung, M., Preparation and Properties of Polypropylene/Clay Nanocomposites for Food Packaging. *Journal of Food Science* **2011,** *76*, 62-67.

18. Laufer, G.; Kirkland, C.; Cain, A. A.; Grunlan, J. C., Oxygen barrier of multilayer thin films comprised of polysaccharides and clay. *Carbohydrate Polymers* **2013,** *95*, 299-302.

19. Dalir, H.; Farahani, R. D.; Nhim, V.; Samson, B.; Lévesque, M.; Therriault, D., Preparation of Highly Exfoliated Polyester-Clay Nanocomposites: Process-Property Correlations. *Langmuir* **2012,** *28*, 791-803.

20. Okada, A.; Usuki, A., The chemistry of polymer-clay hybrids. *Material Science and Engineering: C* **1995,** *3*, 109-115.

21. Barua, S.; Dutta, N.; Karmakar, S.; Chattopadhyay, P.; Aidew, L.; Buragohain, A. K.; Karak, N., Biocompatible high performance hyperbranched epoxy/clay nanocomposite as an implantable material. *Biomedical Materials* **2014,** *9*.

22. Kevadiya, B. D.; Thumbar, R. P.; Rajput, M. M.; Rajkumar, S.; Brambhatt, H.; Joshi, G. V.; Dangi, G. P.; Mody, H. M.; Gadhia, P. K.; Bajaj, H. C., Montmorillonite/poly-(e-caprolactone) composites as versatile layered material: Reservoirs for anticancer drug and controlled release property. *European Journal of Pharmaceutical Science* **2012,** *47*, 265-272.

23. Fogelström, L.; Malmström, E.; Johansson, M.; Hult, A., Hard and Flexible Nanocomposite Coatings using Nanoclay-Filled Hyperbranched Polymers. *Applied Materials & Interfaces* **2010,** *2*, 1679-1684.

24. Meera, K. M. S.; Sankar, R. M.; Murali, A.; Jaisankar, S. N.; Mandal, A. B., Sol–gel network silica/modified montmorillonite clay hybrid nanocomposites for hydrophobic surface coatings. *Colloids and Surfaces B: Biointerfaces* **2012,** *90*, 204-210.

25. Mitrano, D. M.; Motellier, S.; Clavaguera, S.; Nowack, B., Review of nanomaterial aging and transformations through the life cycle of nano-enhanced products. *Environmental International* **2015,** *77*, 132-147.

26. Stern, S. T.; McNeil, S. E., Nanotechnology Safety Concerns Revisited. *Toxicological Sciences* **2008,** *101* (1), 4-21.

27. Dhawan, A.; Sharma, V., Toxicity assessment of nanomaterials: methods and challenges. *Analytical and Bioanalytical Chemistry* **2010,** *398*, 589-605.

28. Kroll, A.; Pillukat, M. H.; Hahn, D.; Schnekenburger, J., Current *in vitro* methods in nanoparticle risk assessment: Limitations and challenges. *European Journal of Pharmaceutics and Biopharmaceutics* **2009,** *72*, 370-377.

29. Lordan, S.; Kennedy, J. E.; Higginbotham, C. L., Cytotoxic effects induced by unmodified and organically modified nanoclays in human hepatic HepG2 cell line. *Journal of Applied Toxicology* **2011,** *31*, 27-35.

30. Maisanaba, S.; Gutièrrez-Praena, D.; Pichardo, S.; Moreno, F. J.; Jordá, M.; A.M., C.; Aucejo, S.; Jos, A., Toxic effects of a modified montmorillonite clay on the human intestinal cell line Caco-2. *Journal of Applied Toxicology* **2013,** *34*, 714-725.

31. Verma, N. K.; Moore, E.; Blau, W.; Volkov, Y.; Babu, P. R., Cytotoxicity evaluation of nanoclays in human epithelial cell line A549 using high content screening and real-time impedance analysis. *Journal of Nanoparticle Research* **2012,** *14*, 1-11.

32. Baek, M.; Lee, J.; Choi, S., Toxicological effects of cationic clay, montmorillonite in vitro and in vivo. *Molecular and Cellular Toxicology* **2012,** *8*, 95-101.

33. Maisanaba, S.; Puerto, M.; Pichardo, S.; Jorda, M.; Moreno, F. J.; Aucejo, S.; Jos, A., In vitro toxicological assessment of clays for their use in food packaging application. *Food and Chemical Toxicology* **2013,** *57*, 266-275.

34. Houtman, J.; Maisanaba, S.; Puerto, M.; Gutièrrez-Praena, D.; Jordá, M.; Aucejo, S.; Jos, A., Toxicity assessment or organomodified clays used in food contact materials on human target cell lines. *Applied Clay Science* **2014,** *90*, 150-158.

35. Sharma, A. K.; Schmidt, B.; Frandsen, H.; Jacobsen, N. R.; Larsen, E. H.; Binderup, M., Genotoxicity of unmodified and organo-modified montmorillonite. *Mutation Research/Genetic Toxicology and Environmental Mutagenesis* **2010,** *700*, 18-25.

36. Souza, P. M. S.; Morales, A. R.; Marin-Morales, M. A.; Mei, L. H. I., PLA and Montmorillonite Nanocoposites: Properties, Biodegradation, and Potential Toxicity. *Journal of Polymers and the Environment* **2013,** *21*, 738-759.

37. Roes, L.; Patel, M. K.; Worrell, E.; Ludwig, C., Preliminary evaluation of risks related to waste incineration of polymer nanocomposites. *Science of the Total Environment* **2012,** *417-418*, 76-86.

38. Lighty, J. S.; Veranth, J. M.; Sarofim, A. F., Combustion aerosols: factors governing their size and composition and implication to human health. *Journal of the Air & Waste Management Association* **2000,** *50* (9), 1565-1618.

39. Knirsch, J. M.; Pulskamp, K.; Krug, H. F., Oops they did it again! Carbon nanotubes hoax scientists in viability assays. *Nano Letters* **2006,** *6*, 1261-1268.

40. Monteiro-Riviere, N. A.; Inman, A. O.; Zhang, L. W., Limitations and relative utility of screening assays to assess engineering nanoparticle toxicity in a human cell line. *Toxicology and Applied Pharmacology* **2009,** *234*, 222-235.

41. Casey, A.; Herzog, E.; Davoren, M.; Lyng, F. M.; Byrne, H. J.; Chambers, G., Spectroscopics analysis confirms the interactions between single walled carbon nanotubes and various dyes commonly used to assess cytotoxicity. *Carbon* **2007,** *45*, 1425-1432.

42. Hoet, P. H.; Brüske-Hohlfeld, I.; Salata, O. V., Nanoparticles-known and unknown health risks. *Journal of Nanobiotechnology* **2004,** *2* (12).

43. Wang, L.; Zhu, J.; Deng, C.; Xing, W.; Cheng, J., An automatic and quantitative on-chip cell migration assay using self-assembled monolayers combined with real-time cellular impedance sensing. *Lab Chip* **2008,** *8*, 872-878.

44. Xi, B.; Yu, N.; Wang, X.; Xu, X.; Abassi, Y. A., The application of cell-based label-free technology in drug discovery. *Biotechnology Journal* **2008,** *3*, 484-495.

45. Xiao, C.; Lachance, B.; Sunahara, G.; Luong, J. H. T., Assessment of Cytotoxicity Using Electric Cell-Substrate Impedance Sensing: Concentration and Time Response Function Approach. *Analytical Chemistry* **2002,** *74*, 5748-5753.

46. Wegener, J.; Keese, C. R.; Giaever, I., Electric Cell-Substrate Impedance Sensing (ECIS) as a Noninvasive Means to Monitor the Kinetics of Cell Spreading to Artificial Surfaces. *Experimental Cell Research* **2000,** *259* (1), 158-166.

47. Erdely, A.; Dahm, M.; Chen, B. T.; Zeidler-Erdely, P. C.; Fernback, J. E.; Birch, M. E.; Evans, D. E.; Kashon, M. L.; Deddens, J. A.; Hulderman, T.; Bilgesu, S. A.; Battelli, L.; Schwegler-Berry, D. E.; Leonard, H. D.; McKinney, W.; Frazer, D. G.; Antonini, J. M.; Porter, D. W.; Castranova, V.; Schubauer-Berigan, M. K., Carbon nanotube dosimetry: from workplace exposure assessment to inhalation toxicology. *Particle and Fibre Toxicology* **2013,** *10*.

48. Hubbs, A.; Greskevitch, M.; Kuempel, E.; Fernando, S.; Toraason, M., Abrasive blasting agents: designing studies to evaluate relative risk. . *Journal of Toxicology and Environmental Health, Part A* **2005,** *68*, 999-1016.

49. Eldawud, R.; Stueckle, T. A.; Manivanna, S.; Elbaz, H.; Chen, M.; Rojanasakul, Y.; Dinu, C. Z., Real-time analysis of the effects of toxic, therapeutic and sub-therapeutic concentrations of digitoxin on lung cancer cells. *Biosensors and Bioelectronics* **2014,** *59*, 192-199.

50. Yin, L. M.; Wei, Y.; Wang, Y.; Xu, Y. D.; Yang, Y. Q., Long term and standard incubations of WST-1 reagent reflect the same inhibitory trend of cell viability in rat airway smooth muscle cells. *International Journal of Medical Sciences* **2013,** *10* (1), 68-72.

51. Giaever, I.; Keese, C. R., Micromotion of mammalian cells measured electrically. *Proceedings of the National Academy of Science* **1991,** *88*, 7896-7900.

52. Zhang, X.; Rongjing, X.; Zenggang, W.; Zhou, C., The synthesis and characterization of polyurethane/clay nanocomposites. *Polymer International* **2003,** *52*, 790-794.

53. Saikia, B. J.; Parthasarathy, G., Fourier Transform Infrared Spectroscopic Characterization of Kaolinite from Assam and Meghalay, Northeastern India. *Journal of Modern Physics* **2010,** *1*, 206-210.

54. Bishop, J.; Madejova, J.; Komadel, P.; Froschl, H., The influence of structural, Fe, Al, and Mg on the infrared OH bands in spectra dioctahedral smectites. *Clay Minerals* **2001,** *37*, 607-616.

55. Shameli, K.; Ahmad, M. B.; Zargar, M.; Yunus, W.; Ibrahim, N. A.; Shabanzadeh, P.; Moghaddam, M. G., Synthesis and characterization of silver/montmorillonite/chitosan bionanocomposites by chemical reduction method and their antibacterial activity. . *International Journal of Nanomedicine* **2011,** *6*, 271-284.

56. Xie, W.; Gao, Z.; Pan, W.; Hunter, D.; Singh, A.; Vata, R., Thermal degradation chemistry of alkyl quaternary ammonium montmorillonite. *Chemistry of Materials* **2001,** *13*, 2979-2990.

57. Rahimi-Razin, S.; Salami-Kalajahi, M.; Haddadi-Asl, V.; Roghani-Mamaqani, H., Effect of different modified nanoclays on the kinetics of preparation and properties of polymer-based nanocomposites. *Journal of Polymer Research* **2012,** *19*, 1-16.

58. Ribeiro, S. P. S.; Estevao, L. R. M.; Nascimento, R. S. V., Effect of clays on the fire-retardant properties of a polyethlenic copolymer containing intumescent formulation. *Science and Technology of Advanced Materials* **2008,** *9*, 1-7.

59. Kendall, M.; Hodges, N. J.; Whitwell, H.; Tyrrell, J.; Cangul, H., Nanoparticle growth and surface chemistry changes in cell-conditioned culture medium. *Philosophical Transactions of the Royal Society B: Biological Sciences* **2015,** *370* (1661).

60. Lordan, S.; Higginbotham, C. L., Effect of serum concentration on the cytotoxicity of clay particles. *Cell Biology International* **2012,** *36*, 57-61.

61. Kuhlbusch, T. A. J.; Asbach, C.; Fissan, H.; Göhler, D.; Stintz, M., Nanoparticle exposure at nanotechnology workplaces: A review. *Particle and Fibre Toxicology* **2011,** *8* (22).

62. Jensen, K. A.; Koponen, I. K.; Clausen, P. A.; Schneider, T., Dustiness behaviour of loose and compacted Bentonite and organoclay powders: What is the difference in exposure risk? *Journal of Nanoparticle Research* **2009,** *11*, 133-146.

63. Tsai, C.; Huang, C.; Chen, S.; Ho, C.; Huang, C.; Chen, C.; Chang, C.; Tsai, S.; Ellenbecker, M. J., Exposure assessment of nano-sized and respirable particles at different workplaces. *Journal of Nanoparticle Research* **2011,** *13*, 4161-4172.

64. Kim, W.; Lee, D. W.; Lee, S., Size Characterization of Incinerator Fly Ash Using Sedimentation/Steric Field-Flow Fractionation. *Analytical Chemistry* **2002,** *74* (848-855).

65. Chang, F.; Wey, M., Comparison of the characteristics of bottom and fly ashes generated from various incineration processes. *Journal of Hazardous Materials* **2006,** *B138*, 594-603.

66. Siegrist, K. J.; Reynolds, S. H.; Kashon, M. L.; Lowry, D. T.; Dong, C.; Hubbs, A. F.; Young, S.; Salisbury, J. L.; Porter, D. W.; Benkovic, S. A.; McCawley, M.; Keane, M. J.; Mastovich, J. T.; Bunker, K. L.; Gena, L. G.; Sparrow, M. C.; Sturgeon, J. L.; Dinu, C. Z.; Sargent, L. M., Genotoxicity of multi-walled carbon nanotubes at occupationally relevant doses. *Particle and Fibre Toxicology* **2014,** *11* (6).

67. Schinwald, A.; Murphy, F. A.; Jones, A.; MacNee, W.; Donaldson, K., Graphene-Based Nanoplatelets: A New Risk to the Respiratory System as a Consequence of Their Unusual Aerodynamic Properties. *ACS Nano* **2012,** *6*, 736-746.

68. Gangwal, S.; Brown, J. S.; Wang, A.; Houck, K. A.; Dix, D. J.; Kavlock, R. J.; Cohen Hubal, E. A., Informing selection of nanomaterial concentration for ToxCast in vitro testing based on occupational exposure potential. *Environmental Health Perspectives* **2011,** *119*, 1539-1546.

69. Benson, K.; Cramer, S.; Galla, H., Impedance-based cell monitoring: barrier properties and beyond. *Fluids and Barriers of the CNS* **2013,** *10* (5), 1-11.

70. Arndt, S.; Seebach, J.; Psathaki, K.; Galla, H.; Wegener, J., Bioelectrical impedance assay to monitor changes in cell shape during apoptosis. *Biosensors and Bioelectronics* **2004,** *19*, 583-594.

71. Xiao, C.; Luong, J. H. T., Assessment of cytotoxicity by emerging impedance spectroscopy. *Toxicology and Applied Pharmacology* **2005,** *206*, 102-112.

72. Male, K. B.; Lachance, B.; Hrapovic, S.; Sunahara, G.; Luong, J. H. T., Assessment of Cytotoxicity of Quantum Dots and Gold Nanoparticles Using Cell-Based Impedance Spectroscopy. *Analytical Chemistry* **2008,** *80*, 5487-5493.

73. Lo, C.; Keese, C. R.; Giaever, I., Impedance Analysis of MDCK Cells Measured by Electric Cell-Substrate Impedance Sensing. *Biophysical Journal* **1995,** *69*, 2800-2807.

74. Driscoll, K. E.; Carter, J. M.; Howard, B. W.; Hassenbein, D. G.; Pepelko, W.; Baggs, R. B.; G., O., Pulmonary Inflammatory, Chemokine, and Mutagenic Responses in Rats after subchronic inhalation of carbon black. *Toxicology and Applied Pharmacology* **1996,** *136*, 372-380.

75. Frisch, S. M.; Francis, H., Disruption of Epithelial Cell-Matrix Interactions Induces Apoptosis. *The Journal of Cell Biology* **1994,** *124* (4), 619-626.

76. Re, F.; Zanetti, A.; Sironi, M.; Polentarutti, N.; Lanfrancone, L.; Dejana, E.; Colotta, F., Inhibition of Anchorage-dependent Cell Spreading Triggers Apoptosis in Cultured Human Endothelial Cells. *The Journal of Cell Biology* **1994,** *127*, 537-546.

77. Dong, C.; Kashon, M. L.; Lowry, D. T.; Dordick, J. S.; Reynolds, S. H.; Rojanasakul, Y.; Sargent, L. M.; Dinu, C. Z., Exposure to Carbon Nanotubes Leads to Changes in the Cellular Biomechanics. *Advanced Healthcare Materials* **2013,** *2*, 1-7.

78. Shen, Y.; Leng, M.; Yu, H.; Zhang, Q.; Luo, X.; Gregersen, H.; Wang, G.; Liu, X., Effect of Amphiphilic PCL-PEG Nano-Micelles on HEpG2 Cell Migration. *Macromolecular Bioscience* **2015,** *15*, 372-384.

79. Zou, J.; Wang, X.; Zhang, L.; Wang, J., Iron Nanoparticles Significantly Affect the *In Vitro* and *In Vivo* Expression of *Id* Genes. *Chemical Research in Toxicology* **2015,** *28*, 373-383.

80. Zhou, X.; Wang, B.; Chen, Y.; Mao, Z.; Gao, C., Uptake of Cerium Oxide nanoparticles and their influences on functions of A549 cells. *Journal of Nanoscience and Nanotechnology* **2013,** *13*, 204-215.

81. Hussain, S.; Thomassen, L. C. J.; Ferecatu, I.; Borot, M.; Andreau, K.; Martens, J. A.; Fleury, J.; Baeza-Squiban, A.; Marano, F.; Boland, S., Carbon black and titanium dioxide nanoparticles elicit distinct apoptotic pathways in bronchial epithelial cells. *Particle and Fibre Toxicology* **2010,** *7* (10).

82. Janer, G.; Fernández-Rosas, E.; Mas del Molino, E.; González-Gáalvez, D.; Vilar, G.; López-Iglesias, C.; Ermini, V.; Vázquez-Campos, S., In vitro toxicity of functionalised nanoclays is mainly driven by the presence of organic modifier. *Nanotoxicology* **2014,** *8*, 279-294.

83. Yoshida, T.; Yoshioka, Y.; Matsuyama, K.; Nakazato, Y.; Tochigi, S.; Hirai, T.; Kondoh, S.; Nagano, K.; Abe, Y.; Kamada, H.; Tsunoda, S.; Nabeshi, H.; Yoshikawa, T.; Tsutsumi, Y., Surface modification of amorphous nanosilica particles suppresses nanosilica-induced cytotoxicity, ROS generation, and DNA damage in various mammalian cells. *Biochemical and Biophysical Research Communications* **2012,** *427*, 748-752.

CHAPTER 3

Early Assessment and Correlations of Nanoclay's Toxicity to their Physical and Chemical Properties

Abstract

Nanoclays' functionalization with organic modifiers increases their individual barrier properties, thermal stability, and mechanical properties and allows for ease of implementation in food packaging materials or medical devices. Previous reports have showed that while organic modifiers integration between the layered mineral silicates leads to nanoclays with different degrees of hydrophobicity that become easily miscible in polymers, they could also pose possible effects at inhalation or ingestion routes of exposure. Through a systematic analysis of 3 organically modified and one pristine nanoclays, we aimed to relate for the first time the physical and chemical characteristics, determined via microscopical and spectroscopical techniques, with the potential of these nanoclays to induce deleterious effects in *in vitro* cellular systems, i.e. immortalized and primary human lung epithelial cell lines. In order to derive information on how functionalization could lead to toxicological profiles throughout nanoclays' life cycle, both as-received and thermally degraded nanoclays were evaluated. Our analyses showed that the organic modifiers chemical composition influenced both the physical and chemical characteristics of the nanoclays, as well as their toxicity. Overall, nanoclays with organic modifiers containing bio-reactive groups displayed lower cellular numbers as well more elongated cellular morphologies relative to the pristine clay and the nanoclay containing a modifier with long carbon chains. Additionally, thermal degradation caused for loss of the organic modifiers, as well as changes in size and shape of the nanoclays, which led to changes in toxicity. Our study provides insight into the synergistic effects of chemical composition, size, and shape of the nanoclays and their toxicological profiles in conditions that mimic exposure in manufacturing and disposal environments respectively, and can help aid in safe-by-design manufacturing of nanoclays with user-controlled functionalization and lower toxicity levels when food packaging applications are considered.

Introduction

With an estimated growth rate of about 25% annually,[1] nanocomposites or composites containing nanoclays incorporated into polymers, are expected to have wide implementation in commercial and industrial products,[2] from food packaging materials[3] to automotive[4] and medical devices.[5] In food packaging for instance, nanoclays are organically modified to allow for better exfoliation within the polymer matrix[4] at a low silicate weight percent,[6] leading to commercial applications of almost 70% of the market volume.[7] The organic modification generally occurs via an ion exchange reaction with the positively-charged ions present between the nanoclay platelets[4] and directly impacts the type of polymer the clay can be exfoliated in, as well as the properties of the resulting nanocomposite. The increased implementation of nanoclays is a result of the improved mechanical strength,[8] barrier properties,[8] UV dispersion,[9] and fire resistance,[10] that they inflict to the polymeric packaging materials thus reducing gas and moisture permeability,[11] allowing for a longer shelf life[4] while still producing a lightweight,[12] transparent[13] material capable of withstanding physical manipulation[12] and other environmental elements, such as light and heat.[12]

Some of the most common nanoclays used in food packaging are Nanomer I.31PS, Nanomer I.34TCN, and Nanomer I.44P respectively. These nanoclays, belonging to the montmorillonite (MMT) clay ”family”, are made up of 2:1 phyllosilicates consisting of 2 silicate-oxygen tetrahedral sheets bounding an aluminum octahedral sheet,[14] with each of the clays containing a different organic modifier that tailors its name as well as its exfoliation ability in the specific types of polymer matrices.[12] Specifically, Nanomer I.31PS is modified with aminopropyltriethoxysilane and octadecylamine, while Nanomer I.34TCN and Nanomer I.44P are modified with methyl dihdroxyethyl hydrogenated tallow ammonium and dimethyl dialkyl amine respectively. Previous results showed that upon such modifications, Nanomer I.31PS and Nanomer I.44P can be exfoliated in polyethylene[15] and polypropylene[16] to result in composites with increased Young’s[15,17] and storage moduli,[15] thermal stability,[17] and tensile strengths[17] that ensures enhanced shelf life of food packaging products. Complementary, addition of Nanomer I.34TCN into polylactide acid[18,13] has resulted in nanocomposites with increased barrier properties,[18,13] thermal stability,[18] and tensile modulus,[18] along with high transparency[13] thus making Nanomer I.34TCN a good candidate for the green food packaging area, i.e., using

biodegradable polymers from renewable resources to allow for a more environmental friendly food packaging material formation.

Previous reports showed that manufacturing and disposal of nanocomposites used in food packaging applications could possibly lead to nanoclays being released from their polymer matrix,[19,20] which can pose health concerns if the exposure is via inhalation or ingestion routes. General *in vitro* assessment has found that both pristine and organically modified nanoclays cause decreased cellular proliferation,[21] mitochondrial damage,[22] reactive oxygen species (ROS) generation,[22] membrane[22] and DNA damage,[23] micronuclei induction,[24] and changes in mRNA expression,[24] in lung epithelial cells,[21,25] liver cells,[22] colon cells,[23] or skin cells,[25] with the degree of toxicity dependent on the cell type, dosage, and the organic modifier itself. Complementary, *in vivo* results revealed significant toxic effects through alteration of protein expressions after organically modified nanoclay was administered orally to rats,[26] as well as robust inflammatory responses characterized by transient neutrophilia for instance.[27]

However, while such reports hint at varying degrees of toxicity, minimal information is available to compare and contrast the effects of the unique physico-chemical properties of the nanoclays across their lifecycle and their effects on biological responses which may differ in degree and mechanism of toxicity due to each clay's unique properties and organic functionalization. During their as-received usages in free forms in manufacturing environments, workers could potentially be exposed to elevated levels of the airborne nanoclays.[28, 29] In addition, high temperatures and the oxidative environment present during the incineration process associated with their disposal[19] can lead to changes in both chemical composition and surface morphology of nanoclays,[20,30] that could potentially change their toxicological effect. Establishing life cycle toxicity assessment profiles are essential to prevent deleterious effects associated with inhalation of such particles by workers in both manufacturing and disposal environments. Specifically, Yuwen et al, observed DNA damage in blood cells for workers exposed to high levels of bentonite particles in factories producing such particles.[29]

We designed a systematic study to help determine the potential for inhalation toxicity of the three organically modified Nanomer nanoclays currently used for food packaging applications. Our study uses human immortalized bronchial epithelial cells (BEAS-2B), and primary small airway epithelial cells (SAECs), as established cell lines for assessing toxicity induced via inhalation since they have previously helped assess toxicity of graphene nanoparticles,[31] asbestos[32]

and carbon nanotubes.[33] The SAECs model expands the impact of our study to a more human-related biological platform as primary cells more closely mimic their tissue of origin and further, reduce misidentification, contamination,[34] general genetic instability,[35] or lack of functions and markers often encountered with immortalized cellular systems. Additionally through the use of two epithelial lung cell lines we will be able to further assess the potential toxicity of nanoclays when they deposit in both the bronchioles and distal airways near the terminal bronchiole and alveolar duct. Our systematic assessment will map and correlate the physical and chemical properties of nanoclays at two points in their life cycle (i.e. production/manufacturing or the end of their life cycle) with their potential to induce toxicity for a better understanding of how nanoclays' deleterious interactions with the cellular systems can be reduced so safe, yet effective materials can be produced and implemented in commercial sectors.

Materials and Methods

Nanoclay Preparation

Four types of commercially available, raw (as-received), montmorillonite (MMT) clays, were obtained from Sigma-Aldrich. Per the manufacturer specifications, Nanomer PGV (PGV) is an unmodified, hydrophilic bentonite, Nanomer I.31PS (I.31PS) is surface modified with aminopropyltriethoxysilane at 0.5-5 wt. % and octadecylamine at 15-35 wt. %, Nanomer I.34TCN (I.34TCN) is surface modified with methyl dihdroxyethyl hydrogenated tallow ammonium at 25-30 wt. % and, Nanomer I.44P (I.44P) is surface modified with dimethyl dialkyl amine at 35-45 wt. %. All the modifications were done at the manufacturing site.

Thermal Degradation

Samples of PGV, I.31PS, I.34TCN, and I.44P were thermally degraded using a TGA701 Thermogravimetric Analyzer from LECO; degradation was used to mimic the disposal generation in municipal solid waste plants.[19] Differences in mass from unheated samples were monitored as a function of temperature and used to calculate % content change. Moisture content of the samples (around 0.5 g each) was determined in the 25 ºC to 105 ºC range, in nitrogen, at a rate of 6 ºC/min, while high temperature volatile content was determined in the 105 ºC to 950 ºC range, in nitrogen, at a rate of 43 ºC/min. Finally, ash content was determined in the 550 ºC to 900 ºC range, in oxygen, at a rate of 15 ºC/min (Table S1). The resulting individual byproduct was collected to serve as the end of life cycle sample assessment, i.e., thermally degraded Nanomer PGV (PGV900), thermally

degraded Nanomer I.31PS (I.31PS900), thermally degraded Nanomer I.34TCN (I.34TCN900), and thermally degraded Nanomer I.44P (I.44P900) respectively.

Material Characterization

Molecular composition of the samples and their thermally degraded byproducts in dry, powder forms, was determined via Fourier Transform Infrared Spectroscopy (FTIR, Digilab FTS 7000) equipped with diamond Attenuated Total Reflection (ATR). For each of the samples, a total of 100 scans in the range of 4000-400 cm^{-1} at a resolution of 4 cm^{-1} were co-added/ averaged to form the final spectrum.

Surface morphology and elemental composition of the samples were investigated using a Hitachi S-4700 Field Emission Scanning Electron Microscope (SEM, Hitachi High-Technologies Corporation) equipped with an energy dispersive X-ray spectroscopy (EDX) unit. For the analyses, dry individual powders were mounted on carbon tape and their surface morphology was examined at 5.0 kV, while their elemental composition was evaluated at 20.0 kV. For surface morphology, samples were also sputter coated for 10 s in vacuum injected with argon using a gold/palladium target. The argon atoms were ionized and collided with the gold/palladium target, causing the metal ions to deposit on the sample in a thin conductive layer of about 3 nm as calculated using the equation d=KIVt, where d is thickness, k is a constant value of 0.17, I is plasma current, V is voltage, and t is the time.

The size distribution of the nanoclays and thermally degraded byproducts was determined by dynamic light scattering (DLS) via the Mastersizer 2000 with a Hydro 2000S accessory (Malvern Instruments). For this, samples of PGV, I31PS, I.3TCN, I.44P, PGV900, I.31PS900, I.34TCN900, or I.44P900 were dispersed either in Dulbecco's Modified Eagle Medium (DMEM, Life Technologies) containing 5% fetal bovine serum (FBS), or in Small Airway Growth Medium (SAGM, Lonza) with SingleQuots Kit (Lonza) containing bovine pituitary extract, hydrocortisone, human Epidermal Growth Factor, epinephrine, transferrin, insulin, retinoic acid, triiodothyronine, gentamicin/amphotericin-B, and 1 % bovine serum albumin (BSA). Also, the nanoclays and byproducts were dispersed in a control, phosphate buffered saline (PBS, Lonza) and in distilled water containing 0.15 mg/ml Survanta®, a pulmonary surfactant.[36] The solutions were then bath sonicated and dropped into the Hydro 2000S until laser obscuration was within 10-20%. The size analysis was performed 3 consecutive times with a stirrer speed of 1750 rpm and under continuous sonication in the Hydro 2000S accessory.

Cell Culture

Immortalized human bronchial epithelial cells (BEAS-2B) from American Type Culture Collection (ATCC) were cultured in 100 mm dishes (Corning, Inc.) in DMEM containing 5% FBS, 1 % L-glutamine, and 1 % penicillin-streptomycin (all reagents were purchased from Life Technologies). The cells were incubated at 37 ^{0}C, 5 % CO_2, and in an 80 % relative humidity; consistent sub-culturing took place using 0.05 or 0.25 % trypsin (Invitrogen). Before each experiment, cells were grown to a monolayer of 90-100% confluency and cells in the 3rd-6th passage were used.

Additionally, small airway epithelial cells (SAECs) were cultured in SAGM with SingleQuots Kit and 1 % penicillin-streptomycin (Life Technologies). Cells were seeded into T-25 flasks (Corning, Inc.), grown to 75-80% confluency and subsequently split (5 passages total). All experiments completed with SAECs were performed using the same passage number.

Half Maximal Inhibitory Concentration (IC_{50})

BEAS-2B cells and SAECs were seeded into 12 well plates (Thermo Scientific) at densities of approximately $1.5x10^5$ and $2.0x10^5$ cells/ml, respectively. After 24 h, the cells were treated with PGV, I.31PS, I.34TCN, I.44P or their thermally degraded byproducts at various doses ranging from 0 to 197 µg/cm^2 (i.e. 0, 0.03, 0.3, 13, 26, 66, 132, and 197 µg/cm^2). To ensure an effective dose metric and uniform dosage distribution per well, the dose is reported in µg/cm^2 with the analysis considering the area of the specific well into which the cells were seeded and the initial dilution of nanoclays to form µg/ml solutions. Before addition to the respective wells, each nanoclay or byproduct sample was sonicated for 10 min in a bath sonicator (2510 Branson; 100 W) with the concentrations used for exposure being serial dilutions from the original stock; cells in only media served as controls. After 24 h of exposure to individual treatment, the treated cells (as well as the controls) were washed to remove the nanoclays and byproducts, trypsinized, and stained with 0.4% trypan blue solution (Invitrogen). Subsequently, 10 µl of the sample containing the stained cells was added to a hemocytometer, and the number of cells in the 4 outer grids was counted through the use of the Leica DM IL optical microscope (Leica Microsystems) and a 10X objective. Analyses of the cellular proliferation post-exposure were used to extrapolate IC_{50} values that would also be used in the remaining cellular assays. At least 6 replicates were performed for BEAS-2B cells at each dose and 4 replicates for SAECs at each dose.

Cellular Imaging

To evaluate changes in cell morphology, BEAS-2B cells and SAECs were seeded at densities of $1.5x10^5$ and $2.5x10^5$ cells/ml, respectively, in 24 well plates. After 24 h the cells were treated with the as-received nanoclays and thermally degraded byproducts, dispersed in media via a bath sonicator, at their respective, determined IC_{50} dose. After 24 h of treatment the cells were imaged through use of a Leica DM IL optical microscope (Leica Microsystems) with a 10X objective. Two replicates were performed with 10 images, per replicate, taken at random spots within the well for each control and treatment.

Extracellular Reactive Oxygen Species (ROS)

BEAS-2B cells were seeded into 24 well plates at a density of approximately $1.5x10^5$ cells/ml. After 24 h, the cells were treated with nanoclays and byproducts dispersed in media through use of a bath sonicator at their respective, determined IC_{50} value; cells exposed to only media served as control samples. After 24, 48, and 72 h of treatment, 50 µl of the media was transferred from the 24 well plate to its respective well in a black-bottomed 96 well plate (Corning, Inc.). Subsequently, 50 µl of PBS was added to each well in the 96 well plate. Fifty µl of the extracellular reactive oxygen species (ROS) assay reagent, Lumigen ECL Plus (Lumigen, Inc.), was also added to each well. The samples were subsequently incubated at room temperature for 5 min, in the dark before luminescence was evaluated using a FLUOstar OPTIMA plate reader (BMG LABTECH) at 600 nm. Media and treated media containing nanoclays or byproducts suspended in solution served as blanks. Respective cellular measurements of the samples were evaluated after subtracting the blanks in order to determine the effect treatment had on extracellular ROS. It has been determined that Lumigen reagent assays generate chemiluminescent responses specific to extracellular ROS.[37] Four replicates were performed for each treatment.

Statistical Analyses

The cellular experiments were repeated at least 4 times for each one of the samples (with the exception of cellular imaging). All tables are presented as the average value (+/-) standard deviation (SD) values. All graphs are presented as the mean value of the number of indicated replicates with (+/-) standard error (SE) bars. Excel and Origin (OriginLab) were used to determine the IC_{50} value for each of the nanoclays and thermally degraded byproducts, through use of a best-fit line (either logistic, exponential, or logarithmic) for each individual replicate with each

nanoclay or byproduct treatment containing at least 4 replicates. Significance was determined by one-way analysis of variance ANOVA with $p<0.05$* indicating significance.

Results and Discussion

We aimed to provide insights into the toxicity mechanisms associated with human exposure to nanoclays in both manufacturing and disposal areas. For this, we first selected a regiment of four nanoclays, namely one pristine (PGV) and three organically modified nanoclays, (I.31PS, I.34TCN, and I.44P), with different physico-chemical properties and with relevant implementation in current food packaging applications.[7] Specifically, the modifier for I.31PS consists of a long alkyl tail and a silane coupling agent (Figure 1a).[17] I.34TCN's modifier consists of a long alkyl chain and 2 hydroxyl molecules,[17] while, the modifier for I.44P consists of 2 long alkyl chains.[17] Secondly, we thermally degraded these nanoclays in conditions aimed to mimic their disposal at the end of their individual life cycles and created resulting byproducts. To assess possible deleterious pulmonary effects, two *in vitro* cellular models were exposed to as-received nanoclays and their incinerated byproducts. Immortalized human bronchial epithelial cells (BEAS-2B) and small airway epithelial cells (SAECs), previously used for pulmonary toxicity in occupational studies, provide sensitive models for known nanoclay deposition areas in the lung[38] and serve as validation tool, as toxicity of nanoclays has shown to differ based on cell line. The results are included below.

Materials Preparation and Characterization

To help evaluate the physico-chemical characteristics of the samples being assessed, we compared nanoclays and their byproducts. Specifically, the thermally degraded byproducts of the pristine (PGV) and the three organically modified nanoclays (I.31PS, I.34TCN, and I.44P) were obtained at temperatures up to 950 °C, in three different temperature regimes known to mimic incineration conditions at the end of food packaging product lifecycle[19] (Figure 1b). The moisture, high temperature volatiles, and ash contents of the resulting byproducts were determined in the range of 25 °C to 105 °C and 105 °C to 950 °C in nitrogen for moisture and volatile contents, while ash content was assessed in the range of 550 ^{0}C to 900 °C in oxygen respectively.

Analyses showed that all the modified nanoclays had significantly lower amount of moisture relative to the pristine nanoclay (Table 1), presumably a result of their greater hydrophobicity resulted from individual chemical functionalization with an organic modifier

known to replace adsorbed water normally found in pristine clays,[39] therefore minimizing the overall amount of free water to be released.[40,41] The modified nanoclays also showed a significantly higher amount of high temperature volatile content and a significantly lower amount of ash content relative to the pristine nanoclay. This is also presumably due to the degradation of the organic modifier which has previously been shown to be released within the 200-500 °C temperature range.[40,41] Further, out of the modified nanoclays themselves, I.44P seemed to have the highest amount of high temperature volatile content of around 39 %, along with the lowest amount of ash content of around 59 % respectively, presumably due to the chemical structure of its organic modifier which is made up of 2 long alkyl chains which differs from the one of I.31PS and I.34TCN, each only having one long alkyl chain.[17]

Table 1: The percent amount of moisture, high temperature volatiles, ash, and fixed carbon present in the Nanomer nanoclays as determined by TGA. The symbol * indicates a significant difference between PGV and the organically modified nanoclays (n=2).

	Moisture	**High Temperature Volatiles**	**Ash**	**Fixed Carbon**
PGV	13.51 +/- 0.71	6.41 +/- 0.06	79.78 +/- 0.67	0.31 +/- 0.10
I.31PS	0.66 +/- 0.05*	30.53 +/- 0.01*	68.50 +/- 0.05*	0.32 +/- 0.08
I.34TCN	2.25 +/- 0.27*	26.50 +/- 0.08*	70.69 +/- 0.18*	0.58 +/- 0.16
I.44P	1.48 +/- 0.13*	39.23 +/- 0.12*	59.20 +/- 0.06*	0.10 +/- 0.06

The modified nanoclays also experienced a greater weight loss when compared to pristine PGV, all within the temperature range of 400-800 °C (Figure 1b), with I.31PS and I.34TCN experiencing similar amounts of weight loss of about 32 and 30 % respectively, while I.44P experienced a greater weight loss of around 40 %. The observed differences are presumably due to the weight percentages (wt. %) and chemical composition of the individual organic modifiers used during functionalization, as well as their roles in the individual nanoclay's degradation profile,[41] with I.44P's organic modifier being added at 45 wt. %, while the organic modifiers of I.31PS and I.34TCN were reported to be added up to 40 and 30 wt. %, respectively, via manufacturer specifications. Our analyses are supported by Xie et al. that showed that the amount of organic modifier released in degradation studies is dependent on the interlayer spacing and

architecture of the modifier and its integration during nanoclay functionalization.[42] Lastly, PGV seemed to have a more gradual weight loss in the 400-800 °C range when compared to the functionalized nanoclays, which is probably associated with the MMT structure breakdown in which hydroxyl groups incorporated within the crystal lattice are being dehydrated within the temperature range of 500-800 ºC.[41]

Physico-chemical characterization of the nanoclays and their thermally degraded byproducts was performed via Fourier Transform Infrared Spectroscopy (FTIR), scanning electron microscopy (SEM) and elemental composition via energy dispersive X-ray spectroscopy (EDX). Results of the thermally degraded byproducts are reported relative to the representative non-degraded form of the respective nanoclay being investigated. Specifically, FTIR analysis of the characteristic peak of montmorillonite (MMT) at 1000 cm^{-1}, indicative of Si-O-Si stretching vibration of silicates,[22,40] was observed for all the nanoclays. However, the peak was shifted to a higher wavelength for the thermally degraded byproducts (Figure 1c,d,e) when compared to their as-received counterparts. Further, all of the as-received nanoclays also displayed a peak at 900 cm^{-1} indicative of Al-OH-Al deformation of aluminates,[22,40,43] while the organically modified as-received nanoclays displayed a peak at 840 cm^{-1} presumably resulted from the deformation of OH linked to Al^{3-} and Mg^{2-} respectively.[43] Previous analysis showed that peaks at 790 and 630 cm^{-1} are associated with Si-O groups[43] and out of the plane vibration of Al-O group,[44] respectively.

Additionally, the three, as-received, organically modified nanoclays also had peaks at 2920, 2850, and 720 cm^{-1} respectively, presumably resulting from the asymmetric and symmetric stretching of their C-H groups included in methylene or alkane rock of CH_2 for alkanes with 7 or more carbons, respectively,[22,40,43] and indicative of the incorporation of their respective organic modifiers. The 3 peaks were however no longer present in the spectra of the thermally degraded byproducts of these nanoclays, confirming their organic modifiers degradation.[40] Additionally, the peak around 3600 cm^{-1} with small repeated peaks moving out towards 3800 cm^{-1} for the as-received clays, indicative of silanol groups on the SiO_2 tetrahedral sheets,[45] was no longer present for the thermally degraded byproducts. Along with the shift recorded for 1000 cm^{-1} peak, the only other peaks remaining for the thermally degraded byproducts were at 780 and 640 cm^{-1} respectively, and are presumably associated with Si-O groups[43] and Si-O-Si bending.[43] Moreover, the peaks associated with Al-OH-Al deformation and OH linked to Al^{3-} and Mg^{2-} were no longer present for any of the

byproducts, again showing the degradation of the alumino-silicate lattice due to the loss of structural water.[40,41,42]

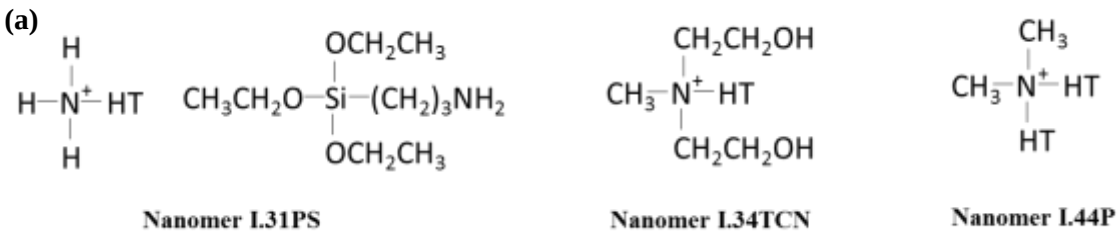

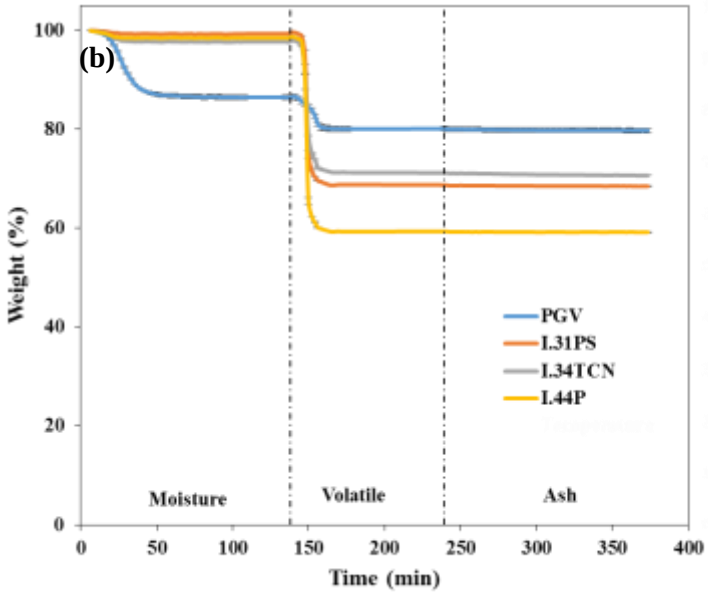

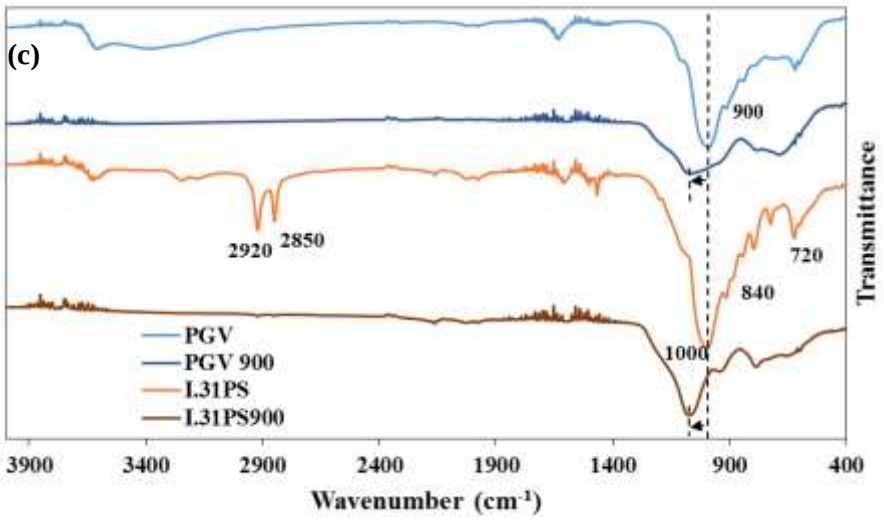

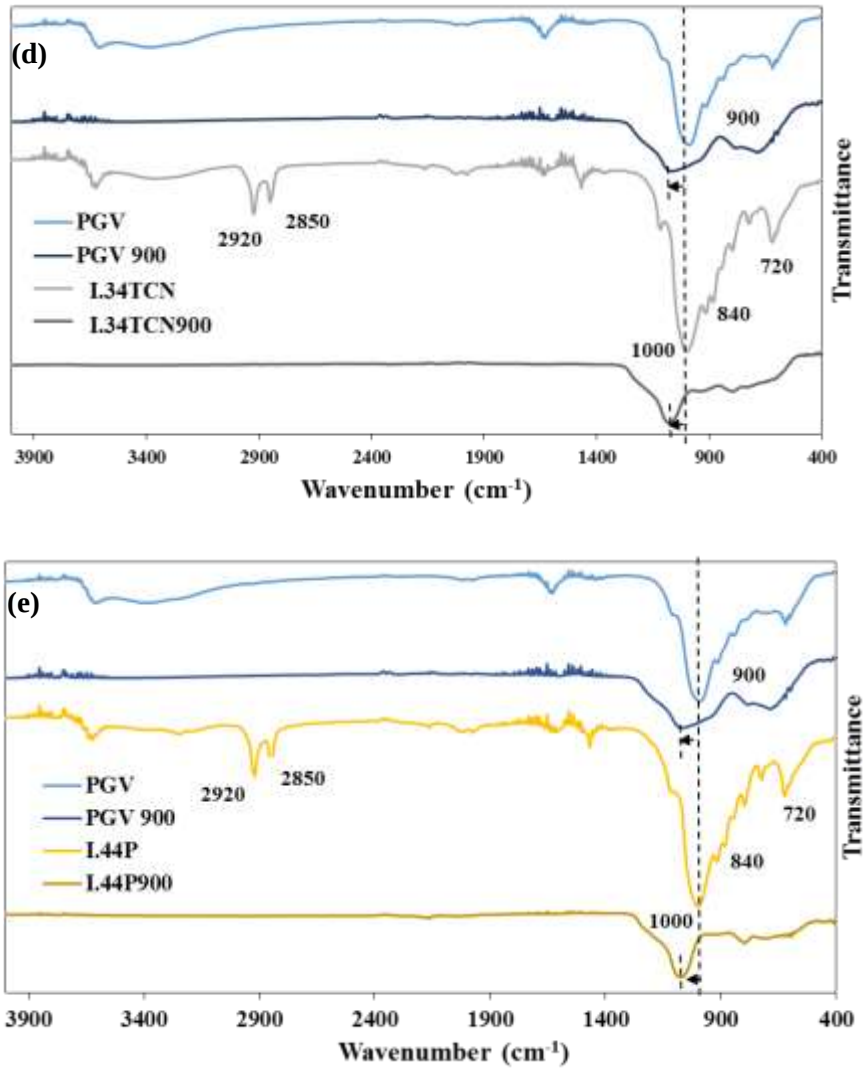

Figure 1: (a) Chemical structures of the organic modifiers present in I.31PS, I.34TCN, and I.44P (b) Thermal degradation profile of PGV and the 3 organically modified nanoclays (n=2). FTIR spectrum for (c) I.31PS, (d) I.34TCN, and (e) I.44P along with their thermally degraded byproducts, all relative to PGV and PGV900 (n=2).

SEM surface morphology analyses revealed layered platelet surfaces (Figure 2a-d) for all the nanoclays being investigated, with I.44P appearing to have a sharper, more defined platelet-like geometry when compared to the other nanoclays being investigated. PGV and I.34TCN displayed similar morphologies in that their platelet edges seemed smoother, i.e., more rounded, relative to I.31PS and I.44P. Also, while I.31PS had a similar morphology to I.44P. It did not seem to contain as many platelets, thus revealing a slightly smoother aspect of its surface.

The observed SEM differences are attributed to the presence of the organic modifiers and their individual integration since previous analyses have showed that functionalization of pristine nanoclays could influence their basal spacing.[46] In particular, basal spacing was shown to increase with increasing cation exchange capacity of a modifier[46] or with increasing its alkyl length.[42] Such increases are presumably due to lowering of the surface energy of the platelets upon introduction of the modifier, thus allowing for their easier separation and better mixing within polymer matrices during manufacturing of composites.[12] The easier dispersion also was shown to allow for better exfoliation within such polymer matrices,[4] thus resulting in nanocomposites with enhanced properties, such as increased mechanical strength[8] and barrier properties,[8] when compared to the neat polymer.[8] Further, previous analysis showed that structure of the nanoclay is influenced by the lateral layer arrangements of the modifiers,[46] and is also dependent on the concentration of the modifier used as well as the degree into which the organic molecules are able to fit/adsorb into the nanoclay individual platelet surface.[46]

Thermal degradation caused for a loss in the platelet morphology for all the byproducts but I.44P900 which seemed to display platelets with smoother edges, relative to its non-degraded form (Figure 2e-h). PGV900 also displayed a smoother surface, while both I.31PS900 and I.34TCN900 displayed a fragmented surface, with platelets jutting out, potentially due to slower degradation due to the organic modifier. The loss in platelet structure recorded upon thermal degradation was most likely caused by the high temperatures encountered which could cause their breakdown likely by dehydroxylation of their aluminosilicates' lattice.[42,46] This is supported by previous study by Ounoughene et al., who also observed a change in morphology of halloysite nanotubes (HNTs) after their exposure to high temperatures (beyond 1000 ºC).[20]

Elemental composition analyses (EDX) showed that the as-received organically modified nanoclays had significantly higher amount of carbon, relative to their pristine counterparts (Figure 3a). Additionally, they also had significantly lower amounts of oxygen, sodium, magnesium, silicon, and calcium, relative to PGV. These changes in elemental composition further confirmed the individual organic modifier functionalization.[39] Moreover, EDX analyses showed that I.34TCN had a lower amount of carbon and higher amount of oxygen relative to I.44P and I.31PS, again, indicative of the presence of the 2 hydroxyl moieties associated with the functionalizing modifier.[17] Additionally, I.31PS had a higher amount of oxygen relative to I.44P, likely due to the presence of the silane coupling agent which contains carbon and oxygen.[17]

After thermal degradation, all of the nanoclays experienced decreases in their respective carbon contents (up to 40-60 % loss) and increases of their oxygen (up to 40-85% increase), magnesium, aluminum, and silicon contents respectively (Figure 3b). These changes were only significant for the organically modified nanoclays, most likely due to the loss of their individual organic modifiers. Lastly, the organically modified clays had around 40% decrease in their iron contents after thermal degradation. The general trends in elemental composition between PGV and the modified nanoclays also persisted after thermal degradation, relative to the as-received forms (Table S2). Further, the only significant difference between PGV and PGV900 was an increase in magnesium, showing that the organic modifiers played a large role in the changes observed in elemental composition due to thermal degradation.

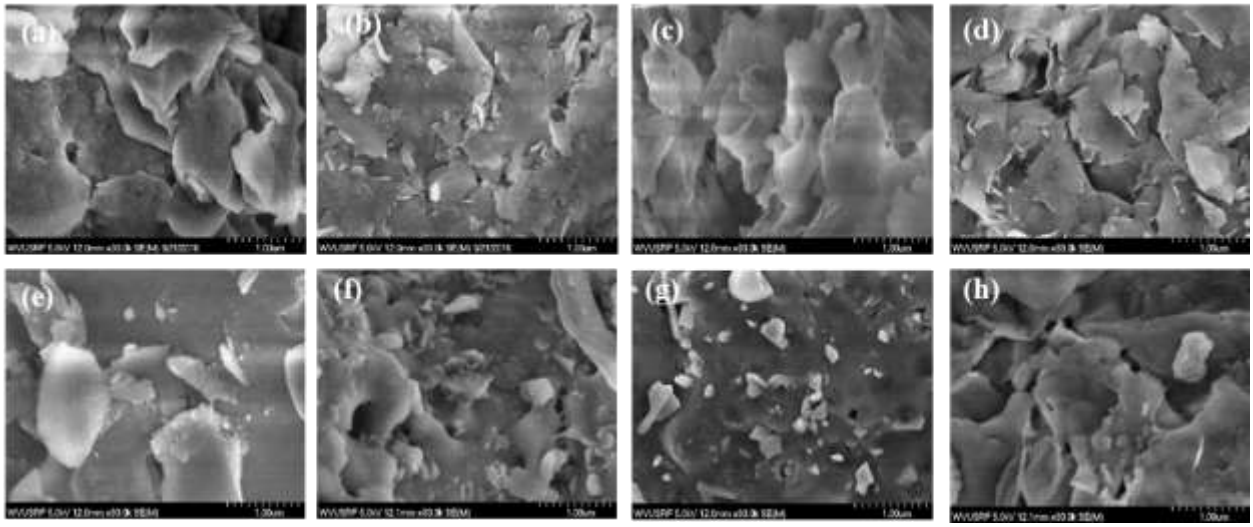

Figure 2: Surface morphology of (a) PGV, (b) I.31PS, (c) I.34TCN, and (d) I.44P and thermally degraded (e) PGV900, (f) I.31PS900, (g) I.34TCN900, and (h) I.44P900 as determined by SEM.

Dispersity Analysis of Nanoclays and Byproducts

Considering that particle size and distribution have been demonstrated to influence the toxicity of materials,[47] as well as internalization into exposed cells,[47] we first assessed nanoclays and byproducts dispersion in cellular media. Such analyses were also expected to provide insights into any sedimentation and/or possible diffusion of the materials thus helping ensure that there are no-mass transfer limitations when exposure to cells is attempted thus limiting an uneven exposure and localized toxicological effects.

Size distributions of the nanoclays and byproducts were assessed by dynamic light scattering (DLS); for this, samples were dispersed in their cell-specific media. A pulmonary surfactant (Survanta) of 90 % lipid and 10 % protein was also used, to provide a model of similar consistency to the pulmonary surfactant environment of humans.[48] How a particle interacts with a pulmonary surfactant will affect its deposition on and interaction with lung cells, its clearance, and overall alveolar surface tension.[49] Analyses are reported relative to control buffer solution (phosphate buffered saline: PBS) normally used for cellular studies.

Overall, the organically modified nanoclays (with the exception of I.44P) had smaller sizes in PBS and DMEM, whereas larger sizes were observed when the modified nanoclays were placed in SAGM and Survanta respectively, all relative to the pristine nanoclay (PGV; Table S3). Specifically, analyses showed that 90 % of the I.44P dispersed in either PBS, DMEM, SAGM, or Survanta all had similar sizes and were smaller than 8 µm (Figure 3c). Moreover, 90 % of the I.31PS and I.34TCN clays dispersed in either control PBS, DMEM, or SAGM were smaller than 0.9 µm. Both I.31PS and I.34TCN displayed an increase in size when in Survanta, with 90 % of these nanoclays being under 8 µm. Lastly, 90% of the PGV dispersed in either SAGM or Survanta were smaller than 0.15 µm. Particle size increased when the nanoclay was placed in PBS and DMEM, with 90 % of it ranging under 9 µm for both solutions respectively. The specific distribution ranges are summarized in Tables S4-7.

The observed differences are likely due to the complex interactions of nanoclays with proteins and lipids in the media they were dispersed in,[50,51] formations of protein corneas,[50] or/and particle repulsion.[52] Specifically, particles that contain long hydrophobic chains, such as I.44P, have been previously shown to have increased protein-binding sites[53] relative to their more hydrophilic counterparts, likely leading to an increased agglomeration via inter-particle-protein bridges.[54] Additionally, the hydrophobic portions of the proteins may associate with the more hydrophobic nanoclays like the I.44P, to further cause for agglomeration.[51]

In the case of PGV, the hydrophilic portions of the proteins may also bind strongly to the nanoclay's hydrophilic surface,[51] also causing for particle agglomeration as seen in DMEM.[50] However, PGV, had a large decrease in size when placed in SAGM (relative to DMEM), signifying the influence of media composition.[55] Specifically, since SAGM has a greater variety of proteins and growth factors present relative to the DMEM, it could possibly allow for a more varied protein adsorption profile to this nanoclay and thus an increase in its dispersity. Similarly, I.34TCN and

I.31PS likely had less agglomeration in both DMEM and SAGM due to their relative intermediate hydrophobicity relative to PGV, resultant from their organic modifiers functionalization which could presumably cause for heterogeneous[51] or less protein adsorption[55] and thus a better dispersion.[55] Additionally, their organic modifiers containing hydroxyl (I.34TCN) and amine (I.31PS) groups could be more prone to interaction with proteins via hydrogen bonding, van der Waals forces, and electrostatic interactions respectively, causing for clay repulsion[52] to be recorded as an increase in their individual dispersity.

Overall, solution type did not appear to largely influence the size distributions of the dispersed byproducts however it did cause for an increase in the individual particle size distributions (Figure 3d). For instance, 90 % of the I.44P900 dispersed in DMEM, SAGM, Survanta and PBS were smaller than 9, 10, 11, and 11 µm, respectively. I.31PS900 displayed similar size distributions in all 4 solutions, with 90 % of its particles smaller than 9 µm in PBS, DMEM, and Survanta and 90 % of its particles smaller than 7 µm in SAGM only. Ninety % of the I.34TCN900 dispersed in DMEM, SAGM, or Survanta were smaller than 10, 9, and 11 µm, respectively; 90 % of the particles in PBS were smaller than 10 µm. Finally, 90 % of the PGV900 dispersed in DMEM, SAGM, or Survanta were smaller than 12, 9, and 8 µm, respectively. Additionally there was no longer any differences between the organically modified nanoclays (i.e. difference in size for I.31PS and I.34TCN relative to I.44P in DMEM, SAGM, and PBS) after thermal degradation, further confirming that once the organic modifier was removed and the platelet structure was melted and fused, no platelet exfoliation or breakup of loose agglomerates might have taken place, thus, the surface chemistry and resulting molecular interactions might have changed. In particular, since the byproducts no longer have their organic modifiers present, this would likely decrease the amount of adsorbed protein and, dependent on the modifier, the variety of proteins being adsorbed, thus in turn decreasing the stability of the suspensions[56] and resulting in the recorded larger sizes.

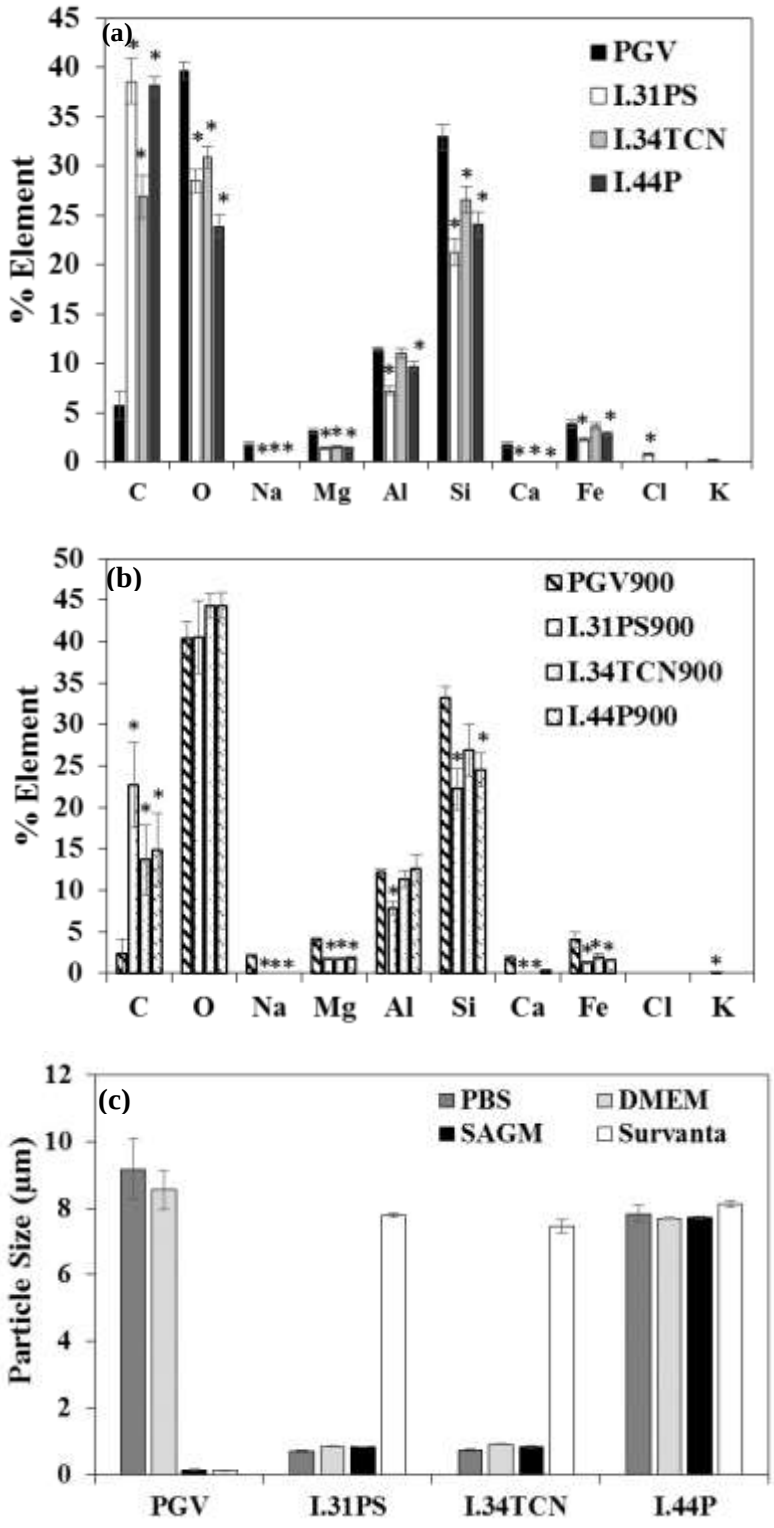
(a)
PGV
I.31PS
I.34TCN
I.44P
% Element
C
O
Na
Mg
Al
Si
Ca
Fe
Cl
K
(b)
PGV900
I.31PS900
I.34TCN900
I.44P900
% Element
(c)
PBS
DMEM
SAGM
Survanta
Particle Size (µm)
PGV
I.31PS
I.34TCN
I.44P

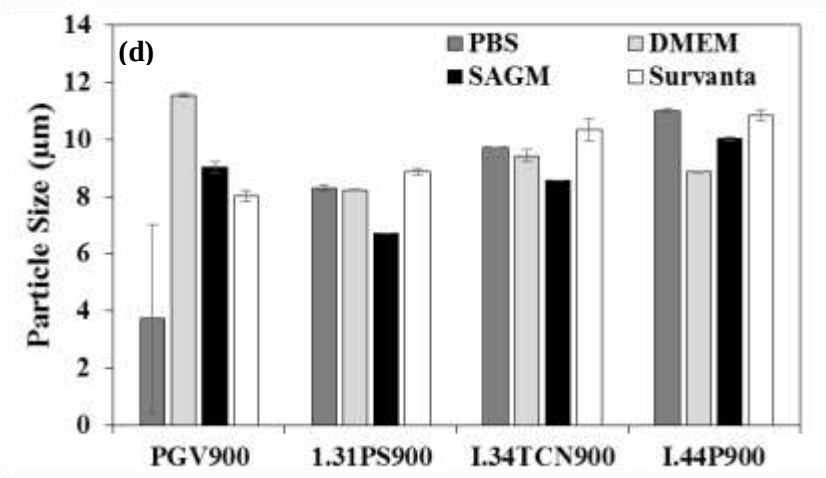

Figure 3: Elemental composition of (a) as-received nanoclay and (b) their thermally degraded byproducts as determined by EDX at 1 µm (n=10). The symbol * indicates significant differences between the unmodified clay (PGV/PGV900) and the organically modified clays. Average size of <90% of (c) the as-received nanoclays in solutions of PBS, DMEM, SAGM, or Survanta (d) as well as their byproducts (n=3).

Lastly, the different size distributions observed for nanoclays or byproducts in Survanta could be a result of Survanta's high content of phospholipids,[49] which could largely change the agglomeration states of the dispersed materials. Specially, the increased hydrophobicity of the modified nanoclays relative to PGV, likely caused for an increased agglomeration and higher interactions with the hydrophobic tails of the phospholipids.[48] Sauer et al. found similar results for hydrophobic nanoparticles that generally seemed to agglomerate more when in the presence of lipids and proteins relative to their more hydrophilic counterparts.[57]

Toxicity Screening Based on Nanoclays' Physico-chemical Properties

Upon dispersity analysis, nanoclays and byproducts dispersed in the complementary media were used in different concentrations (i.e., 0-197 µg/cm^2) and exposed to human bronchial epithelial (BEAS-2B) cells and small airway epithelial cells (SAECs) respectively, for 24 h. The dose range was chosen to mimic exposure in manufacturing and disposal condition areas, with light exposure being defined as minimal concentration that could lead to inhalation in a manufacturing or disposal environment and acute exposure being defined as a 45-year working lifetime exposure based on 8 h/day and 50 weeks/year taking into account particle and lung characteristics.[58] The resulting IC_{50} values (concentration of the nanoclays or byproducts that

inhibit cell growth by 50%) were extrapolated from the dose response trend lines derived from raw data (Table S8). IC_{50} is an acceptable mean for early measure and comparison of particle cytotoxicity,[59] and could help identify early deleterious mechanisms associated with nanoclays exposure to cellular systems.

Overall, the as-received nanoclays, with the exception of I.44P in SAECs, displayed a greater cytotoxicity relative to their thermally degraded byproducts when exposed to both BEAS-2B cells and SAECs respectively (Figure 4a). In addition, organically modified nanoclays showed higher toxicity than their pristine counterpart (PGV), again, with the exception of I.44P in SAECs. The byproducts showed similar toxicity with the PGV900 for the BEAS-2B cells (with PGV900 being the least toxic), while all the byproducts had a similar toxicity to each other for the SAECs. The highest degree of toxicity was observed for I.34TCN (which has a long alkyl chain and 2 hydroxyl molecules),[17] followed by lower degrees of toxicity for I.31PS (which has a long alkyl tail and a silane coupling agent), and finally I.44P (which has 2 long alkyl chains), in both cell lines being investigated. Lastly, SAECs showed a greater sensitivity relative to BEAS-2B cells for all the nanoclays and byproducts, with the exception of I.44P.

We hypothesize that the cytotoxicity differences are based on the different interactions of the organic modifiers-functionalized nanoclays that could influence particle's degree of hydrophobicity. Previous studies have showed that such chains could interact with the cell membrane lipids to cause for changes in membrane integrity.[60] For instance, Farcal et al. showed that TiO_2 nanomaterials with a hydrophobic coating were more toxic than their hydrophilic counterpart in murine alveolar macrophages.[60] Additionally, the increased toxicity of I.34TCN relative to I.31PS and I.44P was likely due to the presence of bio-reactive groups, such as hydroxyl present in its organic modifier. Previous studies on particles containing bio-reactive groups have showed similar results,[61,62] with analysis showing that such particles could interact with biological macromolecules[61] such as phospholipids and proteins[62,63] via hydrogen bonding and electrostatic interactions,[63] disrupt the cell membranes[62,63] and initiate apoptosis.[63] For instance, Zhang et al. showed a decrease in BEAS-2B cell viability upon their exposure to amorphous silica nanoparticles with increased hydroxyl contents.[62] Das et al. found that graphene sheets containing reactive hydroxyl functional groups were more toxic than sheets without these groups and of the same sizes,[61] while Zhang et al. showed that hydroxyl groups can generate reactive oxygen species (ROS)[62] to be responsible for damage to macromolecules, such as nucleic acids, proteins, and

lipids, and for deregulation of cellular signaling pathways associated with cell proliferation, survival, and mitochondrial oxidative stress.[64]

While I.31PS did not contain hydroxyl groups, it did contain a silane coupling agent [17] and an amine group which were shown to also be capable of binding to both organic and inorganic compounds,[65] to allow for interactions with biological molecules containing hydroxyl groups[66] as well as the negatively charged cell membrane.[67] Positively charged particles such as the silane terminated amine groups in I.31PS will also have a better cell internalization[68] which could further contribute to its observed increased toxicity.[63] While the interchange of bio-reactive groups with long alkyl chains has showed a decrease in toxicity, as observed by the reduction in toxicity of I.44P relative to the other two organically modified nanoclays and by previous studies,[68] their presence on particles still caused toxicity most likely because of disturbances of hydrophobic interactions between the lipids and proteins and possibly induced changes in cell signaling.[69]

The byproducts were less toxic relative to their as-received counterparts in both cell lines (except for I.44P/I.44P900 in SAECs). This is presumably due to the recorded loss of their organic modifiers,[25,23,22] reduction of their iron contents, and changes in their platelets morphology[21] as demonstrated by the SEM and EDX analyses or to the loss of the silanol groups on the SiO_2 tetrahedral sheets of the nanoclays[45] as demonstrated by the FTIR analysis. Specifically, our EDX analysis confirmed that iron decreased by around 40% in the byproducts thus causing for lower toxicity as supported by previous analysis that showed that high levels of iron promote cell death,[70] and decrease ATP production.[71] Complementary, silanol groups (especially the disorganized silanols) have been previously hypothesized to contribute to SiO_2 toxicity.[72]

Along with the presence of the organic modifiers, the size and general solubility of the nanoclays and byproducts may also be contributing to the observed differences in cytotoxicity. As seen by the DLS measurements, smaller sized nanoclays (I.34TCN and I.31PS) seemed to show an increase in cytotoxicity relative to the larger as-received nanoclays (PGV and I.44P) as well as their byproducts presumably due to a resultant higher surface area[73] or higher degree of uptake.[74,75] Results are consistent with previous analysis;[74] specifically, Napierska et al. found that smaller sized particles (14-16 nm diameter) were more toxic relative to their larger sized counterparts (19-335 nm), as well as were internalized by human endothelial cells at a faster rate.[74] Additionally, Lin et al. found that smaller Stöber silica nanoparticles had higher hemolytic activity than larger counterparts, most likely resulting from a larger surface area of such particles.[75] However, PGV

displayed the smallest size distribution in SAGM (media for SAECs), yet still had a lower degree of toxicity relative to I.34TCN and I.31PS, showing that the chemical composition of the organic modifiers also plays a large role in the toxicity profiles of these nanoclays, as detailed above. The resultant smaller size of PGV could have attributed to it having a higher degree of toxicity relative to I.44P though in SAECs, which was not observed in the BEAS-2B cells when I.44P and PGV had a similar size distribution.

Overall, SAECs showed a greater sensitivity (of about 4 to 5 times) for all the clays (except I.44P), while the sensitivity of the primary cells exposed to byproducts was only about 2 to 4 times higher relative to BEAS-2B cells. This is presumably due to the fact that primary cells more closely mimic their tissue of human origin; contrary, their immortalized counterparts can undergo mutations as well as contain viral genes to influence their overall stability thus reducing their susceptibility to external agents used for toxicity analysis.[34] Further, immortalized cell lines generally are not as genetically stable as primary cells and lack function and markers often seen *in vivo*.[35] Our results confirm previous experiments in which primary cells displayed a higher degree of toxicity when compared to immortalized cell lines upon exposure to nanoparticles with similar aspect ratios.[38] Moreover, the general trends in our experiments remained the same between the 2 cell lines showing validation of the obtained results and overall confirming that such cell-based systems are suitable models for assessing inhalation toxicity *in vitro*.

Changes in IC_{50} were complemented by the changes in cell morphology (Figure 4b) which is known to be an indicator of overall cell health.[76,77] Specifically, treatment with the nanoclays and byproducts caused for changes in the cellular shape of both cell types relative to the control, more so for the BEAS-2B. These cells were more stretched, thin-like structures relative to the more oval shapes displayed by the controls (especially in regards to their exposure to the byproducts). When comparing BEAS-2B with the primary cells, there was observed that the immortalized cells had a more stretched profile. Generally, treatment with PGV produced more circular cells than any of the other treatments, in both cell lines and also a lower cell confluence especially in primary cells, likely serving as a signal of cell death and thus complementing our IC_{50} values as well as possibly indicating a different mechanistic-based cytotoxic effect.[77] A difference in cytotoxic mechanism is also supported by different slopes of the dose response curves for PGV compared to organically modified nanoclays. For SAECs, exposure seemed to also cause changes in the cell membrane, which could then influence cell-cell and cell-substrate interactions.[76] Additionally,

there were changes in the cell monolayer with all of the treatments causing for a loss of monolayer integrity relative to controls for both cell lines being investigated and over 72 h time period (Figures S1 and S2). Such changes can further provide insights into the integrity of the tight junctions of the epithelial cells and mechanisms of toxicity since it is known that in the lung, the epithelial cells serve as a barrier to prevent the entrance of inhaled particles and pathogens.[78]

Our results overall hint that treatment with nanoclays or byproducts may cause cytoskeleton alterations[76] which may eventually lead to changes in cell mechanics,[79] differentiation, and organization.[80] Similarly, Snyder et al. showed changes in cellular morphology of primary human bronchial epithelial cells, from a cuboidal shape to a spindle-shaped, fibroblastoid appearance upon treatment with multi-walled carbon nanotubes.[78] Further, our systematic analysis showed that the observed differences in cytotoxicity are most likely due to synergistic effects resulting from (1) the presence of the organic modifiers and their surface chemistry, and/or (2) the individual nanoclay or byproduct particle size and surface area and general dispersibility. Synergism has been previously reported for other materials where the combined effects of size, shape, solubility, and/or surface functionalization all contributed to the toxicity profile of the material.[81,82] For instance, Tarantola et al. found that cetyl-trimethyl-ammonium bromide (CTAB)-coated spherical particles were more toxic than rod-shaped ones, due not only due to the shape, but also due to the way such shape influenced cluster formation and release of the CTAB.[81] Xia et al. found that the composition of metal oxide nanoparticles influenced toxicity; however, the degree of toxicity of the metal oxide was also dependent on its solubility in the media.[82] Based on our results, it is likely that the chemical composition of the organic modifier is influencing the degree of toxicity both directly and indirectly due to such modifier composition and effect on the size and dispersibility of the nanoclays. Such toxic effects were diminished when the cells were exposed to the byproducts.

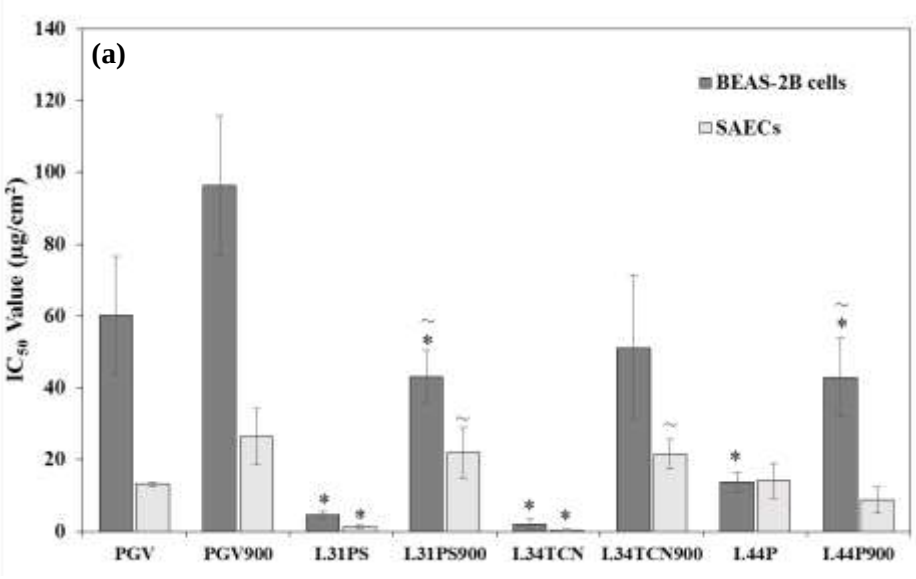

(b)
BEAS-2B Cells

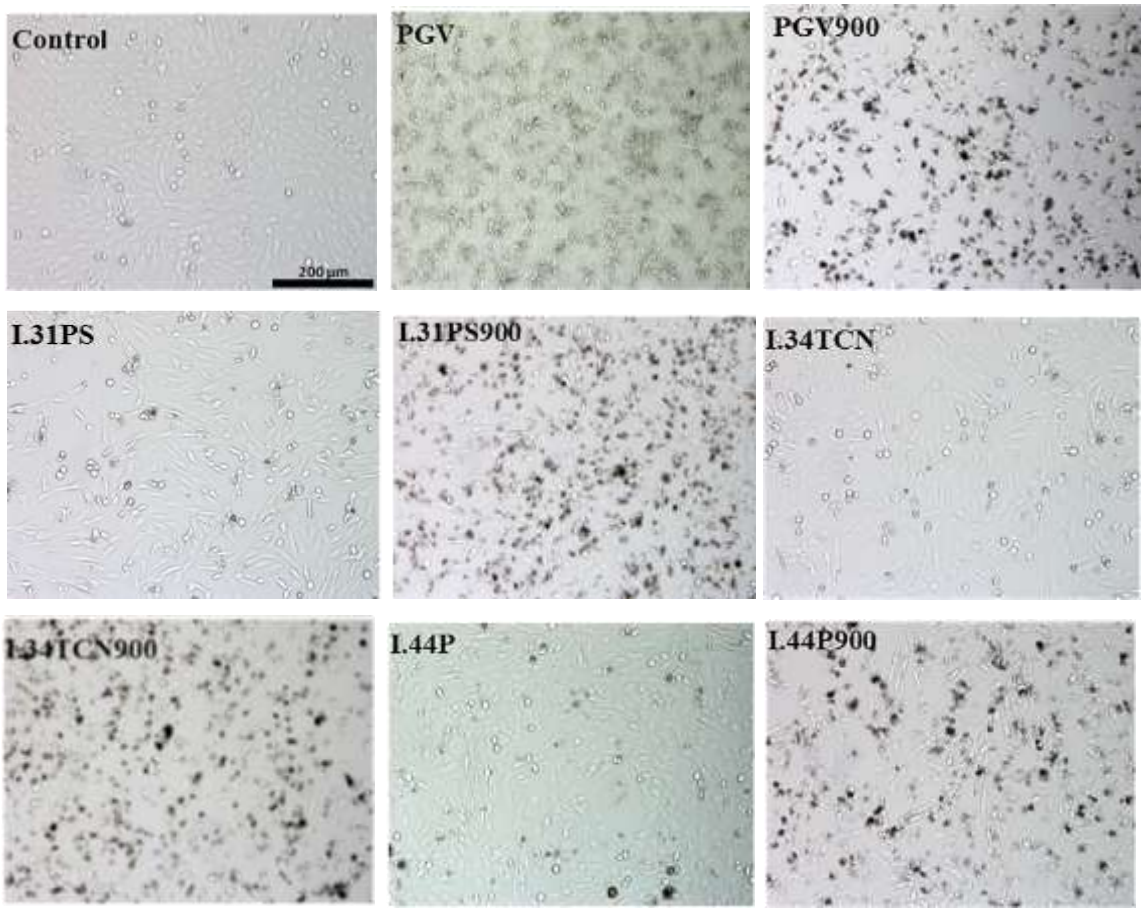

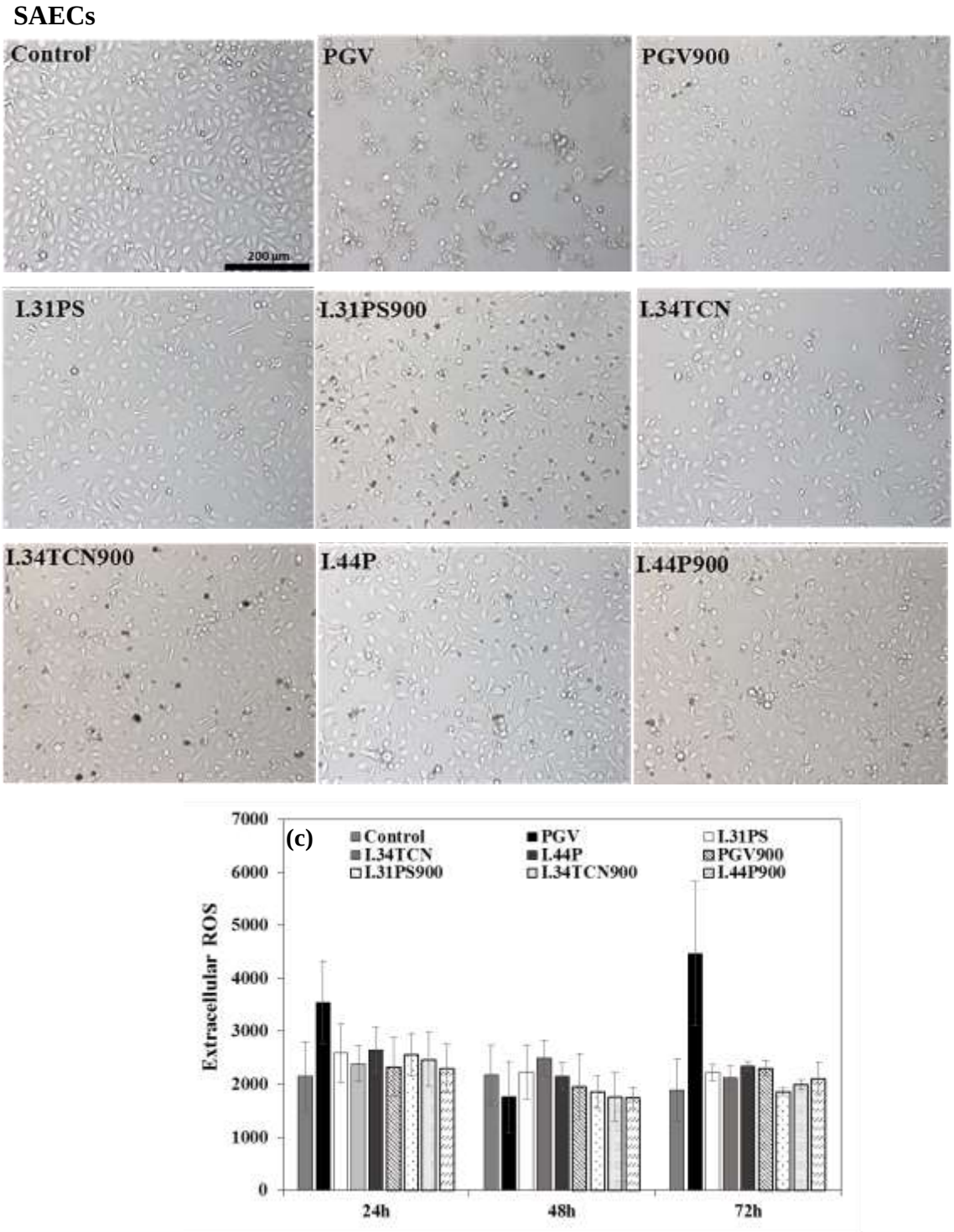

Figure 4: (a) IC_{50} values (µg/cm^2) for BEAS-2B cells and SAECs treated with as-received nanoclays and byproducts. The symbol * and ~ indicate significant differences between the unmodified nanoclay (PGV/PGV900) and the organically modified nanoclays and between the as-received nanoclay and its thermally degraded byproduct, respectively (n≥4 for each treatment). (b)

Representative optical images of BEAS-2B cells and SAECs treated with as-received nanoclays and byproducts at their respective IC_{50} dose after 24 h of exposure. (c) Extracellular ROS production by BEAS-2B cells after treatment with as-received nanoclays and byproducts at their respective IC_{50} dose over 72 h (n=4).

The observed synergism also implies that setting up rather simplistic platforms for toxicity evaluation will not provide a realistic or viable assessment strategy. Extracellular quantitative luminescence reactive oxygen species (ROS) assays,[62] were previously shown to be reliable and help provide information on oxidative stress and cellular metabolism[64] or damage to macromolecules.[64] Indeed, our control analysis showed that when using the extracellular ROS assay our results were inconclusive (Figure 4c). In particular, there was no significant trend observed in the cell response with treatment and moreover, there was a large variability in the extracellular ROS production. A similar response was also observed for doses above and below the IC_{50} value for each clay and byproduct (Figure S3). This could be due to the interaction of the nanoclays with the reagent. Our study accentuates the controversy of using such reagent for toxicity screening, and adds to the bases of other studies that showed[22] or did not show[83] ROS generation for cells exposed to nanoclays. In particular, Maisanaba et al. did not observe any ROS generation for Cloisite Na^+ and Cloisite 30B in HepG2 cells up to a dose of 88 µg/ml;[83] however, Lordan et al. found that Cloisite Na^+ did cause ROS generation in HepG2 cells at doses 50 µg/ml higher.[22]

Our study is the first to show that if one is to implement a platform for toxicity screening of nanoclays during their lifecycle, the overall functionality of the material needs to be tested, with functionality encompassing not only physico-chemical characteristics of the 'as-produced' material, but also its changes in a variety of conditions that reflect product implementation and disposal. Further, our study shows that cellular systems complexity needs to be accounted for, as differences in toxicity may be observed between cell lines and could be due to the different cell lines sensitivity as well as any related cellular changes upon cell line transformation. Only through such a dynamic interplay that could affect both the product "personality" as well as its shelf-life and interactions, one would fully evaluate product safety characteristics and impose viable disposal measures.

Conclusions

Our study showed that the chemical composition of individual organic modifiers used for nanoclays functionalization played large roles in their interactions with cellular systems. Specifically, differences in organic modifiers caused differential size distributions in dispersion cellular media and differential degrees of toxicity upon their or thermally degraded byproducts exposure to lung epithelial cells. The organically modified nanoclays I.34TCN and I.31PS displayed the highest degree of toxicity, followed by I.44P, all relative to the pristine PGV. Based on the chemical structure of their modifiers, it can be determined that modifiers containing bio-reactive groups, such as hydroxyl, are more toxic, relative to the modifiers containing long alkyl chains, likely due to increased interaction with biological macromolecules. Further, the composition of the bio-reactive group was shown to influence toxicity, as the modifier containing hydroxyl (I.34TCN) was more toxic relative to the one containing amine and silane (I.31PS). Finally, the byproducts displayed a loss in toxicity, likely due to the loss of their organic modifier, changes in size, shape, and elemental composition. Such changes in toxicity profiles of the as-received nanoclays relative to their byproducts emphasize the importance of examining such materials at all stages in their life cycle where human exposure might occur. Understanding how the physical and chemical properties of such materials influences toxicity can aid in safer design functionalities, while still maintaining beneficial properties to make them miscible with polymer matrices for food packaging applications.

Acknowledgements

This work was supported by National Science Foundation (NSF) grants 1434503 and 1454230, and the National Institutes of Health (NIH; R01-ES022968). The authors acknowledge use of WVU Shared Research Facilities and the WVU Analytical Lab.

Supporting Information

Chapter 3: Early Assessment and Correlations of Nanoclay's Toxicity to their Physical and Chemical Properties

Materials and Methods

Dispersion analysis

The size distribution of the nanoclays and thermally degraded byproducts was determined by dynamic light scattering (DLS) via the Mastersizer 2000 with a Hydro 2000S accessory (Malvern Instruments). For this, samples of Nanomer PGV (PGV), an unmodified, hydrophilic bentonite, Nanomer I.31PS (I.31PS), a nanoclay surface modified with aminopropyltriethoxysilane at 0.5-5 wt. % and octadecylamine at 15-35 wt. %, Nanomer I.34TCN (I.34TCN), a nanoclay surface modified with methyl dihdroxyethyl hydrogenated tallow ammonium at 25-30 wt. % and, Nanomer I.44P (I.44P), a nanoclay surface modified with dimethyl dialkyl amine at 35-45 wt. %, as well as their thermally degraded byproducts (PGV900, I.31PS900, I.34TCN900, or I.44P900 respectively) were dispersed either in Dulbecco's Modified Eagle Medium (DMEM, Life Technologies) containing 5% fetal bovine serum (FBS), or in Small Airway Growth Medium (SAGM, Lonza) with SingleQuots Kit (Lonza) containing bovine pituitary extract, hydrocortisone, human Epidermal Growth Factor, epinephrine, transferrin, insulin, retinoic acid, triiodothyronine, gentamicin/amphotericin-B, and 1 % bovine serum albumin (BSA). Also, the nanoclays and byproducts were dispersed in a control, phosphate buffered saline (PBS, Lonza) and in distilled water containing 0.15 mg/ml Survanta®, a pulmonary surfactant. The solutions were then bath sonicated and dropped into the Hydro 2000S until laser obscuration was within 10-20%. The size analysis was performed 3 consecutive times with a stirrer speed of 1750 rpm and under continuous sonication in the Hydro 2000S accessory.

Cell Culture

Immortalized human bronchial epithelial cells (BEAS-2B) from American Type Culture Collection (ATCC) were cultured in 100 mm dishes (Corning, Inc.) in DMEM, containing 5% FBS, 1 % L-glutamine, and 1 % penicillin-streptomycin. The cells were incubated at 37 ^{0}C, 5 % CO_2, and in an 80 % relative humidity; consistent sub-culturing took place using 0.05 or 0.25 %

trypsin (Invitrogen). Before each experiment, cells were grown to a monolayer of 90-100% confluency and cells in the 3^{rd}-6^{th} passage were used.

Additionally, small airway epithelial cells (SAECs) were cultured in SAGM with SingleQuots Kit and 1 % penicillin-streptomycin (Life Technologies). Cells were seeded into T-25 flasks (Corning, Inc.), grown to 75-80% confluency and subsequently split (5 passages total). All experiments completed with SAECs were performed using the same passage number.

Half Maximal Inhibitory Concentration (IC_{50})

BEAS-2B cells and SAECs were seeded into 12 well plates (Thermo Scientific) at densities of approximately $1.5x10^5$ and $2.0x10^5$ cells/ml, respectively. After 24 h, the cells were treated with PGV, I.31PS, I.34TCN, I.44P, or their thermally degraded byproducts at various doses ranging from 0 to 197 μg/cm^2. Before addition to the respective wells, each nanoclay or byproduct sample was sonicated for 10 min in a bath sonicator (2510 Branson; 100 W) with the concentrations used for exposure being serial dilutions from the original stock; cells in only media served as controls. After 24 h of exposure to individual treatment, the treated cells (as well as the controls) were washed to remove the nanoclays and byproducts, trypsinized, and stained with 0.4% trypan blue solution (Invitrogen). Subsequently, 10 μl of the sample containing the stained cells was added to a hemocytometer, and the number of cells in the 4 outer grids was counted through the use of the Leica DM IL optical microscope (Leica Microsystems) and a 10X objective. Analyses of the cellular proliferation post-exposure were used to extrapolate IC_{50} values that would also be used in the remaining cellular assays.

Cellular Imaging

BEAS-2B cells and SAECs were seeded at densities of $1.5x10^5$ and $2.5x10^5$ cells/ml, respectively, in 24 well plates. After 24 h the cells were treated with the as-received nanoclays and thermally degraded byproducts, dispersed in media via a bath sonicator, at their respective, determined IC_{50} dose. After 24, 48, and 72 h of treatment the cells were imaged through use of a Leica DM IL optical microscope (Leica Microsystems) with a 10X objective. Two replicates were performed with 10 images, per replicate, taken at random spots within the well for each control and treatment.

Extracellular Reactive Oxygen Species (ROS)

BEAS-2B cells were seeded into 24 well plates at a density of approximately $1.5x10^5$ cells/ml. After 24 h, the cells were treated with nanoclays and byproducts dispersed in media

through use of a bath sonicator at doses above and below their respective, determined IC_{50} value; cells exposed to only media served as control samples. After 24, 48, and 72 h of treatment, 50 µl of the media was transferred from the 24 well plate to its respective well in a black-bottomed 96 well plate (Corning, Inc.). Subsequently, 50 µl of PBS was added to each well in the 96 well plate. Fifty µl of the extracellular reactive oxygen species (ROS) assay reagent, Lumigen ECL Plus (Lumigen, Inc.), was also added to each well. The samples were subsequently incubated at room temperature for 5 min, in the dark before luminescence was evaluated using a FLUOstar OPTIMA plate reader (BMG LABTECH) at 600 nm. Media and treated media containing nanoclays or byproducts suspended in solution served as blanks. Respective cellular measurements of the samples were evaluated after subtracting the blanks in order to determine the effect treatment had on extracellular ROS. Four replicates were performed for each treatment.

Results

Table S1: Equations used to determine the percent moisture, volatile, and ash present in the 4 Nanomer nanoclays upon thermal degradation via the TGA701 Thermogravimetric Analyzer.

Content	**Equation**
Moisture	(([Initial Mass]-[Moisture Mass])/[Initial Mass])*100
Volatile	(([Moisture Mass]-[Volatile Mass])/([Initial Mass])*100
Ash	([Ash Mass]/[Initial Mass])*100

Table S2: Elemental composition of as-received nanoclay and their thermally degraded byproducts as determined by EDX at 1 µm (n=10). The symbol * and ~ indicate significant differences between the unmodified nanoclay (PGV/PGV900) and the organically modified nanoclays and between the as-received nanoclay and its thermally degraded byproduct, respectively.

	PGV	**I.31PS**	**I.34TCN**	**I.44P**	**PGV900**	**I.31PS900**	**I.34TCN900**	**I.44P900**
Carbon	5.70 +/- 4.50	38.59 +/- 7.13*	26.87 +/- 6.70*	38.15 +/- 2.95*	2.33 +/- 5.55	22.67 +/- 16.31*~	13.68 +/- 13.41*~	14.88 +/- 13.92*~
Oxygen	39.67 +/- 2.62	28.49 +/- 3.59*	30.84 +/- 3.55*	23.89 +/- 3.76*	40.34 +/- 6.43	40.42 +/- 13.97~	44.28 +/- 4.63~	44.33 +/- 4.78~
Sodium	1.77 +/- 0.54	0.00 +/- 0.00*	0.00 +/- 0.00*	0.00 +/- 0.00*	2.11 +/- 0.41	0.00 +/- 0.00*	0.00 +/- 0.00*	0.00 +/- 0.00*
Magnesium	3.12 +/- 0.70	1.37 +/- 0.27*	1.46 +/- 0.33*	1.33 +/- 0.31*	4.01 +/- 0.69~	1.75 +/- 0.57*	1.74 +/- 0.47*	1.84 +/- 0.58*~
Aluminum	11.33 +/- 0.76	7.19 +/- 1.33*	10.98 +/- 1.53	9.70 +/- 1.28*	12.12 +/- 1.22	7.86 +/- 2.48*	11.39 +/- 3.33	12.57 +/- 5.01
Silicon	32.93 +/- 4.20	21.21 +/- 4.34*	26.52 +/- 4.34*	24.07 +/- 4.01*	33.14 +/- 4.29	22.22 +/- 7.87*	26.90 +/- 9.82	24.50 +/- 6.33*
Calcium	1.70 +/- 0.77	0.00 +/- 0.00*	0.00 +/- 0.00*	0.00 +/- 0.00*	1.85 +/- 0.98	0.00 +/- 0.00*	0.00 +/- 0.00*	0.29 +/- 0.76*
Iron	3.79 +/- 1.18	2.27 +/- 0.69*	3.62 +/- 1.00	2.86 +/- 0.73*	4.02 +/- 2.83	1.29 +/- 0.51*~	2.02 +/- 1.30~	1.59 +/- 0.50*~
Chlorine	0.00 +/- 0.00	0.78 +/- 0.46*	0.00 +/- 0.00	0.00 +/- 0.00	0.00 +/- 0.00	0.00 +/- 0.00~	0.00 +/- 0.00	0.00 +/- 0.00
Potassium	0.00 +/- 0.00	0.12 +/- 0.38	0.00 +/- 0.00	0.00 +/- 0.00	0.00 +/- 0.00	0.20 +/- 0.24*	0.00 +/- 0.00	0.00 +/- 0.00

Table S3: Average particle size (µm) of <90 % of the four as-received nanoclays and their thermally degraded byproducts in solutions of PBS, DMEM, SAGM, or Survanta with +/- standard deviation (n=3). The symbol * and ~ indicate significant differences between the unmodified nanoclay (PGV/PGV900) and the organically modified nanoclays and between the as-received nanoclay and its thermally degraded byproduct, respectively.

	PGV	**I.31PS**	**I.34TCN**	**I.44P**	**PGV900**	**I.31PS900**	**I.34TCN900**	**I.44P900**
PBS	9.17 +/- 1.59	0.71 +/- 0.05*	0.75 +/- 0.06*	7.83 +/- 0.44	3.72 +/- 5.70	8.28 +/- 0.19~	9.71 +/- 0.01~	10.99 +/- 0.15~
DMEM	8.55 +/- 1.0	0.85 +/- 0.04*	0.92 +/- 0.04*	7.69 +/- 0.02	11.54 +/- 0.09~	8.23 +/- 0.02*~	9.42 +/- 0.36*~	8.85 +/- 0.01*~
SAGM	0.15 +/- 0.02	0.85 +/- 0.01*	0.85 +/- 0.05*	7.73 +/- 0.05*	9.02 +/- 0.34~	6.71 +/- 0.01*~	8.55 +/- 0.01~	10.04 +/- 0.12*~
Survanta	0.12 +/- 0.01	7.79 +/- 0.12*	7.46 +/- 0.35*	8.12 +/- 0.17*	8.03 +/- 0.33~	8.87 +/- 0.21*~	10.33 +/- 0.65*~	10.86 +/- 0.33*~

Table S4: Average particle size (µm) distributions of the 4 as-received nanoclays and their thermally degraded byproducts in PBS with +/- standard deviation (n=3). The symbol * and ~ indicate significant differences between the unmodified nanoclay (PGV/PGV900) and the organically modified nanoclays and between the as-received nanoclay and its thermally degraded byproduct, respectively.

	PGV	**I.31PS**	**I.34TCN**	**I.44P**	**PGV900**	**I.31PS900**	**I.34TCN900**	**I.44P900**
<10%	3.04 +/- 0.38	0.33 +/- 0.02*	0.38 +/- 0.03*	2.81 +/- 0.12	1.22 +/- 1.79	2.87 +/- 0.02~	3.15 +/- 0.00~	3.62 +/- 0.02~
<50%	4.78 +/- 0.72	0.44 +/- 0.03*	0.49 +/- 0.03*	4.11 +/- 0.22	1.88 +/- 2.82	4.30 +/- 0.06~	4.91 +/- 0.00~	5.81 +/- 0.06~
<90%	9.17 +/- 1.59	0.71 +/- 0.05*	0.75 +/- 0.06*	7.83 +/- 0.44	3.72 +/- 5.70	8.28 +/- 0.19~	9.71 +/- 0.01~	10.99 +/- 0.15~

Table S5: Average particle size (μm) distributions of the 4 as-received nanoclays and their thermally degraded byproducts in DMEM with +/- standard deviation (n=3). The symbol * and ~ indicate significant differences between the unmodified nanoclay (PGV/PGV900) and the organically modified nanoclays and between the as-received nanoclay and its thermally degraded byproduct, respectively.

	PGV	**I.31PS**	**I.34TCN**	**I.44P**	**PGV900**	**I.31PS900**	**I.34TCN900**	**I.44P900**
<10%	2.55 +/- 0.14	0.38 +/- 0.02*	0.44 +/- 0.02*	2.84 +/- 0.00*	4.06 +/- 0.01~	2.95 +/- 0.00*~	3.21 +/- 0.10*~	3.25 +/- 0.00*~
<50%	3.81 +/1 0.27	0.50 +/- 0.02*	0.57 +/- 0.02*	4.09 +/- 0.01	6.11 +/1 0.05~	4.28 +/- 0.00*~	4.89 +/- 0.20*~	4.83 +/- 0.01*~
<90%	8.55 +/- 1.0	0.85 +/- 0.04*	0.92 +/- 0.04*	7.69 +/- 0.02	11.54 +/- 0.09~	8.23 +/- 0.02*~	9.42 +/- 0.36*~	8.85 +/- 0.01*~

Table S6: Average particle size (μm) distributions of the 4 as-received nanoclays and their thermally degraded byproducts in SAGM with +/- standard deviation (n=3). The symbol * and ~ indicate significant differences between the unmodified nanoclay (PGV/PGV900) and the organically modified nanoclays and between the as-received nanoclay and its thermally degraded byproduct, respectively.

	PGV	**I.31PS**	**I.34TCN**	**I.44P**	**PGV900**	**I.31PS900**	**I.34TCN900**	**I.44P900**
<10%	0.05 +/- 0.01	0.37 +/- 0.00*	0.41 +/- 0.01*	2.75 +/- 0.02*	3.07 +/- 0.08~	2.52 +/- 0.00*~	2.83 +/- 0.00*~	3.28 +/- 0.01*~
<50%	0.08 +/- 0.02	0.50 +/- 0.02*	0.53 +/- 0.02*	4.03 +/- 0.02*	4.66 +/- 0.19~	3.61 +/- 0.01*~	4.23 +/- 0.00*~	5.11 +/- 0.03*~
<90%	0.15 +/- 0.02	0.85 +/- 0.01*	0.85 +/- 0.05*	7.73 +/- 0.05*	9.02 +/- 0.34~	6.71 +/- 0.01*~	8.55 +/- 0.01~	10.04 +/- 0.12*~

Table S7: Average particle size (μm) distributions of the 4 as-received nanoclays and their thermally degraded byproducts in Survanta with +/- standard deviation (n=3). The symbol * and ~ indicate significant differences between the unmodified nanoclay (PGV/PGV900) and the organically modified nanoclays and between the as-received nanoclay and its thermally degraded byproduct, respectively.

	PGV	**I.31PS**	**I.34TCN**	**I.44P**	**PGV900**	**I.31PS900**	**I.34TCN900**	**I.44P900**
<10%	0.03 +/- 0.00	2.42 +/- 0.16*	2.36 +/- 0.11*	2.64 +/- 0.02*	3.39 +/- 0.19~	2.94 +/- 0.02*~	3.35 +/- 0.21~	4.10 +/- 0.10*~
<50%	0.06 +/- 0.00	3.78 +/- 0.25*	3.63 +/- 0.19*	3.99 +/- 0.05*	4.94 +/1 0.25~	4.44 +/- 0.04*~	5.49 +/- 0.41~	6.34 +/- 0.10*~
<90%	0.12 +/- 0.01	7.79 +/- 0.12*	7.46 +/- 0.35*	8.12 +/- 0.17*	8.03 +/- 0.33~	8.87 +/- 0.21*~	10.33 +/- 0.65*~	10.86 +/- 0.33*~

Table S8: IC_{50} values ($\mu g/cm^2$) of BEAS-2B cells and SAECs treated with as-received nanoclays and thermally degraded byproducts.

	BEAS-2B	**SAECs**
PGV	60.3	13.2
I.31PS	4.5	1.3
I.34TCN	2.1	0.5
I.44P	13.7	14.2
PGV900	96.3	26.3
I.31PS900	43.2	21.8
I.34MN900	51.1	21.6
I.44P900	42.9	8.7

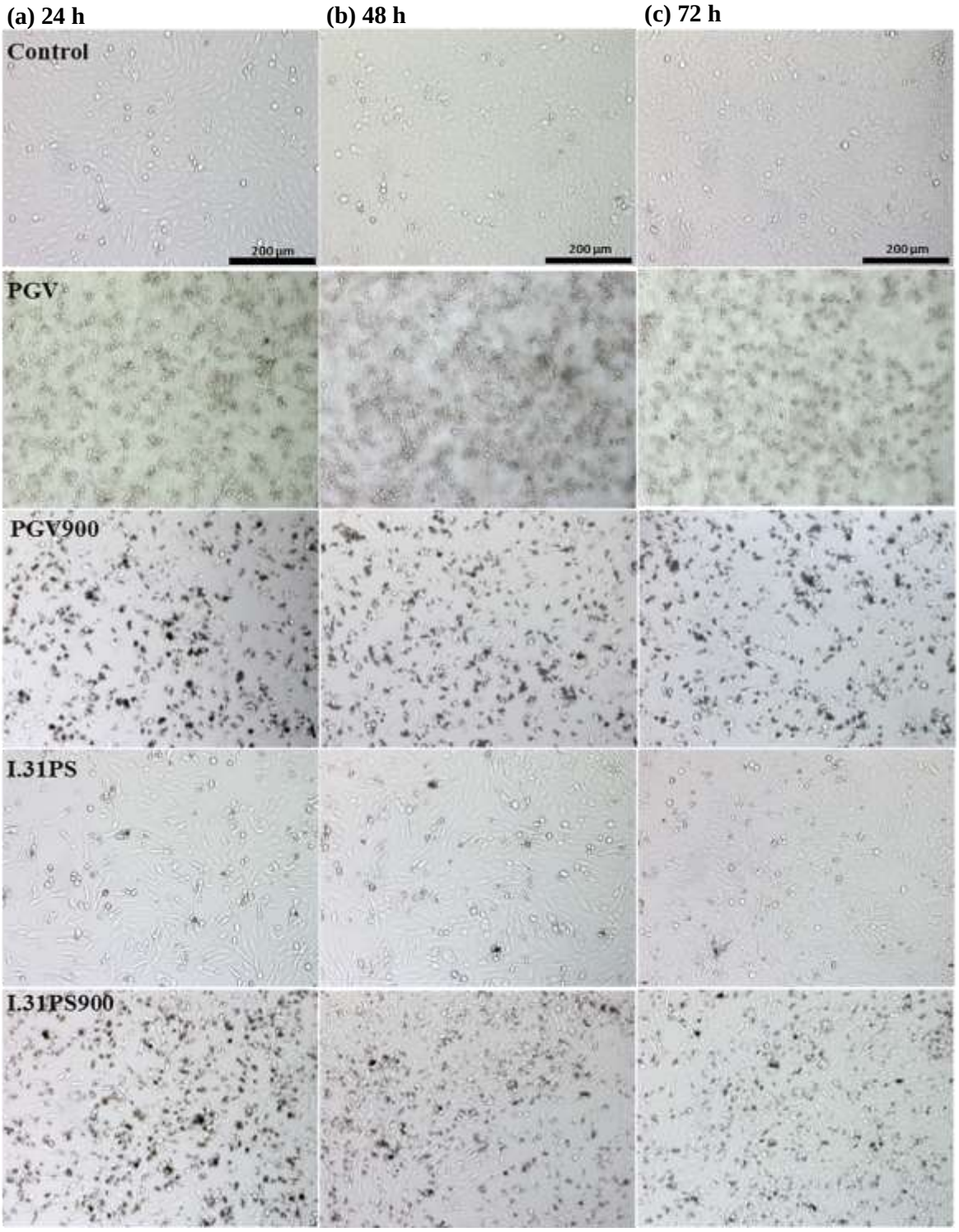
(a) 24 h
(b) 48 h
(c) 72 h
Control
PGV
PGV900
I.31PS
I.31PS900
200 µm
200 µm
200 µm

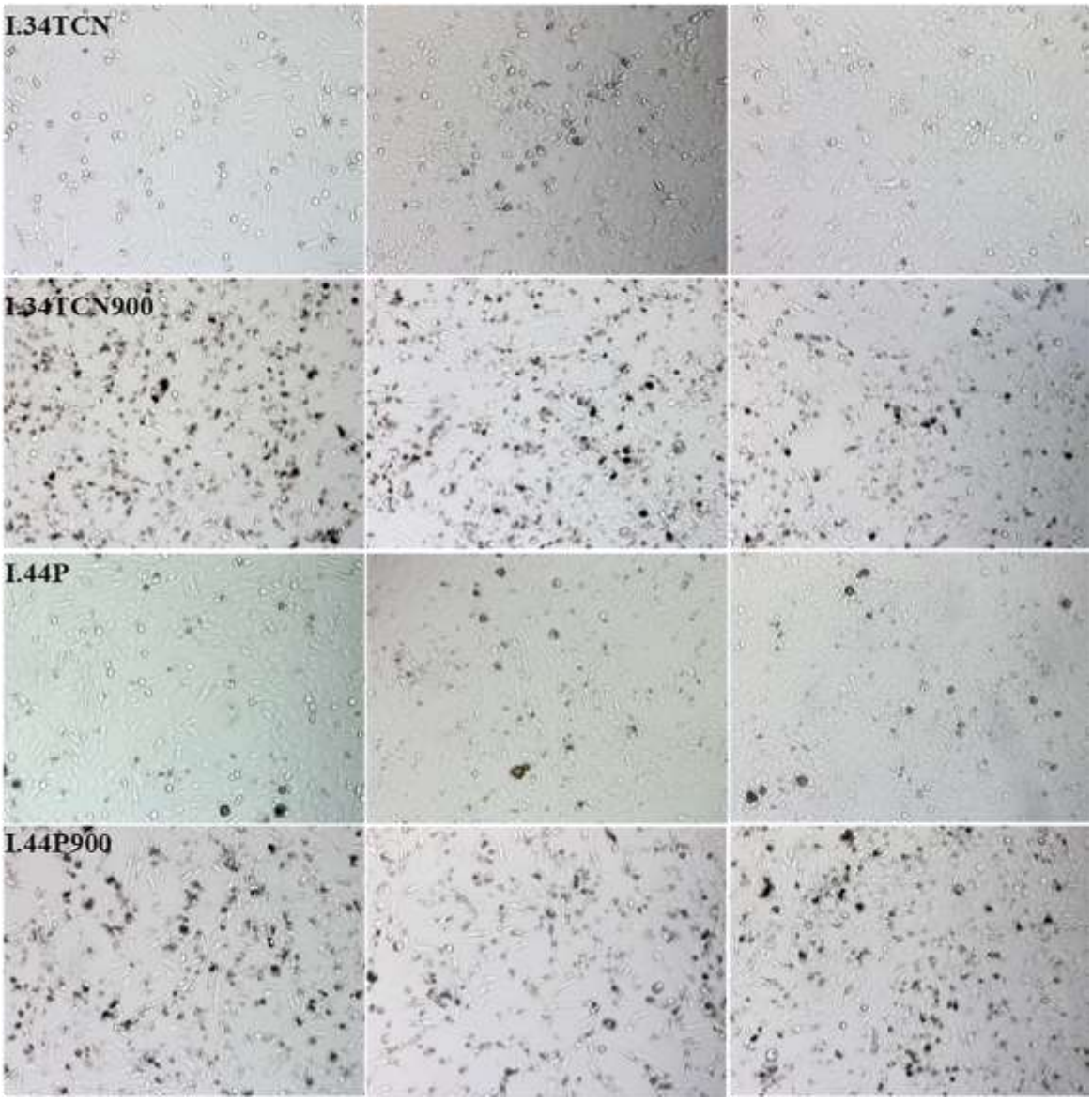

Figure S1: Representative optical images of BEAS-2B cells treated with as-received Nanomer nanoclays and thermally degraded byproducts at their respective IC_{50} doses at (a) 24 h, (b) 48 h, and (c) 72 h post-treatment (n=2).

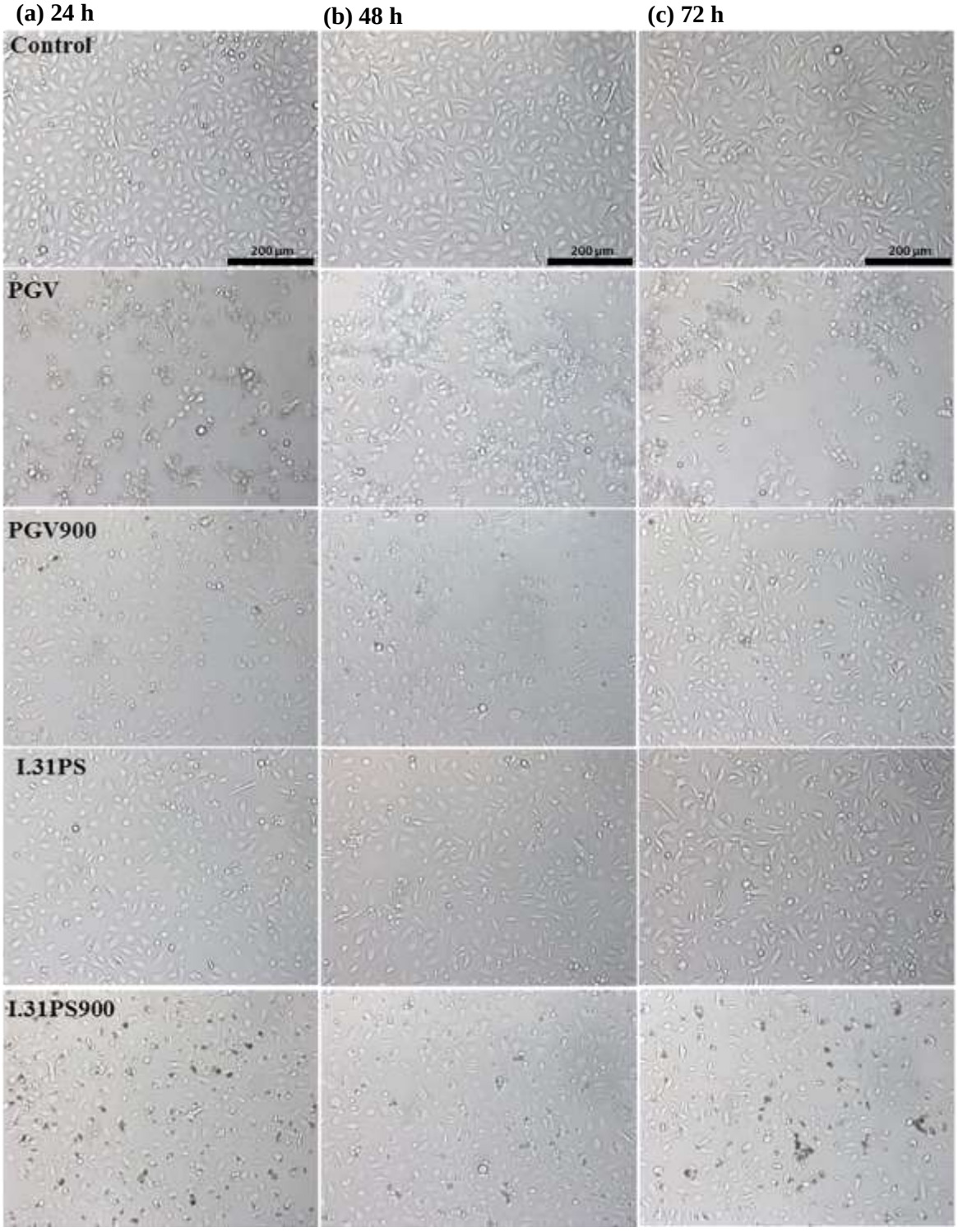
(a) 24 h
(b) 48 h
(c) 72 h
Control
PGV
PGV900
I.31PS
I.31PS900
200 µm
200 µm
200 µm

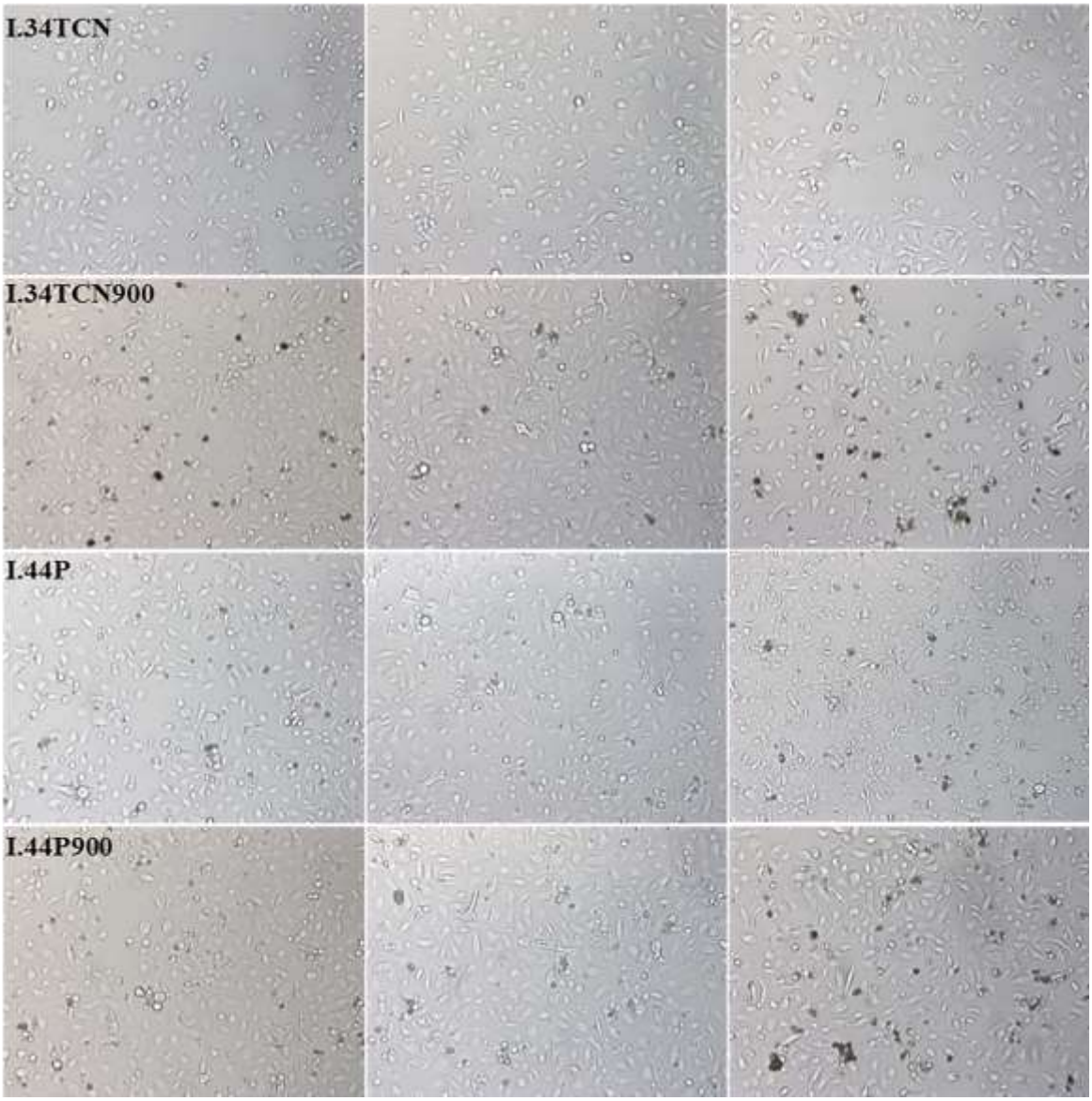

Figure S2: Representative optical images of SAECs treated with as-received Nanomer nanoclays and thermally degraded byproducts at their respective IC_{50} doses at (a) 24 h, (b) 48 h, and (c) 72 h post-treatment (n=2).

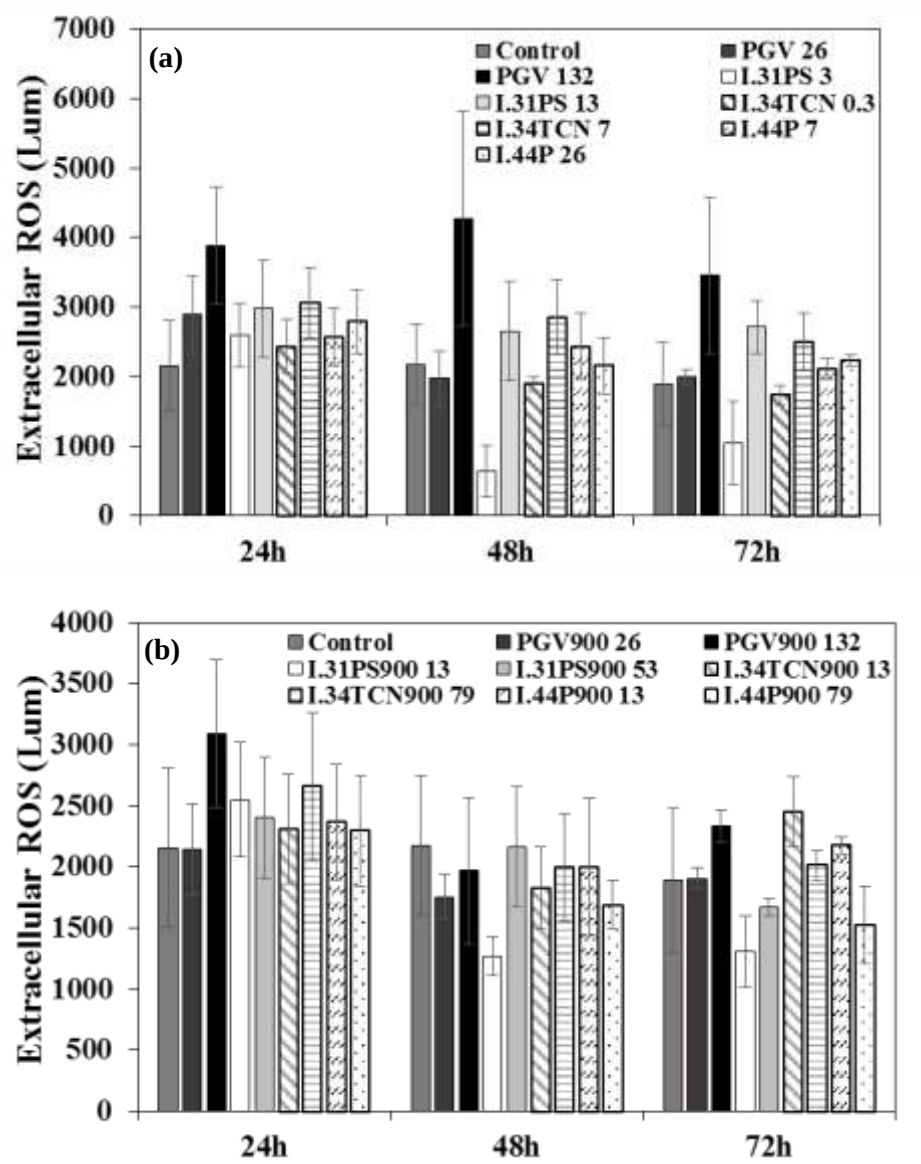

Figure S3: Extracellular ROS production by BEAS-2B cells after treatment with (a) as-received nanoclays above and below their respective IC_{50} dose and (b) thermally degraded byproducts above and below their respective IC_{50} dose over 72 h (n=4).

References

1. Carmargo, P. H. C.; Satyanarayana, K. G.; Wypych, F., Nanocomposites: Synthesis, Structure, Properties and New Application Opportunities. *Materials Research* **2009,** *12*, 1-39.

2. Mitrano, D. M.; Motellier, S.; Clavaguera, S.; Nowack, B., Review of nanomaterial aging and transformations through the life cycle of nano-enhanced products. *Environmental International* **2015,** *77*, 132-147.

3. Pereira de Abreu, D. A.; Paseiro Losada, P.; Angulo, I.; Cruz, J. M., Development of new polyolefin films with nanoclays for application in food packaging. *European Polymer Journal* **2007,** *43*, 2229-2243.

4. Ray, S.; Okamoto, M., Polymer/layered silicate nanocomposites: a review from preparation to processing. *Progress in Polymer Science* **2003,** *28*, 1539-1641.

5. Sahoo, R.; Sahoo, S.; Nayak, P. L., Synthesis and Characterization of Gelatin-Chitosan Nanocomposite to Explore the Possible Use as Drug Delivery Vehicle. *European Scientific Journal* **2013,** *9*, 135-141.

6. Mallakpour, S.; Dinari, M., Synthesis and Properties of Biodegradable Poly (vinyl alcohol)/ Organo-nanoclay Bionanocomposites. *Journal of Polymers and the Environment* **2012,** *20*, 732-740.

7. Silvestre, C.; Duraccio, D.; Cimmino, S., Food packaging based on polymer nanomaterials. *Progress in Polymer Science* **2011,** *36*, 1766-1782.

8. Paul, D. R.; Robeson, L. M., Polymer nanotechnology: Nanocomposites. *Polymer* **2008,** *49*, 3187-3204.

9. Molinaro, S.; Romero, M. C.; Boaro, M.; Sensidoni, A.; Lagazio, C.; Morris, M.; Kerry, J., Effect of nanoclay-type and PLA optical purity on the characteristics of PLA-based nanocomposite films. *Journal of Food Engineering* **2013,** *117*, 113-123.

10. Zheng, X.; Wilkie, C. A., Flame retardancy of polystyrene nanocomposites based on an oligomeric organically-modified clay containing phosphate. . *Polymer Degradation and Stability* **2003,** *81*, 539-550.

11. Manikantan, M. R.; Sharma, R.; Kasturi, R.; Varadharaju, N., Storage stability of banana chips in polypropylene based nanocomposite packaging films. *Journal of Food Science and Technology* **2014,** *51* (11), 2990-3001.

12. Majeed, K.; Jawaid, M.; Hassan, A.; Abu Baker, A.; Abdul Khalil, H. P. S.; Salema, A. A.; Inuwa, I., Potential materials for food packaging from nanoclay/natural fibres filled hybrid composites. *Material and Design* **2013,** *46*, 391-410.

13. Harkki, O., Biaxially oriented PLA-montmorrilonite-nanocomposite for barrier film applications. Sundqvist, H., Ed. VTT Technical Research Centre of Finland: 2012.

14. Floody, M. C.; Theng, B. K. G.; Reyes, P.; Mora, M. L., Natural nanoclays: applications and future trends-a Chilean perspective. *Clay Minerals* **2009,** *44*, 161-176.

15. Campos-Requena, V. H.; Rivas, B. L.; Pérez, M. A.; MGarrido-Miranda, K. A.; Pereira, E. D., Polymer/Clay nanocomposite films as active packaging material: Modeling of antimicrobial release. *European Polymer Journal* **2015,** *71*, 491-475.

16. Tang, Y.; Lewin, M., Maleated polypropylene OMMT nanocomposite: Annealing, structural changes, exfoliated and migration. *Polymer Degradation and Stability* **2007,** *92*, 53-60.

17. Feng, J.; Hao, J.; Du, J.; Yang, R., Effects of organoclay modifiers on the flammability, thermal and mechanical properties of polycarbonate nanocomposites filled with phosphate and organoclays. *Polymer Degradation and Stability* **2012,** *97*, 108-117.

18. Yourdkhani, M.; Mousavand, T.; Chapleau, N.; Hubert, P., Thermal, oxygen barrier and mechanical properties of polylactide-organoclay nanocomposites. *Composites Science and Technology* **2013,** *82*, 47-53.

19. Roes, L.; Patel, M. K.; Worrell, E.; Ludwig, C., Preliminary evaluation of risks related to waste incineration of polymer nanocomposites. *Science of the Total Environment* **2012,** *417-418*, 76-86.

20. Ounoughene, G.; Bihan, O. L.; Chivas-Joly, C.; Motzkus, C.; Longuet, C.; Debray, B.; Joubert, A.; Coq, L. L.; Lopez-Cuesta, J. M., Behavior and Fate of Halloysite Nanotubes (HNTs) When Incinverating PA6/HNTs Nanocomposite. *Environmental Science & Technology* **2015,** *49*, 5450-5457.

21. Verma, N. K.; Moore, E.; Blau, W.; Volkov, Y.; Babu, P. R., Cytotoxicity evaluation of nanoclays in human epithelial cell line A549 using high content screening and real-time impedance analysis. *Journal of Nanoparticle Research* **2012,** *14*, 1-11.

22. Lordan, S.; Kennedy, J. E.; Higginbotham, C. L., Cytotoxic effects induced by unmodified and organically modified nanoclays in human hepatic HepG2 cell line. *Journal of Applied Toxicology* **2011,** *31*, 27-35.

23. Sharma, A. K.; Schmidt, B.; Frandsen, H.; Jacobsen, N. R.; Larsen, E. H.; Binderup, M., Genotoxicity of unmodified and organo-modified montmorillonite. *Mutation Research/Genetic Toxicology and Environmental Mutagenesis* **2010,** *700*, 18-25.

24. Maisanaba, S.; Hercog, K.; Ortuño, N.; Jos, A.; Zegura, B., Induction of micronuclei and alteration of gene expression by an organomodified clay in HepG2 cells. *Chemosphere* **2016,** *154*, 240-248.

25. Janer, G.; Fernández-Rosas, E.; Mas del Molino, E.; González-Gáalvez, D.; Vilar, G.; López-Iglesias, C.; Ermini, V.; Vázquez-Campos, S., In vitro toxicity of functionalised nanoclays is mainly driven by the presence of organic modifier. *Nanotoxicology* **2014,** *8*, 279-294.

26. Maisanaba, S.; Puerto, M.; Gutièrrez-Praena, D.; Llan-Ruíz-Cabello, M.; Pichardo, S.; Mate, A.; Jordá-Beneyto, M.; Cameán, A. M.; Aucejo, S.; Jos, A., In vivo evaluation of activities and expression of antioxidant enzymes in Wistar rats exposed for 90 days to a modified clay. *Journal of Toxicology and Environmental Health, Part A: Current Issues* **2014,** *77*, 456-466.

27. Stueckle, T. A.; Davidson, D.; Derk, R.; Komberg, T. G.; Battelli, L.; Friend, S.; Orandle, M. S.; Wagner, A.; Dinu, C. Z.; Sierros, K.; Agarwal, S.; Gupta, R. K.; Rojanasakul, Y.; Porter, D. W.; Rojanasakul, L. W., Short-term Pulmonary Toxicity Assessment of Pre- and Post-Incinerated Organomodified Nanoclay in Mice. *ACS Nano* **2018**.

28. Tsai, C. S. J.; White, D.; Rodriguez, H.; Munoz, C. E.; Huang, C.-Y.; Tsai, C.-J.; Barry, C.; Ellenbecker, M. J., Exposure assessment and engineering control strategies for airborne nanoparticles: an application to emissions from nanocomposite compounding processes. *Journal of Nanoparticle Research* **2012,** *14* (7), 1-14.

29. Yuwen, H.; Meibian, Z.; Hua, Z.; Xiaxue, L.; Mingluan, X.; Xinglin, F.; Jiliang, H., Genetic damage and lipid peroxidation in workers occupationally exposed to organic bentonite particles. *Mutation Research/Genetic Toxicology and Environmental Mutagenesis* **2013,** *751*, 40-44.

30. Wagner, A.; Eldawud, R.; White, A.; Agarwal, S.; Stueckle, T. A.; Sierros, K. A.; Rojanasakul, Y.; Gupta, R. K.; Dinu, C. Z., Toxicity evaluations of nanoclays and thermally degraded byproducts through spectroscopical and microscopical approaches. *Biochimica et Biophysica Acta-General Subjects* **2017,** *1861*, 3406–3415.

31. Mittal, S.; Kumar, V.; Dhiman, N.; Chauhan, L. K.; Pasricha, R.; Pandey, A. K., Physico-chemical properties based differential toxicity of graphene oxide/reduced graphene oxide in human lung cells mediated through oxidative stress. *Scientific Reports* **2016,** *6*, 39548.

32. Wang, X.; Wu, Y.; Stonehuerner, J. G.; Dailey, L. A.; Richards, J. D.; Jaspers, I.; Piantadosi, C. A.; Ghio, A. J., Oxidant generation promotes iron sequestration in BEAS-2B cells exposed to asbestos. *American journal of respiratory cell and molecular biology* **2006,** *34* (3), 286-92.

33. Eldawud, R.; Wagner, A.; Dong, C.; Rojansakul, Y.; Dinu, C. Z., Electronic platform for real-time multi-parametric analysis of cellular behavior post-exposure to single-walled carbon nanotubes. *Biosensors and Bioelectronics* **2015,** *71*, 269-277.

34. Masters, J. R. W., Human cancer cell lines:fact and fantasy. *Nature Reviews: Molecular Cell Biology* **2000,** *1*, 233-236.

35. Alge, C.; Hauck, S.; Priglinger, S.; Kampik, A.; Ueffing, M., Differential protein profiling of primary versus immortalized human RPE cells identifies expression patterns associated with cytoskeletal remodeling and cell survival. *Journal of Proteome Research* **2006,** *5*, 862-878.

36. Jobe, A. H., Pulmonary Surfactant Therapy. *Drug Therapy* **1993,** *328*, 861-868.

37. Uy, B.; McGlashan, S. R.; Shaikh, S. B., Measurments of Reactive Oxygen Species in the Culture Media Using Acridan Lumigen PS-3 Assay. *Journal of Biomolecular Techniques* **2011,** *22*, 95-107.

38. Rujanapun, N.; Aueviriyavit, S.; Boonrungsiman, S.; Rosena, A.; Phummiratch, D.; Riolueang, S.; Chalaow, N.; Viprakasit, V.; Maniratanachote, R., Human primary erythroid cells as a more sensitive alternative in vitro hematological model for nanotoxicity studies: Toxicological effects of silver nanoparticles. *Toxicology in vitro : an international journal published in association with BIBRA* **2015,** *29* (8), 1982-92.

39. Ribeiro, S. P. S.; Estevao, L. R. M.; Nascimento, R. S. V., Effect of clays on the fire-retardant properties of a polyethlenic copolymer containing intumescent formulation. *Science and Technology of Advanced Materials* **2008,** *9*, 1-7.

40. Cervantes-UC, J. M.; Cauich-Rodriguez, J. V.; Vazquez-Torres, H.; Garfias-Mesias, L. F.; Paul, D. R., Thermal degradation of commercially available organoclays studied by TGA-FTIR. *Thermochimica Acta* **2007,** *457*, 92-102.

41. Xie, W.; Gao, Z.; Liu, K.; Pan, W.; Vaia, R.; Hunter, D.; Singh, A., Thermal characterization of organically modified montmorillonite. *Thermochimica Acta* **2001,** *367-368*, 339-350.

42. Xie, W.; Gao, Z.; Pan, W.; Hunter, D.; Singh, A.; Vata, R., Thermal degradation chemistry of alkyl quaternary ammonium montmorillonite. *Chemistry of Materials* **2001,** *13*, 2979-2990.

43. Saikia, B. J.; Parthasarathy, G., Fourier Transform Infrared Spectroscopic Characterization of Kaolinite from Assam and Meghalay, Northeastern India. *Journal of Modern Physics* **2010,** *1*, 206-210.

44. Bishop, J.; Madejova, J.; Komadel, P.; Froschl, H., The influence of structural, Fe, Al, and Mg on the infrared OH bands in spectra dioctahedral smectites. *Clay Minerals* **2001,** *37*, 607-616.

45. Pavan, C.; Tomatis, M.; Ghiazza, M.; Rabolli, V.; Bolis, V.; Lison, D.; Fubini, B., In Search of the Chemical Basis of the Hemolytic Potential of Silicas. *Chemical Research in Toxicology* **2013,** *26*, 1188-1198.

46. Xi, Y.; Ding, Z.; He., H.; Frost, R. L., Structure of organoclays-an X-ray diffraction and thermogravimetric analysis study. *Journal of Colloid and Interface Science* **2004,** *277*, 116-120.

47. Muller, K. H.; Motskin, M.; Philpott, A. J.; Routh, A. F.; Shanahan, C. M.; Duer, M. J.; Skepper, J. N., The effect of particle agglomeration on the formation of a surface-connected compartment induced by hydroxyapatite nanoparticles in human monocyte-derived macrophages. *Biomaterials* **2014,** *35* (3), 1074-88.

48. Ruge, C. A.; Schaefer, U. F.; Herrmann, J.; Kirch, J.; Canadas, O.; Echaide, M.; Perez-Gil, J.; Casals, C.; Muller, R.; Lehr, C., The Interplay of Lung Surfactant Proteins and Lipids Assimilates the Macrophage Clearance of Nanoparticles. *PLoS One* **2012,** *7*, 1-10.

49. Fan, Q.; Wang, Y. E.; Zhao, X.; Loo, J. S. C.; Zuo, Y. Y., Adverse Biophysical Effects of Hydroxyapatite Nanoparticles on Natural Pulmonary Surfactant. *ACS Nano* **2011,** *5*, 6410-6416.

50. Lordan, S.; Higginbotham, C. L., Effect of serum concentration on the cytotoxicity of clay particles. *Cell Biology International* **2012,** *36*, 57-61.

51. Zeinabad, H. A.; Zarrabian, A.; Saboury, A. A.; Alizadeh, A. M.; Falahati, M., Interaction of single and multi wall carbon nanotubes with the biological systems: tau protein and PC12 cells as targets. *Scientific Reports* **2016,** *6*, 26508.

52. Shannahan, J. H.; Brown, J. M.; Chen, R.; Ke, P. C.; Lai, X.; Mitra, S.; Witzmann, F. A., Comparison of Nanotube-Protein Corona Composition in Cell Culture Media. *Small* **2013,** *9*, 2171-2181.

53. Rahman, M.; Laurent, S.; Tawil, N.; Yahia, L. H.; Mahmoudi, M., Nanoparticle and Protein Corona. **2013,** *15*, 21-44.

54. Saptarshi, S. R.; Duschl, A.; Lopata, A. L., Interaction of nanoparticles with proteins: relation to bio-reactivity of the nanoparticle. *Journal of Nanobiotechnology* **2013,** *11*, 26.

55. Moore, T. L.; Rodriguez-Lorenzo, L.; Hirsch, V.; Balog, S.; Urban, D.; Jud, C.; Rothen-Rutishauser, B.; Lattuada, M.; Petri-Fink, A., Nanoparticle colloidal stability in cell culture media and impact on cellular interactions. *Chemical Society Reviews* **2005,** *44* (6287-6305).

56. Loosli, F.; Vitorazi, L.; Berret, J.; Stoll, S., Towards a better understanding on agglomeration mechanisms and thermodynamic properties of TiO2 nanoparticles interacting with natural organic matter. *Water Research* **2015,** *80*, 139-148.

57. Sauer, U. G.; Aumann, A.; Ma-Hock, L.; Landsiedel, R.; Wohlleben, W., Influence of dispersive agent on nanomaterial agglomeration and implications for biological effects in vivo or in vitro. *Toxicology in vitro : an international journal published in association with BIBRA* **2015,** *29* (1), 182-6.

58. Hubbs, A.; Greskevitch, M.; Kuempel, E.; Fernando, S.; Toraason, M., Abrasive blasting agents: designing studies to evaluate relative risk. . *Journal of Toxicology and Environmental Health, Part A* **2005,** *68*, 999-1016.

59. Yang, A.; Cardona, D. L.; Barile, F. A., In vitro cytotoxicity testing with fluorescence-based assays in cultured human lung and dermal cells. *Cell Biology and Toxicology* **2002,** *18*, 97-108.

60. Farcal, L.; Torres Andon, F.; Di Cristo, L.; Rotoli, B. M.; Bussolati, O.; Bergamaschi, E.; Mech, A.; Hartmann, N. B.; Rasmussen, K.; Riego-Sintes, J.; Ponti, J.; Kinsner-Ovaskainen, A.; Rossi, F.; Oomen, A.; Bos, P.; Chen, R.; Bai, R.; Chen, C.; Rocks, L.; Fulton, N.; Ross, B.; Hutchison, G.; Tran, L.; Mues, S.; Ossig, R.; Schnekenburger, J.; Campagnolo, L.; Vecchione, L.; Pietroiusti, A.; Fadeel, B., Comprehensive In Vitro Toxicity Testing of a Panel of Representative Oxide Nanomaterials: First Steps towards an Intelligent Testing Strategy. *PLOS One* **2015,** *10* (5), e0127174.

61. Das, S.; Singh, S.; Singh, V.; Joung, D.; Dowding, J. M.; Reid, D.; Anderson, J.; Zhai, L.; Khondaker, S. I.; Self, W. T.; Seal, S., Oxygenated Functional Group Density on Graphene Oxide: Its Effect on Cell Toxicity. *Particle & Particle Systems Characterization* **2013,** *30* (2), 148-157.

62. Zhang, H.; Dunphy, D. R.; Jiang, X.; Meng, H.; Sun, B.; Tarn, D.; Xue, M.; Wang, X.; Lin, S.; Ji, Z.; Li, R.; Garcia, F. L.; Yang, J.; Kirk, M. L.; Xia, T.; Zink, J. I.; Nel, A.; Brinker, C. J., Processing pathway dependence of amorphous silica nanoparticle toxicity: colloidal vs pyrolytic. *Journal of the American Chemical Society* **2012,** *134* (38), 15790-804.

63. Tarn, D.; Ashley, C. E.; Xue, M.; Carnes, E. C.; Zink, J. I.; Brinker, C. J., Mesoporous Silica Nanoparticle Nanocarriers: Biofunctionality and Biocompatibility. *Accounts of Chemical Research* **2013,** *46*, 792-801.

64. Ray, P. D.; Huang, B. W.; Tsuji, Y., Reactive oxygen species (ROS) homeostasis and redox regulation in cellular signaling. *Cellular signalling* **2012,** *24* (5), 981-90.

65. Sterman, S.; Marsden, J. G., Silane Coupling Agents. *Reinforced Plastics Symposium* **1966,** *58*, 33-37.

66. Soteropulos, C. E.; Hunt, H. K., Attaching biological probes to silica optical biosensors using silane coupling agents. *Journal of visualized experiments : JoVE* **2012,** (63), e3866.

67. Ojea-Jimenez, I.; Urban, P.; Barahona, F.; Pedroni, M.; Capomaccio, R.; Ceccone, G.; Kinsner-Ovaskainen, A.; Rossi, F.; Gilliland, D., Highly Flexible Platform for Tuning Surface Properties of Silica Nanoparticles and Monitoring Their Biological Interaction. *ACS applied materials & interfaces* **2016,** *8* (7), 4838-50.

68. Meczynska-Wielgosz, S.; Piotrowska, A.; Majkowska-Pilip, A.; Bilewicz, A.; Kruszewski, M., Effect of Surface Functionalization on the Cellular Uptake and Toxicity of Nanozeolite A. *Nanoscale research letters* **2016,** *11* (1), 123.

69. Ibarguren, M.; Lopez, D. J.; Escriba, P. V., The effect of natural and synthetic fatty acids on membrane structure, microdomain organization, cellular functions and human health. *Biochimica et biophysica acta* **2014,** *1838* (6), 1518-1528.

70. Papanikolaou, G.; Pantopoulos, K., Iron metabolism and toxicity. *Toxicology and Applied Pharmacology* **2005,** *202* (2), 199-211.

71. Eaton, J. W.; Qian, M., Molecular Basis of Cellular Iron Toxicity. *Free Radic. Biol. Med.* **2002,** *32*, 833-840.

72. Breznan, D.; Das, D. D.; O'Brien, J. S.; MacKinnon-Roy, C.; Nimesh, S.; Vuong, N. Q.; Bernatchez, S.; DeSilva, N.; Hill, M.; Kumarathasan, P.; Vincent, R., Differential cytotoxic and inflammatory potency of amorphous silicon dioxide nanoparticles of similar size in multiple cell lines. *Nanotoxicology* **2017,** *11*, 223-235.

73. Wallace, W. E.; Keane, M. J.; Murray, D. K.; Chisholm, W. P.; Maynard, A. D.; Ong, T., Phosopholipid lung surfacant and nanoparticle surface toxicity: Lessons from diesel soots and silicate dusts. *Journal of Nanoparticle Research* **2007,** *9*, 23-38.

74. Napierska, D.; Thomassen, L. C. J.; Rabolli, V.; Lison, D.; Gonzalez, L.; Kirsch-Volders, M.; Martens, J. A.; Hoet, P. H., Size-Dependent Cytotoxicity of Monodisperse Silica Nanoparticles in Human Endothelial Cells. *Small* **2009,** *5*, 846-853.

75. Lin, Y.; Haynes, C. L., Impacts of mesoporous silica nanoparticle size, pore ordering, and pore integrty on hemolytic activity. *Journal of the American Chemical Society* **2010,** *132*, 4834-4842.

76. Re, F.; Zanetti, A.; Sironi, M.; Polentarutti, N.; Lanfrancone, L.; Dejana, E.; Colotta, F., Inhibition of Anchorage-dependent Cell Spreading Triggers Apoptosis in Cultured Human Endothelial Cells. *The Journal of Cell Biology* **1994,** *127*, 537-546.

77. Frisch, S. M.; Francis, H., Disruption of Epithelial Cell-Matrix Interactions Induces Apoptosis. *The Journal of Cell Biology* **1994,** *124* (4), 619-626.

78. Snyder, R. J.; Hussain, S.; Rice, A. B.; Garantziotis, S., Multiwalled carbon nanotubes induce altered morphology and loss of barrier function in human bronchial epithelium at noncytotoxic doses. *International Journal of Nanomedicine* **2014,** *9*, 4093-105.

79. Dong, C.; Kashon, M. L.; Lowry, D. T.; Dordick, J. S.; Reynolds, S. H.; Rojanasakul, Y.; Sargent, L. M.; Dinu, C. Z., Exposure to Carbon Nanotubes Leads to Changes in the Cellular Biomechanics. *Advanced Healthcare Materials* **2013,** *2*, 1-7.

80. Zhou, X.; Wang, B.; Chen, Y.; Mao, Z.; Gao, C., Uptake of Cerium Oxide nanoparticles and their influences on functions of A549 cells. *Journal of Nanoscience and Nanotechnology* **2013,** *13*, 204-215.

81. Tarantola, M.; Pietuch, A.; Schneider, D.; Rother, J.; Sunnick, E.; Rosman, C.; Pierrat, S.; Sonnichsen, C.; Wegener, J.; Janshoff, A., Toxicity of gold-nanoparticles: synergistic effects of shape and surface functionalization on micromotility of epithelial cells. *Nanotoxicology* **2011,** *5* (2), 254-68.

82. Xia, T.; Kovochich, M.; Liong, M.; Madler, L.; Gilbert, B.; Shi, H.; Yeh, J. I.; Zink, J. I.; Nel, A. E., Comparison of the mechanism of toxicity of zinc oxide and cerium oxide nanoparticles based on dissolution and oxidative stress properties. *ACS Nano* **2008,** *2* (10), 2121-34.

83. Maisanaba, S.; Puerto, M.; Pichardo, S.; Jorda, M.; Moreno, F. J.; Aucejo, S.; Jos, A., In vitro toxicological assessment of clays for their use in food packaging application. *Food and Chemical Toxicology* **2013,** *57*, 266-275.

CHAPTER 4

Toxicity Assessment of Byproducts Resulted from Nanoclay Composite Disposal by Incineration

Abstract

Addition of nanoclays into a biodegradable polymer matrix leads to nanocomposites with increased mechanical strength, barrier properties, UV dispersion, and thermal stability to be used in plastics for food packaging applications. Because of the plastics' relatively high stored energy values, such nanocomposites make good candidates for disposal via municipal solid waste plants, with the plastics being combusted to allow for the recovery of energy and reduction of waste volume of up to 90 %. However, upon nanocomposite disposal at the end of their lifecycle, increased concerns related to their potential toxicity arise, especially considering that byproducts resulting from nanocomposite incineration could escape disposal filters to cause worker inhalation hazards. Herein, we investigated the deleterious effects that a biodegradable polymer polylactic acid (PLA)-based nanocomposite containing methyl, tallow, bis-2-hydroxyethyl, quaternary ammonium functionalized montmorillonite nanoclay could pose to human lung epithelial cells, used as a model for inhalation exposure, at the end of its lifecycle. Chemical (elemental and molecular compositions) and physical (morphology, mechanical and optical properties, crystallinity and degree of exfoliation of nanoclay in PLA, and hydrodynamic diffusion versus projected area of byproducts, respectively) properties were assessed and correlated with the toxicological profiles of the end of lifecycle byproduct at different exposure doses. The byproducts induced toxic responses, including reductions in cellular viability and proliferation, changes in cellular morphology, and cytoskeletal alterations, but only at high doses. Further, the degree of dispersion of nanoclays in the polymer matrix appeared to influence both the physical and chemical characteristics, thermal degradation, as well as the toxicity. With toxicity of the byproduct occurring at high doses, safety protocols should be considered, along with further investigation into how the material characteristics of such nanocomposites and their disposal profiles could be controlled to help aid in a safer, yet still effective disposal strategy.

Introduction

Biodegradable polymers such as linear aliphatic thermoplastic polyester[1] polylactic acid (PLA),[2-4] made from renewable resources,[2,3,5] have shown good biocompatibility[6-8] and applicability in food packaging[2] and medical areas.[7,8] Biodegradable polymers allow for the reduction of environmental risks resulting from high greenhouse gas emissions and fossil fuel energy usage[5] otherwise encountered at the implementation of conventional petrochemical polymers such as polyethylene (PE), polyethylene terephthalate (PET), polyvinylchloride (PVC), polypropylene (PP), or polystyrene (PS).[5,6,9] Additionally, since biodegradable polymers require 25-55 % less power at their production when compared to the power used to generate petroleum-based polymers,[5] and because of their relatively low production cost resulting from implementation of new processing techniques,[6] it is expected that biodegradable polymers' usage will increase in the future especially when considering the amount of plastics being needed and/or consumed daily.[10,11] However, such biodegradable polymers, including PLA, are still brittle[6,12,13] and lack the barrier,[4,12] thermal,[4,12] and impact resistance properties[13] displayed by the conventional petroleum-based polymers,[6] thus limiting their consumer application.

Recent studies have showed that incorporation of nanoclays, i.e., layered mineral silicates[14,15] with a platelet thickness of about 1 nm and lengths and widths in the micron range,[16,17] could enhance polymers' mechanical strength,[18-20] barrier,[21,22] and thermal properties[6,18,23] when mixed at a low weight percent.[16,18] When such incorporation is attempted, the nanoclays need to be fully exfoliated within the polymer matrix[6] to allow for increased interactions with the polymer, thus minimizing chain mobility and creating reinforcement effects.[18] For the increased interactions, such nanoclays need to be functionalized with organic modifiers to allow for the required miscibility within the polymer,[24,25] as well as a better incorporation/exfoliation.[19] One example of a nanoclay isolated from the clay fraction of soil[14,15] is montmorillonite (MMT) which can be easily modified with methyl, tallow, bis-2-hydroxyethyl, quaternary ammonium (to form Cloisite 30B (CC)) for facile incorporation within PLA.[1,19,26,27] The good miscibility observed upon such nanoclay incorporation is presumably due to interactions of the C=O moieties present in PLA with its modified hydroxyl groups.[1] Due to the resulting increased barrier properties,[20,28,29] UV dispersion,[21,30] transparency,[31] mechanical strength,[28,32] and a longer shelf life,[17] polymer-based nanoclay nanocomposites have shown increased implementation in food packaging with the ability to withstand physical stresses associated with transportation and handling.[33] Further, PLA-

CC nanocomposites were shown to provide a ”green” packaging material that has a lower environmental impact and increased sustainability relative to conventional polymers.[1,12,17] Upon the end of their use, such nanocomposites are known to either be disposed in the landfills, incinerated, or recycled.[34,35] However, due to plastics relatively high stored energy values,[11] the PLA-based nanocomposites make good candidates for disposal via municipal solid waste (MSW) plants, with the waste being combusted to allow for the recovery of energy and reduction of volume of waste of up to 90 %.[11]

Considering the large implementation that is envisioned for such nanocomposites, recent research is focused on determining whether they have toxicological profiles. The need to identify possible deleterious pathways is driven by the minimal studies on their toxicity in both manufacturing and disposal areas, with the available toxicity studies only considering the migration extracts from such nanocomposites,[36,37] and other numerous results showing that nanoclays by themselves can induce toxic effects upon exposure to lung cells[38-41] in such areas.[42-44] Specifically, Maisanaba et al. examined the toxicity of migration extracts from a PLA-Clay 1 (a nanoclay modified with hexadecyltrimethyl-ammonium bromide (HDTA)) and PLA-Clay 2 (a nanoclay modified with HDTA and acetylcholine chloride) nanocomposite on Caco-2 and HepG2 cells and found no significant toxic effects.[36] Similarly, Maisanaba et al. examined the toxicity of a PLA-Clay 1 migration extract on Wistar rats and found no significant toxic effects.[37] However, Zia et al. examined the toxicity of nanocomposite films via investigation of cell attachment and spreading of L-929 cells on a chitin based polyurethane-bentonite nanocomposite and found that nanocomposites with increasing amounts of bentonite had adverse effects on the samples' biocompatibility with less adhesion and dissimilar morphology of the cells relative to control cells.[45] Complementary, we and others showed that nanoclays by themselves decrease cellular proliferation,[38,40] cause mitochondrial[46] and membrane damage,[46,47] induce reactive oxygen species (ROS) generation,[46] and genotoxic effects, such as micronuclei induction[48,49] and changes in mRNA expression.[48]

Considering that ultrafine and fine-sized particles could result from disposal of nanocomposites via MSW plants to potentially escape exhaust filters,[42] and that the high temperatures encountered in the MSW disposal[42] could cause property changes of the incinerated material[50,51] and could potentially create a byproduct with its own toxicological profile,[52,40] we aimed to determine the toxicity of incinerated PLA-CC nanocomposites through the use of a model

in vitro cell line, human bronchial epithelial cells (BEAS-2B).[53] The toxicity of such thermally degraded nanocomposites (i.e., herein called byproducts) is expected to allow for correlation studies between the consumption/usage and disposal stages during the nanocomposite's life cycle, while also allowing the individual toxicological impacts and material characteristics of the components themselves, i.e. PLA and nanoclay, as well as their associated byproducts, to be explored. Such a study could potentially lead to mitigation strategies for worker protection and controlled land field disposal of byproducts.

Materials and Methods

Nanocomposite and Incinerated Byproducts Preparation

Cloisite 30B (CC) was obtained from Southern Clay Products (Gonzales, TX) and, per the manufacturer specifications, organically modified via an ion-exchange reaction with methyl, tallow, bis-2-hydroxyethyl, quaternary ammonium (Scheme S1). Polylactic acid 6752 (PLA; NatureWorks) was melt-mixed with CC loaded at a 5 wt. %, in a Thermo-Haake internal mixer operating at 200 ºC and 80 rpm for 5 min. Thin films were then molded at 200 ºC using a compression press to form PLA-CC nanocomposites (PLACC), as well as PLA films to be used as controls.

Samples of PLA and PLACC (1 g per sample) were thermally degraded using a TGA701 Thermogravimetric Analyzer (LECO) to mimic their disposal. To determine the moisture content, the samples were heated in nitrogen at a rate of 6 ºC/min and in a range of temperatures from 25 ºC to 105 ºC. To determine the volatile content, the samples were heated from 105 ºC to 950 ºC, also in nitrogen and at a rate of 43 ºC/min. Finally, to determine the ash content, the samples were heated from 550 ºC to 900 ºC in oxygen, at a rate of 15 ºC/min. The resulting ash was collected to serve as a model of the byproducts resulted from incineration i.e., thermally degraded PLA-CC nanocomposite (PLACC900).

Materials Characterization

Elemental composition and surface morphology of PLA, PLACC, and PLACC900 were investigated using a Hitachi S-4700 Field Emission Scanning Electron Microscope (SEM, Hitachi High-Technologies Corporation) equipped with energy dispersive X-ray (EDX) spectroscopy. Surface morphology was examined at 5.0 kV while elemental composition was determined at 20.0

kV. For the analyses, dry films or powder samples were mounted onto a carbon tape and then sputter coated with gold/palladium for 10 s in vacuum injected with argon.

Molecular composition of the samples was determined using Fourier Transform Infrared Spectroscopy (FTIR, Digilab FTS 7000) equipped with diamond Attenuated Total Reflection (ATR). Scans were collected in the range of 4000-400 cm^{-1} at a resolution of 4 cm^{-1}; a total of 100 scans were co-added to form the final spectrum for each of the samples.

The crystallinity of PLA and PLACC and the degree of exfoliation of CC in PLACC was determined via X-ray diffraction (XRD): PANalytical X'Pert Pro XRD for crystallinity via a Cu-kα1 8047.2 eV source at 45 kV and 40 mA with a 10 sec/step in a 5-80 º 2θ range and Bruker D8 Discovery XRD for determination of the degree of exfoliation. For the Bruker XRD, thin films were mounted on the sample holder and diffraction was obtained in the 2θ range of 1-10 º at an increment of 0.02 º and scan speed of 10 sec/step via a Cu-kα1 8047.2 eV source at 40 kV and 40 mA. Basal spacing was determined by Bragg's equation

$$n\lambda=2d\sin\theta,$$

where n is an integer, λ is the wavelength of the X-ray radiation (0.1546 nm), d is the spacing between lattice planes, and θ is the measured diffraction angle.

The absorption spectra for PLA and PLACC was determined in the range of 200-800 nm via the Shimadzu UV-Vis spectrophotometer (Shimadzu Scientific Instruments). UV barrier properties of the film were determined by measuring transmission at 280 nm, and transparency of the films was determined by measuring transmission at 660 nm, also via the Shimadzu UV-Vis spectrophotometer.

The tensile strength, Young's Modulus, and elongation at break for films of PLA and PLACC were evaluated via the Instron E1000 (Instron Corporation) under a 2 kN load cell and using the Bluehill 3 software. For this, rectangular films of PLA and PLACC, 5 mm in width x 32 mm in length x 0.3 mm in thickness, were placed in the Instron grips, and the experiments were performed with a crosshead speed set at 5 mm/min. A specimen gauge length of about 25 mm was used for each sample upon gripping in the crosshead.

The size distribution of PLACC900 was determined by dynamic light scattering (DLS) via the Mastersizer 2000 with a Hydro 2000S accessory (Malvern Instruments). For this, solutions of PLACC900 dispersed and bath sonicated in cell culture media (Dulbecco's Modified Eagle Medium: DMEM) containing 5% fetal bovine serum (FBS) or in phosphate buffered saline (PBS)

were dropped into the Hydro 2000S until laser obscuration was within 10-20 %. The size analysis was performed 3 consecutive times with a stirrer speed of 1750 rpm and under continuous sonication.

Cell Culture

Immortalized human bronchial epithelial cells (BEAS-2B) were cultured in DMEM media containing 5% FBS, 1 % L-glutamine, and 1 % penicillin-streptomycin (all reagents were purchased from Life Technologies). The cells were passaged regularly using 0.25 % trypsin (Invitrogen) and incubated at 37 ºC, 5 % CO_2, and 80 % relative humidity. Before each experiment cells were grown to a confluent monolayer.

Dose Response Curve (IC_{50})/ Cell Viability

BEAS-2B were seeded in a 12 well plate (Falcon) at a density of $2.0x10^5$ cells/ml. After 24 h, the cells were exposed to PLACC900 from 0-750 µg/ml, with the doses obtained by serial dilutions. For this, samples were first sonicated for 8-10 min in media by using a bath sonicator (Branson). After 24 h of exposure to PLACC900, the cells were trypsinized and stained with 0.4% trypan blue solution (Invitrogen). Subsequently, 10 µl of the sample containing the stained cells was added to a hemocytometer (Hausser Scientific), and the number of cells in the 4 outer grids was counted through use of the Leica DM IL optical microscope (Leica Microsystems) using a 10X objective. OriginPro (OriginLab Corporation) software was used to determine the IC_{50} value via fit with a sigmoidal curve.

In another assay, BEAS-2B were seeded in a 96 well plate (CellTreat Scientific Products) at a density of $2.0x10^5$ cells/ml. After 24 h, the cells were exposed to PLACC900 at 100, 300, and 500 µg/ml dispersed in media following 8-10 min sonication. Cells in only media served as controls. The 4-[3-(4-Idophenyl)-2-(4-nitrophenyl)-2H-5-tetrazolio]-1,3-benzene disulfonate known as WST-1 assay (Roche, USA) was used to determine cellular metabolic activity since it is known that changes in color of such reagent are produced when cellular dehydrogenases of metabolically active cells reduce it to formazan.[54] Twenty four, 48, and 72 h post exposure to PLACC900, 10 µl of WST was added to the wells. Cells (exposed and control) were incubated for 2 h and absorbance was read at 485 nm using a FLUOstar OPTIMA plate reader (BMG LABTECH). Media and PLACC900 byproduct dispersed in media served as blanks with their absorbance values being subtracted from the cellular measurements counterparts.

Extracellular Reactive Oxygen Species (ROS)

BEAS-2B were seeded in a 12 well plate at a density of $1.5x10^5$ cells/ml. After 24 h, the cells were exposed to 100 or 300 µg/ml of PLACC900 dispersed in media as previously described. After 24, 48, and 72 h of exposure, 50 µl of media from each treatment was transferred to a black-bottomed 96 well plate (Corning, Inc.). Subsequently, 50 µl of PBS and 50 µl of Lumigen ECL Plus (Lumigen, Inc.) were added to each well, and the samples were incubated for 5 min in the dark. Luminescence was read at 600 nm via the FLUOstar OPTIMA plate reader. Media as well as PLACC900 dispersed in media, at each dose, served as blanks. Extracellular reactive oxygen species (ROS) was calculated by subtracting PLACC900 luminescence (determined via subtraction of media from the PLACC900+media blanks) from the respective cellular measurements.

Cellular Imaging

BEAS-2B were seeded on glass coverslips (15 mm diameter; Fisher Scientific) in a 12 well plate at a density of $1.5x10^5$ cells/ml overnight. The cells were subsequently exposed to 100, 300, or 500 µg/ml PLACC900 dispersed in media as previously described. After 24 h, the media was removed and the cells were washed two times with Hank's Balanced Salt Solution (HBSS) (Corning, Inc.), fixed with 4% formaldehyde (Sigma-Aldrich) for 15 min and at 37 ºC, and subsequently washed 3 more times with HBSS to remove any remaining formaldehyde. The cells' plasma membranes and nuclei were then stained with 3 µg/ml Alexa Fluor 594 wheat germ agglutinin (WGA) and 2 µM Hoechst 33342 (Image-iT LIVE Plasma Membrane and Nuclear Labeling Kit, Life Technologies), respectively, both dispersed in HBSS, for 10 min and at 4 ºC. After incubation, cells were washed 2 times with HBSS, the cover slides were mounted on glass coverslips, and imaged under a Nikon Inverted Microscope Eclipse Ti Series (Nikon) and a 40X objective. The NIS-Elements BR 3.1 software was used to analyze the size and morphology of the cells.

Electrical Cell-substrate Impedance Testing

Real-time measurements of BEAS-2B cellular resistance during and after exposure with PLACC900 were performed using an electrical cell-substrate impedance sensing instrument (ECIS-ZΘ, Applied Biophysics, NY). For such cellular studies, a 96 well plate (96W10idf) that contained inter-digitated finger connection electrodes covering an area of about 4 mm^2 of each

well were used. Before addition of the cells, the electrodes were stabilized for 2 h with 200 µl of media to minimize any drift during the experiment.

For exposure, BEAS-2B were seeded on the ECIS electrodes at a density of $2.0x10^5$ cells/ml in a volume of 150 µl/well. After 24 h, the cells were exposed to 100, 300, or 500 µg/ml of PLACC900, dispersed in media; cells in media served as controls. The resistance of the cells was monitored continuously for 72 h. The recovery of the cells was also monitored for 72 h. For this, parallel experiments were performed in which, after 24, 48, and 72 h of exposure, the cells were trypsinized and counted so that $1.0x10^5$ cells/ml could be added to its respective ECIS well at a volume of 150 µl/well.

Cell Cycle

BEAS-2B were seeded in a 6 well plate (Corning, Inc.) at a density of $2.5x10^5$ cells/ml; cells in media served as controls. After 24 h, the cells were exposed to 1-100 µg/ml (1, 10, 25, 50, and 100 µg/ml) of PLACC900 dispersed in media as previously described. After 24 h, the cells were washed 2 times with PBS, trypsinized, pelleted, and washed again. The cells were then resuspended and fixed with 70 % ethanol overnight at -20 ºC. Subsequently, the cells were pelleted and the ethanol decanted. The cells were once again washed and resuspended in 0.2% Tween 20 (Fisher Scientific) for 15 min at 37 ºC. In another step, PBS was added and the cells were pelleted and resuspended in 180 µg/ml Ribonuclease A-PBS (Sigma-Aldrich) for 15 min at room temperature. Finally, the DNA of the cells was stained via a 15 min incubation with 75 µg/ml propidium iodide solution (Sigma-Aldrich) at room temperature. After incubation, the volume was brought up with 300 µl of PBS. The cells' DNA content was then analyzed via the BD LSRFortessa (BD Biosciences) and BDFACSDiva 8.0 software and knowing that the amount of DNA will double in the G2 phase when compared with S phase of the cell cycle. There were 20,000 events contained in the gated area of the live cell population per sample (formed via forward scatter and side scatter) used for analysis.

Statistical Analyses

All cellular experiments were repeated at least 4 times for all samples, with the exception of cellular imaging which was repeated 3 times. All tables are presented as the average value with (+/-) SD values. All graphs are presented as the mean value of the number of indicated replicates with (+/-) SE bars. Significance was determined by one- or two-way analysis of variance ANOVA

with $p<0.05$* indicating significance. OriginPro software was used for determination of the IC_{50} value for PLACC900 by using a sigmoidal dose response fit on the average of the 5 replicates.

Results and Discussion

Considering that nanocomposites (or nanoclay melt-mixed within polymers) have seen increased implementation in food packaging,[55,56] with such products being disposed by incineration because of their energetic costs reduction and cost recovery,[11,57] we aimed to design a platform for meaningful assessment of possible toxicity profiles. The need for toxicity studies is driven by the recent reports that show that nanoparticles resulted from incineration have the potential to escape filters in disposal areas[42,58] and induce toxic effects on lung cells[40,41] of the workers present in such environments. However, no reports assess human exposures in such areas.

To demonstrate the feasibility of the designed platform, we used a model polylactic acid (PLA)-based nanocomposite since PLA has seen a high consumer implementation in the food packaging industry[59,60] due to its known "green polymer" characteristics and granted approval by the Food and Drug Administration.[32,61] In the first part of the assessment strategy, we evaluated the materials' and byproduct resulting from incineration characteristics, while in the second we assessed any induced deleterious effects of such byproducts on model human lung cells and correlated any toxicological mechanistic profiles with the starting material or resulting byproducts physico-chemical characteristics.

Materials Characterization

We first created the PLA-based nanocomposite (PLACC) by melt mixing Cloisite 30B (CC) into PLA.[62-65] Films formed from solely PLA served as controls. Consideration was given to CC as a model nanoclay because of its good miscibility in PLA,[4] large consumer implementation,[66,67] and the available reports on its toxicity on systems such as liver,[68] colon,[69] and lung,[40] where it has shown both reductions in proliferation and viability,[40,68,69] as well as cellular membrane damages,[68] changes in cellular morphology,[40] and increased reactive oxygen species (ROS) generation.[70]

We then aimed to mimic the route of disposal by incineration of such nanocomposites using conditions encountered in MSW plants.[42] Specifically for this, we thermally degraded both PLACC and the PLA control films under temperatures ranging from 25 to 950 ºC and then evaluated the resulting moisture, volatile, and ash contents. As expected, no ash was obtained upon

PLA films incineration, indicating complete degradation of the polymer (Table S1). However, PLACC had around 4 % of its weight remaining as ash, likely due to CC, which was added at 5 wt. %. Additionally, PLACC had a significantly lower amount of volatile content relative to PLA, again, presumably due to the presence of such nanoclay. Such results are supported by Koh et al. who also showed byproduct formation after degradation at up to 700 ºC of PLA containing either Cloisite 15A or Cloisite 20A respectively.[71] However, the ash content identified in our study was larger when compared to the previous one, most likely because of a more prominent char resistance of the CC relative to the other nanoclays[71] as dictated by their different thermal stability as resulting from their respective organic modifier composition (i.e. amount of volatile compounds present) and the wt. % in which the organic modifier was added to them.[41] Specifically the organic modifiers for Cloisite 15A or 20A respectively are made up of 2 tallow groups when compared to CC which is made up of only one tallow group (Scheme S1).[71]

Based on our analysis, both PLA and PLACC lost the majority of their weight in the range of 300-600 ºC, with PLACC showing a slightly slower degradation rate relative to control PLA (Figure 1a). Overall, the differences in degradation rate and onset degradation temperature were fairly minimal between PLA and PLACC, showing that the addition of CC did not appear to significantly influence PLA's thermal stability. It is known that thermal stability of nanocomposites is generally dependent on the degree of dispersion and wt. % of the nanoclays, with a well exfoliated nanocomposite displaying increased stability.[72,73] This is presumably due to the thermal stability of inorganic materials,[71] their interactions with the polymer substrate that allow for the formation of char by hindering the release of volatile products,[71,73,74] or/and to the nanoclays themselves which could potentially be creating a protective barrier when on the surface of the nanocomposite.[72]

The nanocomposites, control films, and their byproducts resulting from incineration were subsequently investigated for their chemical (elemental and molecular compositions) and physical (morphology, mechanical and optical properties, crystallinity and degree of exfoliation of CC in PLA, and hydrodynamic diffusion versus projected area of byproducts, respectively) characteristics.

For chemical characteristics specifically, the elemental composition of PLA, PLACC, and PLACC900 was determined by energy dispersive X-ray (EDX) spectroscopy. Analysis confirmed the presence of carbon and oxygen as the majority of the elements for PLA (Figure 1b), as well as

a significant decrease in carbon content and increase in oxygen and silicon contents respectively in the PLACC nanocomposite presumably resulting from the incorporation of the CC.[14] Upon thermal degradation, the amount of carbon was significantly decreased, confirming the loss of PLA.[75] Additionally, PLACC900 had a significantly higher amount of oxygen, magnesium, aluminum, silicon, and iron, all relative to PLACC with such elements being associated with the presence of the nanoclay itself,[14,76] thus signifying that the ash content was made up mostly of the nanoclay byproduct.

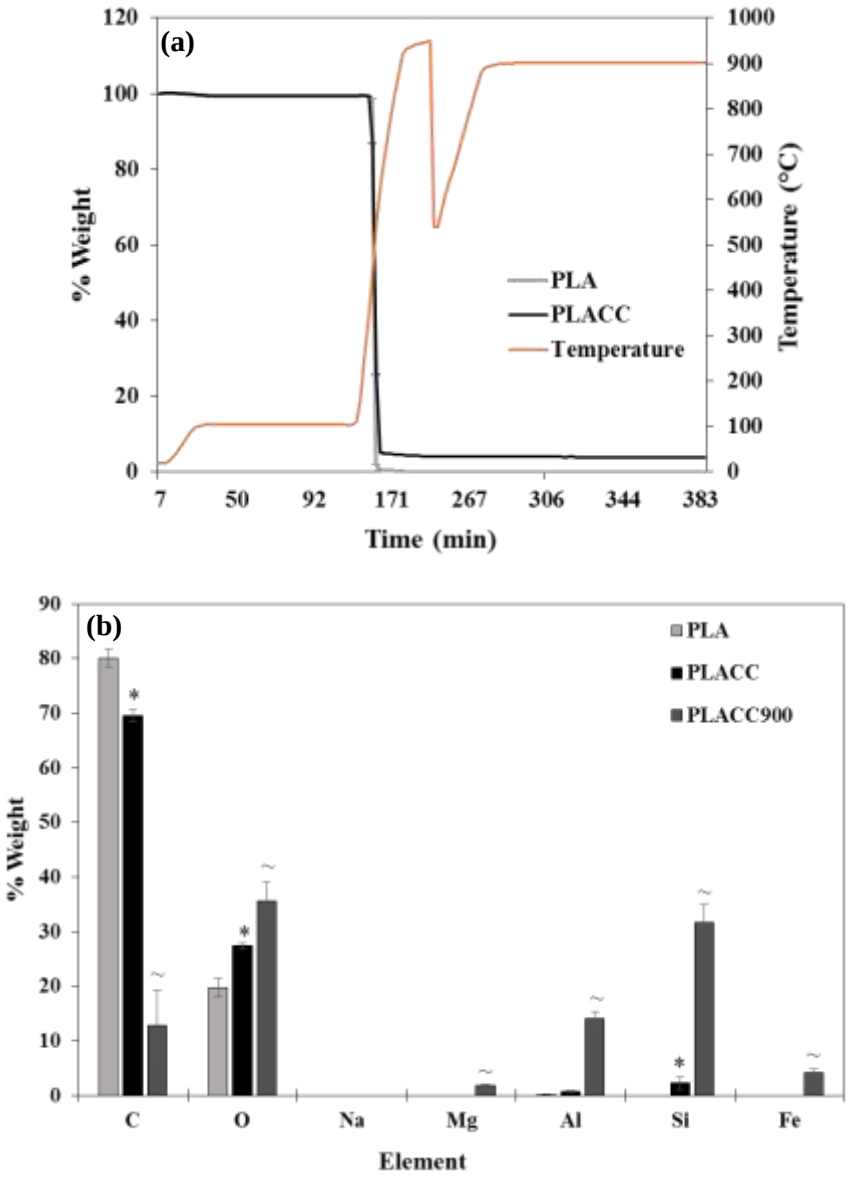

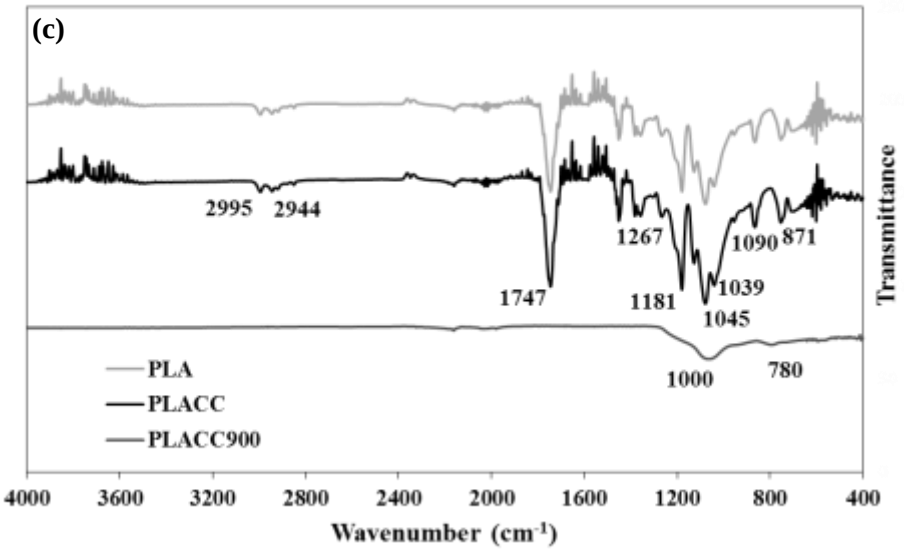

Figure 1: (a) Thermal degradation profile of PLA and PLACC as determined by TGA (n=2). Chemical characteristics analysis. **(**b) Elemental composition of PLA, PLACC, and PLACC900 as determined by EDX (n=5). The symbol * and ~ indicate significant differences between PLA and PLACC and between PLACC and its incinerated byproduct, PLACC900, respectively. (c) FTIR spectra for PLA, PLACC, and PLACC900 (n=2).

Molecular composition of the nanocomposites, PLA control films, and PLACC900 was determined by Fourier Transform Infrared Spectroscopy (FTIR). PLA and PLACC both displayed similar spectra (Figure 1c), as previously reported for PLA itself.[21,77-79] Specifically, both PLA and PLACC displayed peaks at 1267, 1181, 1090, and 1045 cm^{-1}, indicative of -C-O- stretching[77,78] and at 1454, 1384, and 1362 cm^{-1}, indicative of symmetric and asymmetric deformational vibrations of C-H present in the CH_3 groups of the PLA respectively.[21,77-79] Additionally, the peaks present at 2995 and 2944 cm^{-1} and 1747 cm^{-1} were indicative of -CH- [77-79] and C=O stretching,[21,78,79] respectively. Finally, the peak at 871 cm^{-1} was presumably due to -C-C bond formation.[77,78] Peaks specific for CC did not show up in PLACC likely due to the low concentration at which this nanoclay was added when the nanocomposite was formed. Similar results were obtained by Moo-Espinosa et al., when CC was exfoliated into segmented polyurethanes at concentrations of 2, 6, or 10 wt. %.[80]

All of the peaks associated with PLA were no longer present for the byproduct, PLACC900, confirming the degradation of the polymer upon nanocomposite's incineration. The

only 2 peaks remaining for PLACC900 were associated with Si-O-Si stretching vibration of silicate as indicated by the peak around 1000 cm^{-1},[46,81] and Si-O indicated by the peak observed around 780 cm^{-1}.[82] Along with the loss of polymer, the nanoclay itself also lost its organic modifier as confirmed by the absence of peaks at 2920, 2850, and 720 cm^{-1}.[46,81-83] Further, the loss of the alumino-silicate lattice normally displayed by MMT was confirmed by the loss of peaks associated with Al-OH-Al deformation (900 cm^{-1})[46,81] and OH respectively which was previously linked to Al^{3-} and Mg^{2-} (840 cm^{-1}) (Figure S1a).[82]

For physical characteristics we considered that thermal degradation led to an ash byproduct, as such we only investigated the crystallinity of PLA and PLACC, as well as the degree of exfoliation of CC within the polymer, by using X-ray diffraction (XRD) in the 2θ ranges of 5-80 º and 1-10 º, respectively. In the context of our goal to design a platform for meaningful assessment of toxicity, crystallinity was to be evaluated since it has been previously shown to influence toxicity,[84-86] with crystalline materials being known to produce more oxidant species with pronounced deleterious cellular effects.[84,86] Also, exfoliation of nanoparticles has previously shown to influence toxicity, with studies showing that toxicity generally decreased when nanoparticles were properly exfoliated versus when they were in agglomerate forms.[87,88] Further, both crystallinity and exfoliation have been shown to influence degradation of materials,[65,88,89] which in itself could potentially cause for a differential influence in deleterious effects.[90]

Our analysis showed that in the 2θ range of 5-80 º, both PLA and PLACC displayed broad peaks around 15.4 and 18.1 º, respectively (Figure S2a), which are characteristic of neat PLA[91] thus confirming the amorphous structure and low crystallinity of the samples[80,92] likely induced by the high cooling rates used during the molding process of the polymer.[93]

No peaks were observed for PLA in the 1 to 10 º 2θ range which was in contrast with CC and PLACC which both displayed peaks within that range (Figure S2b). Specifically, CC displayed a peak at around 4.8 º, presumably indicating a basal spacing of 1.85 nm.[94] This peak was also present for PLACC, however at a lower intensity, presumably demonstrating that a small amount of the nanoclays were likely agglomerated within the polymer matrix.[12] Additionally, PLACC displayed peaks at smaller angles, i.e., around 1.8 º (basal spacing of 4.92 nm) and 2.5 º (basal spacing of 3.54 nm) respectively, presumably due to the penetration of the polymer chains between the nanoclay platelets and thus resulting in increased basal spacing to confirm intercalation or exfoliation of the nanoclay within the PLA.[12,95-97]

The CC did not seem to be completely surface exfoliated within PLA,[97] as confirmed by surface morphology analysis performed by scanning electron microscopy (SEM). Specifically, results showed that PLACC displayed a slightly rougher morphology relative to PLA used as control (Figure 2a,b). Complementary, upon nanocomposites degradation, the PLACC900 displayed generally two types of morphologies, namely one with a fragmented surface with platelets jutting out, and a second one with a porous conformation (Figure 2c,d). Such different morphologies may be due to differential distribution and degrading of the nanoclay within the polymer matrix, interactions of the nanoclay with the polymer, and/or the different exfoliation noted. Degree of dispersion can be controlled in the future by manufacturing parameters, such as, temperature,[98] time,[22] and feed rate.[99] Previous results by Stueckle et al., showed a porous morphology if only CC was degraded, with the degraded CC's (CC900) morphological changes being attributed to the interactions of the organic modifier with Si-O and Al-O bonds in the pristine clay and an increase in basal spacing of the nanoclay.[52] The porous morphology of the degraded nanocomposite, PLACC900, could also be attributed to the polymer increasing the basal spacing between CC, with the fragmented morphology potentially due to agglomerated CC. Indeed, our control experiments of thermally degraded CC (CC900) showed that the main difference between the thermally degraded nanocomposite (PLACC900) and CC900 respectively, appeared to be related to the physical properties and not changes in the elemental or molecular properties of the two samples (Figure S1).

Additional physical characterizations of transparency and UV dispersion of PLA and PLACC provided further insights into the exfoliation of CC into PLA. Both means of characterizations have previously been shown to be contributing to overall samples' physical characterization and implementation as they allow for a consumer "to see the product" and for the blocking of light/UV transmission to increase product's shelf life[100] by reduction in the UV driven lipid oxidation and discoloration.[101] Analysis showed that PLA and PLACC displayed similar absorbance spectra with peaks around 245 and 270 nm, respectively (Figure S3a). PLACC also had a significantly higher transparency than PLA (Table S2) which could indicate a better orientation of the PLA upon addition of CC in the nanocomposite volume[12,102] since previous analysis showed that cast control films typically have a low degree of crystallinity and transparent appearance due to the rapid cooling.[75] Complementary, both PLA and PLACC generally displayed good UV dispersion properties with around 4 and 3 % transmittance, respectively. The slight

decrease in PLACC's UV dispersion relative to PLA was most likely due to the presence of the nanoclays which are known to enhance the scattering of the UV light.[103] Additionally, upon incorporation of CC, PLACC displayed a color change (to a brown color, Figure S3b,c), further known to be preferable for preventing UV transmission in food packaging.[104]

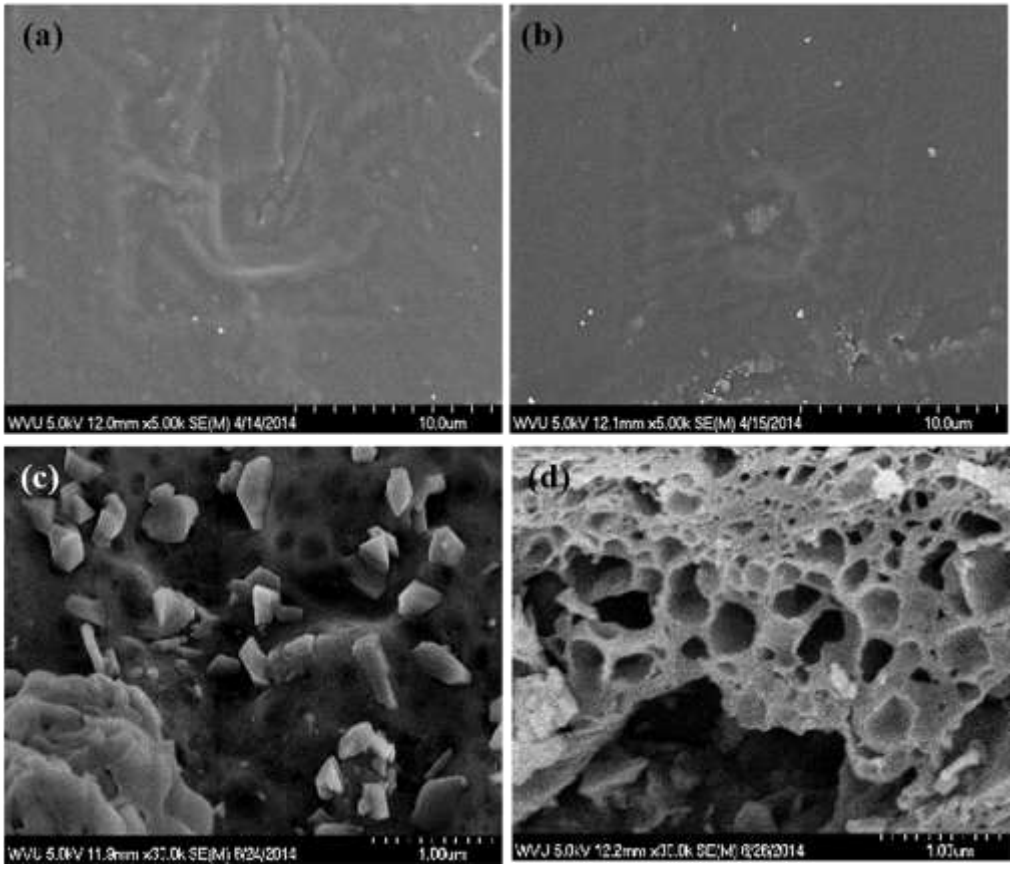

Figure 2: Surface morphology of (a) PLA, (b) PLACC, and (c), (d) the two morphologies displayed by PLACC900 as determined by SEM.

Mechanical properties analysis of the nanocomposite showed that PLACC had a significantly higher Young's Modulus relative to PLA films, thus indicating that CC interacted with the polymer within the volume of the nanocomposite (Table S3).[72] However, both elongation and tensile strength were lower for the nanocomposites when compared to control, presumably due to an uneven dispersion of CC[105] and resulting reduction in strength.[106] Further, such agglomerated nanoclays cause poor interfacial bonding, leading to the formation of microcracks,[105,107] as well as lower plasticity.[108]

Lastly, the hydrodynamic diffusion versus projected area of byproducts was evaluated via dynamic light scattering (DLS) since previous analysis have showed that the size of a particle could influence its toxicity[109] and internalization profiles.[109] Specifically, spherical particles less than 10 µm can be inhaled[110,111] with particles smaller than 2.5 µm potentially reaching the alveoli.[110] Further, particles of up to 25 µm in diameter were shown to be deposited in ciliated airways if they had a platelet like morphology and a thickness of less than 0.1 µm.[112] Our analysis showed that PLACC900 displayed size distributions in the micrometer range in both media and control buffer, PBS (Figure S4). Specifically, 90 % of the particles were under 13 µm, with 50 % of such particles being under 5 µm (Table S4) presumably due to the recorded loss of the organic modifier from CC and the majority of the polymer matrix.[41]

Toxicity Evaluation

Thermally degraded PLACC byproduct (i.e., PLACC900) was exposed to model human bronchial epithelial cells (BEAS-2B). BEAS-2B were chosen for inhalation toxicity assessment due to their ease of handling and previous feasibility studies.[113-116]

A dose response curve was initially performed to identify the PLACC900 concentrations that would create a differential effect on the cell viability. Specifically, cells were exposed to doses of 0.1, 1, 50, 100, 250, 300, 500, and 750 µg/ml for 24 h (Figure 3a). The large number of doses was chosen to mimic what a worker might inhale in areas of disposal, where it is known that concentrations could vary based on the point of emission, time of day, the amount and incorporation of the nanoparticle in the material being disposed, and the amount of the material being disposed, respectively.[43,117,118] Additionally, such doses represent different working lifetimes by taking into account total work hours, and particle and lung characteristics of the worker.[119]

Analysis showed that the IC_{50} value (i.e., concentration of PLACC900 required to inhibit cell growth by 50%) of PLACC900 was 435 µg/ml. No significant decrease in cell viability was observed for cells exposed to 100 µg/ml (below IC_{50}) over the 72 h (Figure 3b). However, after 24 h of exposure a significant decrease in cellular viability (around 20 and 50 %) was observed for cells exposed to PLACC900 at 300 and 500 µg/ml, respectively. This effect continued for BEAS-2B exposed to 500 µg/ml PLACC900 throughout the 72 h of exposure. When examining the effect of doses under the IC_{50} value of PLACC900 over time on cellular proliferation, there were not any significant decreases even after 72 h of exposure (Figure S5).

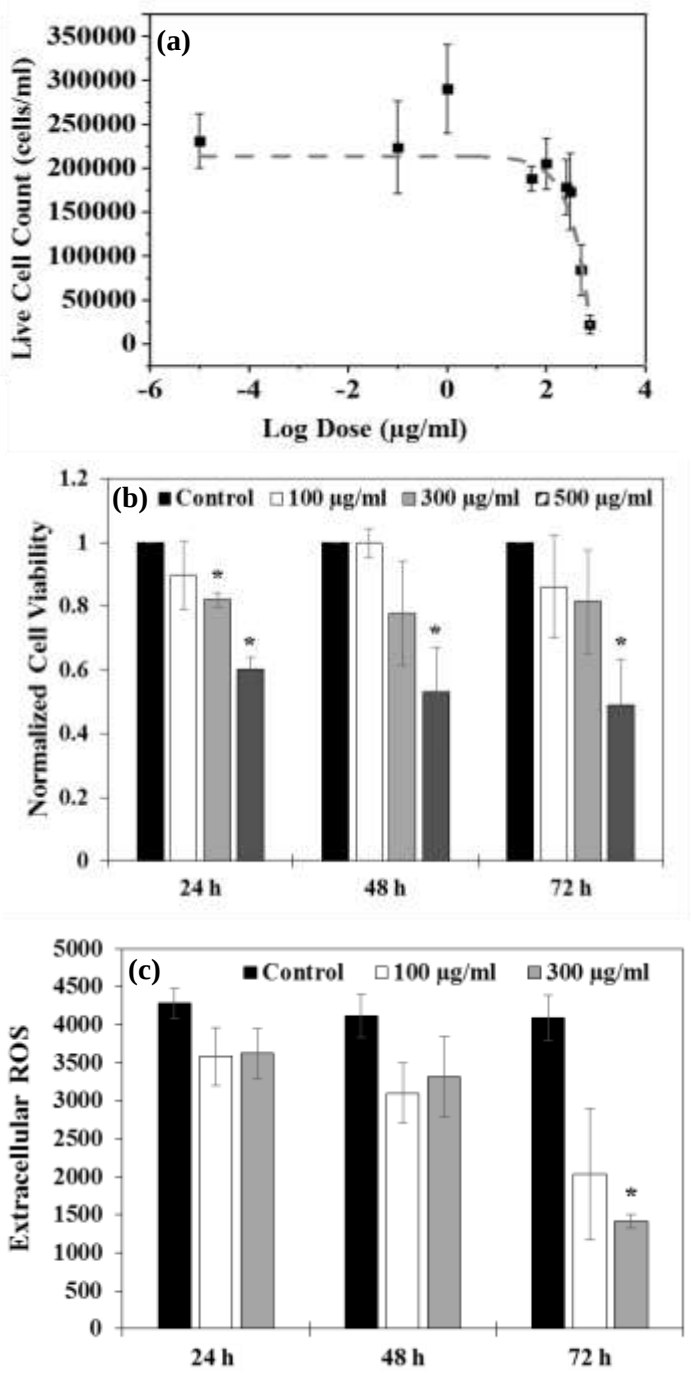

Figure 3: (a) Dose response curve (based on live cell counts) for BEAS-2B cells exposed to PLACC900 from 0-750 µg/ml (n=5). (b) Cellular viability (based on WST assay) for cells exposed to PLACC900 (n=6). The symbol * indicates a significant difference between the control cells and exposed cells. The values are normalized relative to the controls. (c) Extracellular ROS of cells exposed to varying doses of PLACC900 (n=4). The symbol * indicates a significant difference between the control cells and exposed cells.

The decrease in cellular viability could be due to the accumulation of reactive oxygen species (ROS) and the effects that such accumulation could induce on the cells.[120] In particular, previous studies have showed that CC by itself could induce internal ROS[70] to lead to cellular membrane damage and cell morphology changes from an oval to a more circular profile.[121,122] Our results showed that the cells exposed to 300 µg/ml PLACC900 had a significant decrease in external ROS after 72 h of exposure, indicating that ROS may be building up within individual cells,[120] to potentially cause damage to internal organelles or cell membrane and shape[46] (Figure 3c). The observed error bars are attributed to the byproducts interaction with the reagent[123] or to the variability in the surface morphology of the byproduct (Figure S6).[38]

Cellular imaging complemented the above results showing a dose-dependent behavior for cells exposed to PLACC900 at 100, 300, and 500 µg/ml over a 24 h period (Figure 4a-d). Analysis showed that at 24 h of exposure, the control and cells exposed to 100 µg/ml displayed a confluent monolayer with oval cells. However, the cells were no longer confluent upon exposure to doses of 300 µg/ml and higher. Further, the cells seemed to assume irregular shapes, with stretched or circular profiles being noted. Cells exposed to 500 µg/ml PLACC900 displayed the greatest loss in cell monolayer.

The observed change in shape as well as the loss of the cellular monolayer and buildup of ROS could indicate that cells may have begun to lose their ability to attach to substrates, as well as to other cells, two mechanisms hinting at deleterious effects and potential toxicity[121,122,124,125] of the byproducts. Indeed, our electrical cell-substrate impedance sensing (ECIS) analysis indicated that cells exposed to PLACC900 at 100, 300, and 500 µg/ml and subsequently monitored for 72 h (Figure 5a) had changes in their resistance pathways which were both time and dose dependent. ECIS is known to monitor changes in cell-cell and cell-substrate interactions, cell morphology, and coverage in real time,[126,127] with such changes being quantitatively analyzed, at a nanoscale resolution, and in a non-invasive,[123,128] and high-throughput manner.[126,127,129,130] Specifically, while cells exposed to 100 µg/ml had very similar resistance values relative to the control over the whole exposure time, cells exposed to 300 and 500 µg/ml of the byproducts displayed an initial increase in resistance, with the increase being more dramatic and longer for the 500 µg/ml dose. However, after 24 h, the resistances lowered with such drops in resistance complementing the observed decreases in cell viability, proliferation, monolayer's coverage and cell shape.[126,127]

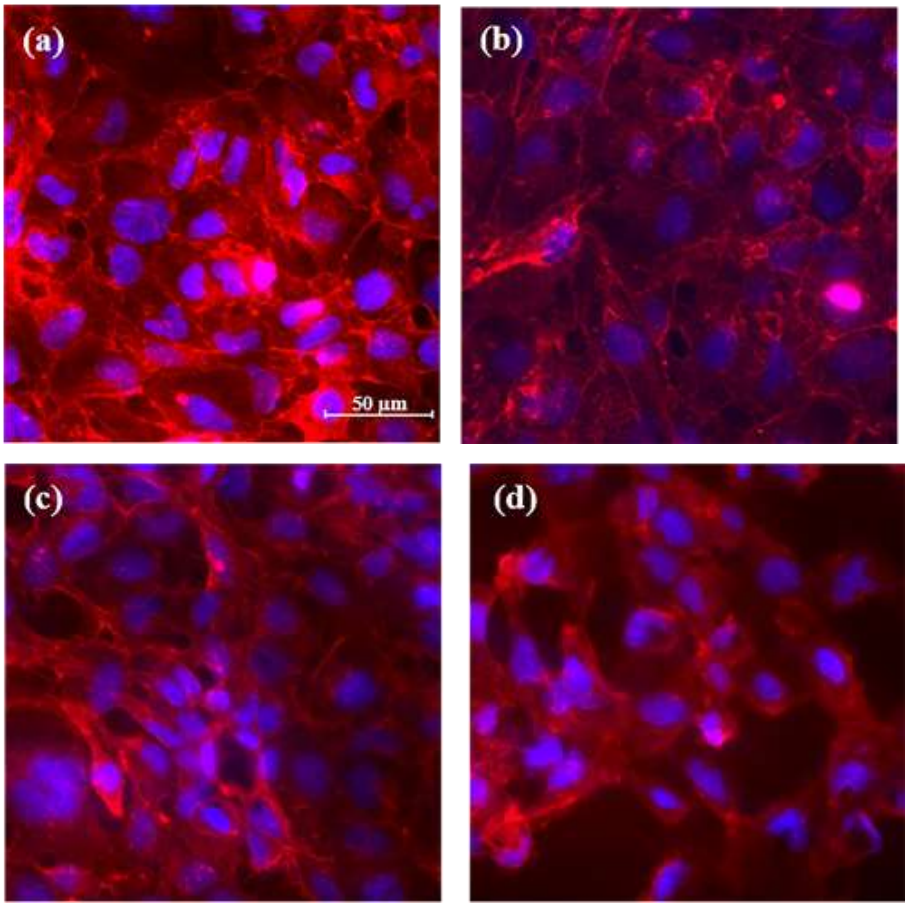

Figure 4: Fluorescent images of the cell membrane (red) and nucleus (blue) for (a) control cells and cells exposed to PLACC900 at (b) 100 µg/ml, (c) 300 µg/ml, and (d) 500 µg/ml after 24 h.

The recovery of cells exposed to PLACC900 was also non-invasively monitored with only 100 and 300 µg/ml doses being used in order to allow for an adequate number of cells to be added to the electrodes. Overall, the cells ability to recover was dose dependent. Specifically, analysis showed that after 24 h of exposure to 100 and 300 µg/ml of PLACC900, the cells showed lower resistance relative to the control (Figure 5b). However, cells exposed to 100 µg/ml PLACC900 had similar resistances to the control within 48 h of recovery, while cells exposed to 300 µg/ml had similar resistances to the control within 60 h of recovery. After a 48 h exposure to PLACC900, cells exposed to 100 µg/ml also had slightly lower resistance values relative to the control again over the first 48 h of recovery, but eventually had the similar resistances to the control cells by 40 h of recovery (Figure 5c). Cells exposed to 300 µg/ml of PLACC900 had slightly lower resistances relative to the control cells over the full 72 h of recovery. Finally, after 72 h of exposure to the byproduct, cells exposed to 100 µg/ml had higher resistances relative to the control for the first 40

h of recovery, while cells exposed to 300 µg/ml had lower resistances relative to the control over the full 72 h of recovery (Figure 5d). Similarly, AshaRani et al. noted that cells exposed to 400 µg/ml of silver nanoparticles took a month to recover when compared to cells exposed to 100 or 200 µg/ml which were able to recover within 5 or 15 days, respectively.[131]

The ability of the cells to recover was also confirmed by cell cycle analysis (Figure 5e) with analysis showing that there were no significant differences in cell cycle phases for G1, G2, or S after exposure to any of the doses, all relative to the control cells. While previous studies have shown genotoxic effects of nanoclays, ranging from DNA strand breaks[68] to condensed chromatin[132] and micronuclei,[133] as well as, changes in gene expression,[133] the lack of cell cycle arrest and normal progression through the cell cycle for cells exposed to PLACC900 hints at DNA stability[134] and lack of DNA damage[135] at lower doses.

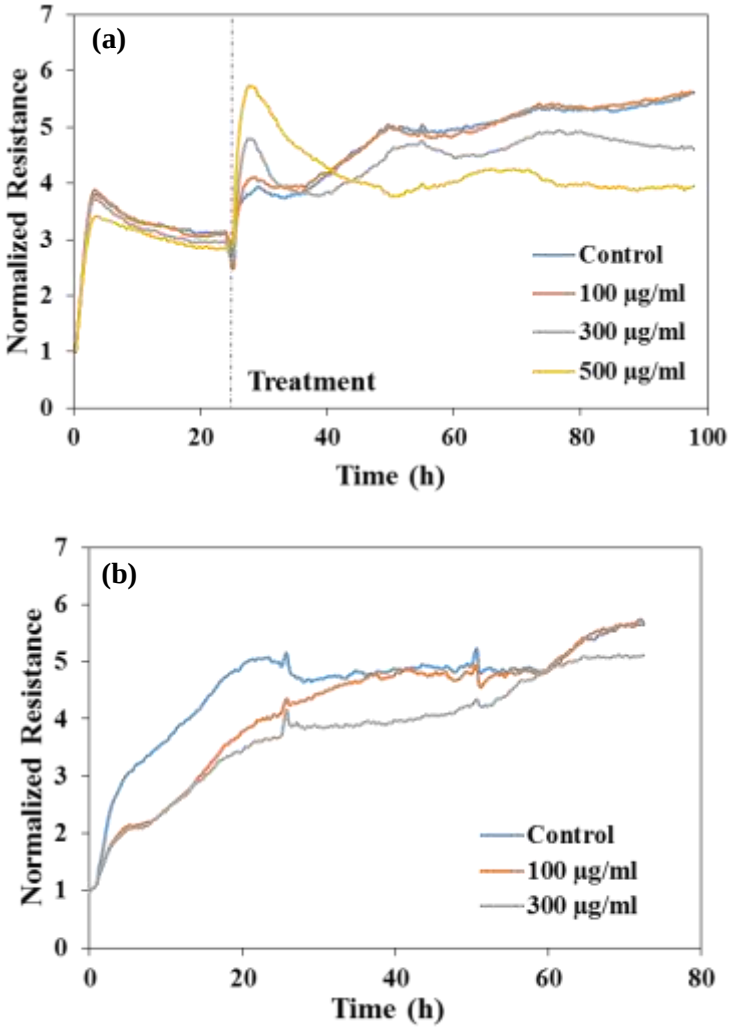

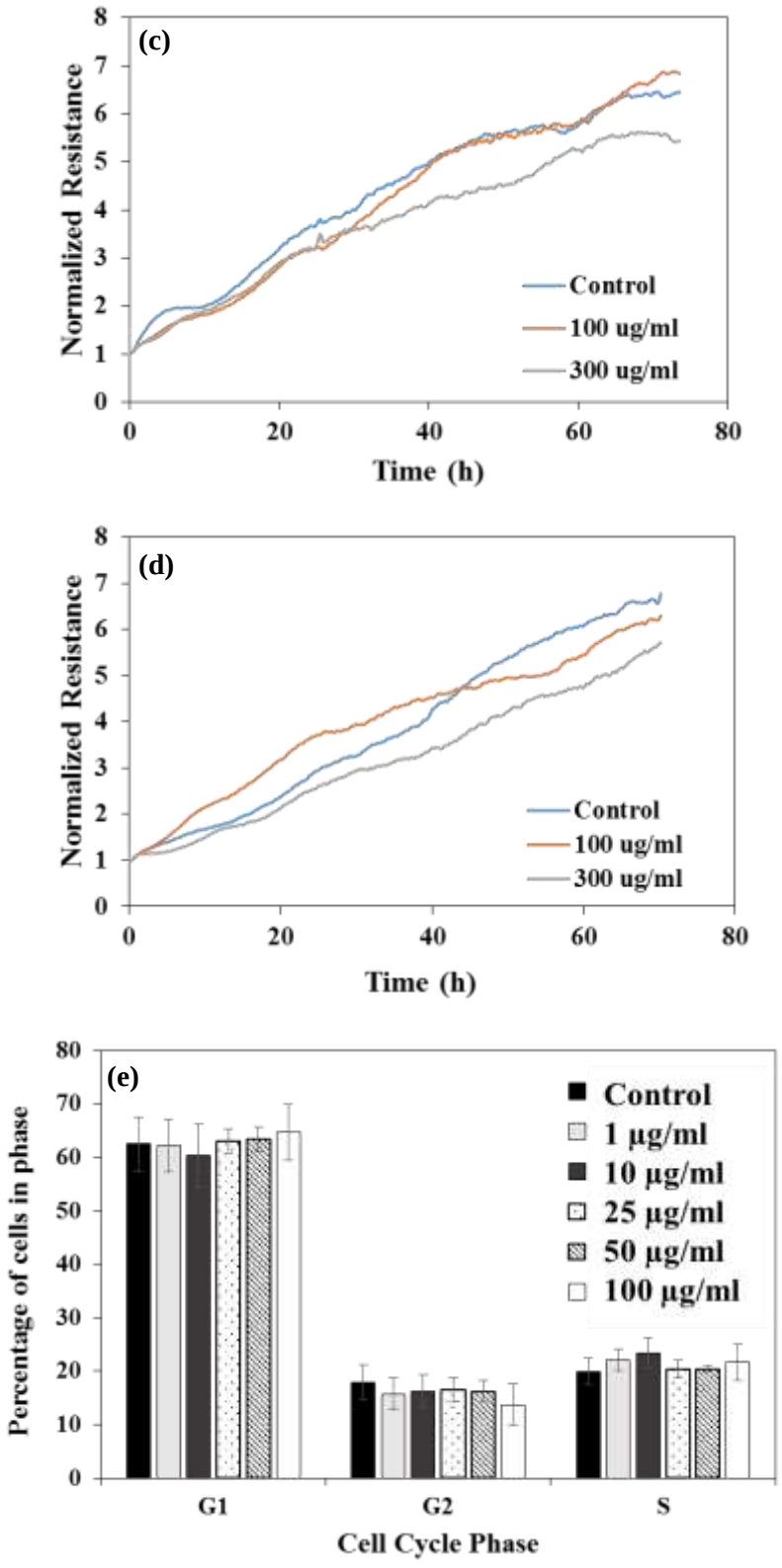

Figure 5: (a) Representative real-time measurements of normalized resistance for BEAS-2B cells before and during exposure to PLACC900 from 100-500 µg/ml. Representative real-time

measurements of normalized resistance for the recovery of BEAS-2B cells over 72 h after exposure to PLACC900 for (b) 24 h, (c) 48 h, and (d) 72 h. (e) Percentage of cells in the G1, G2, or S phase of the cell cycle after exposure to 1-100 μg/ml PLACC900 (n=4).

The observed recovery after removal of the exposure could be attributed to a volume-based dilution of the internalized byproducts and/or lower toxicity that such byproducts have. First, previous analysis showed that internalized gold nanoparticles were devised between the surviving cells to lead to a cell recovery profile dependent on the cell growth/division.[136] However, in such studies, the nanoparticles were around 45 and 13 nm.[136] For the second, PLACC900 seems to be following a similar toxicity profile to thermally degraded nanoclays which have previously been shown to be less toxic relative to their as-received counterparts.[40,41] Previous results showed wide ranges in toxicity of nanoclays with IC_{50} values as low as around 1 μg/ml[39] to more than 1000 μg/ml,[137] generally with the organic modifier being the variant.[39,68-70] In particular, thermally degraded byproducts of one pristine and three organically modified nanoclays had higher IC_{50}s relative to their as-received counterparts.[41] Such lower toxicity was attributed to loss of the organic modifier, along with changes in morphology, size, and molecular and elemental composition of the byproduct itself. Additional changes may exist herein most likely due to morphology, size, or potential entrapment of polymer species within the byproduct. For instance, while some of the smaller PLACC900 particles may be internalized,[138,139] larger particles could disrupt the membrane and potentially cause damage[88] due to their uneven, jagged profile (SEM),[87,88] however with such damage to be recovering in a time-dependent manner (real-time analysis). Additionally, the variability observed in toxic effects may be due to the different surface morphologies and sizes of the byproducts. Finally, PLACC900 itself may have effects similar to that of crystalline silica, i.e., inflammation and collagen deposition, since it contains similar CC900 properties previously shown to produce a low, persistent inflammation profile in mice.[52]

Our results indicate that while more information is required to determine mechanisms for nanocomposites degradation and ultimately toxicity of its end of life cycle byproduct, proper engineering control and protocols for workers in areas of disposal should be implemented to help lessen deleterious inhalation exposure.

Acknowledgements

This work was supported by National Science Foundation (NSF) grants 1434503 and 1454230, and the National Institutes of Health (NIH; R01-ES022968). The authors acknowledge use of WVU Shared Research Facilities and the WVU Analytical Lab.

Supporting Information

Chapter 4: Toxicity Assessment of Byproducts Resulted from Nanoclay Composite Disposal by Incineration

Material and Methods

Nanocomposite Preparation

Polylactic acid 6752 (PLA) was melt-mixed with Cloisite 30B (CC) loaded at a 5 wt. %, in a Thermo-Haake internal mixer operating at 200 ºC and 80 rpm for 5 min. Thin films were then molded at 200 ºC using a compression press to form PLA-CC nanocomposites (PLACC), as well as PLA films to be used as controls. Cloisite 30B was obtained from Southern Clay Products (Gonzales, TX) and, per the manufacturer specifications, organically modified via an ion-exchange reaction with methyl, tallow, bis-2-hydroxyethyl, quaternary ammonium at a concentration of 90 meq/100 g clay.

Thermal Degradation of PLACC and CC

PLACC (1 g per sample) and CC (0.5 g per sample) were thermally degraded using a TGA701 Thermogravimetric Analyzer (LECO). To determine the moisture content, the samples were heated in nitrogen at a rate of 6 ºC/min and in a range of temperatures from 25 ºC to 105 ºC. To determine the volatile content, the samples were heated from 105 ºC to 950 ºC also in nitrogen and at a rate of 43 ºC/min. Finally, to determine the ash content, the samples were heated from 550 ºC to 900 ºC in oxygen, at a rate of 15 ºC/min.

Material Characterization of PLA, PLACC, and Associated Nanoclays or Byproducts

Molecular composition of CC, thermally degraded CC (CC900), and thermally degraded PLACC (PLACC900) was determined using Fourier Transform Infrared Spectroscopy (FTIR, Digilab FTS 7000) equipped with diamond Attenuated Total Reflection (ATR). Scans were collected in the range of 4000-400 cm^{-1} at a resolution of 4 cm^{-1}; a total of 100 scans were co-added to form the final spectrum for each of the samples. Elemental composition of PLACC900 and CC900 was investigated using a Hitachi S-4700 Field Emission Scanning Electron Microscope (SEM, Hitachi High-Technologies Corporation) equipped with energy dispersive X-ray (EDX) spectroscopy at 20.0 kV.

The crystallinity of PLA and PLACC and the degree of exfoliation of CC in PLACC was determined via X-ray diffraction (XRD). The PANalytical X'Pert Pro XRD was used to determine crystallinity via a Cu-kα1 8047.2 eV source at 45 kV and 40 mA with a 10 sec/step in a 5-80 º 2θ range. The Bruker D8 Discovery XRD was used to determine the degree of exfoliation; thin films were mounted on the sample holder and diffraction was obtained in the 2θ range of 1-10 º at an increment of 0.02 º and scan speed of 10 sec/step via a Cu-kα1 8047.2 eV source at 40 kV and 40 mA. Basal spacing was determined by Bragg's equation

$$n\lambda=2d\sin\theta,$$

where n is an integer, λ is the wavelength of the X-ray radiation (0.1546 nm), d is the spacing between lattice planes, and θ is the measured diffraction angle.

The absorption spectra for PLA and PLACC was determined in the range of 200-800 nm via the Shimadzu UV-vis spectrophotometer (Shimadzu Scientific Instruments). UV barrier properties of the film were determined by measuring transmission at 280 nm, and transparency of the films was determined by measuring transmission at 660 nm, also via the Shimadzu UV-Vis spectrophotometer.

The tensile strength, Young's Modulus, and elongation at break for films of PLA and PLACC were evaluated via the Instron E1000 (Instron Corporation) under a 2 kN load cell and using the Bluehill 3 software. For this, rectangular films of PLA and PLACC, 5 mm in width x 32 mm in length x 0.3 mm in thickness, were placed in the Instron grips, and the experiments were performed with a crosshead speed set at 5 mm/min. A specimen gauge length of about 25 mm was used for each sample upon gripping in the crosshead.

The size distribution of PLACC900 was determined by dynamic light scattering (DLS) via the Mastersizer 2000 with a Hydro 2000S accessory (Malvern Instruments). For this, solutions of PLACC900 dispersed and bath sonicated in cell culture media (Dulbecco's Modified Eagle Medium: DMEM) containing 5% fetal bovine serum (FBS) or in phosphate buffered saline (PBS), were dropped into the Hydro 2000S until laser obscuration was within 10-20 %. The size analysis was performed 3 consecutive times with a stirrer speed of 1750 rpm and under continuous sonication.

Cell Culture

Immortalized human bronchial epithelial cells (BEAS-2B) were cultured in Dulbecco's Modified Eagle Medium (DMEM) containing 5% FBS, 1 % L-glutamine, and 1 % penicillin-

streptomycin (all reagents were purchased from Life Technologies). The cells were passaged regularly using 0.25 % trypsin (Invitrogen) and incubated at 37 ºC, 5 % CO_2, and 80 % relative humidity. Before each experiment cells were grown to a confluent monolayer.

Live Cell Count

BEAS-2B were seeded in a 12 well plate (Falcon) at a density of $2.0x10^5$ cells/ml. After 24 h, the cells were exposed to PLACC900 at 100 and 300 µg/ml, which were first sonicated for 8-10 min in media via a bath sonicator (Branson). Cells in only media served as controls. Twenty four, 48, and 72 h post exposure to PLACC900 the cells were trypsinized and stained with 0.4% trypan blue solution. Subsequently, 10 µl of the sample containing the stained cells was added to a hemocytometer, and the number of cells in the 4 outer grids were counted through use of the Leica DM IL optical microscope using a 10X objective.

Reactive Oxygen Species (ROS) Generation of PLACC900

PLACC900 was dispersed in media via a bath sonicator at doses of 100 and 300 µg/ml. The solutions were then placed in a 12 well plate with media only serving as the control. After 24, 48, and 72 h of incubation at 37 ºC, 5 % CO_2, and 80 % relative humidity, 50 µl of the PLACC900+media from each dose (and media only as control) was transferred to a black-bottomed 96 well plate. Subsequently, 50 µl of PBS and 50 µl of Lumigen ECL Plus (Lumigen, Inc.) were added to each well, and the samples were incubated for 5 min in the dark. Luminescence was read at 600 nm via the FLUOstar OPTIMA plate reader.

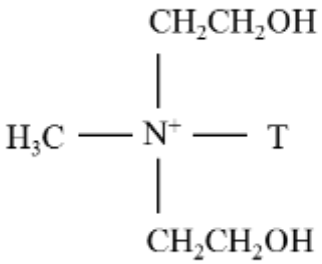

Scheme S1: Organic modifier of CC; methyl, tallow, bis-2-hydroxyethyl, quaternary ammonium.

Results

Table S1: The amount of moisture, volatile, and ash present in PLA and PLACC as determined by TGA. The symbol * indicates a significant difference between PLA and PLACC (n=4).

	Moisture	**Volatile**	**Ash**
PLA	0.49 +/- 0.18	99.70 +/- 0.27	0 +/- 0
PLACC	0.60 +/- 0.17	95.37 +/- 0.43*	3.92 +/- 0.10*

Table S2: UV dispersion (determined by Transmittance at 280 nm (T_{280nm})) and Transparency (determined by Transmittance at 660 nm (T_{660nm})) of PLA and PLACC. The symbol * indicates a significant difference between PLA and PLACC (n=5).

	T_{280nm}	**T_{660nm}**
PLA	3.85 +/- 0.12	4.88 +/- 0.08
PLACC	3.35 +/- 0.21*	7.11 +/- 0.20*

Table S3: Mechanical properties of PLA and PLACC as determined via the Instron. The symbol * indicates a significant difference between PLA and PLACC (n=5).

	Tensile Strength (MPa)	**Elongation at Break (mm)**	**Young's Modulus (MPa)**
PLA	81.2 +/- 19.0	0.436 +/- 0.093	9291.3 +/- 850.9
PLACC	66.8 +/- 22.3	0.270 +/- 0.053*	11055.8 +/- 1517.6*

Table S4: Average particle size distributions (μm) of PLACC900 in cellular media and control buffer, PBS (n=3).

	PBS	**Media**
<10%	3.00 +/- 0.01	3.12 +/- 0.08
<50%	4.57 +/- 0.01	4.84 +/- 0.29
<90%	12.67 +/- 0.03	12.14 +/- 1.14

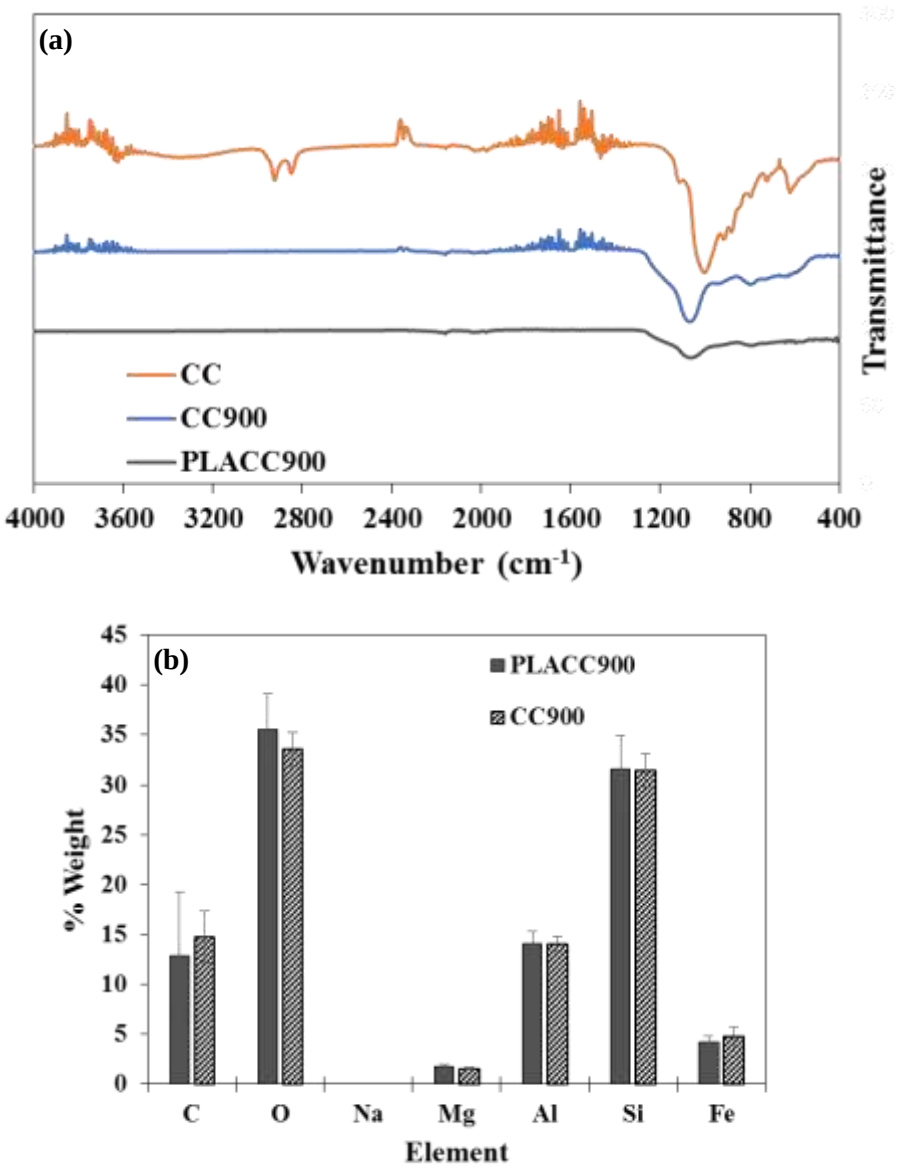

Figure S1: (a) FTIR spectra for CC, CC900, and PLACC900 (n=2). (b) Elemental composition of PLACC900 and CC900 as determined by EDX (n=5).

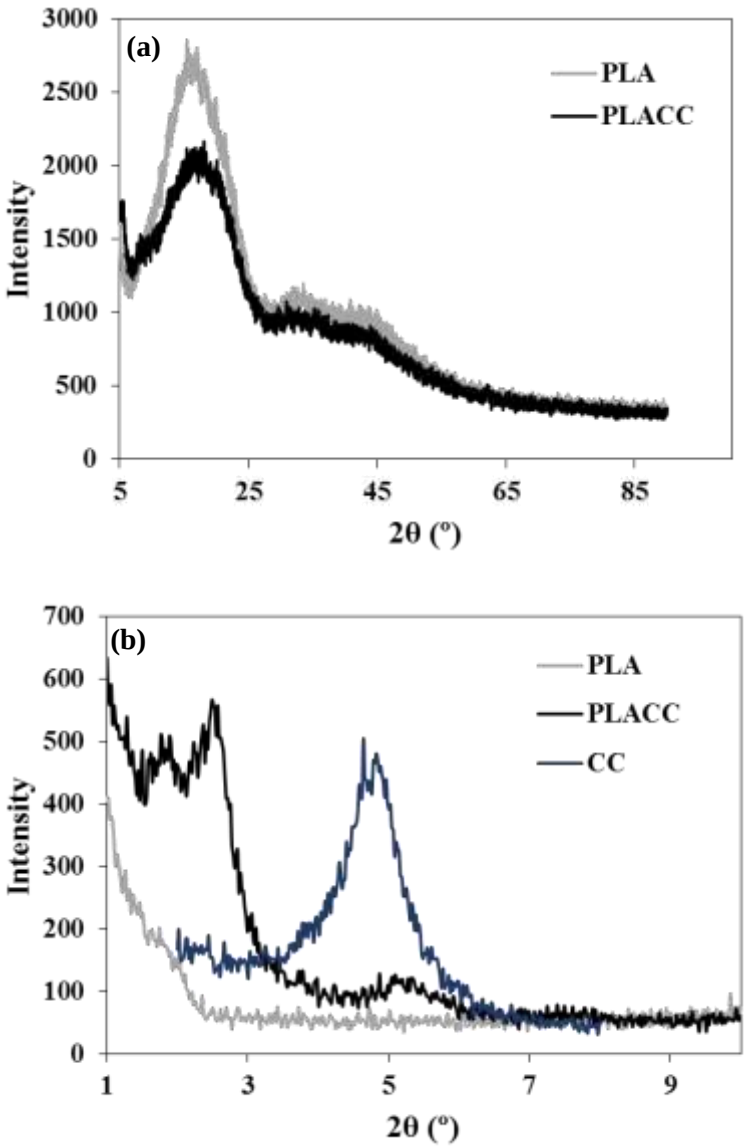

Figure S2: Physical characteristics analysis. (a) Crystallinity of PLA and PLACC as determined via XRD. (b) Exfoliation of CC in PLACC as determined via XRD.

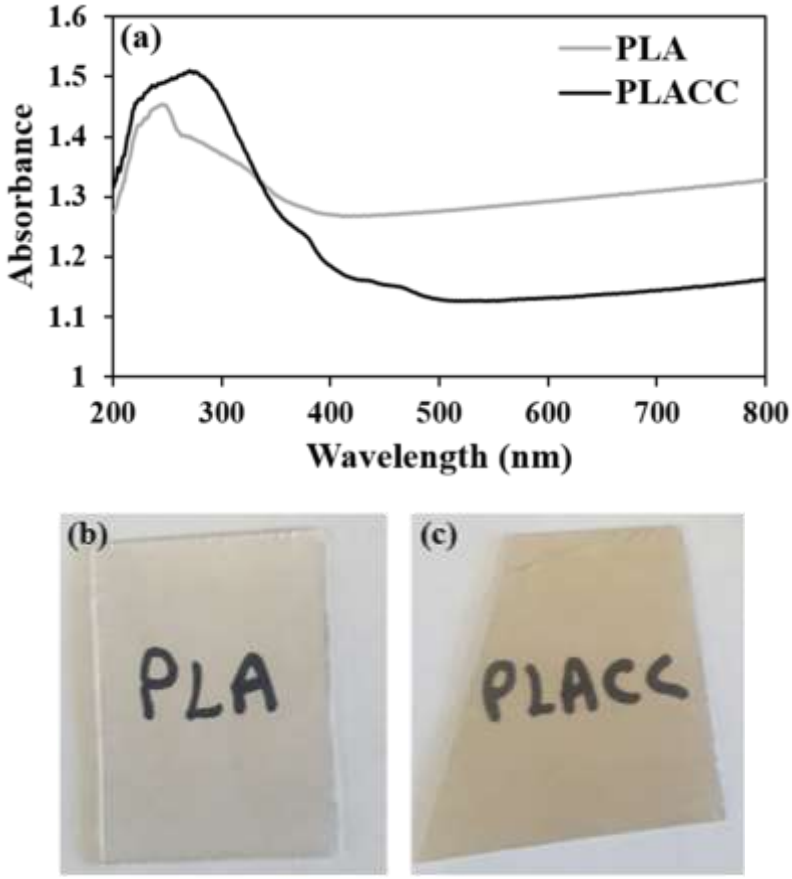

Figure S3: (a) Absorbance spectra for PLA and PLACC from 200-800 nm (n=3). Representative films of (b) PLA and (c) PLACC.

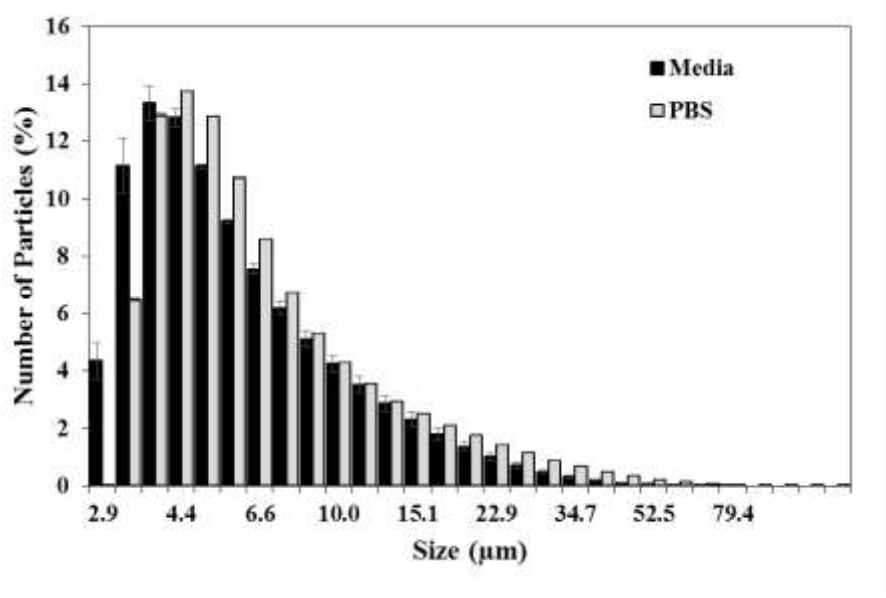

Figure S4: Average particle diameter size distribution of PLACC900 in cellular media or control buffer, PBS (n=3).

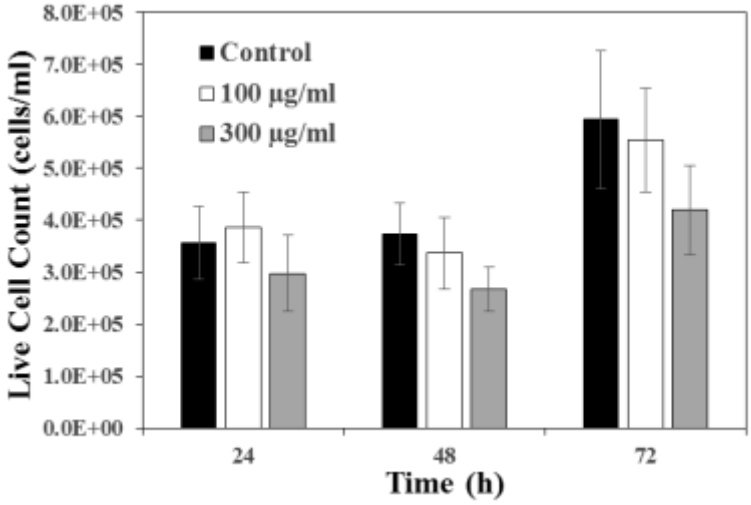

Figure S5: Live cell count of BEAS-2B cells exposed to PLACC900 over 72 h (n=6).

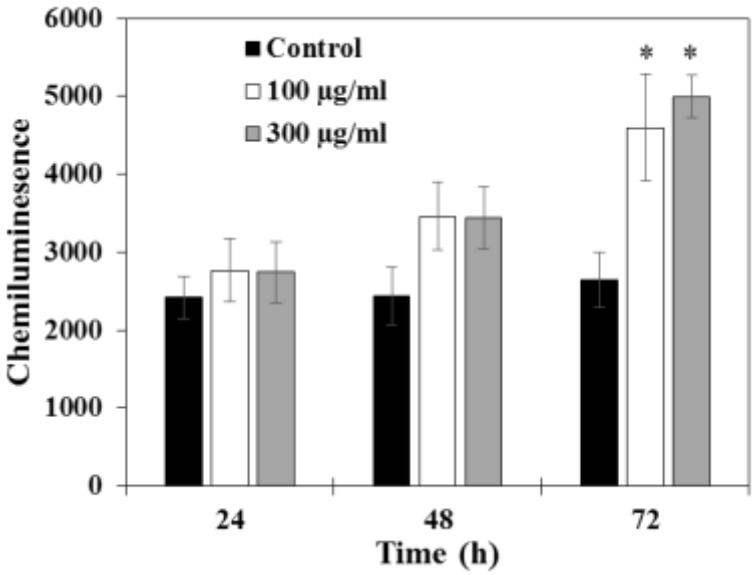

Figure S6: ROS generation of PLACC900 at varying doses in DMEM (n=6). The symbol * indicates a significant difference between the control and PLACC900.

References

1. Zaidi, L.; Bruzaud, S.; Bourmaud, A.; Mederic, P.; Kaci, M.; Grohens, Y. Relationship Between Structure and Rheological, Mechanical and Thermal Properties of Polylactide/Cloisite 30B Nanocomposites. *Journal of Applied Polymer Science* **2010,** *116*, 1357-1365.

2. Jin, T.; Zhang, H. Biodegradable Polylactic Acid Polymer with Nisin for Use in Antimicrobial Food Packaging. *Journal of Food Science* **2008,** *73*, M127-M134.

3. Holm, V. K.; Ndoni, S.; Risbo, J. The Stability of Poly(lactic acid) Packaging Films as Influenced by Humidity and Temperature. *Journal of Food Science* **2006,** *71*, E40-E44.

4. Zaidi, L.; Mustapha, K.; Bruzaud, S.; Bourmad, A.; Grohens, Y. Effect of natural weather on the structure and properties of polylactide/Cloisite 30B nanocomposites. *Polymer Degradation and Stability* **2010,** *95*, 1751-1758.

5. Vink, E. T. H.; Rabago, K. R.; Glassner, D. A.; Gruber, P. R. Applications of life cycle assessment to NatureWorks^{TM} polylactide (PLA) production. *Polymer Degradation and Stability* **2003,** *80*, 403-419.

6. Lim, L.-T.; Auras, R.; Rubino, M. Processing technologies for poly(lactic acid). *Progress in Polymer Science* **2008,** *33*, 820-852.

7. Pawar, R. P.; Tekale, S. U.; Shisodia, S. U.; Totre, J. T.; Domb, A. J. Biomedical Applications of Poly(Lactic Acid). *Recent Patents on Regenerative Medicine* **2014,** *4*, 40-51.

8. Eldesoqi, K.; Henrich, D.; El-Kady, A. M.; Arbid, M. S.; Abd El-Hady, B. M.; Marzi, I.; Seebach, C. Safety evaluation of a bioglass-polylactic acid composite scaffold seeded with progenitor cells in a rat skull critical-size bone defect. *PLOS One* **2014,** *9* (2), e87642.

9. Siracusa, V.; Rocculi, P.; Romani, S.; Rosa, M. D. Biodegradable polymers for food packaging: a review. *Food Science and Technology* **2008,** *19*, 634-643.

10. Lagaron, J. M.; Lopez-Rubio, A. Nanotechnology for bioplastics: opportunities, challenges and strategies. *Trends in Food Science & Technology* **2011,** *22*, 611-617.

11. Subramanian, P. M. Plastics recycling and waste management in the US. *Resources, Conservation and Recycling* **2000,** *28*, 253-263.

12. Rhim, J.; Hong, S.; Ha, C. Tensile, water vapor barrier and antimicrobial properties of PLA/nanoclay composite films. *LWT-Food Science and Technology* **2009,** *42*, 612-617.

13. Cabedo, L.; Feijoo, J. L.; Villanueva, M. P.; Lagaron, J. M.; Gimenez, E. Optimization of Biodegradable Nanocomposites Based on aPLA/PCL Blends for Food Packaging Applications. *Macromolecular Symposia* **2006**.

14. Floody, M. C.; Theng, B. K. G.; Reyes, P.; Mora, M. L. Natural nanoclays: applications and future trends-a Chilean perspective. *Clay Minerals* **2009,** *44*, 161-176.

15. Calabi, M.; Jara, A.; Bendall, J.; Welland, M.; Mora, M. Structural characterization of natural nanomaterials: potential use to increase the phosphorus mineralization. In *19th World Congress of Soil Science, Soil Solutions for a Changing World*, Brisbane, Australia, 2010; Vol. 1-6, pp 29-32.

16. Patel, H. A.; Somani, R. S.; Bajaj, H. C.; Jasra, R. V. Nanoclays for polymer nanocomposites, paints, inks, greases and cosmetics formulations, drug delivery vehicle and waste water treatment. *Bulletin of Materials Science* **2006,** *29* (2), 133-145.

17. Ray, S.; Okamoto, M. Polymer/layered silicate nanocomposites: a review from preparation to processing. *Progress in Polymer Science* **2003,** *28*, 1539-1641.

18. Prakalathan, K.; Mohanty, S.; Nayak, S. K. Polylactide/modified layered silicates nanocomposites: A critical analysis of morphological, mechanical and thermal properties. *Journal of Reinforced Plastics and Composites* **2012,** *31*, 1300-1310.

19. Krikorian, V.; Pochan, D. J. Poly (L-Lactic Acid)/Layered silicate nanocomposite: fabrication, characterization, and properties. *Chemistry of Materials* **2003,** *15*, 4317-4324.

20. Paul, D. R.; Robeson, L. M. Polymer nanotechnology: Nanocomposites. *Polymer* **2008,** *49*, 3187-3204.

21. Molinaro, S.; Romero, M. C.; Boaro, M.; Sensidoni, A.; Lagazio, C.; Morris, M.; Kerry, J. Effect of nanoclay-type and PLA optical purity on the characteristics of PLA-based nanocomposite films. *Journal of Food Engineering* **2013,** *117*, 113-123.

22. Pereira de Abreu, D. A.; Paseiro Losada, P.; Angulo, I.; Cruz, J. M. Development of new polyolefin films with nanoclays for application in food packaging. *European Polymer Journal* **2007,** *43*, 2229-2243.

23. Zheng, X.; Wilkie, C. A. Flame retardancy of polystyrene nanocomposites based on an oligomeric organically-modified clay containing phosphate. *Polymer Degradation and Stability* **2003,** *81*, 539-550.

24. Udon, F. Clays, Nanoclays, and Montmorillonite Minerals. *Metallurgical and Materials Transactions A* **2008,** *39A*, 2804-2814.

25. Singla, P.; Mehta, R.; Upadhyay, S. N. Clay modification by the use of organic cations. *Green and Sustainable Chemistry* **2012,** *2*, 21-25.

26. Paul, M. A.; Alexandre, M.; Degee, P.; Calberg, C.; Jerome, R.; Dubois, P. Exfoliated Polylactide/Clay Nanocomposites by In-Situ Coordination–Insertion Polymerization. *Macromolecular Rapid Communications* **2003,** *24* (561-566).

27. Paul, M. A.; Alexandre, M.; Degee, P.; Henrist, C.; Rulmont, A.; Dubois, P. New nanocomposite materials based on plasticized poly(L-lactide) and organo-modified montmorillonites: thermal and morphological study. *Polymer* **2003,** *44*, 443-450.

28. Yourdkhani, M.; Mousavand, T.; Chapleau, N.; Hubert, P. Thermal, oxygen barrier and mechanical properties of polylactide-organoclay nanocomposites. *Composites Science and Technology* **2013,** *82*, 47-53.

29. Bartel, M.; Remde, H.; Bohn, A.; Ganster, J. Barrier properties of poly(lactic acid)/cloisite 30B composites and their relation between oxygen permeability and relative humidity. *Journal of Applied Polymer Science* **2017,** *134* (5).

30. Ligot, S.; Benali, S.; Ramy-Ratiarison, R.; Murariu, M.; Snyders, R.; Dubois, P. Mechanical, Optical and Barrier Properties of PLA-layered Silicate Nanocomposites Coated with Organic Plasma Polymer Thin Films. *Material Science and Engineering with Advanced Research* **2015,** *1* (1), 20-30.

31. Harkki, O. *Biaxially oriented PLA-montmorrilonite-nanocomposite for barrier film applications* [Online]; VTT Technical Research Centre of Finland: 2012.

32. Darie, R. N.; Pâslaru, E.; Sdrobis, A.; Pricope, G. M.; Hitruc, G. E.; Poiată, A.; Baklavaridis, A.; Vasile, C. Effect of Nanoclay Hydrophilicity on the Poly(lactic acid)/Clay Nanocomposites Properties. *Industrial & Engineering Chemistry Research* **2014,** *53* (19), 7877-7890.

33. Majeed, K.; Jawaid, M.; Hassan, A.; Abu Baker, A.; Abdul Khalil, H. P. S.; Salema, A. A.; Inuwa, I. Potential materials for food packaging from nanoclay/natural fibres filled hybrid composites. *Material Design* **2013,** *46*, 391-410.

34. Hopewell, J.; Dvorak, R.; Kosior, E. Plastics recycling: challenges and opportunities. *Philosophical Transactions of the Royal Society* **2009,** *364* (2115-2126).

35. Song, J. H.; Murphy, R. J.; Narayan, R.; Davies, G. B. H. Biodegradable and compostable alternatives to conventional plastics. *Philosophical Transactions of the Royal Society B* **2009,** *364*, 2127-2139.

36. Maisanaba, S.; Pichardo, S.; Jordá-Beneyto, M.; Aucejo, S.; Cameán, A. M.; Jos, A. Cytotoxicity and mutagenicity studies on migration extracts from nanocomposites with potential use in food packaging. *Food and Chemical Toxicology* **2014,** *66*, 366-372.

37. Maisanaba, S.; Gutiérrez-Praena, D.; Puerto, M.; Llan-Ruíz-Cabello, M.; Pichardo, S.; Moyano, R.; Blanco, A.; Jordá-Beneyto, M.; Jos, A. In vivo Toxicity Evaluation of the Migration Extract of an Organomodified Clay-Poly(lactic) Acid Nanocomposite. *Journal of Toxicology and Environmental Health, Part A* **2014,** *77*, 731-746.

38. Verma, N. K.; Moore, E.; Blau, W.; Volkov, Y.; Babu, P. R. Cytotoxicity evaluation of nanoclays in human epithelial cell line A549 using high content screening and real-time impedance analysis. *Journal of Nanoparticle Research* **2012,** *14*, 1-11.

39. Janer, G.; Fernández-Rosas, E.; Mas del Molino, E.; González-Gáalvez, D.; Vilar, G.; López-Iglesias, C.; Ermini, V.; Vázquez-Campos, S. In vitro toxicity of functionalised nanoclays is mainly driven by the presence of organic modifier. *Nanotoxicology* **2014,** *8*, 279-294.

40. Wagner, A.; Eldawud, R.; White, A.; Agarwal, S.; Stueckle, T. A.; Sierros, K. A.; Rojanasakul, Y.; Gupta, R. K.; Dinu, C. Z. Toxicity evaluations of nanoclays and thermally degraded byproducts through spectroscopical and microscopical approaches. *BBA-General Subjects* **2017,** *1861*, 3406–3415.

41. Wagner, A.; White, A. P.; Stueckle, T. A.; Banerjee, D.; Sierros, K. A.; Rojanasakul, Y.; Agarwal, S.; Gupta, R. K.; Dinu, C. Z. Early Assessment and Correlations of Nanoclay's Toxicity to Their Physical and Chemical Properties. *ACS Applied Materials & Interfaces* **2017,** *9* (37), 32323-32335.

42. Roes, L.; Patel, M. K.; Worrell, E.; Ludwig, C. Preliminary evaluation of risks related to waste incineration of polymer nanocomposites. *Science of the Total Environment* **2012,** *417-418*, 76-86.

43. Yuwen, H.; Meibian, Z.; Hua, Z.; Xiaxue, L.; Mingluan, X.; Xinglin, F.; Jiliang, H. Genetic damage and lipid peroxidation in workers occupationally exposed to organic bentonite particles. *Mutatation Research/Genetic Toxicology and Environmental Mutagenesis* **2013,** *751*, 40-44.

44. Tsai, C. S. J.; White, D.; Rodriguez, H.; Munoz, C. E.; Huang, C.-Y.; Tsai, C.-J.; Barry, C.; Ellenbecker, M. J. Exposure assessment and engineering control strategies for airborne nanoparticles: an application to emissions from nanocomposite compounding processes. *Journal of Nanoparticle Research* **2012,** *14* (7), 1-14.

45. Zia, K. M.; Zuber, M.; Barikani, M.; Hussain, R.; Jamil, T.; Anjum, S. Cytotoxicity and mechanical behavior of chitin–bentonite clay based polyurethane bio-nanocomposites. *International Journal of Biological Macromolecules* **2011,** *49*, 1131-1136.

46. Lordan, S.; Kennedy, J. E.; Higginbotham, C. L. Cytotoxic effects induced by unmodified and organically modified nanoclays in human hepatic HepG2 cell line. *Journal of Applied Toxicology* **2011,** *31*, 27-35.

47. Baek, M.; Lee, J.; Choi, S. Toxicological effects of cationic clay, montmorillonite in vitro and in vivo. *Molecular & Cellular Toxicology* **2012,** *8*, 95-101.

48. Maisanaba, S.; Hercog, K.; Ortuño, N.; Jos, A.; Zegura, B. Induction of micronuclei and alteration of gene expression by an organomodified clay in HepG2 cells. *Chemosphere* **2016,** *154*, 240-248.

49. Meibian, Z.; Xiaoxue, L.; Yezhen, L.; Xinglin, F.; Qing, C.; Mingluan, X.; Jiliang, H. Studying the genotoxic effects induced by two kinds of bentonite particles on human B lymphoblast cells in vitro. *Mutatation Research/Genetic Toxicology and Environmental Mutagenesis* **2011,** *720*, 62-66.

50. Derrough, S.; Raffin, G.; Locatelli, D.; Nobile, P.; Durand, C. Behaviour of nanoparticles during high temperature treatment (Incineration type). In *Nanosafe 2012: International Conferences on Safe Production and Use of Nanomaterials*, 2012.

51. Lighty, J. S.; Veranth, J. M.; Sarofim, A. F. Combustion aerosols: factors governing their size and composition and implication to human health. *Journal of the Air & Waste Management* **2000,** *50* (9), 1565-1618.

52. Stueckle, T. A.; Davidson, D.; Derk, R.; Komberg, T. G.; Battelli, L.; Friend, S.; Orandle, M. S.; Wagner, A.; Dinu, C. Z.; Sierros, K.; Agarwal, S.; Gupta, R. K.; Rojanasakul, Y.; Porter, D. W.; Rojanasakul, L. W. Short-term Pulmonary Toxicity Assessment of Pre- and Post-Incinerated Organomodified Nanoclay in Mice. *ACS Nano* **2018**; DOI 10.1021/acsnano.7b07281.

53. Park, Y.; Kim, D.; Dai, J.; Zhang, Z. Human bronchial epithelial BEAS-2B cells, an appropriate in vitro model to study heavy metals induced carcinogenesis. *Toxicology and Applied Pharmacology* **2015,** *287*, 240-245.

54. Yin, L. M.; Wei, Y.; Wang, Y.; Xu, Y. D.; Yang, Y. Q. Long term and standard incubations of WST-1 reagent reflect the same inhibitory trend of cell viability in rat airway smooth muscle cells. *International Journal of Medical Sciences* **2013,** *10* (1), 68-72.

55. Bratovcic, A.; Odobasic, A.; Catic, S.; Sestan, I. Application of polymer nanocomposite materials in food packaging. *Croatian Journal of Food Science and Technology* **2015,** *7* (2), 86-94.

56. Bandyopadhyay, J.; Ray, S. S. *Applications of Nanoclay-Containing Polymer Nanocomposites* [Online]; Springer: Tokyo, 2017.

57. Holder, A. L.; Vejerano, E. P.; Zhou, X.; Marr, L. C. Nanomaterial disposal by incineration. *Environmental Science: Processes & Impacts* **2013,** *15*.

58. Kohler, A. R.; Som, C.; Helland, A.; Gottschalk, F. Studying the potential release of carbon nanotubes throughout the application life cycle. *Journal of Cleaner Production* **2008,** *16*, 927-937.

59. Rhim, J.-W.; Park, H.-M.; Ha, C.-S. Bio-nanocomposites for food packaging applications. *Progress in Polymer Science* **2013,** *38* (10-11), 1629-1652.

60. Arora, A.; Padua, G. W. Review: nanocomposites in food packaging. *Journal of Food Science* **2010,** *75* (1), R43-9.

61. Tyler, B.; Gullotti, D.; Mangraviti, A.; Utsuki, T.; Brem, H. Polylactic acid (PLA) controlled delivery carriers for biomedical applications. *Advanced Drug Deliverery Reviews* **2016,** *107*, 163-175.

62. Finniss, A.; Agarwal, S.; Gupta, R. Retarding hydrolytic degradation of polylactic acid: Effect of induced crystallinity and graphene addition. *Journal of Applied Polymer Science* **2016**.

63. Agarwal, S.; Khan, M. M. K.; Gupta, R. K. Thermal conductivity of polymer nanocomposites made with carbon nanofibers. *Polymer Engineering & Science* **2008,** *48* (12), 2474-2481.

64. Mohapatra, A. K.; Mohanty, S.; Nayak, S. K. Poly(lactic acid) and layered silicate nanocomposites prepared by melt mixing: Thermomechanical and morphological properties. *Polymer Composites* **2012,** *33* (12), 2095-2104.

65. Chrissafis, K.; Paraskevopoulos, K. M.; Pavlidou, E.; Bikiaris, D. Thermal degradation mechanism of HDPE nanocomposites containing fumed silica nanoparticles. *Thermochimica Acta* **2009,** *485* (1-2), 65-71.

66. Beltrán, A.; Valente, A. J. M.; Jiménez, A.; Garrigós, M. C. Characterization of Poly(Ɛ-caprolactone)-Based Nanocomposites Containing Hydroxytyrosol for Active Food Packaging. *Journal of Agricultural and Food Chemistry* **2014,** *62*, 2244-2252.

67. Abreu, A. S.; Oliveira, M.; de Sá, A.; Rodrigues, R. M.; Cerqueira, M. A.; Vicente, A. A.; Machado, A. V. Antimicrobial nanostructured starch based films for packaging. *Carbohydrate Polymers* **2015,** *129*, 127-134.

68. Maisanaba, S.; Puerto, M.; Pichardo, S.; Jorda, M.; Moreno, F. J.; Aucejo, S.; Jos, A. In vitro toxicological assessment of clays for their use in food packaging application. *Food and Chemical Toxicology* **2013,** *57*, 266-275.

69. Sharma, A. K.; Schmidt, B.; Frandsen, H.; Jacobsen, N. R.; Larsen, E. H.; Binderup, M. Genotoxicity of unmodified and organo-modified montmorillonite. *Mutatuation Research/Genetic Toxicology and Environmental Mutagenesis* **2010,** *700*, 18-25.

70. Maisanaba, S.; Gutièrrez-Praena, D.; Pichardo, S.; Moreno, F. J.; Jordá, M.; A.M., C.; Aucejo, S.; Jos, A. Toxic effects of a modified montmorillonite clay on the human intestinal cell line Caco-2. *Journal of Applied Toxicology* **2013,** *34*, 714-725.

71. Koh, H. C.; Park, J. S.; Jeong, M. A.; Hwang, H. Y.; Hong, Y. T.; Ha, S. Y.; Nam, S. Y. Preparation and gas permeation properties of biodegradable polymer/layered silicate nanocomposite membranes. *Desalination* **2008,** *233*, 201-209.

72. Ibrahim, N.; Jollands, M.; Parthasarathy, R. Mechanical and thermal properties of melt processed PLA/organoclay nanocomposites. *IOP Conf. Series: Materials Science and Engineering* **2017,** *191*, 1-7.

73. Corcione, C.; Frigione, M. Characterization of Nanocomposites by Thermal Analysis. *Materials* **2012,** *5* (12), 2960-2980.

74. Eng, C. C.; Ibrahim, N. A.; Zainuddin, N.; Ariffin, H.; Yunus, W. M. Z. W.; Then, Y. Y.; Teh, C. C. Enhancement of Mechanical and Thermal Properties of Polylactic Acid/Polycaprolactone Blends by Hydrophilic Nanoclay. *Indian Journal of Materials Science* **2013,** *2013*, 1-11.

75. Jamshidian, M.; Tehrany, E.; Imran, M.; Jacquot, M.; Desobry, S. Poly-Lactic Acid: Production, Applications, Nanocomposites, and Release Studies. *Comprehensive Reviews in Food Science and Food Safety* **2010,** *9*, 552-571.

76. Xi, Y.; Ding, Z.; He., H.; Frost, R. L. Structure of organoclays-an X-ray diffraction and thermogravimetric analysis study. *Journal of Colloid Interface Science* **2004,** *277*, 116-120.

77. Zaidi, L.; Kaci, M.; Bruzaud, S.; Bourmaud, A.; Grohens, Y. Effect of natural weather on the structure and properties of polylactide/Cloisite 30B nanocomposites. *Polymer Degradration and Stability* **2010,** *95*, 1751-1758.

78. Copinet, A.; Bertrand, C.; Govindin, S.; Coma, V.; Couturier, Y. Effects of ultraviolet light (315 nm), temperature and relative humidity on the degradation of polylactic acid plastic films. *Chemosphere* **2004,** *55*, 763-773.

79. Orozco, V. H.; Brostow, W.; Chonkaew, W.; Lo´pez, B. L. Prepartation and Characterization of Poly(Lactic Acid)-g-Maleic Anhydride + Startch Blends. *Macromolecular Symposia* **2009,** *277*, 69-80.

80. Moo-Espinosa, J. I.; Solis-Correa, R.; Vargas-Coronado, R.; Cervantes-UC, J. M.; Cauich-Rodriguez, J. V.; Owen, P. Q.; Aguilar-Santamaria, M. A.; Gutièrrez, M. F.; San Roman del Barrio, J. Physicochemical and biological characterization of nanocomposites made of segmented polyurethanes and Cloisite 30B. *Journal of Biomaterials Applications* **2013,** *28*, 38-48.

81. Cervantes-UC, J. M.; Cauich-Rodriguez, J. V.; Vazquez-Torres, H.; Garfias-Mesias, L. F.; Paul, D. R. Thermal degradation of commercially available organoclays studied by TGA-FTIR. *Thermochimica Acta* **2007,** *457*, 92-102.

82. Saikia, B. J.; Parthasarathy, G. Fourier Transform Infrared Spectroscopic Characterization of Kaolinite from Assam and Meghalay, Northeastern India. *Journal of Modern Physics* **2010,** *1*, 206-210.

83. Frankowski, D. J.; Capracotta, M. D.; Martin, J. D.; Khan, S. A.; Spontak, R. J. Stability of organically modified montmorillonites and their polystyrene nanocomposites after prolonged thermal treatment. *Chemical Materials* **2007,** *19*, 2757-2767.

84. Sayes, C. M. The Relationships among Structure, Activity, and Toxicity of Engineered Nanoparticles. *KONA Powder and Particle Journal* **2014,** *31*, 10-21.

85. Love, S. A.; Maurer-Jones, M. A.; Thompson, J. W.; Lin, Y. S.; Haynes, C. L. Assessing nanoparticle toxicity. *Annual Review of Analytical Chemistry* **2012,** *5*, 181-205.

86. Selim, A. A.; Al-Sunaidi, A.; Tabet, N. Effect of the surface texture and crystallinity of ZnO nanoparticles on their toxicity. *Materials Science and Engineering: C* **2012,** *32* (8), 2356-2360.

87. Lahiri, D.; Dua, R.; Zhang, C.; de Socarraz-Novoa, I.; Bhat, A.; Ramaswamy, S.; Agarwal, A. Graphene nanoplatelet-induced strengthening of ultrahigh molecular weight polyethylene and biocompatibility in vitro. *ACS Applied Materials & Interfaces* **2012,** *4* (4), 2234-41.

88. Osman, A. F.; TF, M. F.; Rakibuddin, M.; Hashim, F.; Tuan Johari, S. A.; Ananthakrishnan, R.; Ramli, R. Pre-dispersed organo-montmorillonite (organo-MMT) nanofiller: Morphology, cytocompatibility and impact on flexibility, toughness and biostability of biomedical ethyl vinyl acetate (EVA) copolymer. *Materials Science & Engineering. C, Materials for Biological Applications* **2017,** *74*, 194-206.

89. Song, Y. M.; Chen, W. C.; Yu, T. L.; Linliu, K.; Tseng, Y. H. Effect of lsocyanates on the Crystallinity and Thermal Stability of Polyurethanes. *Journal of Applied Polymer Science* **1996,** *62*, 827-834.

90. Álvarez, Z.; Mateos-Timoneda, M. A.; Hyrossava, P.; Castano, O.; Planell, J. A.; Perales, J. C.; Engel, E.; Alcantara, S. The effect of the composition of PLA films and lactate release on glial and neuronal maturation and the maintenance of the neuronal progenitor niche. *Biomaterials* **2013,** *34*, 2221-2233.

91. Silverajah, V. S.; Ibrahim, N. A.; Zainuddin, N.; Yunus, W. M.; Hassan, H. A. Mechanical, thermal and morphological properties of poly(lactic acid)/epoxidized palm olein blend. *Molecules* **2012,** *17* (10), 11729-11747.

92. Buzarovska, A.; Bogoeva-Gaceva, G.; Fajgar, R. Effect of the talc filler on structural, water vapor barrier and mechanical properties of poly(lactic acid) composites. *Journal of Polymer Engineering* **2016,** *36*, 181-188.

93. Tábi, T.; Sajó, I. E.; Szabó, F.; Luyt, A. S.; Kovács, J. G. Crystalline structure of annealed polylactic acid and its relation to processing. *eXPRESS Polymer Letters* **2010,** *4*, 659-668.

94. Charlon, S.; Marais, S.; Dargent, E.; Soulestin, J.; Sclavons, M.; Follain, N. Structure–barrier property relationship of biodegradable poly(butylene succinate) and poly[(butylene succinate)-co-(butylene adipate)] nanocomposites: influence of the rigid amorphous fraction. *Physical Chemistry Chemical Physics* **2015,** *17*, 29918-29934.

95. Chandran, N.; Chandran, S.; Maria, H. J.; Thomas, S. Compatibilizing action and localization of clay in a polypropylene/natural rubber (PP/NR) blend. *RSC Advances* **2015,** *5*, 86265-86273.

96. Liu, W.; Hoa, S. V.; Pugh, M. Fracture toughness and water uptake of high-performance epoxy/nanoclay nanocomposites. *Composites Science and Technology* **2005,** *65*, 2364-2373.

97. Kim, S.; Lofgren, E. A.; Jabarin, S. A. Dispersion of Nanoclays with Poly(ethylene terephthalate) by Melt Blending and Solid State Polymerization. *Journal of Applied Polymer Science* **2013**, 2201-2212.

98. Lertwimolnun, W.; Vergnes, B. Influence of compatibilizer and processing conditions on the dispersion of nanoclay in a polypropylene matrix. *Polymer* **2005,** *46*, 3462-3471.

99. Lertwimolnun, W.; Vergnes, B. Effect of Processing Conditions on the Formation of Polypropylene/Organoclay Nanocomposites in a Twin Screw Extruder. *Polymer Engineering & Science* **2006**, 314-323.

100. Krehula, L. K.; Papić, A.; Krehula, S.; Gilja, V.; Foglar, L.; Hrnjak-Murgić, Z. Properties of UV protective films of poly(vinyl-chloride)/TiO2 nanocomposites for food packaging. *Polymer Bulletin* **2016,** *74* (4), 1387-1404.

101. Ramos, O. L.; Reinas, I.; Silva, S. I.; Fernandes, J. C.; Cerqueira, M. A.; Pereira, R. N.; Vicente, A. A.; Poças, M. F.; Pintado, M. E.; Malcata, F. X. Effect of whey protein purity and glycerol content upon physical properties of edible films manufactured therefrom. *Food Hydrocolloids* **2013,** *30*, 110-122.

102. Cele, H. M.; Ojijo, V.; Chen, H.; Kumar, S.; Land, K.; Joubert, T.; de Villiers, M. F. R.; Ray, S. S. Effect of nanoclay on optical properties of PLA/clay composite films. *Polymer Testing* **2014,** *36*, 24-31.

103. Sanchez-Garcia, M. D.; Lopez-Rubio, A.; Lagaron, J. M. Natural micro and nanobiocomposites with enhanced barrier properties and novel functionalities for food biopackaging applications. *Trends in Food Science & Technology* **2010,** *21*, 528-536.

104. Kanmani, P.; Rhim, J. Physical, mechanical and antimicrobial properties of gelatin based active nanocomposite films containing AgNPs and nanoclay. *Food Hydrocolloids* **2014,** *35*, 644-652.

105. Kord, B. Effect of nanoparticles loading on properties of polymeric composite based on Hemp Fiber/Polypropylene. *Journal of Thermoplastic Composite Materials* **2011,** *25* (7), 793-806.

106. Islam, M. S.; Masoodi, R.; Rostami, H. The Effect of Nanoparticles Percentage on Mechanical Behavior of Silica-Epoxy Nanocomposites. *Journal of Nanoscience* **2013,** *2013*, 1-10.

107. Song, Y. S.; Youn, J. R. Influence of dispersion states of carbon nanotubes on physical properties of epoxy nanocomposites. *Carbon* **2005,** *43*, 1378-1385.

108. Chow, W. S.; Ishak, Z. A. M.; Ishiaku, U. S.; Karger-Kocsis, J.; Apostolov, A. A. The Effect of Organoclay on the Mechanical Properties and Morphology of Injection-Molded Polyamide 6/Polypropylene Nanocomposites. *Journal of Applied Polymer Science* **2004,** *91*, 175-189.

109. Muller, K. H.; Motskin, M.; Philpott, A. J.; Routh, A. F.; Shanahan, C. M.; Duer, M. J.; Skepper, J. N. The effect of particle agglomeration on the formation of a surface-connected compartment induced by hydroxyapatite nanoparticles in human monocyte-derived macrophages. *Biomaterials* **2014,** *35* (3), 1074-88.

110. Hoet, P. H.; Brüske-Hohlfeld, I.; Salata, O. V. Nanoparticles-known and unknown health risks. *Journal of Nanobiotechnology* **2004,** *2* (12).

111. Heyder, J. Deposition of inhaled particles in the human respiratory tract and consequences for regional targeting in respiratory drug delivery. *ATSJournals* **2004,** *1*, 315-320.

112. Schinwald, A.; Murphy, F. A.; Jones, A.; MacNee, W.; Donaldson, K. Graphene-Based Nanoplatelets: A New Risk to the Respiratory System as a Consequence of Their Unusual Aerodynamic Properties. *ACS Nano* **2012,** *6*, 736-746.

113. Eldawud, R.; Wagner, A.; Dong, C.; Rojansakul, Y.; Dinu, C. Z. Electronic platform for real-time multi-parametric analysis of cellular behavior post-exposure to single-walled carbon nanotubes. *Biosensors and Bioelectronics* **2015,** *71*, 269-277.

114. Siegrist, K. J.; Reynolds, S. H.; Kashon, M. L.; Lowry, D. T.; Dong, C.; Hubbs, A. F.; Young, S.; Salisbury, J. L.; Porter, D. W.; Benkovic, S. A.; McCawley, M.; Keane, M. J.; Mastovich, J. T.; Bunker, K. L.; Gena, L. G.; Sparrow, M. C.; Sturgeon, J. L.; Dinu, C. Z.; Sargent, L. M. Genotoxicity of multi-walled carbon nanotubes at occupationally relevant doses. *Particle and Fibre Toxicology* **2014,** *11* (6).

115. Mittal, S.; Kumar, V.; Dhiman, N.; Chauhan, L. K.; Pasricha, R.; Pandey, A. K. Physico-chemical properties based differential toxicity of graphene oxide/reduced graphene oxide in human lung cells mediated through oxidative stress. *Scientific Reports* **2016,** *6*, 39548.

116. Wang, X.; Wu, Y.; Stonehuerner, J. G.; Dailey, L. A.; Richards, J. D.; Jaspers, I.; Piantadosi, C. A.; Ghio, A. J. Oxidant generation promotes iron sequestration in BEAS-2B cells exposed to asbestos. *American Journal of Respiratory Cell and Molecular Biology* **2006,** *34* (3), 286-92.

117. Biswas, P.; Wu, C. Nanoparticles and the Environment. *Journal of the Air & Waste Management Association* **2005,** *55*, 708-746.

118. Som, C.; Berges, M.; Chaudhry, Q.; Dusinska, M.; Fernandes, T. F.; Olsen, S. I.; Nowack, B. The importance of life cycle concepts for the development of safe nanoproducts. *Toxicology* **2010,** *269*, 160-169.

119. Hubbs, A.; Greskevitch, M.; Kuempel, E.; Fernando, S.; Toraason, M. Abrasive blasting agents: designing studies to evaluate relative risk. *Journal of Toxicology and Environmental Health, Part A* **2005,** *68*, 999-1016.

120. Uy, B.; McGlashan, S. R.; Shaikh, S. B. Measurments of Reactive Oxygen Species in the Culture Media Using Acridan Lumigen PS-3 Assay. *Journal of Biomolecular Techniques* **2011,** *22*, 95-107.

121. Frisch, S. M.; Francis, H. Disruption of Epithelial Cell-Matrix Interactions Induces Apoptosis. *The Journal of Cell Biology* **1994,** *124* (4), 619-626.

122. Re, F.; Zanetti, A.; Sironi, M.; Polentarutti, N.; Lanfrancone, L.; Dejana, E.; Colotta, F. Inhibition of Anchorage-dependent Cell Spreading Triggers Apoptosis in Cultured Human Endothelial Cells. *The Journal of Cell Biology* **1994,** *127*, 537-546.

123. Knirsch, J. M.; Pulskamp, K.; Krug, H. F. Oops they did it again! Carbon nanotubes hoax scientists in viability assays. *Nano Letters* **2006,** *6*, 1261-1268.

124. Kim, S.; Turnbull, J.; Guimond, S. Extracellular matrix and cell signalling: the dynamic cooperation of integrin, proteoglycan and growth factor receptor. *Journal of Endocrinology* **2011,** *209*, 139-151.

125. Hussain, S.; Thomassen, L. C. J.; Ferecatu, I.; Borot, M.; Andreau, K.; Martens, J. A.; Fleury, J.; Baeza-Squiban, A.; Marano, F.; Boland, S. Carbon black and titanium dioxide nanoparticles elicit distinct apoptotic pathways in bronchial epithelial cells. *Particle and Fibre Toxicology* **2010,** *7* (10).

126. Giaever, I.; Keese, C. R. Micromotion of mammalian cells measured electrically. *Proceedings of the National Academy of Sciences* **1991,** *88*, 7896-7900.

127. Wegener, J.; Keese, C. R.; Giaever, I. Electric Cell-Substrate Impedance Sensing (ECIS) as a Noninvasive Means to Monitor the Kinetics of Cell Spreading to Artificial Surfaces. *Experimental Cell Research* **2000,** *259* (1), 158-166.

128. Monteiro-Riviere, N. A.; Inman, A. O.; Zhang, L. W. Limitations and relative utility of screening assays to assess engineering nanoparticle toxicity in a human cell line. *Toxicology and Applied Pharmacology* **2009,** *234*, 222-235.

129. Xi, B.; Yu, N.; Wang, X.; Xu, X.; Abassi, Y. A. The application of cell-based label-free technology in drug discovery. *Biotechnology Journal* **2008,** *3*, 484-495.

130. Xiao, C.; Lachance, B.; Sunahara, G.; Luong, J. H. T. An In-Depth Analysis of Electric Cell-Substrate Impedance Sensing to Study the Attachment and Spreading of Mammalian Cells. *Analytical Chemistry* **2002,** *74*, 1333-1339.

131. AshaRani, P.V.; Hande, M.P.; Valiyaveettil, S. Anti-Proliferative activity of silver nanoparticles. *BMC Cell Biology* **2009**, *10*.

132. Liu, Q.; Liu, Y.; Xiang, S.; Mo, X.; Su, S.; Zhang, J. Apoptosis and cytotoxicity of oligo(styrene-*co*-acrylonitrile)-modified montmorillonite. *Applied Clay Science* **2011,** *51*, 214-219.

133. Maisanaba, S.; Hercog, K.; Filipic, M.; Jos, A.; Zegura, B. Genotoxic potential of montmorillonite clay mineral and alteration in the expression of genes involved in toxicity mechanisms in the human hepatoma cell line HepG2. *Journal of Hazardous Materials* **2016,** *304*, 425-433.

134. Shackelford, R. E.; Kaufmann, W. K.; Paules, R. S. Cell Cycle Control, Checkpoint Mechanisms, and Genotoxic Stress. *Environmental Health Perspectives* **1999,** *107*.

135. Kastan, M. B.; Bartek, J. Cell-cycle checkpoints and cancer. *Nature* **2004,** *432*, 316-323.

136. Mironava, T.; Hadjiargyrou, M.; Simon, M.; Jurukovski, V.; Rafailovich, M. H. Gold nanoparticles cellular toxicity and recovery: Effect of size, concentration and exposure time. *Nanotoxicology* **2010,** *4*, 120-137.

137. Li, P.; Wei, J.; Chiu, Y.; Su, H.; Peng, F.; Lin, J. Evaluation on cytotoxicity and genotoxicity of the exfoliated silicate nanoclay. ACS *Applied Materials & Interfaces* **2010,** *2*, 1608-1613.

138. Geh, S.; Yücel, R.; Duffin, R.; Albrecht, C.; Borm, P. J. A.; Armbruster, L.; Raulf-Heimsoth, M.; Brüning, T.; Hoffman, E.; Rettenmeier, A. W.; Dopp, E. Cellular uptake and

cytotoxic potential of respirable bentonite particles with different quartz contents and chemical modifications in human lung fibroblasts. *Archives of Toxicology* **2006,** *80*, 98-106.

139. Papageorgiou, I.; Marsh, R.; Tipper, J. L.; Hall, R. M.; Fisher, J.; Ingham, E. Interaction of micron and nano-sized particles with cells of the dura mater. *Journal of Biomedical Materials Research Part B* **2014,** *102B*, 1496-1505.

CONCLUSIONS

The analysis performed in this thesis showed that nanoclays, throughout their life cycle, induced toxic responses upon exposure to lung epithelial cell lines, with such analysis hinting at nanoclay's potential to induce toxicity when inhaled. The effects were more pronounced on small airway epithelial cells (SAECs) than on immortalized human bronchial epithelial (BEAS-2B) cells since the primary cell lines more closely mimic their tissue of origin. Moreover, our analysis showed that a model nanocomposite formed upon incorporation of the nanoclays into a biodegradable polymer, polylactic acid, influenced material's properties throughout its life cycle, its degradation, and ultimately toxicity. In such studies, general toxicological profiles included decreases in viability and proliferation of the exposed cells, as well as changes in cellular morphology, mitochondrial activity, cellular attachment, and membrane integrity. The differences in toxicity were correlated to the physical and chemical properties of the nanoclays or nanocomposites and how such changes were influenced by the life cycle. Such differences were analyzed and validated through both single point as well as real-time assays.

More specifically, our studies were the first to show that thermally degraded nanoclays, used to mimic the end of life cycle or the disposal stage of nanoclay systems, had different toxicological profiles relative to their as-received counterparts, used to mimic the manufacturing stage of the nanoclay systems' life cycle. Specifically, the thermally degraded nanoclays generally showed a lower degree of toxicity relative to their as-received counterparts; this was presumably due to changes in their physical and chemical properties upon degradation.

Moreover, our studies also showed that organically modified nanoclays generally induced higher degrees of toxicity in lung cells relative to pristine (non-modified) nanoclays. Further, the degree of toxicity of organically modified nanoclays was dependent not only on the presence of the organic modifier, but also on the composition of the modifier, with the organic modifier directly and indirectly contributing to toxicity via its composition. Briefly, organic modifiers with bio-reactive groups (i.e. hydroxyls and amines) showed a greater degree of toxicity relative to organic modifiers with long carbon chains. No large differences in toxicity (or chemical properties) were however displayed by the organically modified nanoclays' thermally degraded byproducts, further verifying the large role the organic modifier plays towards contributing to physical and chemical properties and ultimately toxicity of nanoclays.

Complementary, the thermally degraded nanoclays showed lower degrees of toxicity due to the loss of their aluminosilicate lattice and platelet-like morphology. Further, the thermally degraded nanoclays no longer had silanol groups present presumably leading to lower membrane disruptions and reactive oxygen species generation when compared with as-received samples.

Based on our results, detection and mitigation strategies should be implemented in nanoclay/nanocomposite manufacturing and disposal areas to minimize worker inhalation hazards. Specifically, further investigations into the amount and sizes of particles workers are being exposed to should be performed and used to help set up proper occupational exposure limits and protection equipment that allows for the filtering of nanoparticles of certain sizes. Further, engineering controls such as better ventilation and encasing appropriate release areas of process equipment used in nanocomposite manufacturing should be implemented. Finally, with such toxicity information, safe-by-design manufacturing can be implemented. For instance, nanoclays functionalized with modifiers containing long carbon chains instead of bio-reactive groups can be used in the manufacturing of nanocomposites to help make safe, yet still effective products. Also, further investigations into the manufacturing parameters that influence nanoclay exfoliation within a polymer, such as temperature, processing time, and processing conditions can be performed to help decrease the toxicity of nanocomposites in addition to building a more effective product. With a combinatorial approach of lessening nanoclay exposure and designing safer products with an understanding of both material properties along with toxicity, the effects of these systems throughout their life cycle can be minimized.